Evolution of complex traits in carnivorous plants

食虫植物における複合形質の進化

Kenji Fukushima

福島 健児

DOCTOR OF PHILOSOPHY

Department of Basic Biology
School of Life Science
The Graduate University for Advanced Studies

2015

TABLE OF CONTENTS

LIST OF TABLES

LIST OF FIGURES

ABSTRACT

Gradual, stepwise evolution occurs by the accumulation of small changes, but how complex traits evolve remains unclear, since evolutionary intermediates may be less adaptive than the starting state, or the final state. In the evolution of carnivorous plants, the use of insects as a nutrient source requires multiple novel traits, such as the production of specialized leaf morphology and the secretion of digestive fluids; together, these traits are known as 'carnivorous syndrome'. Acquisition of partial components of carnivorous traits may not be adaptive without concurrent establishment of other traits. Therefore, evolutionary pathways may have circumvented less-adaptive intermediates. In this study, I examined development of pitcher leaves and evolution of digestive enzymes of carnivorous plants to understand how complex traits evolve.

In carnivorous plants, morphological evolution often involves changes that facilitate a trapping strategy and construction of functional pitfall traps requires drastic morphological changes. Here, I first review the developmental mechanisms of leaf shape diversification in flowering plants, and then describe developmental analyses of pitcher leaves in *Sarracenia purpurea*. I show that the pitcher leaves of *Sarracenia purpurea* develop through cell division patterns that are distinct from those in bifacial and peltate leaves, subsequent to regular expression of adaxial and abaxial marker genes. Differences in the orientation of cell divisions in the adaxial domain cause bifacial growth in the distal region and adaxial ridge protrusion in the middle region. These different growth patterns in the leaf establish the pitcher morphology. A computer simulation suggests that the orientation of the cell division plane is critical for the acquisition of the pitcher morphology. Our results imply that tissue-specific changes in the orientation of cell division underlie the development of a morphologically complex leaf.

To facilitate molecular understanding of carnivorous syndrome, my colleagues and I established *Cephalotus follicularis* as a new model system. This plant can produce both carnivorous pitcher and non-carnivorous flat leaves. Using this phenotypic plasticity, we can compare the two types of leaves in a single species to infer evolutionary processes. By analyzing leaf fates in response to various environmental factors, I succeeded in controlling the leaf dimorphism under experimental conditions. In addition, the *C. follicularis* nuclear genome has been sequenced and gene knockdown techniques have been developed, making this species tractable for molecular and genetic analyses. Using these resources, I identified transcription factors that show expression changes correlated with leaf fates. This model system will enable further analyses of the molecular mechanisms of carnivorous syndrome.

Carnivorous plants repeatedly evolved from non-carnivorous ancestors, indicating multiple, independent origins of carnivorous traits, including secretion of digestive enzymes. To understand the genetic basis of repeated emergence of carnivorous traits, I analyzed digestive enzyme genes

from four carnivorous plants covering three independent origins of carnivorous syndrome. First, partial amino acid sequences of secreted proteins were determined, and then the corresponding genes were identified by transcriptome sequencing of trap leaves. The identified genes were not specific to carnivorous plants, but rather were homologs of pathogenesis-related hydrolytic enzymes in non-carnivorous plants. These orthologous genes likely were co-opted as digestive enzymes in parallel. Furthermore, several digestive enzymes share convergent amino acid substitutions, particularly in exposed residues at the protein-environment interface; these convergent substitutions may affect molecular adaptation to digestive fluid-specific micro-environments.

The evolution of leaf morphology and digestive enzymes has likely co-opted preexisting mechanisms and modified these mechanisms to serve novel functions. Such evolutionary modifications may require fewer genetic changes than constructing these traits from ground zero, and thus have the potential to drive evolution of complex traits.

1. GENERAL INTRODUCTION

Stepwise phenotypic evolution can be explained by the gradual accumulation of small changes; however, the mechanism by which complex traits evolve remains unclear, since intermediate steps are likely to be less adaptive than either the starting state, or the final state (Barton et al. 2007). In the evolution of carnivorous plants, use of insects as a nutrient source requires multiple novel traits, such as development of specialized leaf morphology and secretion of digestive fluids (Juniper et al. 1989). Acquisition of a partial component of carnivorous traits should not be adaptive without concurrent acquisition of the other traits. Therefore, an evolutionary pathway may exist to circumvent less-adaptive intermediates.

Previous work has revealed possible mechanisms of evolution of novel traits. In the adaptive landscape of flower color evolution in *Antirrhinum* spp., an adaptive ridge connects two distinct, naturally predominating phenotypes; therefore, intermediate states are as adaptive as parental flower colors (Whibley et al. 2006). This demonstrates that stepwise evolution can occur for simple phenotypes like flower color. In saltation, an alternative hypothesis to gradualism, a variation with large effect causes discontinuous phenotypic changes (Futuyma 2009). Genotype-phenotype relationships may also affect evolution of novel traits, as organisms can exhibit phenotypic changes without genetic changes under certain selective pressures; this phenotypic plasticity can be genetically fixed later, a process called genetic assimilation (Pigliucci et al. 2006; Waddington 1953). Genetic changes can also accumulate without phenotypic changes and these cryptic genetic variations can also drive the evolution of novel traits (Gibson and Dworkin 2004). Additional evolutionary pathways also include co-option from preexisting traits and emergence from scratch (Shubin et al. 2009). However, whether those pathways act in complex trait evolution remains unknown. Especially in saltatory evolution, how a change of large effect occurs is unclear.

Carnivorous plants have suitable features for the study of novel characters in a complex trait. First, evolution of pitcher leaves can be considered as a typical example of saltation. Pitcher-shaped pitfall traps evolved from flat leaves in three independent lineages of flowering plants (Albert et al. 1992), with no apparent intermediate status. Developmental comparison of pitcher and flat leaves thus may give insights into saltatory evolution. A carnivorous plant that stably produces pitcher leaves, like *Sarracenia purpurea*, can be used for inter-species comparison with flat-leaved species. Moreover, *Cephalotus follicularis*, a herbaceous plant native to south west Australia, produces both carnivorous pitcher leaves and non-carnivorous flat leaves (Juniper et al. 1989; Lloyd 1942). If we can control leaf fates, coexistence of presumably ancestral and derived characters in a single species will enable comparative analyses in identical genetic backgrounds.

Second, genes regulating carnivorous traits, particularly digestive functions, can be readily examined. Carnivorous plants secrete hydrolytic enzymes into their digestive fluids for degradation of insect bodies (Juniper et al. 1989). Digestive fluids can be collected in sufficient quantities for

biochemical analyses, enabling identification of digestive enzyme genes. Indeed, several digestive enzyme genes have been isolated since the identification of the aspartic proteases NEPENTHESIN I and II from the digestive fluids of *Nepenthes* spp. (Athauda et al. 2004). Finally, carnivorous plants evolved multiple times in five independent orders of flowering plants (Albert et al. 1992). This provides an opportunity to examine evolutionary trends by comparing independently evolved lineages.

Recent advances in sequencing technology have facilitated genomics approaches in non-model organisms (reviewed in Hawkins et al. 2010). In addition, the establishment of widely applicable gene-silencing techniques has facilitated analyses of gene function (reviewed in Becker and Lange 2010). By taking advantage of these technologies, we can dissect the genetic basis of carnivory-related traits and thus reveal the mechanisms of evolution of complex traits.

In this thesis, I analyzed pitcher leaf development and digestive enzyme evolution of carnivorous plants to understand how complex traits evolve. Chapter 2 provides a literature review summarizing current knowledge on the developmental basis of leaf shape diversification in flowering plants. Chapter 3 describes developmental analyses of pitcher leaves in *S. purpurea* and provides evidence of the role of oriented cell division in drastic morphological changes. Chapter 4 details culture conditions for experimentally controlling leaf fate, and describes genome sequencing and knockdown analyses of developmental genes in *C. follicularis*. Chapter 5 describes the origin and molecular evolution of digestive enzymes in four carnivorous plants from lineages that independently originated carnivory. Possible mechanisms of complex trait evolution in carnivorous plants are discussed.

2. PREVIOUS STUDIES AND CONTEMPORARY PROBLEMS ON LEAF SHAPE DIVERSIFICATION

2.1 Introduction

Leaves are lateral organs that have diversified during the evolution of flowering plants. Although the flat shape of typical leaves is efficient for their primary function as the site of photosynthesis, flowering plants have also evolved morphologically distinct leaves with novel functions. For example, some climbing plants produce leaf tendrils to support their body, and some carnivorous plants develop pitcher-shaped leaves to capture small animals as a nutrient source (Bell and Bryan 2008).

Leaves are produced at the tips of leaf-bearing branches called shoots (reviewed in Groff and Kaplan 1988). The shoot apex contains stem cells and proliferative tissues, together called the shoot apical meristem (SAM) (Esau 1977). The first morphogenetic signature of leaf initiation is a periclinal cell division, which forms a new cell wall parallel to the organ surface, in the inner tissues of the SAM periphery (*e.g.* Cunninghame and Lyndon 1986; Tepfer 1960). Along with subsequent cell proliferation, leaf primordia acquire organ polarities. Adaxial–abaxial polarity is determined based on position relative to the SAM. The cells close to the SAM differentiate into the adaxial domain, and those far from the SAM become the abaxial domain, generating a bifacial structure in the leaves (Fig. 2.1). Leaf margins are formed in the boundary of the adaxial and abaxial domains (Steeves and Sussex 1989). During leaf blade development, prolonged proliferative activity is induced at the marginal region (Esau 1977). As leaf development proceeds, cell proliferation is gradually replaced by cell differentiation, including increases in cell size (reviewed in Tsukaya 2013). Finally, leaf primordia develop into mature leaves with two anatomically distinct faces, the adaxial and abaxial sides corresponding to the upper and lower sides, respectively (Fig. 2.2). Leaves with only bifacial parts are termed conventional bifacial leaves, whereas leaves exhibiting different facialities are classified into other leaf type categories (Fig. 2.3) (reviewed in Franck 1976).

The developmental mechanisms of conventional bifacial leaves have been well studied in model plants including Arabidopsis (*Arabidopsis thaliana*) and maize (*Zea mays*) (Fig. 2.4), and those of other leaf types are being progressively elucidated in different plant species. In this review, I summarize what is known mainly about the development of conventional bifacial leaves and then discuss mechanisms underlying the diversification of leaf shape, with emphasis on adaxial–abaxial polarity.

2.2 Terminology related to adaxial–abaxial polarity

The concept of adaxial–abaxial polarity refers to asymmetry in tissue differentiation associated with position relative to the SAM (reviewed in Kaplan 2001). In this article, I use adaxial/abaxial "side" to describe positional relationships, whereas adaxial/abaxial "character" is reserved to denote

gene expression and tissue differentiation, characteristic of the adaxial/abaxial side of conventional bifacial leaves (Fig. 2.1). Adaxial/abaxial "domain" indicates leaf tissue with adaxial/abaxial characters. The adaxial/abaxial "surface" is the surface layer of the domains. These designations are helpful in dissecting the faciality of diverse leaf types, especially in those with complicated patterns of adaxial and abaxial domains.

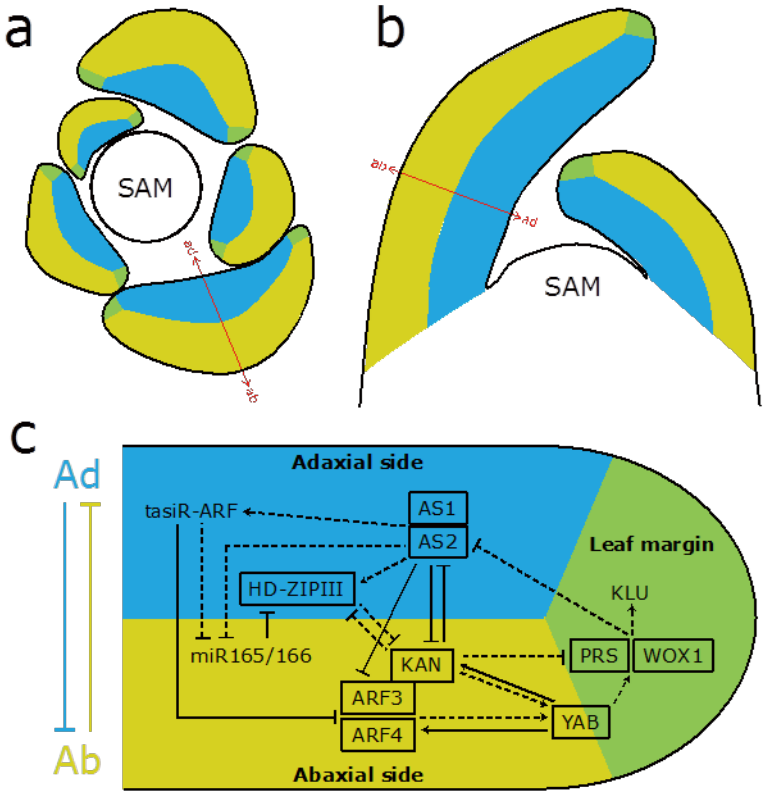

Figure 2.1. Patterning and regulation of adaxial–abaxial polarity in Arabidopsis. (a-b) Schematic representations of transverse (a) and longitudinal (b) sections of the shoot apex. Blue, yellow, and green indicate adaxial side, abaxial side, and leaf margin, respectively. **(c)** Transcriptional network regulating antagonistic interactions between the adaxial and abaxial domains, and the downstream pathway promoting laminar growth activity. Transcription factors are boxed. Solid lines denote direct regulation. Dashed lines indicate indirect or unconfirmed interactions.

2.3 Asymmetric tissue differentiation with regard to adaxial–abaxial polarity

Leaf tissues are organized into a layered structure and differentiate asymmetrically along the adaxial–abaxial axis. The adaxial epidermis of Arabidopsis is composed of jigsaw puzzle-shaped pavement cells, with more trichomes, and fewer stomata than found on the abaxial epidermis (Bowman 1994). The inner tissues of the leaf also display polarity. The adaxial inner tissue contains palisade mesophyll, composed of elongated cells perpendicular to the surface that form a cell layer optimized for light capture (Fig. 2.2a). In the abaxial side, spongy mesophyll has loosely packed cells surrounded by air space that facilitates photosynthetic gas exchange through abaxial stomata. This arrangement enables the adaxial light-harvesting tissue to be in the vicinity of the photosynthetic substrate, namely carbon dioxide, supplied from the abaxial tissue. As such, the

layered organization serves as an adaptation for efficient photosynthesis (Braybrook and Kuhlemeier 2010; Kaplan 2001).

Vascular tissue also has adaxial–abaxial polarity in leaves. In Arabidopsis, vascular bundles differentiate in a collateral arrangement with xylem and phloem on the adaxial and abaxial sides, respectively (Fig. 2.2c; Fig. 2.3a, b). In addition, some plants develop bicollateral vascular bundles, which have additional phloem on the adaxial side (Dengler and Kang 2001; Esau 1977).

Asymmetric tissue differentiation has been subject to structural modification during adaptation to a specific habitat. For example, bifacial leaves of *Eucalyptus* spp. (Fig. 2.2b) have palisade mesophyll on both the adaxial and abaxial sides. Despite the anatomical symmetry of the mesophyll layers, *Eucalyptus* leaves have adaxially positioned xylem and abaxially positioned phloem (Fig. 2.2d), and therefore are considered to represent a form of bifacial leaves with reduced asymmetry. In natural habitats, two faces of adult leaf blades of *E. globulus* tend to face east and west (James and Bell 2000), and these so-called equifacial *Eucalyptus* leaves are considered to utilize incident light from the sun at low angle by both the adaxial and abaxial assimilatory tissues (Kaplan 2001).

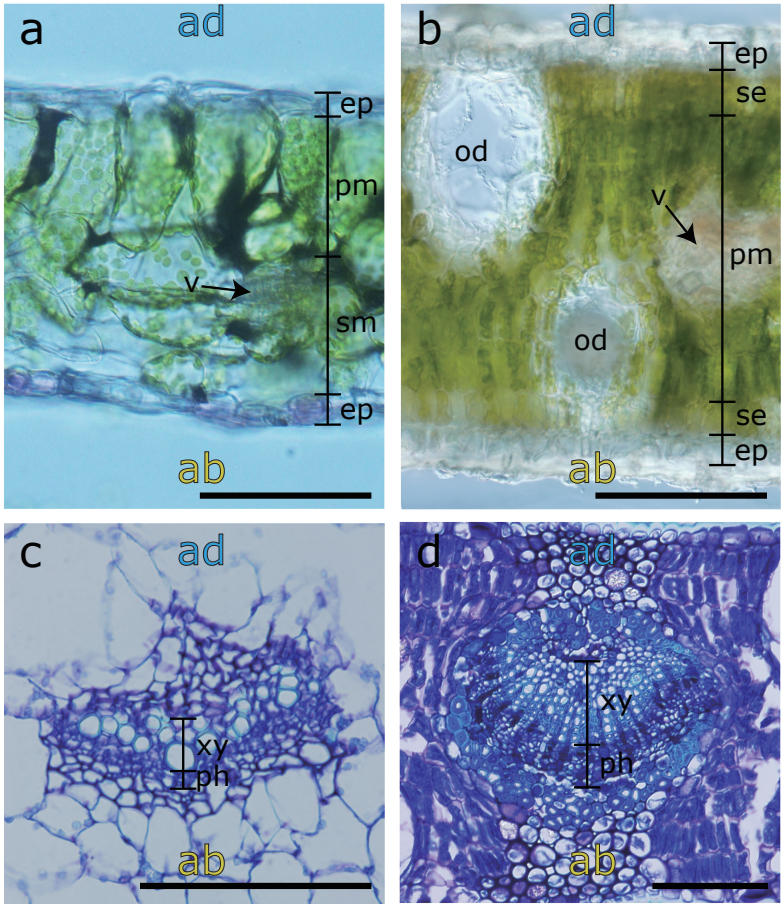

Figure 2.2. Cross sections of mature leaves showing asymmetric tissue differentiation along the adaxial–abaxial axis. Leaves of Arabidopsis **(a, c)** differentiate adaxial palisade and abaxial spongy mesophyll layers, whereas that of *Eucalyptus camaldulensis* **(b, d)** develops well-packed palisade tissue on both sides. Both species show clear vascular polarity in leaves. Scale bar denotes 100 µm. Abbreviations are as follows: ad, adaxial side; ab, abaxial side; ep, epidermal layer; se, sub-epidermal layer; pm, palisade mesophyll; sm, spongy mesophyll; v, vascular bundle; xy, xylem; ph, phloem; od, oil duct.

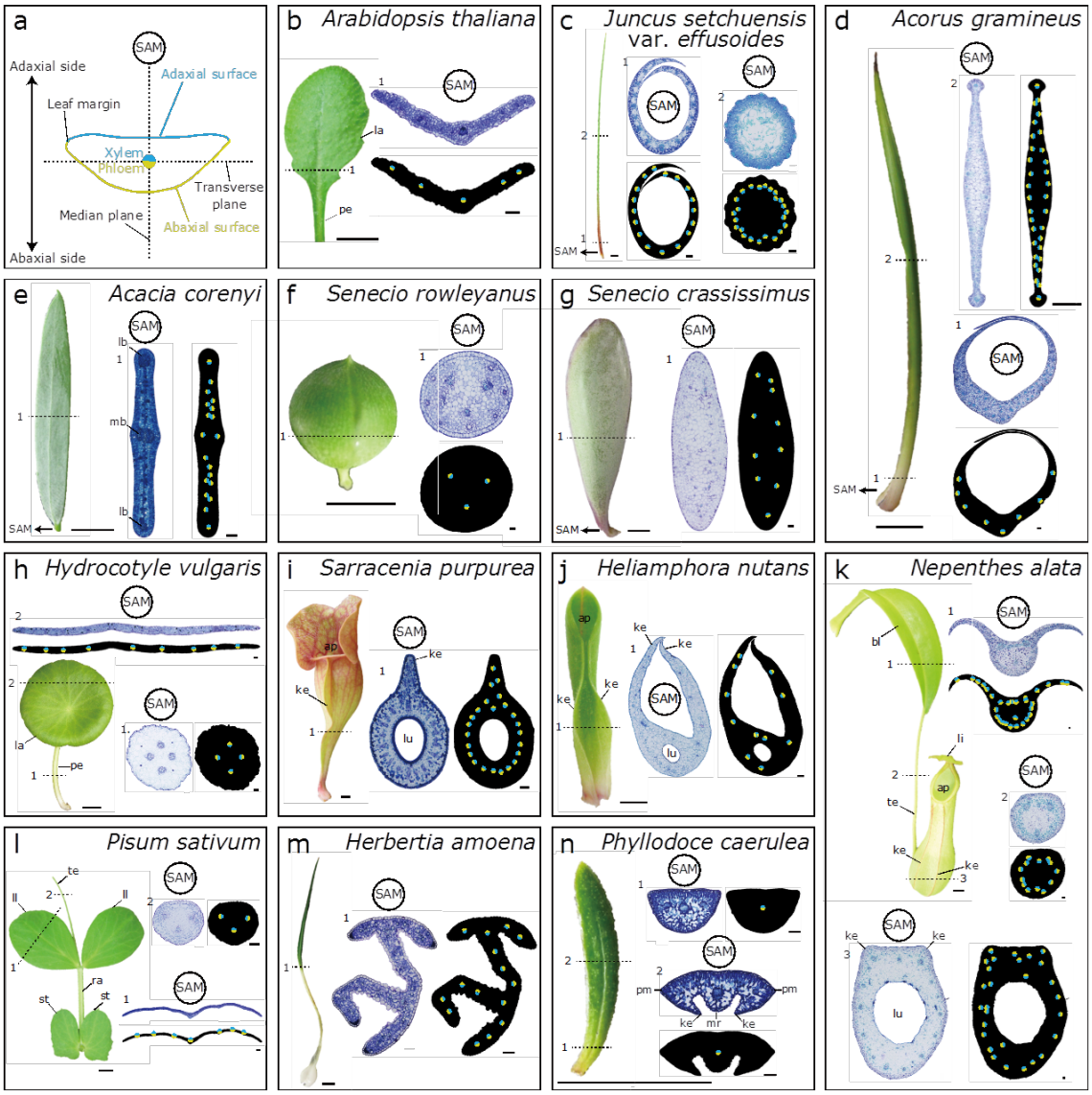

Figure 2.3. Typical examples of different leaf types. (a) Schematic representation of a transverse section of a conventional bifacial leaf. **(b-l)** Leaf appearance, toluidine blue-stained transverse section, and vascular polarity are shown. The positions at which the sections were prepared are indicated by the dashed lines. **(b)** Conventional bifacial leaf of Arabidopsis. **(c)** Terete leaf of *Juncus setchuensis* var. *effusoides*. **(d)** Ensiform leaf of *Acorus gramineus*. **(e)** Phyllode of *Acacia corenyi*. **(f)** Spherical leaf of *Senecio rowleyanus*. **(g)** Leaf flattened along the median plane in *Se. crassissimus*. **(h)** Peltate leaf of *Hydrocotyle vulgaris*. **(i)** Keeled pitcher leaf of *Sarracenia purpurea*. **(j)** Bi-keeled pitcher leaf of *Heliamphora nutans*. **(k)** Pitcher leaf of *Nepenthes alata*. **(l)** Compound leaf with a terminal tendril in *Pisum sativum*. **(m)** Foliated leaf of *Herbertia amoena*. **(n)** Ericoid leaf of *Phyllodoce caerulea*. Solid circles in the section contours indicate vascular bundles: blue, xylem; yellow, phloem. Scale bars denote 5 mm and 100 µm for leaf appearance and cross sections, respectively. Abbreviations are as follows: SAM, shoot apical meristem; pe, petiole; la, lamina; lb, lateral vascular bundle; mb, main vascular bundle; ke, keel; ap, aperture; lu, pitcher lumen; bl, basal laminar portion; te, tendril; li, lid; st, stipule; ra, rachis; ll, leaflet; pm, primary margin; mr, midrib.

2.4 Specification of adaxial domain

During the establishment of adaxial–abaxial polarity, leaf primordia are hypothesized to receive mobile signal(s) from the SAM. Surgical experiments have shown that a leaf primordium that has been physically separated from the shoot apex gives rise to an abaxialized bladeless leaf, raising the possibility that the positional information to specify the adaxial domain originates from the SAM

(Snow and Snow 1959; Snow and Snow 1954; Sussex 1951; 1954; 1955). Laser ablation of epidermal cells between a leaf primordium and the SAM also causes leaf abaxialization, indicating that the adaxializing signal is mediated by the epidermal layer (Reinhardt et al. 2005).

The molecular identity of the adaxialization signal remains unknown, although a clue regarding its nature comes from analysis of the Arabidopsis mutant *enlarged fil expression domain1* (*enf1*), which exhibits disturbed expression of a gene that is normally expressed abaxially (Toyokura et al. 2011). *ENF1* encodes SUCCINIC SEMIALDEHYDE DEHYDROGENASE (SSADH), a component of the GABA metabolic pathway. Exogenously supplied small metabolites in the GABA shunt, including succinic semialdehyde (SSA) and its derivatives, confer adaxial characters in abaxial sides (Toyokura et al. 2011). This suggests that a metabolite in the GABA shunt is involved in establishment of the adaxial domain.

Flowering plants are able to develop multiple shoots by branching from axillary meristems. In *Zelkova serrata*, the adaxial surface is not always oriented toward the SAM of the axillary bud from which the leaf originated, but can face the main branch instead (Charlton 1993; Soma 1965). This orientation emerges from the outset, and thus is not the result of secondary twisting. These observations suggest that there can be interference in the adaxial specification between the main and axillary shoot apices in a plant body.

2.5 Coordination of adaxial–abaxial polarity by transcription factors and small RNAs in conventional bifacial leaves

The first insight revealing a genetic connection between adaxial–abaxial polarity and leaf morphogenesis came from analysis of the loss-of-function mutant *phantastica* (*phan*) in *Antirrhinum majus* (snapdragon). *PHAN* encodes a MYB family transcription factor of *ASYMMETRIC LEAVES1*/*ROUGH SHEATH2*/*PHANTASTICA* (ARP) orthologous group and functions to promote adaxial characters (Byrne et al. 2000; Waites and Hudson 1995; Waites et al. 1998). The *phan* mutant produces a series of abaxialized leaves wherein the adaxial side exhibits a mosaic of adaxial and abaxial characters. Blade-like outgrowths called lamina ridges are formed at the ectopic boundaries of the adaxial and abaxial domains (Fig. 2.4b). Waites and Hudson (1995) proposed that the adaxial–abaxial boundary induces lamina growth activity and that both adaxial and abaxial surfaces are required for lamina formation. Similar phenotypes have been observed in loss-of-function mutants of ARP genes from other eudicot species (Kim et al. 2003a; Kim et al. 2003b; McHale and Koning 2004b; Tattersall et al. 2005; Zoulias et al. 2012). Likewise, some ornamental plants (*e.g. Xanthosoma atrovirens*, *Begonia hispida* var. *cucullifera*) exhibit growth activity at ectopic adaxial–abaxial boundaries, supporting the idea that the boundary induces a novel growth axis (Kidner and Wrigley 2010; Korn 2010).

Although *PHAN* plays a central role in adaxial–abaxial patterning in snapdragon, the extent of

ARP activity to the polarity formation is different among plant species. For example, loss-of-function mutants of Arabidopsis ortholog *ASYMMETRIC LEAVES1* (*AS1*) exhibits abaxialized phenotypes at a low frequency (Xu et al. 2003), whereas mutants of maize ortholog *ROUGH SHEATH2* (*RS2*) do not show clear phenotype in adaxial–abaxial patterning (Schneeberger et al. 1998; Timmermans et al. 1999; Tsiantis et al. 1999). These indicate that the regulatory mechanism of adaxial–abaxial patterning differentiates among plant species with conventional bifacial leaves.

Extensive genetic screening subsequently identified several factors involved in polarity establishment (Fig. 2.1c). In Arabidopsis, AS1 and its structurally unrelated interactor AS2 positively regulate class III homeodomain-leucine zipper (HD-ZIP III) transcription factors that function in specification of the adaxial domain (Emery et al. 2003; Fu et al. 2007; McConnell et al. 2001; Semiarti et al. 2001; Xu et al. 2003). Three HD-ZIP III family genes, *PHABULOSA* (*PHB*), *PHAVOLUTA* (*PHV*), and *REVOLOTA* (*REV*), redundantly function on the adaxial side to promote adaxial differentiation (Emery et al. 2003; McConnell and Barton 1998; Prigge et al. 2005; Talbert et al. 1995). Their mRNAs harbor a microRNA recognition site and their expression domains are tightly regulated by miR165/166-guided mRNA cleavage (Mallory et al. 2004; Rhoades et al. 2002; Tang et al. 2003). Plant small RNAs are able to move cell-to-cell (Dunoyer et al. 2010; Molnar et al. 2010). In accord with this, miR165/166 precursors are predominantly transcribed in the abaxial side (Miyashima et al. 2013; Yao et al. 2009), and are suggested to move toward the adaxial side (Juarez et al. 2004a). miR165 is known to act non-cell-autonomously in roots, where it is transferred through plasmodesmata (Carlsbecker et al. 2010; Miyashima et al. 2011; Vatén et al. 2011). Defects in ARGONAUTE1 (AGO1), which functions in miR165/166 loading into the RNA-induced silencing complex (RISC), bring about leaf adaxialization (Bohmert et al. 1998; Kidner and Martienssen 2004). By contrast, another AGO protein, ZWILLE/PINHEAD/AGO10, binds to miR165/166 without inducing target cleavage, thereby acting as a decoy to inactivate miR165/166 in the adaxial side (Liu et al. 2009; Zhu et al. 2011). Mutations in HD-ZIP III genes at the miRNA binding site cause ectopic expression of miRNA-resistant mRNA, giving rise to adaxialized leaves in Arabidopsis, maize, and *Nicotiana sylvestris* (Fig. 2.4e) (Emery et al. 2003; Juarez et al. 2004a; Juarez et al. 2004b; McConnell and Barton 1998; McConnell et al. 2001; McHale and Koning 2004a).

KANADIs (KANs), *ETTIN*/*AUXIN RESPONSE FACTOR 3* (*ETT*/*ARF3*), and *ARF4* are expressed in the abaxial side and cooperatively function in abaxial specification (Eshed et al. 1999; Kerstetter et al. 2001; Pekker et al. 2005; Sessions et al. 1997; Sessions and Zambryski 1995). KANADI genes encode GARP family of transcription factors that abaxially expressed in Arabidopsis, *Oryza sativa* (rice), and maize (Candela et al. 2008; Kerstetter et al. 2001; Yan et al. 2008; Zhang et al. 2009). In Arabidopsis, KANADIs act antagonistically to *AS2* and HD-ZIP III

genes, repressing adaxialization in the abaxial side (Emery et al. 2003; Iwasaki et al. 2013; Wu et al. 2008). Abaxialized phenotype of *KAN1* misexpression is suppressed in *ett*/*arf3* mutant (Pekker et al. 2005), which is concordant with the formation of a KANADI and ETT/ARF3 protein complex (Kelley et al. 2012). *ARF4* is a sister gene of *ETT*/*ARF3*, and is found in all of previously examined angiosperms except rice, maize, and their relatives (Finet et al. 2013; Finet et al. 2010). In Arabidopsis and tomato, *ARF4* mRNA localizes to the abaxial side, while *ETT*/*ARF3* mRNA expresses also in the adaxial side as well as the abaxial side (Pekker et al. 2005; Yifhar et al. 2012). Despite the broad expression of mRNA, its protein localizes to the abaxial side in wild-type Arabidopsis (Chitwood et al. 2009). An open reading frame in the 5' region of *ARF3*/*ETT* mRNA modulates the translation of ETT/ARF3, although its spatial regulation in leaf tissues remains unknown (Nishimura et al. 2004; Nishimura et al. 2005; Rosado et al. 2012).

Accumulation and abaxial localization of *ETT*/*ARF3* and *ARF4* is regulated by tasiR-ARF, a member of a class of endogenous small RNA called *trans*-acting small-interfering RNA (tasiRNA) (Adenot et al. 2006; Allen et al. 2005; Garcia et al. 2006; Williams et al. 2005). Whereas *TAS3a*, which is a precursor non-coding RNA, is expressed only in the adaxial side, the mature 21-nucleotide tasiR-ARF shows a wider distribution as a result of intercellular movement toward the abaxial side, forming a gradient of distribution (Chitwood et al. 2009; Garcia et al. 2006; Nogueira et al. 2007; Schwab et al. 2009). Arabidopsis mutants defective in tasiRNA biogenesis overaccumulate *ARF3*/*ETT* mRNA and misexpress its protein throughout leaf primordia (Adenot et al. 2006; Chitwood et al. 2009), although such mutants do not show polarity phenotypes similar to those found in rice and maize mutants (Nagasaki et al. 2007; Nogueira et al. 2007). However, the tasiRNA biogenesis mutants with *as1* or *as2* background formed abnormal leaves, in which adaxial surface harbors patches of adaxial and abaxial identities (Li et al. 2005; Xu et al. 2006). This suggests that both pathways redundantly function in Arabidopsis. In addition, biogenesis of the tasiRNA (tasiR-ARF) itself is positively regulated by the AS1-AS2 protein complex through up-regulation of miR390 and *RDR6* expression (Iwasaki et al. 2013). Simulation of the small RNA-mRNA interaction illustrated that diffusible tasiR-ARF could form the sharp boundary of target ARF expression domain (Levine et al. 2007). However, in maize, tasiR-ARF biogenesis is required for proper expression level of *ARF3* but not for abaxial localization of its transcript, suggesting that tasiR-ARF-independent mechanism polarize *ARF3* expression in this species (Douglas et al. 2010).

Together, the analyses of genetic interactions reveal a generalized view of the regulatory relationships between adaxial and abaxial factors: adaxially localized transcription factors repress abaxial factors and *vice versa* (Fig. 2.1c). Accumulating evidence indicates that small RNAs are the key players for intercellular signaling in the transcriptional network across the two domains. The work to date supports a model in which antagonistic interactions coordinate the mutually exclusive specification of adaxial and abaxial cell fates, and thereby facilitate precise tissue differentiation.

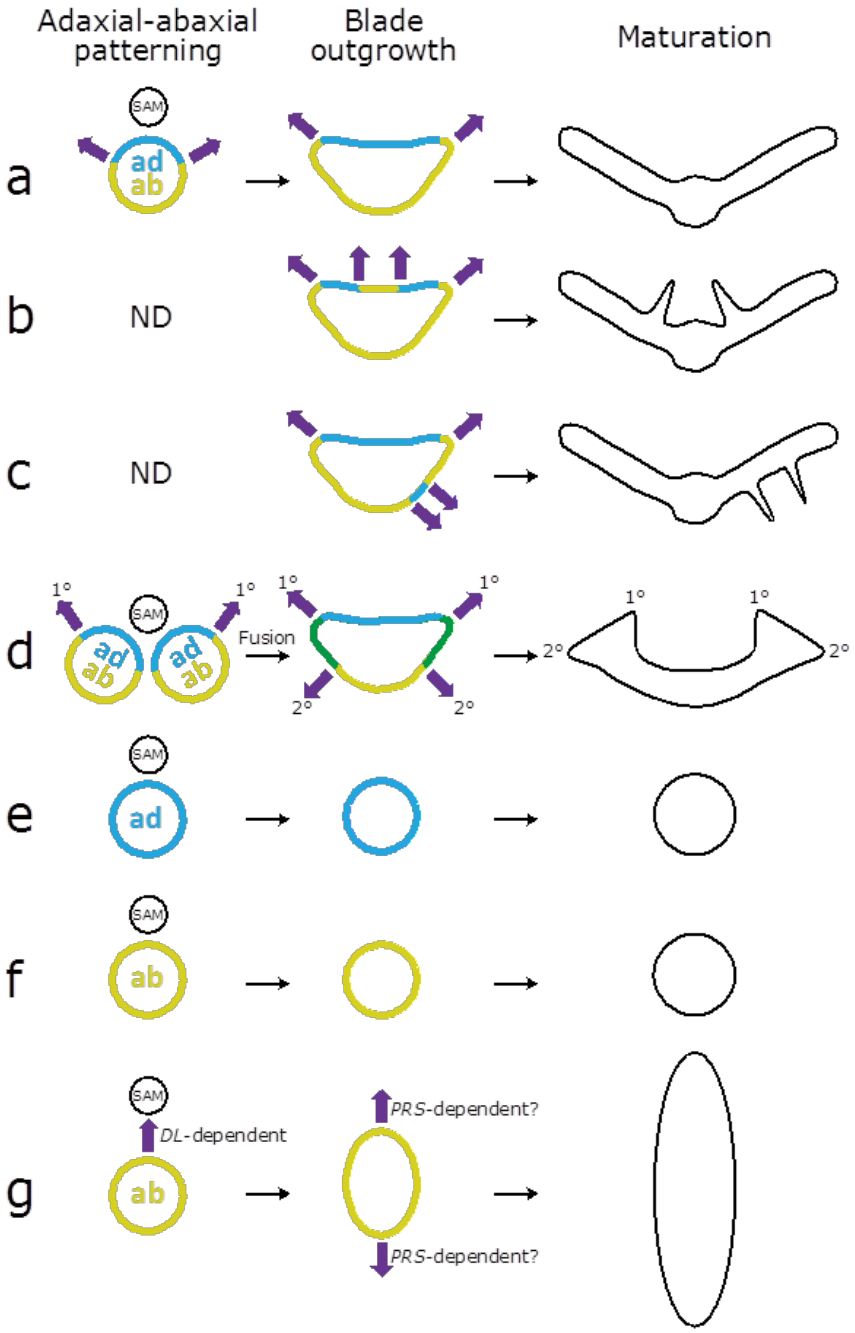

Figure 2.4. Schematics representing development of leaves with different shapes in relation to the growth activity at the adaxial–abaxial boundary. Cross-sectional views of leaf primordia at the establishment of adaxial–abaxial polarity (left), blade outgrowth (middle), and maturation (right) are shown. **(a)** Conventional bifacial leaf, like those of wild-type Arabidopsis. **(b)** Weak phenotype of *phantastica* (*phan*) mutant in snapdragon (Waites and Hudson 1995) and knock-down phenotype of *Nicotiana sylvestris PHAN* ortholog (McHale and Koning 2004b). **(c)** Maize *milkweed pod1* mutant (Candela et al. 2008). **(d)** Wild-type prophyll in maize (Johnston et al. 2010). **(e)** Severe phenotype of *phabulosa-1d* in Arabidopsis (McConnell and Barton 1998). **(f)** Naturally occurring terete leaf (Yamaguchi et al. 2010) or severely compromised leaf of *phan* in snapdragon (Waites and Hudson 1995). **(g)** Ensiform leaf of *Juncus prismatocarpus* (Yamaguchi et al. 2010). See text for detail. Blue and yellow lines denote the adaxial and abaxial surfaces in developing leaves, respectively. Green in (d) indicates expanded adaxial domain. Black lines show transectional contours of mature leaves. SAM indicates the position of the shoot apical meristem. Purple arrows show growth direction. The primary and secondary growth axes are indicated by 1° and 2°, respectively, in (d). ND, not determined.

2.6 Blade formation in bifacial leaves

After the establishment of adaxial–abaxial polarity, a dome-shaped primordium develops into a flat structure partly as a result of active cell division at the marginal region, where the adaxial and abaxial domains are juxtaposed (Fig. 2.4a) and characteristic margin cells develop (Esau 1977). Interaction between the adaxial and abaxial domains is necessary for the onset of the directed growth that forms leaf blades. Although the mechanism by which directed growth activity is initiated remains largely unknown, analyses of YABBY and WUSCHEL-RELATED HOMEOBOX (WOX) genes have provided evidence linking adaxial–abaxial polarity and the growth activity.

Expression of YABBY genes *FILAMENTOUS FLOWER* (*FIL*/*YAB1*) and *YAB3* marks the abaxial domain and marginal regions of primordial leaves in Arabidopsis (Sawa et al. 1999; Siegfried et al. 1999). Abaxial expression is conserved in a snapdragon ortholog *GRAMINIFOLIA* (Golz et al. 2004). In maize and rice, the YABBY orthologs show adaxial and uniform expression, respectively (Dai et al. 2007; Juarez et al. 2004b), although ancestral expression pattern in angiosprems was inferred to be abaxial (Yamada et al. 2011). In Arabidopsis, YABBY genes are up-regulated by KANADIs, *ETT*/*ARF3*, and *ARF4* (Eshed et al. 2004; Garcia et al. 2006), and, in turn, *FIL*/*YAB1* and *YAB3* promote the expression of *KAN1* and *ARF4*, forming positive feedback loops (Bonaccorso et al. 2012; La Rota et al. 2011). In the absence of all YABBY activities, leaf primordia establish adaxial–abaxial polarity but fail to initiate lamina outgrowth (Sarojam et al. 2010). Moreover, loss of YABBY activity abolishes ectopic outgrowths in the *kan1 kan2* double mutant (Eshed et al. 2004). These findings indicate that YABBY genes mediate the induction of growth activity related to adaxial–abaxial polarity.

YABBY genes positively regulate a member of the WOX gene family, *PRESSED FLOWER* (*PRS*), which is expressed in the leaf margin and promotes blade outgrowth (Fig. 2.1c) (Nakata et al. 2012). *PRS* cooperatively functions with *WOX1*, and the *prs wox1* double mutant exhibits a narrower-leaf phenotype in Arabidopsis (Nakata et al. 2012; Vandenbussche et al. 2009). Likewise, mutants disrupted in *PRS* or *WOX1* orthologs in other species show compromised leaf blades (Cho et al. 2013; Ishiwata et al. 2013; McHale 1993; Nardmann et al. 2004; Tadege et al. 2011; Vandenbussche et al. 2009). *lamina1* (*lam1*), a loss-of-function mutant of a *WOX1* ortholog from *Nicotiana sylvestris*, retains the capacity to specify blade founder cells, but fails to commence blade outgrowth, suggesting that *LAM1* has a role in blade formation after adaxial–abaxial specification (McHale 1993).

The WOX genes act in leaf blade formation differently in plant lineages. *WOX1* are conserved in eudicots but is absent from rice and maize (Nardmann et al. 2007; Zhang et al. 2010). In Arabidopsis, *prs wox1* double mutant displays reduced cell proliferation in the marginal region of leaf primordium (Nakata et al. 2012), whereas the compromised leaf blades in loss-of-function mutant of maize *PRS* orthologs are largely attributed to the failure in founder-cell recruitment into leaf blades from SAM

(Nardmann et al. 2004; Scanlon et al. 2000; Scanlon and Freeling 1997; Scanlon et al. 1996). This may reflect the difference in the developmental mechanisms of leaf blade initiation between these species.

The *PRS*- and *WOX1*-dependent blade outgrowth is, in part, mediated by an as-yet-unidentified mobile signal(s) processed by the cytochrome P450 KLUH/CYP78A5 (KLU) in Arabidopsis (Nakata et al. 2012). *KLU* non-cell-autonomously promotes cell division activity in aerial organs including leaves (Anastasiou et al. 2007). The loss-of-function mutant of *KLU* exhibits reduced organ sizes, and a series of *KLU*-restored lines show different organ sizes in correlation with the restored *KLU* expression level. This dose-dependent effect of *KLU* is attributed changes in the longevity of the cell proliferative stage, but not in the growth rate.

Auxin appears to be another signal acting in blade formation (Wang et al. 2011), independent of KLU (Anastasiou et al. 2007). Multiple loss-of-function mutants of the *YUCCA* (*YUC*) auxin-biosynthetic genes show defective blade outgrowth, raising the possibility that auxin participates in the regulatory network for directed growth activity (Wang et al. 2011). YUCCA-dependent growth activity is ectopically activated in *as2 rev* and *kan1 kan2* double mutants, indicating that auxin biosynthesis is coordinated by adaxial and abaxial factors.

2.7 Unifacial leaves and their analogs

Nonequivalent development of adaxial and abaxial tissues gives rise to mature leaf morphology different from that of conventional bifacial leaves (Fig. 2.4). Abaxialization usually causes a cylindrical leaf type with radialized symmetry, referred to as unifacial (reviewed in Franck 1976). Vascular bundles in these leaves are arranged in a radial pattern with phloem outside and xylem inside (section 2 in Fig. 2.3c). Unifacial leaves with cylindrical leaf blades, called terete leaves, are prevalent in monocots. Whereas the distal portion of monocotyledonous terete leaves is fully abaxialized, a basal part usually retains adaxial characters (section 1 in Fig. 2.3c). Ensiform leaves, another type of unifacial leaf, have a flat blade along the median plane, yet exhibit radial symmetry in terms of vascular polarity (*e.g. Acorus gramineus*, Fig. 2.3d) (Arber 1921). In these leaves, the *ETT*/*ARF3* ortholog is expressed throughout the entire surface of the flattened blade, whereas the *PHB* ortholog is confined to the adaxial side of the basal part, consistent with their anatomical features including vascular polarity (Yamaguchi et al. 2010). Terete and ensiform leaves have evolved repeatedly in monocots (Rudall and Buzgo 2002).

Ensiform leaves develop into flattened structures in the absence of adaxial–abaxial juxtaposition, suggesting that they utilize an alternative mechanism for blade outgrowth (Yamaguchi and Tsukaya 2010). The *YABBY* gene *DROOPING LEAF* (*DL*) was recently identified as a regulator of this process. In ensiform leaves of *Juncus prismatocarpus*, incipient leaf primordia acquire proliferative activity in the adaxial side, where *DL* is expressed (Fig. 2.4g) (Yamaguchi et al. 2010). This

morphogenetic event is called adaxial growth (Kaplan 1975), and it is not observed in cylindrical unifacial leaves of *J. wallichianus* (Fig. 2.4f). Consistent with this, *DL* expression is not detected in the adaxial side of *J. wallichianus* leaves (Yamaguchi et al. 2010). Results from crosses between the two species suggest that the *DL* locus regulates the specific growth activity of ensiform leaves. After the adaxial growth, proliferative activity is induced in both margins of a leaf primordium, where *PRS* orthologs are expressed (Fig. 2.4g) (Yamaguchi et al. 2010). In conventional bifacial leaves of rice, *DL* is expressed in the medial part of primordia, where the midrib develops, and promotes midrib thickening (Yamaguchi et al. 2004), suggesting that the expression patterns and gene functions are partly conserved between ensiform leaves of *J. prismatocarpus* and conventional bifacial leaves of rice.

Terete-like and ensiform-like leaves also evolved in eudicots, although their exact faciality has not been determined conclusively. *Acacia* phyllodes are composed mainly of an abaxialized rachis-petiole that is flattened along the median plane like ensiform leaves (Fig. 2.3e) (Arber 1918; 1921; Boke 1940; Kaplan 1970). These phyllodes are produced by adaxial growth that causes the primordium to become a planar structure (Boke 1940). Unlike in monocot ensiform leaves, bidirectional growth does not occur in *Acacia* phyllodes, and unilateral adaxial growth continues until maturation. In another example from eudicots, the succulents *Senecio rowleyanus* and *Se. crassissimus* produce terete-like and ensiform-like leaves, respectively (Fig. 2.3f, g). Primordia in both species first develop into transversely flat structures like conventional bifacial leaves. Subsequently, by adaxial growth, they are rounded out to be terete-like or flattened along the median plane to be ensiform-like (Hillson 1979; Ozerova and Timonin 2009). Growth patterns in this process suggest that the abaxial surface expands in the mediolateral direction, but the adaxial surface does not. As a result, the abaxial surface dominates at maturity and this type of leaf is classified as subunifacial (Ozerova and Timonin 2009). Subunifacial leaves also evolved in some species of *Peperomia* including *P. dolabriformis* (Kaul 1977). The molecular mechanisms of ensiform-like leaf development remain unknown in eudicots.

2.8 Peltate leaves and their analogs

Peltate leaves are widespread in at least 40 flowering plant families (Gleissberg et al. 2005). Whereas conventional bifacial leaves have a lamina that is basifixed to a bifacial petiole, peltate leaves have a unifacial petiole attached to the abaxial side of the lamina, forming a shield-like structure (Fig. 2.3h) (Franck 1976). The peltate structure is hypothesized to enable efficient light capture on an erect petiole (Givnish and Vermeij 1976). In the emerging stage, peltate leaf primordia are indistinguishable from those of conventional bifacial leaves (Hagemann and Gleissberg 1996). Subsequently, the “cross zone” characteristic of peltate leaf development is formed (Fig. 2.5). The cross zone corresponds to the basal portion of the incipient lamina, where leaf margins are

congenitally fused (Troll 1932).

A glimpse into the molecular mechanisms of peltate leaf development was provided by the *phan* mutant, in which conventional bifacial leaves are sometimes converted into peltate leaves (Waites and Hudson 1995). Abaxialization of a proximal portion of the leaf has been proposed to be the cause of the *phan* peltate-leaf phenotype (Waites and Hudson 1995). Arabidopsis and other model plants that normally produce conventional bifacial leaves also can produce peltate leaves as a result of mutations that impair adaxial–abaxial patterning (summarized in Table 2.1, often referred to as "lotus" or "trumpet" leaves in the original reports). Two types of peltate leaves, epipeltate and hypopeltate, can be differentiated based on the arrangement of the adaxial and abaxial surfaces (reviewed in Franck 1976). Epipeltate leaves show a distal-adaxial proximal-abaxial arrangement, and arise in loss-of-function mutants of the adaxial determinants *AS1*, *AS2*, and HD-ZIP III genes (Prigge et al. 2005; Sun et al. 2002; Xu et al. 2003; Xu et al. 2002). The hypopeltate leaf type exhibits the opposite polarity: distal-abaxial and proximal-adaxial. Gain-of-function mutants of HD-ZIP III genes develop hypopeltate leaves due to adaxialization of the basal part of the leaf (McConnell and Barton 1998; McConnell et al. 2001; Zhong and Ye 2004).

Peltate leaves can be funnel-shaped or follicule-shaped. Such leaves are termed epiascidiate or hypoascidiate leaves depending on their adaxial–abaxial patterning, in the same manner as described in the previous paragraph (Franck 1976). Epiascidiate leaves are often associated with specialized functions, especially in carnivorous plants (Fig. 2.3i, j, k). Three phylogenetically independent families, the Nepenthaceae, the Sarraceniaceae, and the Cephalotaceae, form epiascidiate leaves that function as pitfall traps to capture small animals (Albert et al. 1992; Juniper et al. 1989). Hypopeltate or hypoascidiate leaves are also widely distributed in flowering plants including *Tococa* and *Maieta* in the Melastomataceae, *Cassiope* in the Ericaceae, *Dischidia* in the Apocynaceae, and *Celmisia* in the Asteraceae (Franck 1976).

All examples described above are peltate leaves with undivided leaf blades, but compound leaves, which are composed of a set of leaflets, can also be peltate. In peltately palmate compound leaves, leaflets are attached to the tip of a unifacial rachis, which is structurally equivalent to the petiole of simple peltate leaves. Kim et al. (2003a) examined *PHAN* expression in eight compound-leaved species sampled across eudicots, and found that the expression domain correlates to the adaxial fate and leaflet initiation sites in peltately palmate compound leaves. In non-peltately palmate compound leaves and pinnate compound leaves, *PHAN* genes are expressed in the adaxial side from the tip to the basal portion of leaf primordia including the rachis. By contrast, *PHAN* expression marks a distal portion of peltately palmate compound leaf primordia where leaflets initiate. Those expression patterns are reminiscent of the developmental model for simple peltate leaves (Waites and Hudson, 1995). Knock-down of the *PHAN* ortholog in *Solanum lycopersicum* (tomato) converts pinnate compound leaves into peltately palmate compound leaves (Kim et al. 2003a). A mutation in the

PHAN ortholog of *Pisum sativum* (pea) causes peltate leaflets rather than peltately palmate compound leaves to form (Tattersall et al. 2005). Taken together, those results suggest that similar expression changes in the adaxial and abaxial determinants underlie peltation in simple leaves, compound leaves, and leaflets.

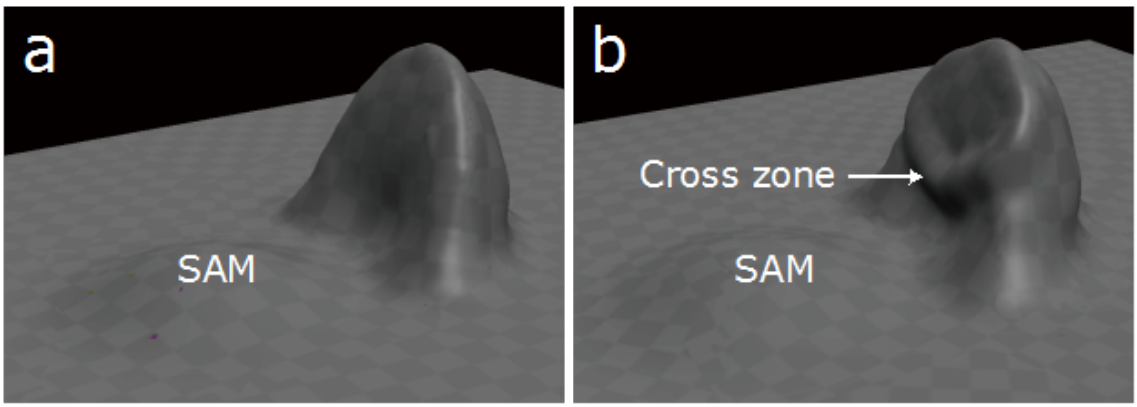

Figure 2.5. Leaf primordium morphology. Primordia of a conventional bifacial leaf **(a)** and an epipeltate leaf **(b)** are shown. SAM indicates the position of the shoot apical meristem. The cross zone characteristic of epipeltate leaf primordia is indicated in (b).

Table 2.1. Peltate-leaf phenotypes caused by genetic changes affecting adaxial–abaxial polarity.

Species	Mutation/treatment *	Peltate-leaf phenotype	Reference
Arabidopsis thaliana	*as1*	Epipeltate leaf	Sun et al. 2002 Xu et al. 2003
	as2	Epipeltate leaf	Xu et al. 2002 Xu et al. 2003
	phb-1d (gain-of-function)	Hypopeltate leaf	McConnell and Barton 1998 McConnell et al. 2001
	35S::PHB (miRNA-resistant form)	Hypopeltate leaf	Magnani and Barton 2011
	rev (gain-of-function)	Hypopeltate leaf Hypopeltate/conventional bifacial-combined leaf	Zhong and Ye 2004
	35S::REV (miRNA-resistant form)	Hypopeltate leaf	Wenkel et al. 2007 Magnani and Barton 2011
	pREV::REV (miRNA-resistant form)	Hypopeltate leaf	Emery et al. 2003
	rev phv (loss-of function)	Epipeltate leaf	Prigge et al. 2005
	35S::MIR165a/rdr6	Epipeltate leaf	Li et al. 2005
	hat3 athb4	Epipeltate leaf	Turchi et al. 2013
	ago1	Epipeltate leaf	Kidner and Martienssen 2004 Yang et al. 2006
	lug luh/+	Epipeltate leaf	Stahle et al. 2009
	elo1	Epipeltate leaf	Xu et al. 2012
	elo2	Epipeltate leaf	Xu et al. 2012
	elo3	Epipeltate leaf	Xu et al. 2012
	elo3 ago7	Epipeltate/conventional bifacial-combined leaf	Kojima et al. 2011
	elo3 rdr6	Epipeltate/conventional bifacial-combined leaf	Kojima et al. 2011
	ae3	Epipeltate leaf	Huang et al. 2006
	ae7 rdr6	Epipeltate leaf	Yuan et al. 2010
	35S:*miR396a*	Epipeltate leaf	Mecchia et al. 2013
	AS1:*miR396a*	Epipeltate leaf	Mecchia et al. 2013
Nicotiana sylvestris	*phv1/+* (gain-of-function)	Hypopeltate leaf	McHale and Koning 2004a
Solanum lycopersicum	*wiry*	Epipeltate leaflet	Kim et al. 2003b
	wiry3	Epipeltate leaf	Kim et al. 2003b
	wiry6	Epipeltate leaf	Kim et al. 2003b
	35S::PHAN antisense	Epipeltate leaf	Kim et al. 2003a Kim et al. 2003b
Pisum sativum	*crispa*	Epipeltate leaflet	Tattersall et al. 2005

* Mutations/treatments that enhance peltate-leaf phenotypes in *as1*, *as2*, and other mutant backgrounds are omitted from the list if no novel structural phenotype is observed.

2.9 Tendrils

Climbing plants have tendrils, which are twining organs filamentous in shape (Fig. 2.3l) (Bell and Bryan 2008). Leguminous species form leaf tendrils, which fully lack a laminar portion and are interpreted as abaxialized leaflets or rachises (Tattersall et al. 2005). *Tendrill-less* (*Tl*) encodes a structurally unusual Class I HD-ZIP protein and was isolated as a regulator of terminal tendril formation in pea (Hofer et al. 2009). Loss-of-function *tl* mutants develop a leaflet in place of the terminal tendril. *Tl* mRNA accumulates in tendril primordia at the stage when organ fate is determined, indicating that *Tl* functions in the establishment of tendril identity including the absence of blade outgrowth (Hofer et al. 2009). *Tl* expression is up-regulated by *LATHYROIDES*, a *WOX1* ortholog in pea (Zhuang et al. 2012). *Tl* orthologs have been identified in tendrilled legumes including *Vicia* spp., *Lens culinaris*, and *Lathyrus odoratus*, but not in the non-tendrilled plants Arabidopsis and *Medicago truncatula* (Hofer et al. 2009), suggesting that *Tl* function is specific to tendril formation.

2.10 Ectopic laminas

Protrusive laminar structures arise in various leaf types. These ectopic laminas can be circular (*i.e.* closed margin) or linear (*i.e.* open margin). In the latter case, the structure is specifically referred to as a keel. Ectopic laminas increase the morphological complexity of leaves. For example, foliated leaves of some species in the Iridaceae bear keels in an iterative manner (*e.g. Herbertia amoena*, Fig. 2.3m) (Arber 1921), and, as a result, the keels comprise a large portion of those leaves. Ectopic laminas can also be related to novel functions. A pair of keels on the abaxial surface of some ericoid leaves form a humid chamber immediately outside stomatal pores (*e.g. Phyllodoce caerulea*: Fig. 2.3n), which is considered to be advantageous in dry environments (Böcher 1981; Hagerup 1946; Kron et al. 2002). The keels on pitcher leaves in the carnivorous plant genus *Sarracenia* can compensate for the inefficient photosynthetic activity (Ellison and Gotelli 2002) and reinforce structural strength of pitcher leaves (Fig. 2.3i) (Juniper et al. 1989).

An ectopic lamina can be bifacial or unifacial. Accumulating evidence suggests that the initiation of bifacial ectopic laminas depends on growth activity at the adaxial–abaxial boundary. The *milkweed pod1* (*mpw1*) loss-of-function mutant of a KANADI gene in maize develops bifacial ectopic laminas on the abaxial surface (Candela et al. 2008). In the leaves of the *mpw1* mutant, adaxial characters are ectopically conferred to the abaxial surface and growth activity is induced, presumably in response to the ectopic adaxial–abaxial boundary (Fig. 2.4c) (Candela et al. 2008; Johnston et al. 2010). More evidence for the importance of the adaxial–abaxial boundary came from analysis of the maize prophyll, the first leaf of a shoot. In the Poaceae, prophylls are intrinsically bi-keeled and are formed by congenital fusion of two primordia (Arber 1923). Based on the expression pattern of a HD-ZIP III gene in maize, Johnston et al. (2010) proposed that the bifacial

keels initiate due to the new adaxial–abaxial boundaries generated by transient expression of adaxial determinant(s) on the abaxial surface (Fig. 2.4d). Opposite to *mpw1* in maize, knock-down of a *PHAN* ortholog in *Nicotiana sylvestris* results in the formation of bifacial laminas on the adaxial surface (Fig. 2.4b) (McHale and Koning 2004b). Sporadic abaxial characters on the adaxial side may underlie this ectopic lamina formation (McHale and Koning 2004b). Because bifacial ectopic laminas are frequently formed over or on a flank of veins, Kidner and Wrigley (2010) hypothesized that the prolonged expression of adaxial–abaxial determinants like HD-ZIP IIIs and KANADIs in vascular elements can contribute to reversing the previously determined polarity and therefore to establishing a new adaxial–abaxial boundary on the founder region of bifacial ectopic laminas.

Compared with bifacial ectopic laminas, unifacial ectopic laminas are poorly characterized and their developmental mechanisms remain unclear.

2.11 Combinations of different adaxial–abaxial patterning within a leaf

A leaf is divided into distinct portions along the proximal–distal axis: a leaf base, a petiole, and a lamina, as well as each leaflet in the case of compound leaves. Differential regulation of adaxial–abaxial patterning in proximal–distal segments is a source of leaf shape diversity. For example, the pitcher, tendril, and basal laminar portion of *Nepenthes* leaves presumably correspond to the lamina, petiole, and leaf base of conventional bifacial leaves, respectively (Franck 1976; Kaplan 1973; Troll 1932), and show distinct adaxial–abaxial patterning judged from vascular bundle orientation (Fig. 2.3k). In another example, monocotyledonous unifacial leaves of both terete and ensiform types have bifacial and unifacial portions in their basal and distal parts, respectively (Fig. 2.3c, d).

Disturbance of adaxial–abaxial polarity can have local effects, giving rise to different faciality within a leaf. The pea mutant *crispa* and the tomato mutant *wiry6* exhibit phenotypes in which a portion of the leaflets are peltate despite others retaining conventional bifacial structure (Kim et al. 2003b; Tattersall et al. 2005). Some Arabidopsis mutants develop malformed leaves wherein a peltate distal portion is connected with a proximally located bifacial structure by a midrib without a leaf blade (Table 2.1) (Kojima et al. 2011; Zhong and Ye 2004). Structurally similar leaves spontaneously arise in *Codiaeum variegatum* var. *pictum* f. *appendiculatum* (Fig. 2.6a) (De Vries 1905) and *Camellia japonica* cv. ‘Kingyobatsubaki’ (Fig. 2.6b). As these examples come only from phenotypes observed in various mutants and cultivars, solid evidence for their adaptive significance is yet to be identified. However, these observations indicate that genetic changes related to adaxial–abaxial patterning can result in further segmentation or addition of novel segments in leaves from a broad range of taxa.

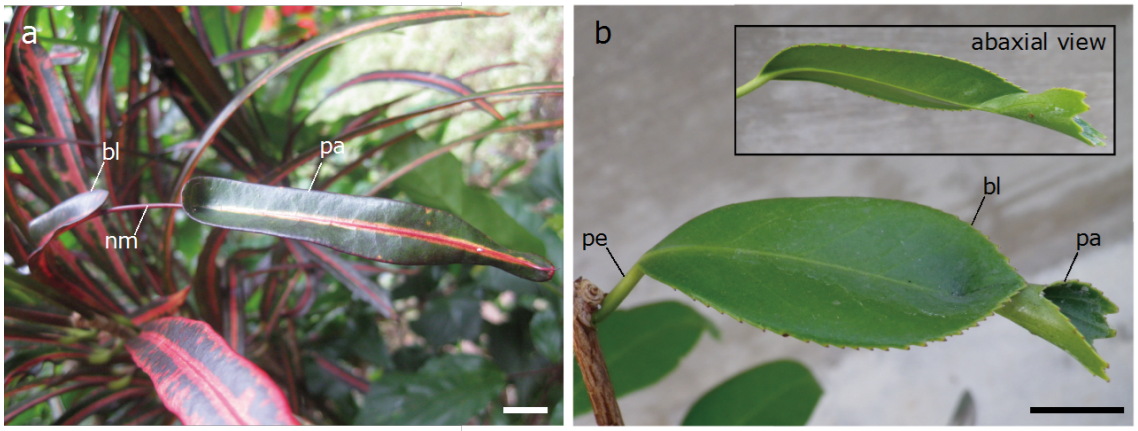

Figure 2.6. Examples of leaf segmentation with regard to adaxial–abaxial polarity. Leaves of *Codiaeum variegatum* var. *pictum* f. *appendiculatum* **(a)** and *Camellia japonica* cv. 'kingyobatsubaki' **(b)** are subdivided along the proximal–distal axis. The basal lamina (bl) is connected to a peltate appendage (pa) with or without naked midrib (nm). pe, petiole. Bars denote 10 mm.

2.12 Rearrangement of the expression domains of adaxial–abaxial determinants

In some cases, the expression of adaxial–abaxial determinants are not static. In Arabidopsis leaf development, *FIL*/*YAB1* shrinks its expression domain in parallel with the expansion of miR165/166-free domain (Tameshige et al. 2013). Stamen development provides an explicit example of expression rearrangement. Leaves and floral organs are both formed laterally and share part of the same developmental gene network, including the interactions between adaxial and abaxial determinants. Among lateral organs in flowering plants, stamens are substantially differentiated in terms of morphology. Based on analyses of rice stamen morphogenesis, Toriba et al. (2010) proposed that growth activity is induced at the expression boundary of the adaxial and abaxial determinants to form pollen sacs, and that the expression patterns are rearranged during stamen development. Initially, the expression domains of *ETT*/*ARF3* and *PHB* orthologs occupy the abaxial and adaxial sides, respectively, as in conventional bifacial leaves. However, as stamen development proceeds, the expression domains are rearranged into a complex pattern that generates four expression boundaries where pollen sacs initiate. This rearrangement does not disturb the complementary patterns: an *ETT*/*ARF3* ortholog comes to occupy both adaxial and abaxial corners, while the *PHB* ortholog localizes to two lateral corners between the two expression domains of the *ETT*/*ARF3* ortholog (Toriba et al. 2011). The *rod-like lemma* mutant shows compromised expression patterns of *ETT*/*ARF3* and *PHB* orthologs, and a reduced number of pollen sacs (Toriba et al. 2010). These observations substantiate the idea that expression rearrangement of polarity determinants mediates the development of non-planar organs like stamens.

Another example of expression rearrangement is found in the peltate-leaved species *Tropaeolum majus*. In leaf primordia, *TmFIL* mRNA is localized to the abaxial side at an early stage, reminiscent of *FIL*/*YAB1* localization in conventional bifacial leaves of Arabidopsis (Gleissberg et al. 2005). This expression pattern is concordant with the observation that peltate leaves of this species arise

from fully bifacial primordia (Hagemann and Gleissberg 1996). Later, the *TmFIL* expression domain expands into the adaxial side of the petiole (Gleissberg et al. 2005) and the initially bifacial petiole is secondarily compensated by additional growth to form radially symmetric structure (Hagemann and Gleissberg 1996). This suggests that the *TmFIL* expression domain is rearranged to generate a new adaxial–abaxial boundary at the cross-zone, where growth activity is induced (Fig. 2.5).

Although the mechanism by which expression domains are rearranged remains unclear, it is clear that expression rearrangement contributes to the morphological diversification of lateral organs.

2.13 Conclusion

As discussed above, changes of adaxial–abaxial polarity plays a role in leaf shape diversification in flowering plants. So far, spatiotemporal expression changes of polarity determinants have been recognized as a widespread mechanism of the polarity changes and other mechanisms are poorly characterized. In the next chapter, I discuss on a mechanism of leaf shape evolution without expression changes of polarity determinants, on the basis of developmental analyses of pitcher leaves in *Sarracenia purpurea*.

3. ORIENTED CELL DIVISION SHAPES CARNIVOROUS PITCHER LEAVES OF *SARRACENIA PURPUREA*

3.1 Introduction

The emergence of novel morphology usually involves modifications of preexisting developmental programs, but its basic mechanisms remain unclear, particularly for some drastic changes, such as the evolution of pitcher-shaped leaves in carnivorous plants. Leaves are usually planar, to allow efficient photosynthesis, but species in the family Sarraceniaceae produce pitcher-shaped leaves that function as pitfall traps to capture small animals.

Changes in adaxial–abaxial patterning contribute to the diversification of leaf morphology, as discussed in Chapter 2 (Fukushima and Hasebe 2014; Waites and Hudson 1995). In a primordium of a conventional bifacial leaf (Franck 1976), such as that of *A. thaliana*, the complementary expression patterns of *PHB* and *FIL* are maintained from the tip to the base (McConnell et al. 2001; Sawa et al. 1999; Siegfried et al. 1999; Tameshige et al. 2013) and blade outgrowth initiates at their expression boundary in the primordium, to form a flat structure (Fig. 3.1). By contrast, *Tropaeolum majus* produces peltate leaves, which have a unifacial petiole attached to the central part of a bifacial leaf blade, rather than at the margin (Gleissberg et al. 2005). The abaxial *FIL* expression pattern in the primordium of a peltate leaf is initially indistinguishable from that of a conventional bifacial leaf, but later *FIL* is expressed on both adaxial and abaxial sides of the primordium, in the proximal region where the unifacial petiole develops, leaving a bifacial structure in the distal region where the lamina forms (Gleissberg et al. 2005) (Fig. 3.1). In addition, a mutation that attenuates the expression of adaxial determinants, including *PHB,* converts the conventional bifacial leaves of *A. thaliana* to peltate leaves (Prigge et al. 2005; Waites and Hudson 1995; Xu et al. 2003). Thus, the establishment of peltate leaves is related to changes in the expression patterns of the polarity genes (Gleissberg et al. 2005; Kim et al. 2003a). Early studies showed that the outer morphology of young primordia in pitcher leaves of *Darlingtonia californica* resembles that in peltate leaves (Franck 1975; Roth 1952), suggesting that peltate and pitcher leaves share a common developmental mechanism (Franck 1975; 1976). However, the development of the early primordia, and the genes involved in polarity formation, have not been examined.

In this study, I analyzed leaf development in the purple pitcher plant *Sarracenia purpurea*. I first examined the spatiotemporal expression of *FIL* and *PHB* orthologs to test the hypothesis that pitcher leaves and peltate leaves develop by similar mechanisms. However, unlike peltate leaf primordia, pitcher leaf primordia did not show the prevailed *FIL* expression. I then examined the cell division pattern during pitcher development and found that oriented cell divisions in the adaxial tissue form a novel morphogenetic pattern that is distinct from that of both conventional bifacial and peltate leaves. A computer simulation showed that site-specific changes in the cell division plane could explain the novel morphogenetic pattern of the pitcher leaf. Taken together, our results show that local changes

in the orientation of cell division lead to the novel morphology of pitcher leaves.

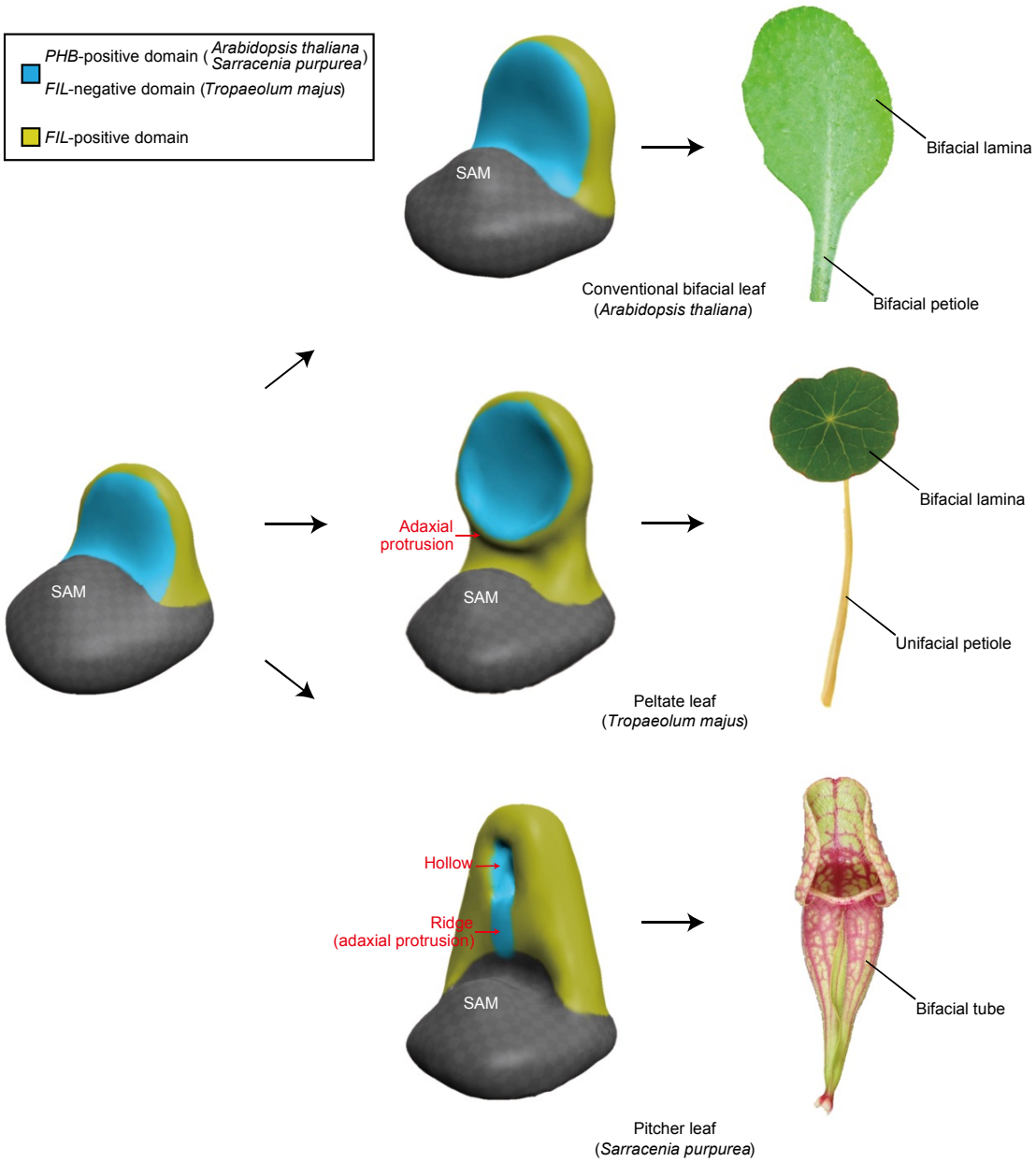

Figure 3.1. A model of leaf development through differential patterning of polarized gene expression. Expression patterns of *PHABULOSA* (*PHB*) and *FILAMENTOUS FLOWER* (*FIL*) mRNA are indicated in blue and yellow, respectively, based on studies in *Arabidopsis thaliana* (McConnell et al. 2001; Sawa et al. 1999; Siegfried et al. 1999; Tameshige et al. 2013) and *Tropaeolum majus* (Gleissberg et al. 2005) as well as this study on *Sarracenia purpurea*. *PHB* expression in peltate leaves has not been studied and I postulated that *PHB* would be expressed in a *FIL*-negative domain. SAM: shoot apical meristem.

3.2 Materials and methods

Plant materials. *Sarracenia purpurea* ssp. *venosa* L. plantlets were purchased from Daisho-en Nursery (Numazu, Japan) and cultivated in a greenhouse. Axenically grown plants were obtained from CZ Plants Nursery (Trebovice, Czech Republic) and were subcultured on half-strength Murashige and Skoog plate medium (Murashige and Skoog 1962) supplemented with 3% sucrose, 1x Gamborg's vitamins, 0.1% 2-(N-morpholino)ethanesulfonic acid, 0.05% Plant Preservative Mixture (Plant Cell Technology), and 0.3% Phytagel, at 25°C under continuous light. Voucher specimens were deposited in The Herbarium of the University of Tokyo (TI). Accession numbers are KF001 and KF002 for axenically grown and greenhouse-grown plants, respectively.

RNA extraction. Fresh shoot apices of approximately 10 mm diameter were excised from soil-grown plants, washed with tap water, and ground in liquid nitrogen with a mortar and pestle. Total RNA was extracted using PureLink Plant RNA Reagent (Life Technologies).

Cloning of *SpPHB* and *SpFIL*. cDNA was synthesized from total RNA using SuperScript III Reverse Transcriptase (Life Technologies). Gene fragments were amplified with degenerate primers (Table 3.1), cloned into pGEM-T Easy Vector (Promega), and sequenced with the ABI Prism 3100 Genetic Analyzer (Applied Biosystems). Next, 3'-terminal sequences were obtained by rapid amplification of cDNA ends using GeneRacer (Invitrogen) and gene-specific primers (Table 3.1). Corresponding transcript sequences retrieved from RNA-seq data of HiSeq 2000 (Illumina) were also included (details will be published elsewhere). DDBJ accession numbers are as follows: *SpPHB*, AB938211; *SpFIL*, AB938212; and *SpHIS4*, AB938214.

Table 3.1. Oligonucleotide primers used in the work of Chapter 3.

Gene	Primer name	Primer sequence (5' to 3')	Usage	References
SpPHB	dPHB-d7	TGCGGTACACCCCCGARCARGTNGA	degenerate PCR (1st round)	This study
	dPHB-u8	AGGAGGGCCGGTCCTTNARDATYTC	degenerate PCR (1st round)	This study
	dPHB-d5	CGAGCCCAAGCAGATCAARGTNTGGTT	degenerate PCR (nested following to dPHB-d7)	Nakayama et al. 2012
	dPHB-u6	GGGCTCCAGGTTCACCARNCCRCANGC	degenerate PCR (nested following to dPHB-u8)	Nakayama et al. 2012
	PHB-F1	GTCAATGGGTTTATGGATGATGGTTGG	3'-RACE	This study
	PHB-F2	ATAATGGGTAGCGATGGTGTGGAG	3'-RACE	This study
SpFIL	dYABd1	TGTTCAAGACCGTGACCGTNMGNTGYGG	degenerate PCR	This study
	dYABu4	CGGCCATGGAGAAGGCYTCNCKRTG	degenerate PCR	This study
	FIL-F1	ACTGCACCAACCTCTTGTCTGTG	3'-RACE	This study
	FIL-F2	AACATGCGTGGTCTGCTGCTTC	3'-RACE	This study
SpHIS4	dH4-d1	GGAAGGTGCTGCGGGAYAAYATHCA	degenerate PCR	Yamaguchi et al. 2010
	dH4-u2	CCGCTTCAGGGCGTACACNACRTCCAT	degenerate PCR	Yamaguchi et al. 2010
-	M13-21	TGTAAAACGACGGCCAGT	TA-cloning	-
	RV-17me	CAGGAAACAGCTATGAC	TA-cloning	-

Phylogenetic analysis. Phylogenetic relationships among *SpPHB, SpFIL,* and their homologs in the annotated genomes of *Arabidopsis thaliana* (TAIR10, Swarbreck et al. 2008), *Populus trichocarpa* (v3, Tuskan et al. 2006), *Mimulus guttatus* (v1.1, distributed by Department of Energy Joint Genome Institute [JGI] at http://www.jgi.doe.gov/), *Solanum lycopersicum* (ITAG2.3, Tomato Genome Consortium 2012), *Aquilegia coerulea* (distributed by JGI), *Oryza sativa* (MSU Release 7.0, Ouyang et al. 2007), and *Picea abies* (Nystedt et al. 2013) were analyzed. Coding sequence (CDS) datasets were obtained from The Arabidopsis Information Resource (TAIR, http://www.arabidopsis.org/), Phytozome v9.1 (http://www.phytozome.net/), and ConGenIE (http://congenie.org/). TBLASTX (Altschul et al. 1997) searches of *SpPHB* and *SpFIL* sequences were performed against the above CDS datasets with E-value cutoffs of 1e-160 and 1e-20, respectively. After sequence retrieval, multiple alignments were prepared with MAFFT 6.956 (Katoh and Standley 2013), and ambiguous codons were removed using trimAl (Capella-Gutierrez et al. 2009) with the "gappyout" option implemented in Phylogears2-2.0.2013.03.15 (http://www.fifthdimension.jp/products/phylogears/). Phylogenetic trees were reconstructed by the maximum likelihood method using RAxML 7.5.3 (Stamatakis 2006) with the general time-reversible model of nucleotide substitution and four discrete gamma categories of rate heterogeneity (GTRGAMMA option). Support for nodes was estimated by rapid bootstrapping with 1000 replications.

Scanning electron microscopy. Shoot apices and leaves of axenically grown plants were excised with fine forceps, frozen in liquid nitrogen, and immediately observed with a scanning electron microscope XL30 (FEI, Hillsboro, Oregon, USA), with an accelerating voltage of 10 kV.

Serial section preparation and toluidine blue staining. Shoot apices of soil-grown plants were fixed overnight in 4% paraformaldehyde (pH 7.2). The fixative solution was sequentially replaced with a series of water-ethanol, ethanol-xylene, and xylene-Paraplast Plus (Sigma-Aldrich) to prepare paraffin-embedded samples. Serial sections were made using a rotary microtome (Leica RM 2155, Leica), and were affixed to glass slides overnight at 42°C. Then, 9-µm-thick serial sections were rehydrated through xylene-ethanol and ethanol-water series, and stained with 0.1% toluidine blue in 0.1 M phosphate buffer (pH 7.0). The preparations were mounted in Entellan New (Merck Millipore). Section images were taken using a digital camera (DP70, Olympus) coupled to a microscope (BX-51, Olympus).

RNA *in situ* hybridization and signal quantification. Cloned gene fragments were amplified using the M13-21 and RV-17mer primers (Table 3.1). Digoxigenin (DIG)-labeled antisense RNA probes were prepared using the DIG RNA Labeling Kit (Roche Applied Science). Then, 9-µm-thick serial sections were rehydrated, treated with 0.5 µg/ml Proteinase K for 30 min at 37°C, re-fixed in 4% paraformaldehyde (pH 7.2) for 10 min, and then dehydrated in a water-ethanol series. RNA probe hybridization was performed overnight in a humid chamber at 50°C. After the samples were washed twice with 4x saline sodium citrate (SSC) buffer at 50°C for 20 min, the slides were treated with 50 µg/ml RNase A at 37°C for 60 min, washed twice in 0.5x SSC at 50°C for 20 min, and then blocked with Blocking Reagent (Roche Applied Science). Signals were detected by incubating the samples in Anti-DIG-AP (Roche Applied Science) for 90 min and NBT/BCIP solution (Roche Applied Science) overnight. After brief dehydration in water-ethanol and ethanol-xylene series, the preparations were mounted in Entellan New (Merck Millipore). Section images were taken using a digital camera (DP71, Olympus). Using ImageJ 1.47k (National Institutes of Health, MD, USA), segmented lines were drawn through the centers of the epidermal cells, and gray values were obtained for each pixel along these lines (Fig. 3.2). Subsequently, a B-spline curve was drawn through the data points. The boundary of signal-positive and -negative cells was determined by calculating the local maximum and local minimum of backward difference of fitted values (Fig. 3.2).

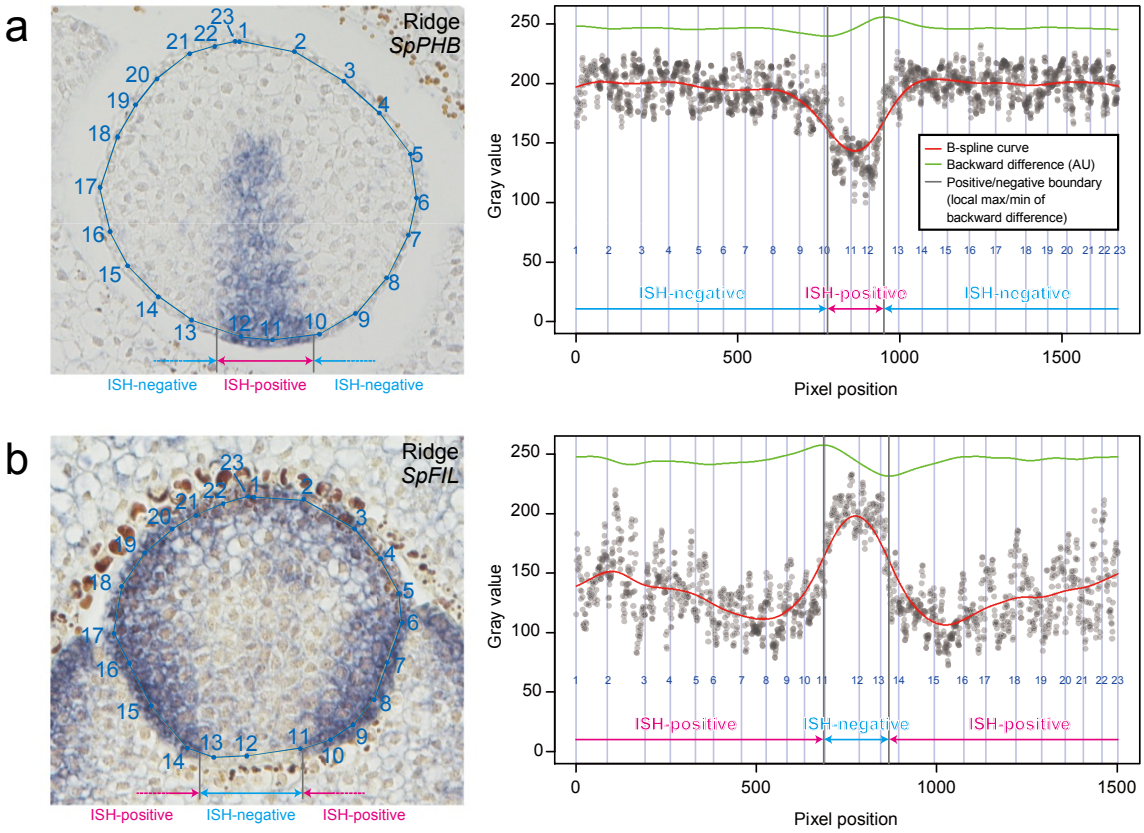

Figure 3.2. Determination of *in situ* hybridization (ISH)-positive and ISH-negative epidermal cells. Transverse sections in Fig. 3.6b are shown as examples of signal detection for *SpPHB* (**a**) and *SpFIL* (**b**) (left). The gray value of each pixel was measured along the blue segmented lines. Numbers indicate the position of vertices of segmented lines, and correspond to pixel positions in the graph (right). The boundary of ISH-positive and ISH-negative epidermal cells was determined by calculating the local maximum and local minimum from fitted values of the B-spline curve.

Analyses of cell division orientation. To visualize spindle equators in inner tissues, 8-µm-thick serial sections were prepared from axenically grown plants. The prepared sections were rehydrated on slides, stained with 1 µg/ml DAPI in McIlvaine's buffer (pH 7.0), and then mounted in 50% glycerol. Mitotic chromosomes were observed using the filter set WU (Olympus) on a microscope (BX51, Olympus).

Hormone treatments. Axenically grown plants were transferred to the half-strength Murashige and Skoog medium containing 2, 10, or 50 µM of NAA or NPA, and were grown at 25°C under continuous light for 4 weeks.

Statistical analyses. All statistical analyses were performed using R 3.0.1. Comparisons were considered statistically significant when P values were <0.05. Multiple comparisons were corrected with Bonferroni's procedure. Angular data were processed with R package 'circular'.

Model (i) Vertex model. Leaf primordium development was modeled to examine the effect of cell division orientation by coupling vertex dynamics and chemical dynamics. To simplify the model system, transverse sections of primordia, in which each cell is represented by a polygon specified by surrounding vertices, were considered. If it is assumed that vertices are embedded in a viscous medium and have no mass, the equation of motion for vertices is given by

$$\eta \frac{d\boldsymbol{x}_j}{dt} = \boldsymbol{F}_j, \tag{1}$$

where $\boldsymbol{x}_j$ is the position vector of vertex j, $\boldsymbol{F}_j$ is the total force acting on vertex j, and η is the viscosity coefficient. The acting force is often described using potential U as follows:

$$\eta \frac{d\boldsymbol{x}_j}{dt} = -\frac{\partial U}{\partial \boldsymbol{x}_j}. \tag{2}$$

Thereby, vertices move so as to minimize the potential energy, and we can describe various dynamics of vertices by changing potential energy function (Farhadifar et al. 2007; Fletcher et al. 2014; Nagai and Honda 2001). Vertex model has been extensively used for investigating cellular mechanisms of morphogenesis in animals (see references cited in Fletcher et al. 2014) and in plants (Abera et al. 2014; Dupuy et al. 2008; Fozard et al. 2013; Gibson et al. 2011; Lee et al. 2014; Merks et al. 2011; Prusinkiewicz and Lindenmayer 1990; Rudge and Haseloff 2005). In models used in these studies, acting force on vertex is frequently described based on the elasticity of cell area and bond tension of cell edge. Accordingly, in our model, potential energy is given by the following simple form with some modifications:

$$U = \sum_i K_S \left(S_i - s_i\right)^2 + \sum_j \left(K_B L_j + K_R / L_j\right) + \sum_k K_E \left(L_k / L_E - 1\right)^2, \tag{3}$$

where S_i is the area of cell i, L_j is the length of edge j, L_k is the length of outermost edge k, and K_S, K_B, K_R, K_E, and L_E are constants. The first term of the right-hand side represents area elasticity, where cell i has a target area s_i that depends on its edge number N_i and is given by the relative area of N_i-sided regular polygon to that of regular hexagon, namely, $s_i = N_i \tan(\pi/6)/6\tan(\pi/N_i)$. K_S denotes the elastic constant. The second term describes the conservation force of edge length, where each edge has the target length $\sqrt{K_R/K_B}$ at which the potential energy function reaches a minimum. This condition ensures that neighboring vertices do not become extremely close because of repulsive force. The third term indicates the elastic force that maintains the outermost edges at a constant length L_E with the elastic coefficient K_E, which reflects that the outer cell wall is usually thickened and stiffened by a cuticle.

In animal cell models, it is usually assumed that vertices are reconnected to mimic cell movement if an edge becomes extremely short (Farhadifar et al. 2007; Fletcher et al. 2014; Nagai

and Honda 2001). In contrast, because the plant cell wall prevents changes in the relative position of cells, such reconnection process is not permitted in our model. In addition, neighboring vertices are prohibited to be extremely close by potential energy as described above.

Programs were written in C, and the vertex position ($\boldsymbol{x}_j$) was iteratively calculated every time step $\Delta t = 0.005$, using the fourth order Runge-Kutta method.

Model (ii) Cell division in epidermal cells. In epidermis, longitudinal divisions are observed in the adaxial domain where inner cells divide longitudinally, but rarely in the ridge part where inner cells divide periclinally (Fig. 3.8j). This evidence, together with a previous report on inter-cell-layer signaling (Kawade et al. 2013), suggests that epidermal cells divide in coordination with inner cell proliferation. In transverse sections of leaf primordia in *S. purpurea*, it is observed that most epidermal cells have less than five neighboring cells (Fig. 3.3). Accordingly, in our model, when an epidermal cell has five neighboring cells (or six edges), it is longitudinally divided by a line through the midpoints of the outermost and innermost edges, and then returns to having four neighboring cells (Fig. 3.14e, dark yellow cells). This division condition ensures that an epidermal cell proliferates while keeping less than five neighboring cells throughout primordial growth.

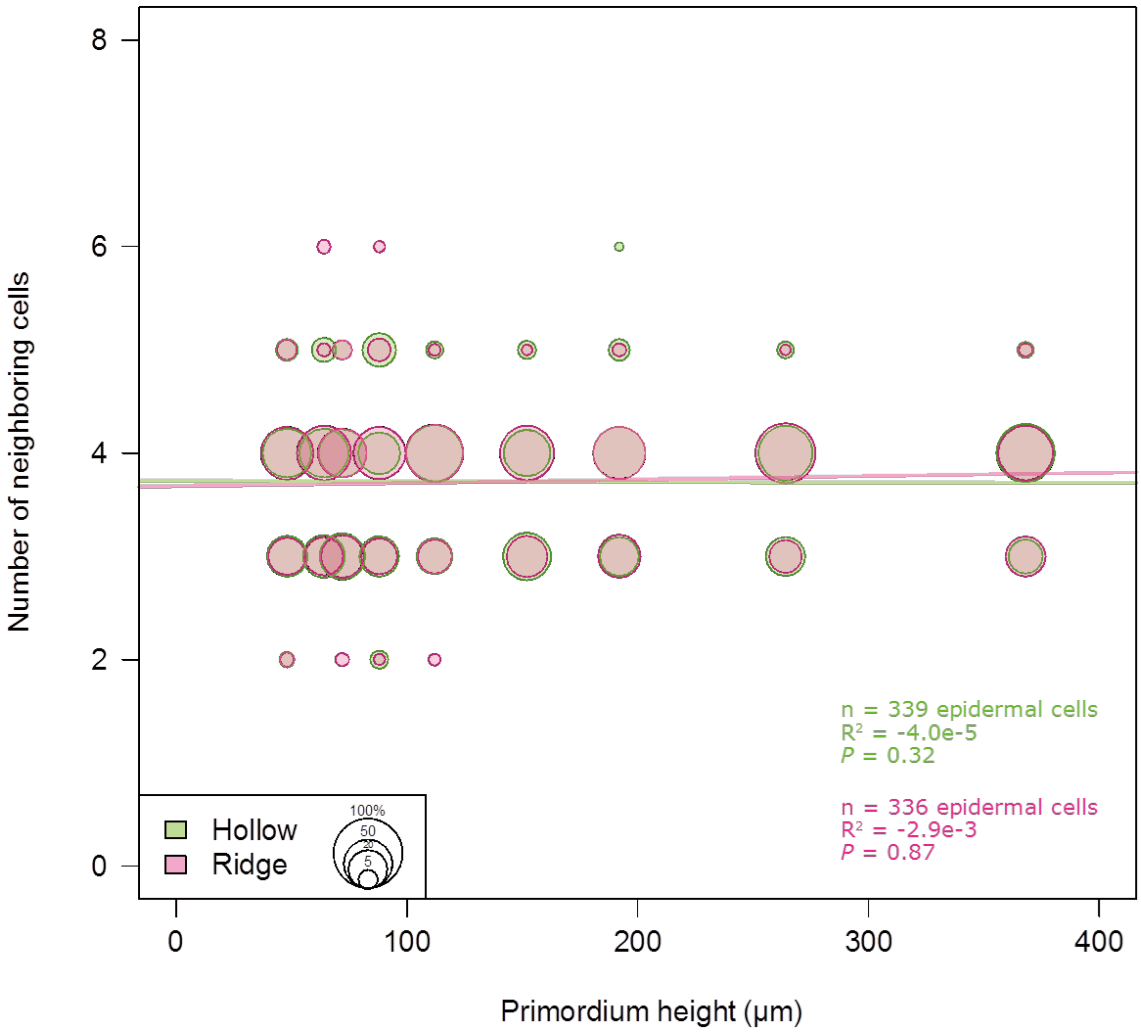

Figure 3.3. Neighboring cell numbers of epidermal cells in pitcher development. Cells that an epidermal cell contacts are counted in transverse sections and shown as a bubble plot. Data were acquired from 9 primordia with different developmental stages. Linear regression line, number of measured cells, adjusted R^2, and *P* value are shown in a plot. *P* values indicate a significant difference of R^2 from 0.

Model (iii) Cell division clock. Epidermal cells are differentiated into *PHB*-positive and *FIL*-positive states, which correspond to adaxial and abaxial L1 cells, respectively, which are shown in blue and yellow, respectively in Fig. 3.14h-i. Cell division is active in the leaf margin (see Results), that is, near the epidermal boundary of the adaxial and abaxial domains. Thus I and colleagues introduced a morphogen that promotes cell division:

$$\frac{du_i}{dt} = \begin{cases} A_u - B_u u_i + D_u \sum_j (u_j - u_i) & \text{for adaxial-abaxial boundary L1 cells} \\ -B_u u_i + D_u \sum_j (u_j - u_i) & \text{otherwise} \end{cases}, \qquad (4)$$

where u_i and u_j are the morphogen concentrations of cell i and its neighboring cell j, respectively, and A_u, B_u, and D_u are the synthesis rate, degradation rate, and diffusion coefficient, respectively. Morphogen u is synthesized in L1 cells of the adaxial–abaxial boundary, diffuses and decreases in concentration with distance from the boundary, and stimulates cell division as described below (Fig.

3.14h-i, magenta).

In contrast to the epidermis, non-epidermal cells divide depending on their cell division clock, which is promoted by the morphogen (u_i) and cell area (S_i) as follows:

$$\frac{d\,clock_i}{dt} = P_0\left(1 + P\frac{u_i^n}{u_0^n + u_i^n}\right)\frac{S_i^m}{S_0^m + S_i^m}, \quad (5)$$

where $clock_i$, u_i, and S_i are the clock, morphogen concentration, and area of cell i, respectively, and P_0, P, u_0, S_0, n, and m are constants. Cells divide if their clock exceeds a threshold (i.e., $clock_i > C_i$) and then the clock is reset to zero in their daughter cells, where C_i is the threshold of cell i and is given by C with 10% fluctuation.

Model (iv) Cell division orientation in inner cells. Cell division orientation is determined according to experimental observations (Fig. 3.8j). That is, cells divide longitudinally or periclinally in the outermost three cell layers (i.e., L1, L2, and L3) (Fig. 3.14a). On the other hand, more inner cells than L3 cells divide perpendicular to their long cell axis. To determine the long axis of a dividing cell, the line L_θ that runs through the cell center ($\boldsymbol{x}_c$) and forms angle θ with the x-axis was considered (Fig. 3.14g). L_θ satisfies

$$f(\boldsymbol{x};\theta) = \boldsymbol{n}\cdot(\boldsymbol{x} - \boldsymbol{x}_c) = 0, \quad (6)$$

where $\boldsymbol{n} = (-\sin\theta, \cos\theta)$ is a normal vector of L_θ, $\boldsymbol{x}_c = \frac{1}{N_i}\sum_j \boldsymbol{x}_j$ and N_i is the center position and vertex number of dividing cell i, respectively, and $\boldsymbol{x}_j$ is the position of vertex j. The sum of squared distances was then introduced:

$$R(\theta) = \sum_j r_j^2 = \sum_j \left| f(\boldsymbol{x}_j;\theta) \right|^2, \quad (7)$$

where r_j is the distance between vertex j and line L_θ. $R(\theta)$ reaches a minimum at

$$\theta = \theta_0 = \begin{cases} \arctan(Y/X)/2 & \text{for } X > 0 \\ \arctan(Y/X)/2 + \pi/2 & \text{for } X < 0 \end{cases}, \quad (8)$$

where $X = \sum_j (x_j^2 - y_j^2)$, $Y = 2\sum_j x_j y_j$, and $(x_j, y_j) = \boldsymbol{x}_j - \boldsymbol{x}_c$. This indicates that the line L_0 satisfying $f(\boldsymbol{x},\theta_0) = 0$ corresponds to the long cell axis, and accordingly the focal cell is divided by the line that runs through the cell center $\boldsymbol{x}_c$ and is perpendicular to L_0 (Fig. 3.14g, blue line).

Model (v) Longitudinal and periclinal cell divisions in L2 and L3 cells. In L2 and L3, cells divide longitudinally, with the exception of adaxial L2 and L3 cells of the ridge region, which divide periclinally (Fig. 3.8j). Adaxial L2 and L3 are defined as the L2 and L3 cells that are connected with adaxial L1 and L2, respectively. To determine the orientations of the longitudinal and periclinal divisions, assumed morphogens were introduced as follows:

$$\frac{dv_i}{dt} = \begin{cases} A_v - B_v v_i + D_v \sum_j (v_j - v_i) & \text{for L1 cells} \\ -B_v u_i + D_v \sum_j (v_j - v_i) & \text{otherwise} \end{cases}, \quad (9)$$

$$\frac{dw_i}{dt} = \begin{cases} A_w - B_w u_i + D_w \sum_j (w_j - w_i) & \text{for adaxial L1 cells} \\ -B_w u_i + D_w \sum_j (w_j - w_i) & \text{otherwise} \end{cases}, \quad (10)$$

where the notations are the same as those in equation (4) after replacing u with v or w. Morphogens v and w are synthesized in the epidermis and adaxial epidermis, respectively, diffuse and decrease in concentration with distance from their synthesis region (Fig. 3.14c,d), and affect the orientations of longitudinal and periclinal cell divisions, respectively, in L2 and L3. Next, the following was introduced

$$\boldsymbol{s}_k = z_k \frac{\boldsymbol{r}_k - \boldsymbol{x}_c}{|\boldsymbol{r}_k - \boldsymbol{x}_c|} \quad (z = v \text{ or } w), \quad (11)$$

where $\boldsymbol{x}_c$ is the center position of the dividing cell i, z_k (= v_k or w_k) is the morphogen concentration of neighboring cell k, and $\boldsymbol{r}_k$ is the midpoint position of the edge shared with cell i and cell k (Fig. 3.14f). Vector $\boldsymbol{s}_k$ is oriented towards cell k with the same size as the morphogen concentration of cell k (i.e., $|\boldsymbol{s}_k| = z_k$). When the polygon consisting of the vertices with position vector $\boldsymbol{s}_k$ is considered, this polygon elongates towards higher concentrations of morphogen z, and thereby its long axis will be oriented longitudinally. This long axis can be determined by the same method as that described in the previous section, and is denoted here as L_z by morphogen z (= v or w). As a result, in L2 and L3, a cell is divided by the line that runs through the cell center and is parallel to L_v in the case of longitudinal division (Fig. 3.14f, blue line), and by the line perpendicular to L_w in periclinal division (Fig. 3.14f, magenta line).

Model (vi) Initial and parameter conditions. At an initial stage of leaf primordium development (70 μm in size), the transverse sections of the hollow and the ridge regions are similar to each other in shape and adaxial–abaxial patterning (Fig. 3.8a,b). Thus I and colleagues used this primordial stage as an initial condition for numerical simulations, in which primordial sections consist of approximately 100 cells and have a round shape with a small depression in the adaxial side. Initial adaxial L1 is given as a string of six epidermal cells at the depression, and the other epidermal cells are defined as initial abaxial L1 (Fig. 3.14h-i, 100 cells). Parameter values used in Fig. 3.14h-i are as follows: $\eta = 1.0$, $K_S = 1.0$, $K_B = 0.1$, $K_R = 0.001$, $K_E = 0.005$, $L_E = 1.3$, $A_u = 2.0$, $A_v = 1.0$, $A_w = 1.0$, $B_u = 1.0$, $B_v = 1.0$, $B_w = 1.0$, $D_u = 1.0$, $D_v = 0.2$, $D_w = 0.2$, $P_0 = 1.0$, $P = 20.0$, $u_0 = 0.03$, $S_0 = 1.2$, $n = 2$, $m = 8$, and $C = 10000.0$.

Programs were written in C, and morphogen concentrations (u_i, v_i, and w_i) and cell division clock ($clock_i$) were iteratively calculated every time step $\Delta t = 0.005$, using Euler's method.

3.3 **Results**

Development of pitcher leaves. Mature pitcher leaves of *S. purpurea* are mainly composed of a tube, a keel, and a sheath (Fig. 3.4a,b). In the tube, phloem bundles point toward the outer surface and xylem toward the inner (Fig. 3.4c,d), indicating that this structure is bifacial, like the blades of conventional, planar leaves. In the keel, phloem bundles point toward the outer surface but xylem vessels face each other (Fig. 3.4d), indicating that the keel forms a distinct structure from the bifacial tube. I investigated the early development of *S. purpurea* pitcher leaves using scanning electron microscopy. The adaxial surface of the incipient leaf primordium is flat (Fig. 3.4e,f), similar to that in conventional bifacial leaves (Eshed et al. 2001; McConnell et al. 2001; Nakata et al. 2012). When a primordium becomes approximately 100 μm long, an adaxial ridge connecting both sides of a leaf margin appears in the middle of the primordium (Fig. 3.4g), which is similar to the "cross zone" protrusions in peltate leaves of *Tropaeolum majus* (Gleissberg et al. 2005) and pitcher leaves of *D. californica* (Franck 1975). In *S. purpurea*, the adaxial ridge develops into a keel (Fig. 3.4a,b). When the primordium reaches approximately 200 μm in length, it becomes obvious that the proximal and distal parts of the adaxial ridge will form a keel and the adaxial side of the tube, respectively (Fig. 3.4h). As a result of growth in the leaf margin and the adaxial ridge, a hollow structure develops in the distal part of the primordium (Fig. 3.4i) and the continued growth of these regions deepens the hollow to form a pitcher shape (Fig. 3.4j).

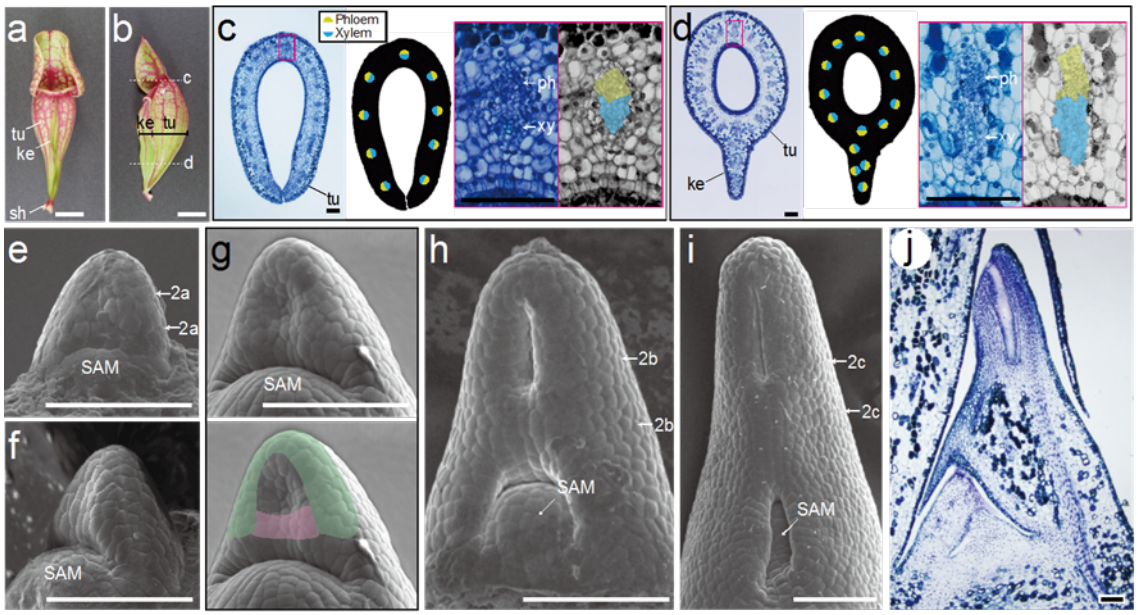

Figure 3.4. Morphology of *Sarracenia purpurea* pitcher leaves. (**a**,**b**) External morphology of mature pitchers: adaxial view (**a**) and lateral dissected view (**b**). tu: tube; ke: keel; sh, sheath. Dissected planes corresponding to those in **c** and **d** are indicated. (**c,d**) Transverse sections of immature pitchers of ca. 20 mm in length, stained with toluidine blue (left). Schematics of vascular polarity (middle) and magnified views of vascular bundles (right) are indicated. Vascular polarity is shown by the positions of adaxial element xylem (blue) and abaxial element phloem (yellow). ph, phloem; xy, xylem. (**e-i**) Scanning electron micrographs of developing pitcher primordia of ca. 70 µm (**e**,**f**), 100 µm (**g**), 200 µm (**h**), and 400 µm (**i**) in length. Adaxial (**e**) and lateral (**f**) views of ca. 70-µm primordia are shown. The leaf margin and adaxial ridge are shown in green and pink, respectively, in the lower panel of **g**. Approximate positions of sections in Fig. 3.6**a**, **b**, and **c** are indicated by arrows in Fig. 3.4**e**, **h**, and **i**, respectively. SAM, shoot apical meristem. (**j**) A longitudinal section of a pitcher primordium of ca. 1 mm in length. The scanning electron micrographs and toluidine blue-stained sections represent three to ten leaf primordia. Bars = 100 µm.

Polarity gene expression does not predict pitcher morphology in *S. purpurea*. *PHABULOSA* (*PHB*) and *FILAMENTOUS FLOWER* (*FIL*) transcription factors are expressed in the adaxial and abaxial surfaces, respectively, of some eudicot leaves (Golz et al. 2004; Kim et al. 2003b; McConnell and Barton 1998; Sawa et al. 1999; Siegfried et al. 1999). *KANADI* (*KAN*) is expressed in abaxial domains of both eudicots and monocots (reviewed in Chapter 2) but transcripts of its ortholog was not detected in *S. purpurea*. I isolated *PHB* and *FIL* orthologs in *S. purpurea* (*SpPHB* and *SpFIL*; Fig. 3.5) and analyzed their mRNA expression patterns during pitcher development (Fig. 3.6). Hybridization signals were not detected in sense probe experiments (Supplementary Fig. 3.7). In *S. purpurea*, the shape of each primordium varies slightly, likely because they are densely packed within the meristem. I therefore classified leaf primordia of similar heights as being in the same developmental stage. At least three primordia were examined for each developmental stage in RNA *in situ* hybridization (Fig. 3.6). In primordia that are approximately 70 µm long, *SpPHB* and *SpFIL* are expressed in the adaxial and abaxial surfaces of the incipient leaf primordia, respectively (Fig. 3.6a). I could not detect any difference in expression patterns between the distal and middle parts of primordia of this length. These expression patterns are similar to those in conventional bifacial leaves of *A. thaliana* (McConnell et al. 2001; Nakata et al. 2012; Sawa et al. 1999; Tameshige et al. 2013), although the relative sizes of the two expression domains may differ between *S. purpurea* and

A. thaliana. In primordia that were approximately 100 µm in height, I detected *SpPHB* expression in the inner side of the hollow and in approximately six cell lines in the adaxial side of the ridge (Fig. 3.6b,c). Both signals were also detected in provascular cells. Unlike the peltate primordia of *T. majus*, *SpFIL* expression did not extend into the adaxial ridge (Fig. 3.6b, c), suggesting that pitcher and peltate leaves use different developmental mechanisms.

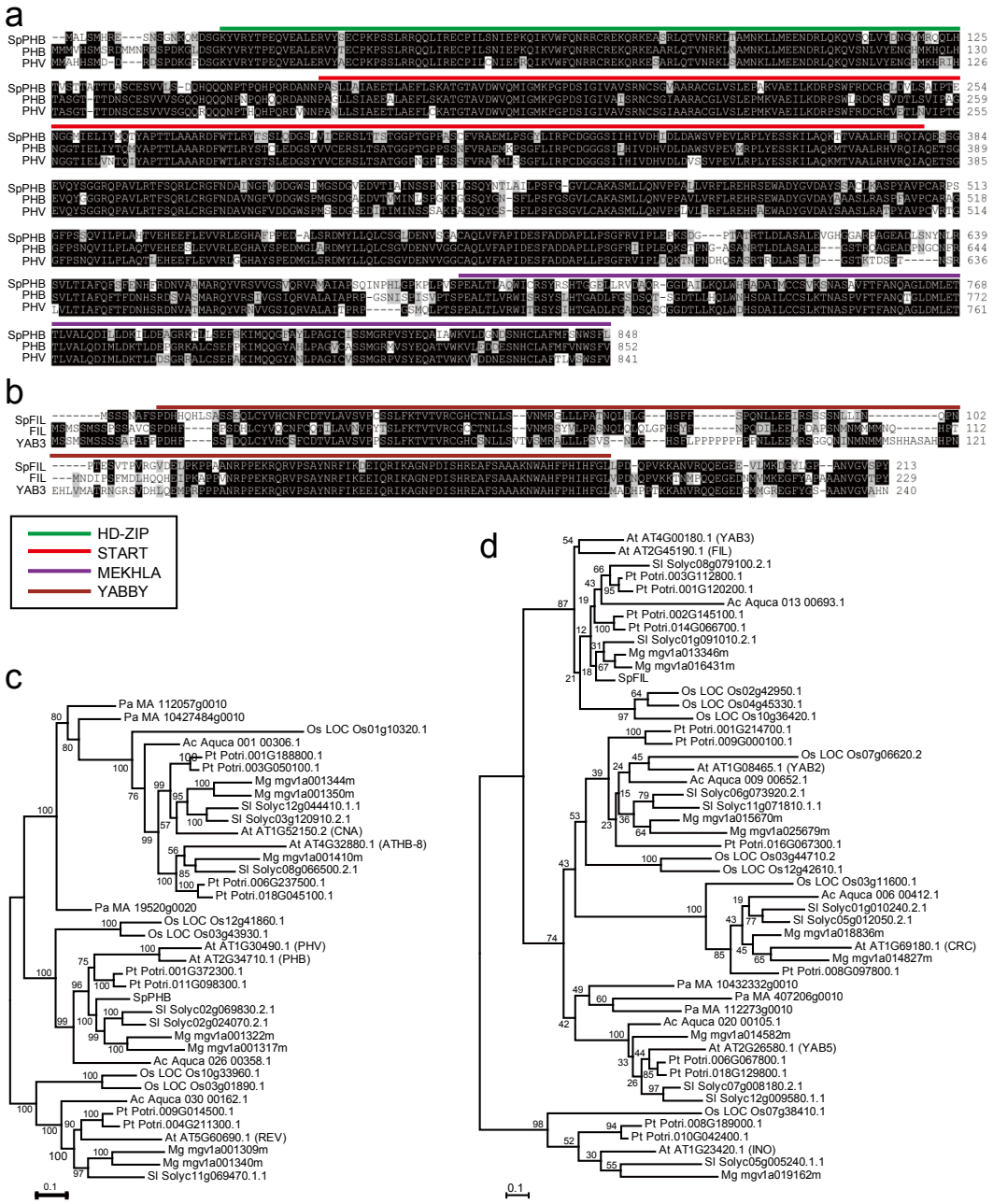

Figure 3.5. Identification of *PHABULOSA* and *FILAMENTOUS FLOWER* orthologs in *S. purpurea*. (**a,b**) Alignment of amino acid sequences of *SpPHB* (**a**) and *SpFIL* (**b**) with that of *A. thaliana* orthologs. Green, red, purple, and brown bars above the alignments indicate HD-ZIP, START, MEKHLA, and YABBY domains, respectively. (**c, d**) Unrooted maximum likelihood trees of *SpPHB* (**c**) and *SpFIL* (**d**) and their representative seed plant homologs. First two letters denote plant species and are followed by gene ID. At: *Arabidopsis thaliana*; Pt: *Populus trichocarpa*; Mg: *Mimulus guttatus*; Sl: *Solanum lycopersicum*; Ac: *Aquilegia coerulea*; Os: *Oryza sativa*; Pa: *Picea abies*. Names of *A. thaliana* genes are given in parentheses. Numbers on branches are bootstrap percentages of 1000 replicates.

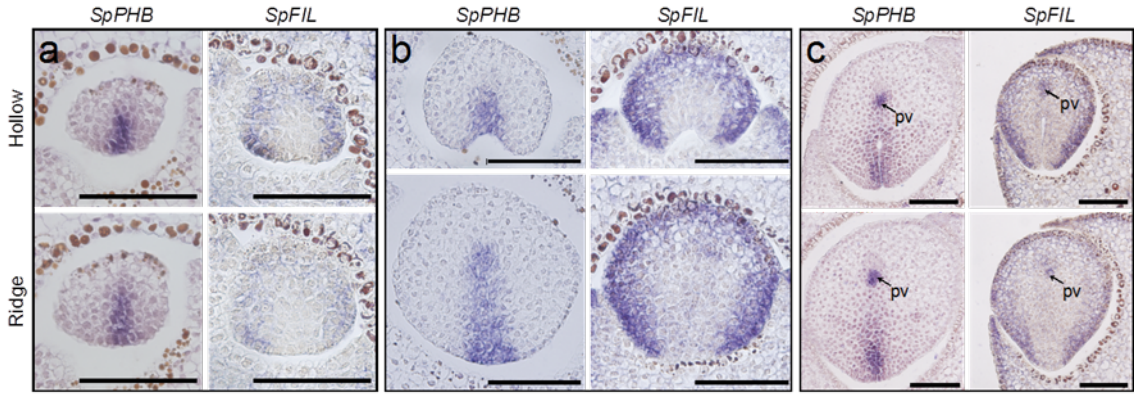

Figure 3.6. Expression patterns of *SpPHB* and *SpFIL* during pitcher development. (**a-c**) RNA *in situ* hybridization of *SpPHB* and *SpFIL* in pitcher primordia. Sections of primordia of ca. 70 µm (all sections in **a**), 160 µm (all sections in **b**), 370 µm (left sections in **c**), and 310 µm (right sections in **c**) in length. Sections are oriented with the abaxial side up and the adaxial side down. pv, provascular cells. Bars = 100 µm.

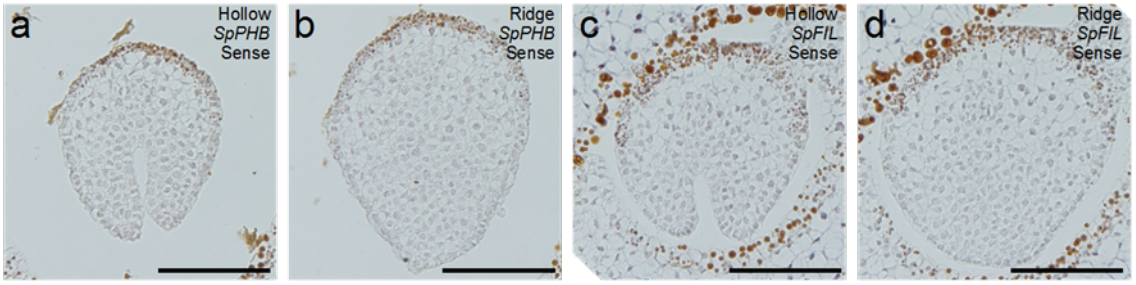

Figure 3.7. Negative control experiments of RNA *in situ* hybridization using sense probes of *SpPHB* and *SpFIL*. Transverse sections of hollow (**a**,**c**) and ridge (**b**,**d**) regions of primordia in height of ca. 210 µm (**a**,**b**) and 240 µm (**c**,**d**) are hybridized with sense probes of *SpPHB* (**a**,**b**) and *SpFIL* (**c**,**d**). The images represent three leaf primordia. Bars = 100 µm.

Oriented cell division in adaxial tissues leads to differential morphology of the hollow and ridge. In pitcher leaf primordia, the distal and middle regions develop a hollow and a ridge, respectively. Expression patterns of *SpPHB* and *SpFIL* were indistinguishable between the two regions in incipient flat primordia (Fig. 3.6a). These observations suggest that *SpPHB* and *SpFIL* expressions are not directly related to the morphological differentiation between the hollow and ridge. Plant development depends on the regulation of cell division planes, because of the immobile nature of plant cells (Wolpert et al. 2011). Therefore, I next examined the orientations of cell divisions in these two regions. Cell layers of each region were classified into layer 1 to 3 (L1 to L3) from the outermost to innermost layers, in transverse sections (Fig. 3.8a-d). I defined the *SpPHB* expression domain as the putative adaxial domain. In the hollow region, L1 cells of the inner side of the developing hollow and adjacent L2 and L3 cells were defined as adaxial cells (Fig. 3.8a,c). In the ridge region, six adaxial cell files were defined as the adaxial domain (Fig. 3.8b,d), since *SpPHB* was expressed in approximately six epidermal cells (6.17 ± 1.66 cells, mean ± standard deviation). The remaining cells were defined as abaxial cells, which presumably correspond to the *SpFIL* expression domain (Fig. 3.8a-d). In a primordium composed of five layers, the central layer was

named the middle L3 layer. To measure the orientation of division, I identified M-phase cells in transverse sections stained with 4',6-diamidino-2-phenylindole (DAPI) (Fig. 3.8. e-h). I measured the angle between the tissue surface and the spindle equator (Fig. 3.9). Although some plant tissues decouple the spindle equator from division plane by equator reorientation, the angle of spindle equators was not significantly different between metaphase and anaphase-telophase, at which point equator reorientation may occur (Mineyuki et al. 1988; Oud and Nanninga 1992; Palevitz and Hepler 1974) (Fig. 3.10). This indicates that the position of a spindle equator corresponds to that of a division plane in the pitcher leaves of *S. purpurea*.

Longitudinal divisions, which increase the number of cells in a cell layer, predominated in cells except adaxial L2 and L3 cells in the ridge region, in which division planes were periclinal (Fig. 3.8i,j; Table 3.2). These findings indicate that leaf tissues enlarge the area of a cell layer, rather than the thickness, except in the adaxial L2 and L3 cells of the middle section, which undergo periclinal divisions to increase the number of cell layers, forming the ridge of the adaxial protrusion (Fig. 3.8d). The periclinal orientation was maintained until the primordia became at least 540 μm long (Fig. 3.11). Simultaneously, the hollow region increased in area and the ridge region increased in thickness in the adaxial domain. The growth of the hollow region resembles the bifacial growth of conventional bifacial leaves, in which both adaxial and abaxial surfaces increase in area (Esau 1977). By contrast, the thickening growth of the ridge region observed in this study is characteristic to pitcher leaves, and the two different growth modes together produce the pitcher shape.

Since the mobile plant hormone auxin has been implicated in division plane regulation (Yoshida et al. 2014), next I examined effects of auxin on pitcher development. Plantlets were grown on a medium containing a synthetic auxin 1-Naphthaleneacetic acid (NAA) or an auxin transport inhibitor 1-N-Naphthylphthalamic acid (NPA) for 4 weeks, and morphology of newly-formed primordia was observed. Even in the presence of NAA or NPA in concentrations of 2 to 50 μM, leaves of *S. purpurea* clearly differentiated hollow and ridge regions (Fig. 3.12). This result reduces the possibility of differential division plane regulation in hollow and ridge regions by auxin.

I also analyzed how cell shape affects division plane in adaxial L2 and L3 cells. As a default mechanism, both animal and plant cells tend to make division plane at a right angle to cell long axis (Gibson et al. 2011; Lewis 1928). I measured geometry of dividing cells in transverse sections and compared contributions of cell shape-dependent “long-axis division rule” and cell position-dependent periclinal/longitudinal orientation. While division planes in both hollow and ridge regions were moderately correlated to periclinal/longitudinal orientation, almost no correlation was found between division plane and cell long axis (Fig. 3.13). This indicates that cell position-dependent mechanisms mainly coordinate division plane orientation in adaxial L2 and L3 cells in both hollow and ridge regions.

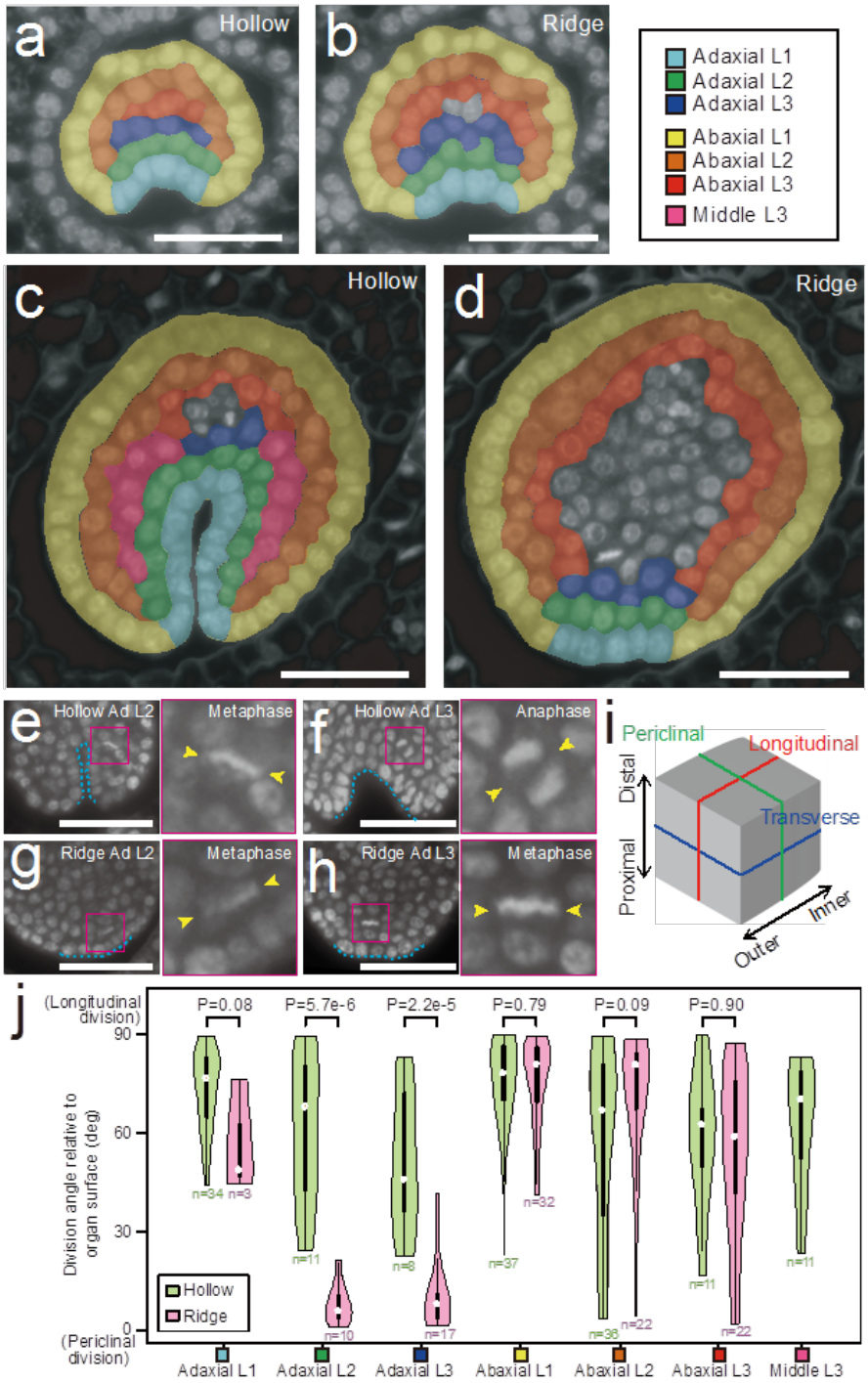

Figure 3.8. Oriented cell divisions in the hollow and ridge regions. (**a-d**) Classification of cell positions in transverse sections. Adaxial and abaxial layers 1 to 3 (L1 to L3) and middle layer 3 are indicated with different colors in sections of primordia of approximately 70 (**a, b**) and 250 (**c, d**) µm in height. (**e-h**) Examples of mitotic cells: longitudinal divisions in adaxial L2 (**e**) and adaxial L3 (**f**) cells of the hollow region, and periclinal divisions in adaxial L2 (**g**) and adaxial L3 (**h**) cells of the ridge region. Dashed lines denote adaxial L1 cells. A magnified view of dividing cells are shown as an inset (magenta). Arrowheads indicate the spindle equator of dividing cells. (**i**) Definition of cell division planes. (**j**) Polarity of cell division orientation in transverse sections. In total, 254 metaphase cells from a total of 2,022 transverse sections prepared from 67 leaf primordia between 40 and 560 µm in height were measured. Division angles are illustrated as a violin plot. White circles indicate the median. Thick and thin lines cover ±1 and ±1.5 interquantile ranges, respectively. The vertical curve is an estimator of the density. Values close to 0° indicate periclinal division, whereas those close to 90° indicate longitudinal division. Cell division polarity in the hollow (green) and ridge (pink) regions was compared by the Mann-Whitney *U* test. Bars = 100 µm.

Table 3.2. Kolmogorov-Smirnov test for uniformity of division angles in transverse sections.

Tissue	Cell position	Number of cells examined	*P* value
Hollow region	Adaxial L1	34	7.1e-10
	Adaxial L2	11	0.18
	Adaxial L3	8	0.62
	Abaxial L1	37	7.0e-13
	Abaxial L2	36	1.4e-3
	Abaxial L3	11	0.11
	Middle L3	11	0.061
Ridge region	Adaxial L1	3	0.34
	Adaxial L2	10	1.3e-06
	Adaxial L3	17	8.2e-09
	Abaxial L1	32	5.3e-10
	Abaxial L2	22	4.0e-06
	Abaxial L3	22	0.071

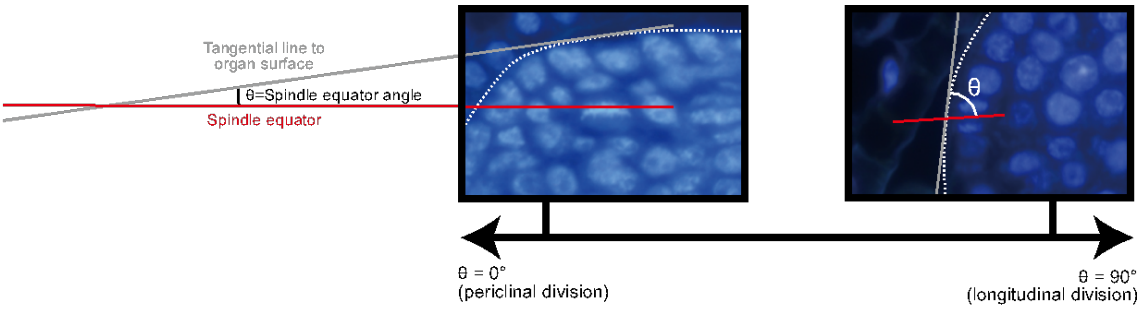

Figure 3.9. Measurement of spindle equator orientation in transverse sections. The example on the left shows measurement of the spindle equator angles during periclinal division, whereas that on the right shows measurement during longitudinal division. Dashed lines denote the organ surface.

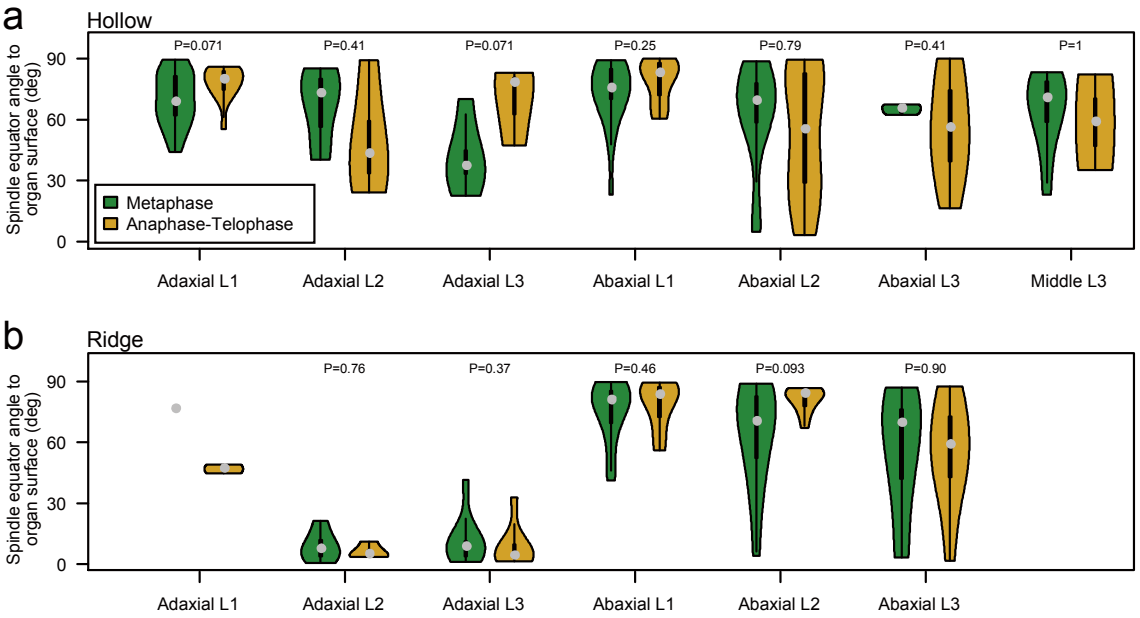

Figure 3.10. Comparison of spindle equator orientation in different cell division stages. (**a**,**b**) Differences of spindle equator orientation in the hollow (**a**) and ridge (**b**) regions. Angles of spindle equators are illustrated as violin plots. Gray circles indicate median values. Thick and thin lines cover ±1 and ±1.5 interquantile ranges, respectively. The vertical curve is an estimator of the density. *P* values indicate significant differences as determined by a Mann-Whitney *U* test.

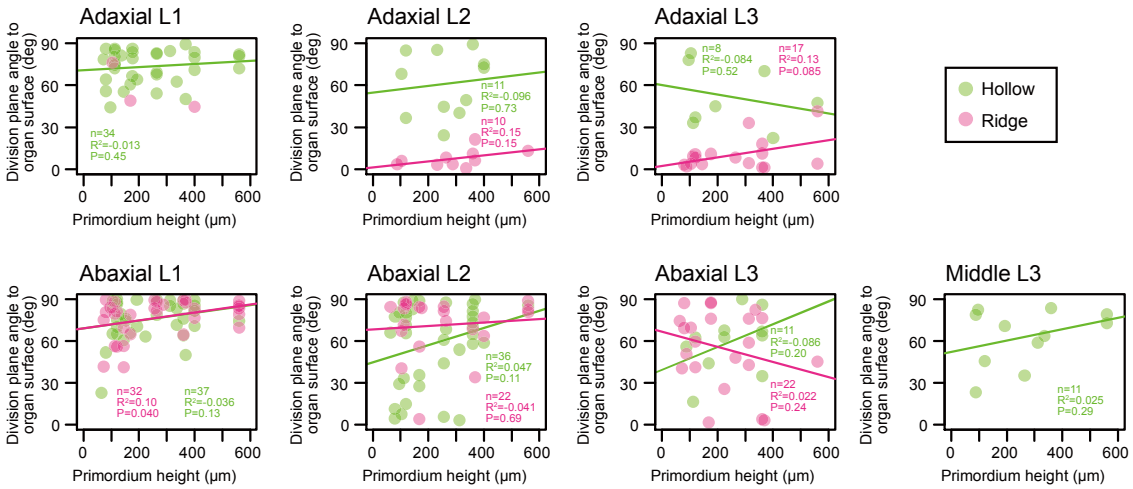

Figure 3.11. Polarity of cell division orientation in transverse sections. Division angles of different types of cells during pitcher development. Specification of cell positions is the same as in Fig. 3.8. Linear regression line, number of samples, adjusted R^2, and *P* value are shown in a plot. *P* values indicate a significant difference of R^2 from 0.

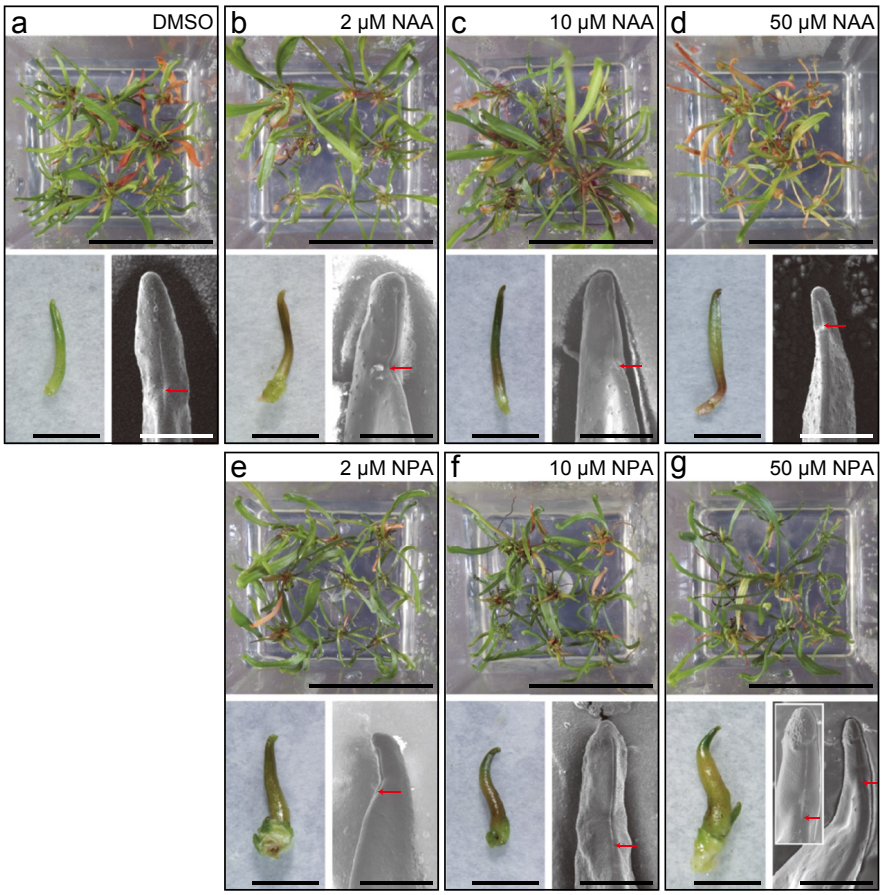

Figure 3.12. Effects of auxin addition on pitcher leaf development. Dimethyl sulfoxide (DMSO, **a**), 1-Naphthaleneacetic acid (NAA, **b-d**), and 1-N-Naphthylphthalamic acid (NPA, **e-g**) in a concentration of 2 μM (**b**,**e**), 10 μM (**c**,**f**), or 50 μM (**d**,**g**) are added to a growing medium, on which *S. purpurea* plantlets were cultivated for 4 weeks. In each panel, an upper image shows plantlets growing on the medium. A lower left image is a dissected leaf primordium in height of 5 to 10 mm. The primordium is oriented with the adaxial side right and the abaxial side left. A lower right image shows scanning electron micrograph of a leaf primordium in height of 5 to 10 mm. An inset in the lower right image of **g** is a magnified view of the distal part. Each micrograph represents at least three leaf primordia. Red arrows denote the boundary between hollow and ridge regions. Bars indicate 50 mm, 5 mm, and 500 μm for upper, lower left, and lower right images, respectively.

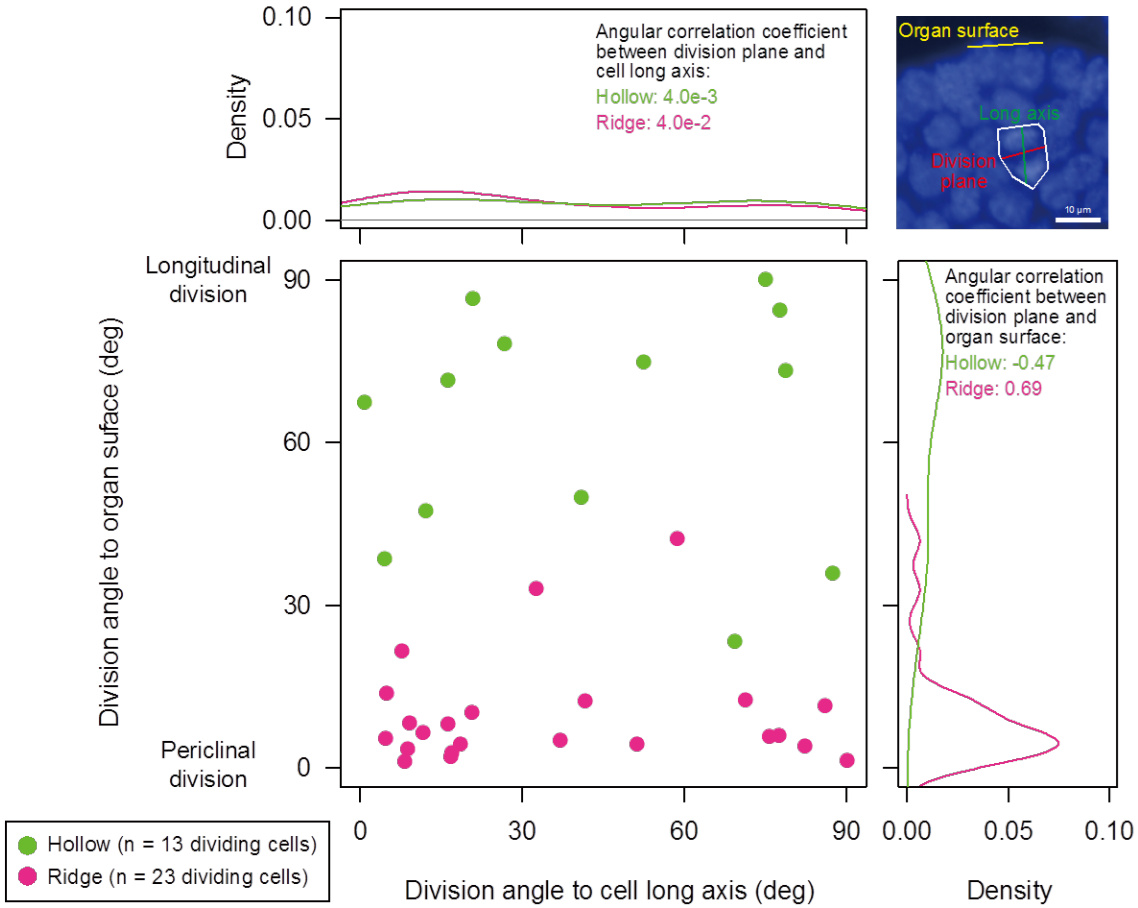

Figure 3.13. Contribution of cell shape and cell position to division orientation in adaxial L2 and L3 cells. Cell shape of dividing cells are measured in transverse sections and cell long axis is determined as the same procedure described in Model (iv) section in Methods. Upper right panel shows an example of analyzed cells. Angles formed by division plane, cell long axis, and organ surface are shown as scatter plot (bottom left). Angular correlation coefficients between division plane and organ surface are provided in density plot of bottom right panel, and those between division plane and cell long axis are shown in the plot of upper left panel.

Computational modeling of pitcher leaf morphogenesis. To examine whether the different cell division patterns are sufficient to explain bifacial growth in the hollow region and protruding growth in the ridge, I and colleagues developed a computational model based on the previously established vertex dynamics model (Nagai and Honda 2001; Staple et al. 2010) to simulate proliferating plant tissues (Fig. 3.14a-g, see Methods for detail). Plant organs develop by cell division and cell expansion (reviewed in Gonzalez et al. 2012). In early leaf development, cells actively divide and cell sizes are relatively constant and small. Cell divisions later cease and cell expansion activity intensifies instead. Because cell sizes were constant and its increase was undetectable during the developmental stage I analyzed (Fig. 3.15), I concluded that hollow and ridge differentiate within the cell division phase. Therefore, I and colleagues constructed a computational model focusing on cell division in which cell expansion occurs after cell division only to maintain constant cell sizes. Transverse sections of plant tissues were modeled as a two-dimensional aggregate of polygonal cells

drawn as connections of vertices. Upon cell division, a new vertex connection was introduced to divide one cell into two daughter cells. Since I observed higher cell division activity in the marginal regions than in other regions (Fig. 3.16), as found in *A. thaliana* (Nakata et al. 2012), I and colleagues introduced a cell division-promoting morphogen that diffuses from the boundary of adaxial and abaxial epidermal cells (magenta in Fig. 3.14h-i). Leaf primordia before pitcher morphogenesis have a slight depression in the adaxial side (Fig. 3.8a,b), and this was found to be important for simulating leaf morphogenesis because proper bifacial growth was suppressed when simulations were started from cell aggregates with round shape (Fig. 3.17). Therefore, pitcher leaf morphogenesis was simulated using initial shape with depression in adaxial side. When starting with 100 cells and forcing L1, L2, and L3 cells of both adaxial and abaxial tissues to divide longitudinally as observed in the hollow region of actual leaf primordia (Fig. 3.8j), bifacial growth was recapitulated (Fig. 3.14h). When adaxial L2 and L3 cells were forced to divide periclinally (Fig. 3.8j), an adaxial protrusion formed (Fig. 3.14i).

To understand how cell division activity affects growth patterns, I and colleagues changed three parameters related to division activity: the diffusion coefficient of the cell division-promoting morphogen, the synthesis rate of the morphogen, and the division-inducing efficiency of the morphogen (Fig. 3.18). Although simulated morphology fluctuates when the parameters are changed, the model stably reconstructed bifacial growth and adaxial protrusion. This indicates that the morphological differences between the two growth patterns result from differences in cell division orientation.

Together, these modeling results indicate that differences in the orientations of cell divisions in the adaxial tissues should be sufficient to produce the distinct growth patterns of bifacial growth and adaxial protrusion, which combine to form the pitcher morphology.

a

Cell	Division condition	Division orientation
Adaxial L1	Neighboring cells ≥ 5	Longitudinal
Abaxial L1	Neighboring cells ≥ 5	Longitudinal
Adaxial L2/L3 in hollow part	$clock_i > C_i$	Longitudinal
Adaxial L2/L3 in ridge part	$clock_i > C_i$	Periclinal
Abaxial L2/L3	$clock_i > C_i$	Longitudinal
L4 and inner	$clock_i > C_i$	Perpendicular to long axis

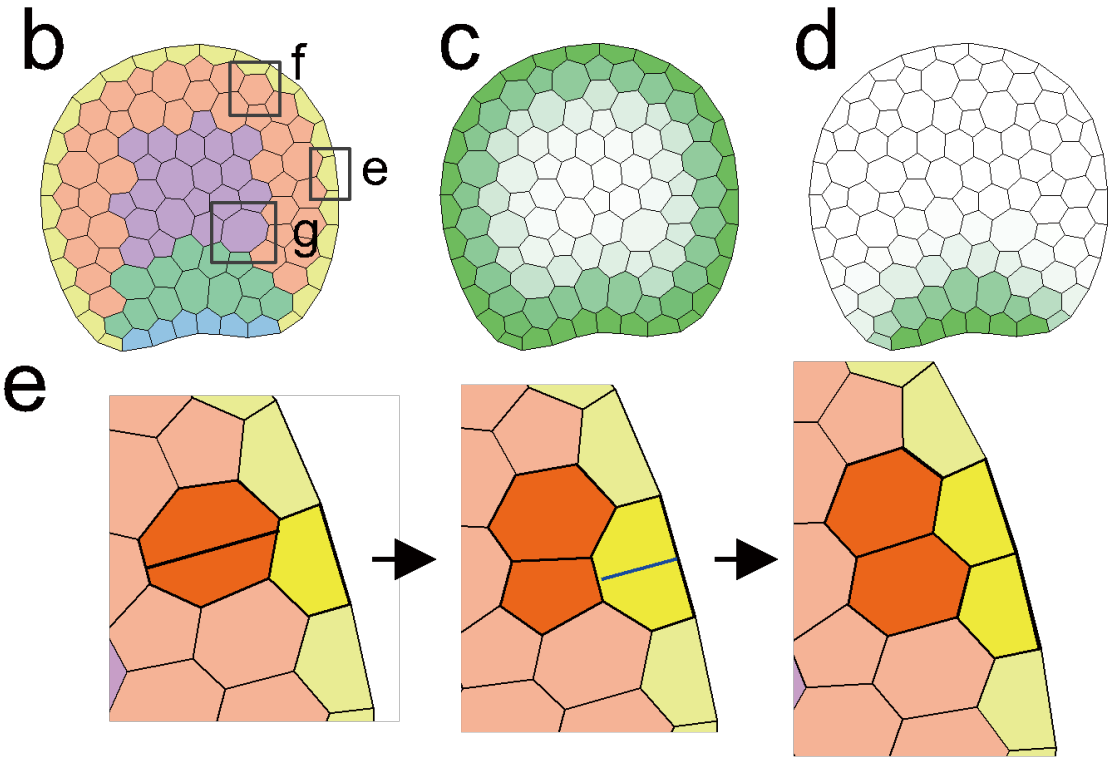

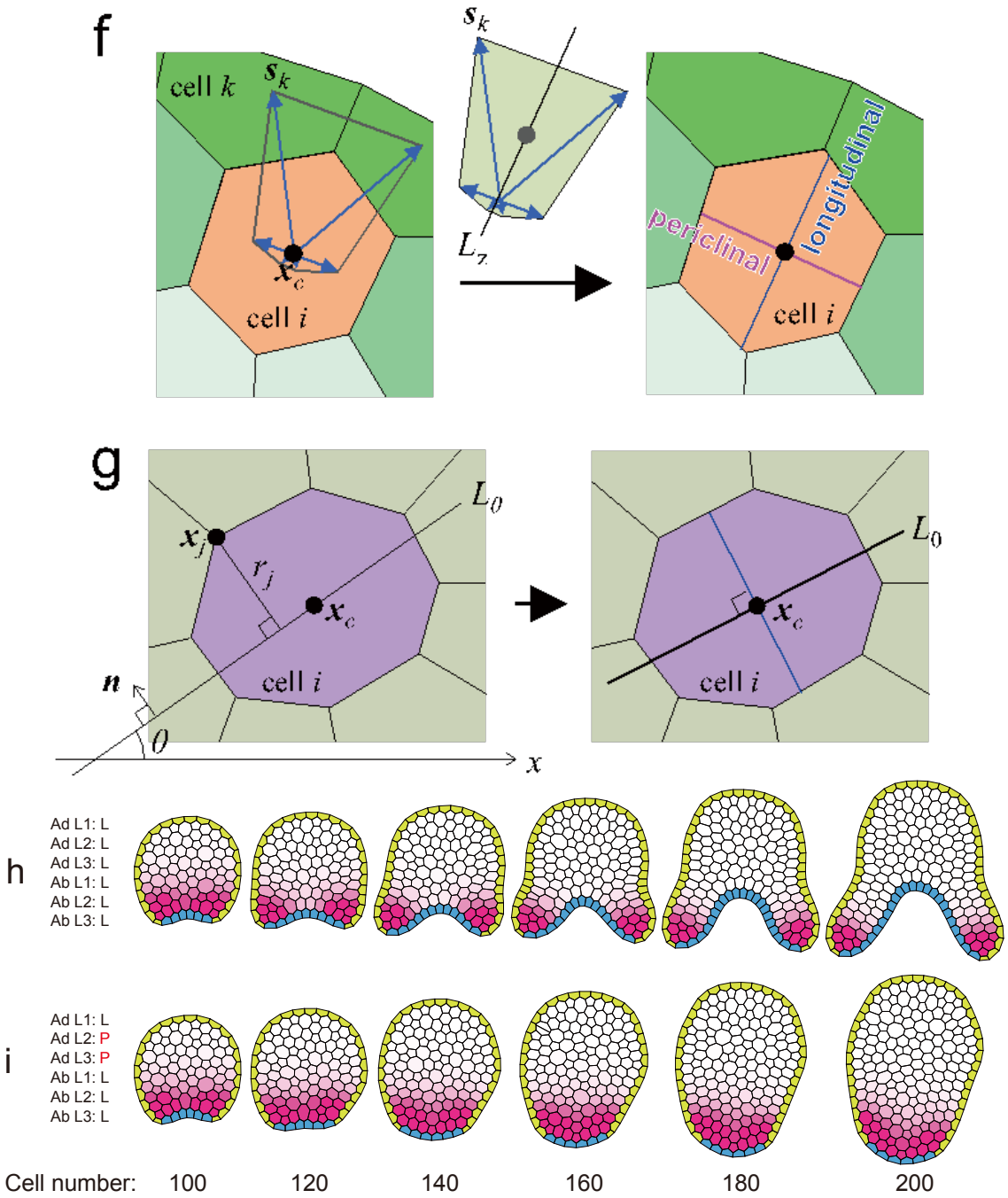

Figure 3.14. Computational simulation of cell proliferation during leaf development. (**a**) Summary of cell division condition and orientation according to cell position. (**b**) Example of classification of cell positions, which are distinguished by colors corresponding to those in (**a**). Cells in squares are examples of L1, L2/L3, and inner cells, which are illustrated in (**e**), (**f**), and (**g**), respectively. (**c,d**) Distribution of morphogens *v* (**c**) and *w* (**d**), with the darker shade representing a higher concentration. (**e-g**) L1 cells divide longitudinally (blue line) in coordination with inner cell proliferation (**e**), L2/L3 cells divide longitudinally (blue line) or periclinally (magenta line) in response to the presence of a morphogen (green) (**f**), and more inner cells divide perpendicular to their long axis L_0 (blue line) (**g**). (**h**) Cells in the outermost three layers are forced to divide longitudinally. (**i**) Adaxial L2 and L3 cells are forced to divide periclinally, while cells in other positions undergo longitudinal division. Simulations in (**h**) and (**i**) are performed with the same initial status. Adaxial and abaxial L1 cells are shaded blue and yellow, respectively. Magenta indicates the concentration of cell division-promoting morphogen, which diffuses from the boundary of adaxial and abaxial L1 cells. Darker shade represents higher concentration. Preset division planes of cell layers are indicated on the left side: L, longitudinal division; P, periclinal division.

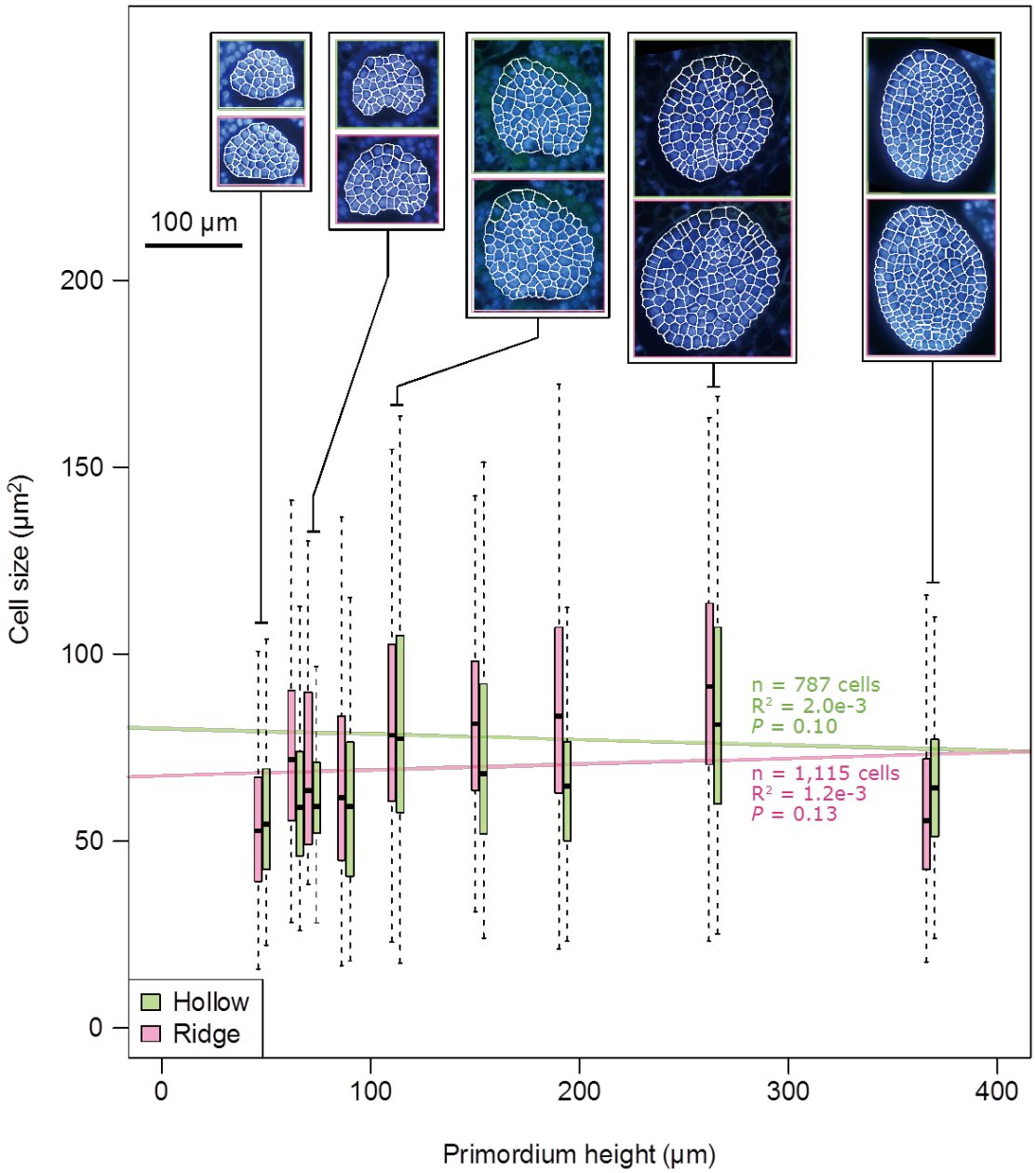

Figure 3.15. Cell size distribution in pitcher development. Cell sizes are measured in transverse sections of hollow and ridge parts and shown as a box plot. Nine primordia in different developmental stages were examined. Representative pictures of transverse sections are shown as insets. Linear regression lines, the number of measured cells (n), adjusted R^2, and *P* value are shown in the plot. *P* values indicate a significant difference of R^2 from 0. A bar indicates 100 µm for the microscopic images of transverse sections.

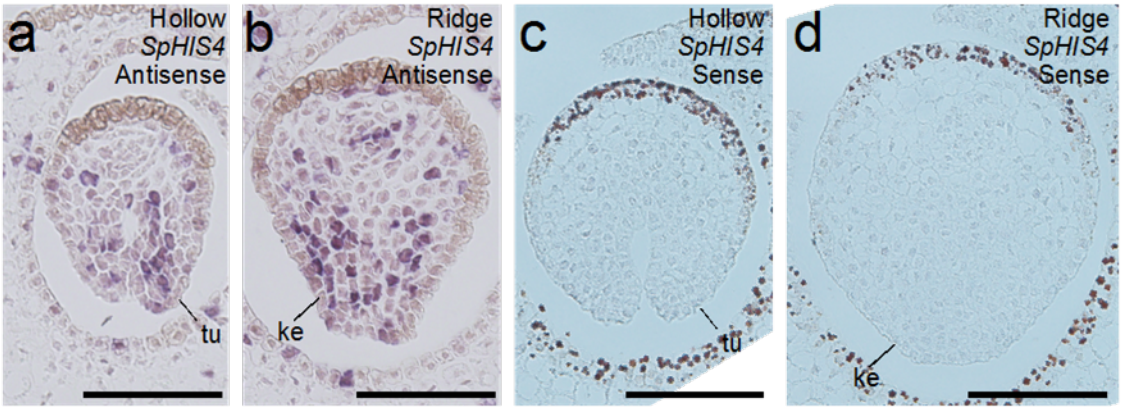

Figure 3.16. mRNA localization of *Sarracenia purpurea HistoneH4* (*SpHIS4*) in pitcher development as an indicator of cell division activity. Antisense (**a**,**b**) and sense (**c**,**d**) probes are hybridized to transverse sections of the hollow (**a,c**) and ridge (**b,d**) regions of primordia of ca. 370 µm (**a**,**b**) and 306 µm (**c**,**d**) in length. The section images of antisense and sense probe experiments represent ten and three leaf primordia, respectively. tu: tube, ke: keel. Bars = 100 µm.

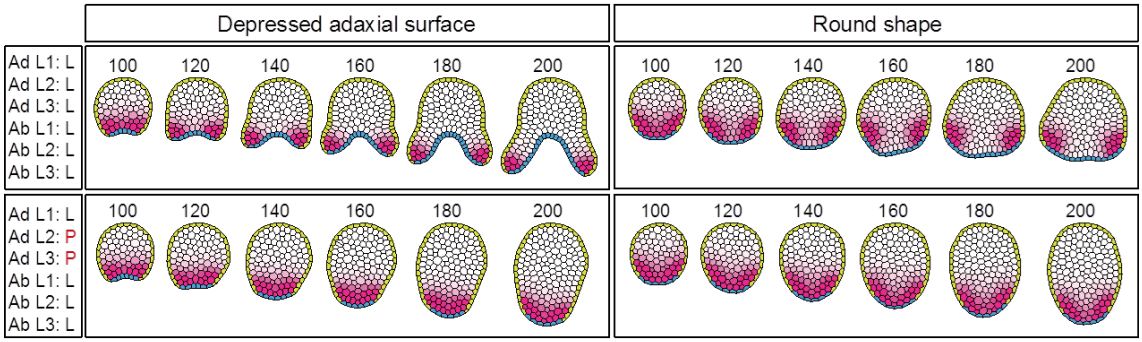

Figure 3.17. Effects of initial morphology on simulated leaf morphogenesis. Simulations are started from cell aggregates with round shape (right) and those with depressed adaxial surface (left). The preset division plane of each cell layer is indicated on the left side: L, longitudinal division; P, periclinal division.

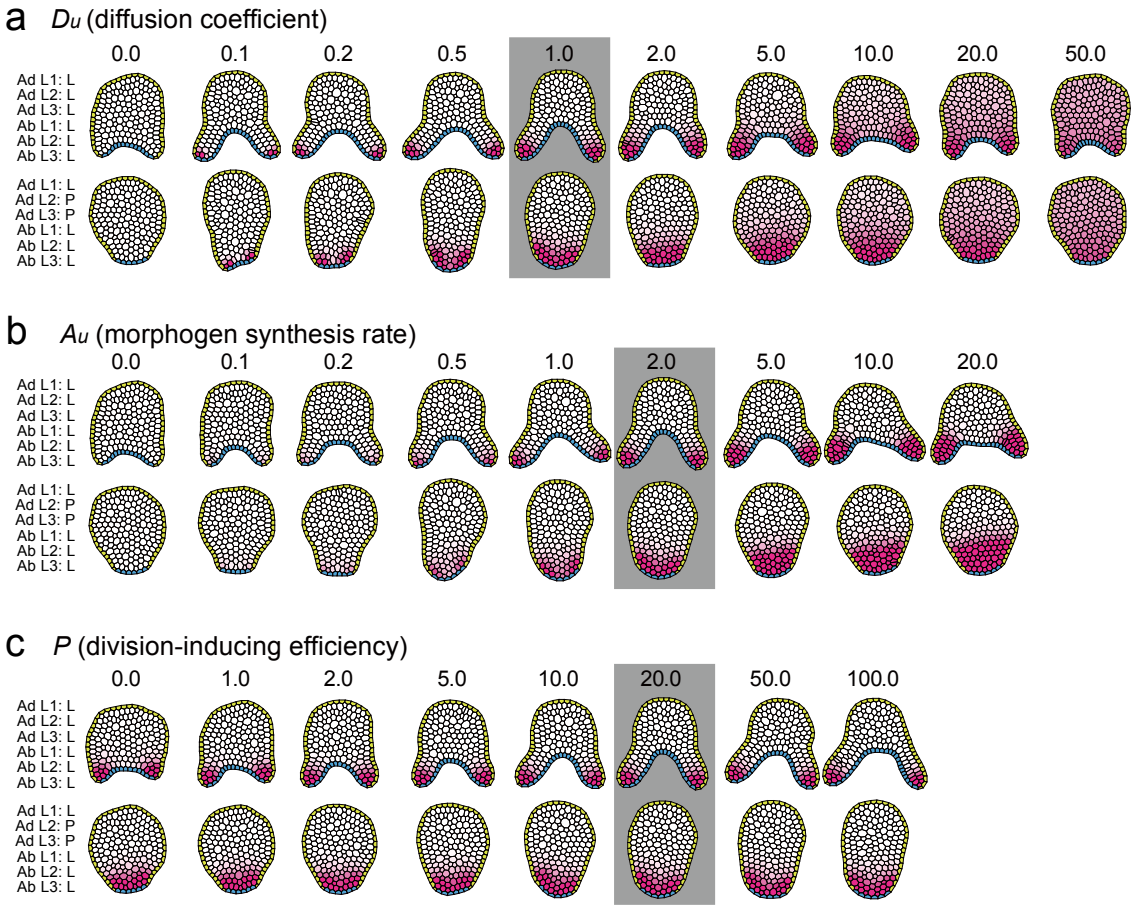

Figure 3.18. Effects of a cell division-promoting morphogen on simulated leaf morphogenesis. Diffusion coefficient (**a**), morphogen synthesis rate in adaxial-abaxial boundary cells (**b**), and a constant that affects the cell division inducing efficiency of the morphogen (**c**) are examined. The preset division plane of each cell layer is indicated on the left side: L, longitudinal division; P, periclinal division. Parameters used in Fig. 3.14 are shaded. Darker shade represents higher concentration.

3.4 Discussion

In the present study, I analyzed pitcher leaf development in *S. purpurea* and found that the pitcher shape is established through differential cell division patterns between the hollow and ridge regions of a leaf primordium. The morphology of the pitcher primordium and the expression patterns of *PHB* and *FIL* orthologs before formation of the hollow are similar to those of conventional bifacial leaves and peltate leaves during the early developmental stages (Fig. 3.6a). Subsequently, pitcher morphology is established through differential cell division patterns in the leaf primordium (Fig. 3.8). In the hollow part of the leaf primordium, longitudinal cell divisions predominated in L1, L2, and L3 cells of both the adaxial and abaxial surfaces (Fig. 3.8), as in conventional bifacial leaves (Esau 1977). By contrast, in the ridge region, periclinal cell divisions predominated in the L2 and L3 cells of the adaxial surface (Fig. 3.8), and resulted in a protruding ridge that formed a keel (Fig. 3.4a,b). The different modes of growth between the hollow and ridge regions form a tube structure. Therefore, the spatial regulation of oriented cell divisions in the leaf primordium is key for pitcher formation.

I and colleagues used computer simulation to examine the effect of growth parameters because of difficulty in experimental manipulation of multicellular dynamics *in planta*. As well as cell division orientation resulting in the specific morphology of hollow and ridge regions (Fig. 3.14), initial morphology (Fig. 3.17) and spatial distribution of cell division frequency (Fig. 3.18) appear to contribute to leaf development. Changes in these two parameters result in attenuation of bifacial growth, and this raises the possibility that proper initial morphology and cell division frequency are required for blade formation in hollow region of pitcher leaves as well as in a leaf blade of other types of leaves. This view is concordant with previously-described phenotypes of Arabidopsis mutants defective in two *WUSCHEL-RELATED HOMEOBOX* (*WOX*) genes that have been proven to function in leaf blade formation (Nakata et al. 2012; Vandenbussche et al. 2009). Double mutants of *wox1* and *pressed flower* abolish higher cell division activity in leaf margins and show attenuated blade formation (Nakata et al. 2012), exhibiting patterns similar to simulated morphogenesis (Fig. 3.18). While division plane determines basic morphology of hollow and ridge regions, other parameters are likely to additionally function to form final shapes for proper leaf development.

The *PHB* and *FIL* expression patterns of incipient leaf primordia are conserved in conventional bifacial leaves of diverse flowering plants including *A. thaliana* (McConnell et al. 2001; Sawa et al. 1999), *Antirrhinum majus* (Golz et al. 2004), and *Cabomba caroliniana* (Yamada et al. 2011). The expression patterns in the early primordia are also conserved in leaves with varied morphology, including peltate leaves (Gleissberg et al. 2005). Together with our results on pitcher development, these observations show that polarized gene expression at the initial stage is evolutionarily conserved in different types of leaves. However, after the conserved stage of polarity establishment, organ-specific differences appear, including spatial expression changes of polarity markers in peltate

leaves, and cell division patterns without polarity marker expression changes in pitcher leaves.

Because of the partly similar developmental processes between peltate and pitcher leaves, pitcher leaves have been hypothesized to be a modified form of the peltate leaf (Franck 1976; Juniper et al. 1989). I found that the pitcher leaf architecture is established through modified cell division patterns, rather than a change of leaf polarity indicated by polarity marker gene expression, which underlies peltate leaf development (Gleissberg et al. 2005; Waites and Hudson 1995) (reviewed in Fukushima and Hasebe 2014). Therefore, the developmental mechanisms of pitcher leaves appear to be distinct from those of peltate leaves. Although the mechanisms of division plane regulation remain largely unknown, both chemical and physical signals are implicated in this process. It is reported that auxin participates in division plane regulation in embryonic development (Yoshida et al. 2014), although auxin addition did not disturb hollow and ridge formations (Fig. 3.12). Given that auxin acts in a tissue-specific manner (e.g. Pinon et al. 2013), visualization of endogenous auxin distribution in transgenic plants with auxin-responsive marker genes may give clearer results to test the hypothesis of auxin's involvement of division plane regulation in pitcher development. Another candidate of division plane regulator is physical properties. Although our results showed that so-called "long-axis division rule" does not act in the tissues I analyzed (Fig. 3.13), physical properties can orient division plane without affecting cell shapes by mechanical feedback, in which mechanical forces coordinate growth dynamics by modulating chemical signals (Bozorg et al. 2014; Buchmann et al. 2014). Signaling molecules or physical properties that do not alter the expression of polarity markers might have been differentially regulated during the evolution of pitcher leaves. Further sophistication of the model may be beneficial for more detailed analyses because of the complexity of multicellular dynamics. Incorporation of the experimentally measured dynamics of cell shape and growth rate will allow more robust modeling. Furthermore, application of three-dimensional vertex modeling (Honda et al. 2004; Okuda et al. 2013) to pitcher morphogenesis may give additional insights into how distinct growth patterns are coordinated and integrated in a pitcher primordium.

Carnivorous plants evolved at least five times in flowering plants, and pitcher morphology evolved three times (Albert et al. 1992). However, the leaf morphology of sister taxa does not provide insight into the intermediate morphology of pitcher leaf evolution. In addition, fossil records are scarce. Therefore, the evolutionary processes and mechanisms underlying pitcher leaf formation have remained mostly unknown (Juniper et al. 1989). Major morphological changes appear to be due mainly to mutations with large effects or to the accumulation of many changes with small effects (Barton et al. 2007). As cell walls limit the mobility of plant cells, cell division activity and direction usually have critical roles in shaping plant organs. Changes at the cellular level, such as the changes of oriented cell divisions found in this study, likely function as the source of major morphological changes at the organ level during the evolution of pitcher leaves and other distinctive organs.

4. THE GENOME OF *CEPHALOTUS FOLLICULARIS* PROVIDES INSIGHTS INTO THE EVOLUTION OF PITCHER LEAVES

4.1 Introduction

Carnivorous plants form specialized leaves capable of attracting, trapping, and digesting prey and absorbing nutrients (Juniper et al. 1989). These unusual plants evolved from non-carnivorous ancestors (Albert et al. 1992) but their evolutionary process is mostly unknown. The Australian pitcher plant *Cephalotus follicularis* (Cephalotus) produces both carnivorous pitcher and non-carnivorous flat leaves (Juniper et al. 1989; Lloyd 1942), enabling us to study carnivory-related genes by comparative approaches in a single species. By taking advantage of this unique opportunity, we can study the evolution of novel traits in carnivorous plants, using Cephalotus as a model system. This study requires manipulation of gene expression and access to genome and transcriptome information to link phenotypic evolution and genetic changes. However, none of these molecular biological technologies have been applied to this species. Moreover, experimental control of the leaf dimorphisms has not yet been achieved.

To understand the genetic changes associated with the evolution of carnivory, my colleagues and I sequenced the 2-Gbp genome of *C. follicularis*. In addition, I established experimental regulation of leaf dimorphisms and virus-induced gene silencing (VIGS) to study the molecular mechanisms of pitcher morphogenesis. I then examined candidate genes regulating pitcher morphogenesis by transcriptome comparisons and knockdown experiments. This approach successfully identified transcription factors that cause morphological defects when silenced by VIGS. This study provides key infrastructure enabling molecular biological examination of carnivorous syndrome.

4.2 Materials and Methods

Plant materials and culture conditions. Axenically grown plants of *Cephalotus follicularis* were obtained from CZ Plants Nursery (Trebovice, Czech Republic) and were maintained in polycarbonate containers (60x60x100 mm) containing half-strength Murashige and Skoog solid medium (Murashige and Skoog 1962) supplemented with 3% sucrose, 1x Gamborg's vitamins, 0.1% 2-(N-morpholino)ethanesulfonic acid, 0.05% Plant Preservative Mixture (Plant Cell Technology), and 0.3% Phytagel, at 25°C under continuous light.

Culture conditions for leaf fate regulation. Shoot apices with one or two expanded leaves were collected with fine forceps from plants grown at 25°C, and planted on the medium. Unless mentioned otherwise, the plantlets were grown for 12 weeks under a light intensity of 20 to 40 µmol m^{-2} s^{-1}. Numbers of pitcher and flat leaves in the youngest expanded leaves of the main shoot were counted for each plantlet. Leaves with intermediate shapes were counted as either of the two categories based on morphological similarity.

RNA extraction. Plant materials were ground in liquid nitrogen with a mortar and pestle. Total RNA was extracted using the PureLink Plant RNA Reagent (Life Technologies) and subsequently purified using the RNeasy Mini Kit (QIAGEN). DNase treatment was performed during the column purification. Total RNA was qualified using a 2100 Bioanalyzer (Agilent).

Construction of the pTRV2-CfPDS clone. cDNA was synthesized from total RNA using SuperScript III Reverse Transcriptase (Life Technologies). A partial coding sequence of *PHYTOENE DESATURASE* (*PDS,* gene ID: Cfol_v3_02526) was amplified with oligonucleotide primers CfPDS-F-XbaI and CfPDS-R-BamH1, which have extra bases for restriction sites (Table 4.1). The *PDS* fragment was sequentially digested with XbaI and BamH1, and was subsequently cloned into the multiple cloning site of pTV00 plasmid (Fig. 4.1), in which *Tobacco Rattle Virus* (*TRV*) RNA 2 is integrated (Ratcliff et al. 2001). Cloned sequences were amplified with the primer pair pYL156F and pYL156R (Table 4.1), and sequenced with the ABI Prism 3100 Genetic Analyzer (Applied Biosystems) to confirm plasmid integrity. Target gene fragments for knockdown experiments were amplified with primer pairs containing restriction sites for *Xba*I and *Eco*RI. The amplicon was then digested with *Xba*I and *Eco*RI, and cloned into TRV2-CfPDS construct.

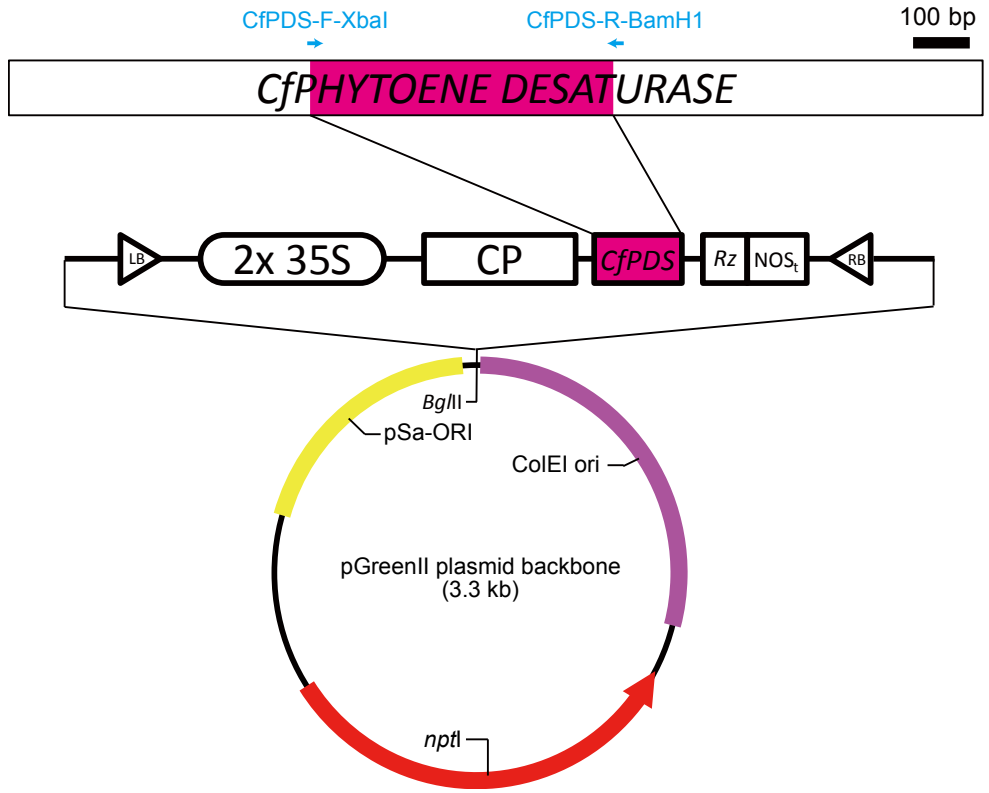

Figure 4.1. Schematic representation of the TRV2-CfPDS vector. Abbreviations: 2x 35S, tandemly-conjugated CaMV 35S promoter; CP, coat protein; Rz, self-cleaving ribozyme; NOSt, transcription terminator of Nopaline synthase; LB, left border; RB, right border.

Table 4.1. Oligonucleotide primers used in the work in Chapter 4.

Target	Primer name	Primer sequence (5' to 3')	Usage	References
CfPDS	CfPDS-F-XbaI	GGTCTAGACAGCCGATTTGATTTTCCTG	Restriction site addition to *CfPDS* fragment	This study
	CfPDS-R-BamH1	AAGGATCCGTGAATTAAGCCTGACTTCG	Restriction site addition to *CfPDS* fragment	This study
TRV2	pYL156F	GGTCAAGGTACGTAGTAGAG	Restriction cloning, detection of TRV2 plasmid	(Hileman et al. 2005)
	pYL156R	CGAGAATGTCAATCTCGTAGG	Restriction cloning, detection of TRV2 plasmid	(Hileman et al. 2005)
TRV1	OYL195	CTTGAAGAAGAAGACTTTCGAAGTCTC	Detection of TRV1 plasmid	(Hileman et al. 2005)
	OYL198	GTAAAATCATTGATAACAACACAGACAAAC	Detection of TRV1 plasmid	(Hileman et al. 2005)

Virus-induced gene silencing (VIGS). The pBINTRA6 construct containing the *Tobacco rattle virus* (*TRV*) RNA 1 (Ratcliff et al. 2001) and TRV2-CfPDS-Target gene construct were separately introduced into electro-competent cells of Agrobacterium strain GV3101:MP90. The transformed Agrobacterium was propagated on LB medium containing 50 mg/L Kanamycin, 50 mg/L Rifampicin, and 50 mg/L Gentamycin. A single Agrobacterium colony was picked and grown overnight in 30-ml LB liquid medium containing the three antibiotics and 200 nM acetosyringone at

28°C with vigorous shaking (180-200 rpm). The Agrobacterium suspension was diluted to adjust the OD600 to 0.3, cultured for an additional 2 h, and resuspended in half-strength MS liquid medium supplemented with 2% sucrose, 0.2% glucose, 200 nM acetosyringone, and 0.03% Silwet L-77. Separately prepared Agrobacterium suspensions for TRV1 and TRV2-CfPDS-Target gene were combined at a volume ratio of 1 : 1. Petri dishes were used for plant culture to obtain etiolated, well-branching Cephalotus plantlets suitable for VIGS experiments. The plantlets were dipped into the combined Agrobacterium suspension, and simultaneous infection was performed by vacuum infiltration for 2 min (- 0.08 MPa). After repeated washing, plantlets were placed onto half-strength MS medium containing 1x Gamborg's vitamins, 3% sucrose, 0.05% PPM, 0.1% MES, 0.3% Phytagel, and 150 mg/L Cefotaxime. Infected plants were grown at 25°C under continuous light for one to two months.

Chromosome preparation. Fresh root tips of *Cephalotus follicularis* were treated with 0.05% colchicine for 4 h, fixed with 70% EtOH, and then washed in ice-cold water for 60 min. The tissues were macerated in an enzymatic mixture containing 0.4% Cellulase Onozuka R-10 (Yakult Pharmaceutical Industry Co., Ltd., Tokyo, Japan) and 0.2% Pectolyase Y-23 (Kikkoman Co. Ltd., Tokyo, Japan) for 60 min at 37°C. After washing with distilled water, root tips were placed onto a glass slide and spread with ethanol–acetic acid (3:1). The slides were air dried overnight. The preparations were stained with 1 μg/ml 4',6-diamidino-2-phenylindole (DAPI). Chromosome images were taken by a digital camera (DP70, Olympus) on a microscope (Olympus BX51, Olympus).

DNA isolation. Total genomic DNA was isolated from young flat leaves and pitcher leaves of axenically grown plants. Collected leaves were homogenized in liquid nitrogen using a mortar and a pestle. The homogenate was transferred into 2x CTAB buffer preheated to 80°C, and was gently agitated at 60°C for 1 h. An equal amount of chloroform : isoamyl alcohol (25:1) was added, and agitated using a rotator at 20 rpm for 10 min at room temperature. After centrifugation at 10,000 rpm for 30 min at room temperature, supernatants were transferred to new tubes and supplemented with 1/10 volume of 10% CTAB and an equal amount of chloroform : isoamyl alcohol (25:1). The tubes were shaken with a rotator for 10 min. After centrifugation, supernatants were again transferred to new tubes and an equal amount of isopropanol was added. The tubes were centrifuged, and supernatants were discarded. The crude DNA pellet was rinsed with 5 ml of 70% EtOH and air-dried for 10 min. The pellet was dissolved in 200 μl of TE (pH 8.0) containing 0.1 mg/ml RNase A, and gently agitated for 60 min at 37°C. A 1/20 volume of 20 mg/ml Proteinase K was added, and tubes were incubated at 56°C for 30 min. Subsequently, the DNA solution was further purified using Qiagen Genomic-tip, following the manufacturer's instructions. DNA concentration was determined using fluorometry with Qubit 2.0 (Life Technologies).

Genome sequencing. Whole-genome shotgun short-read sequences to a depth of approximately 100 fold of the 2-Gb Cephalotus genome were generated using paired-end and mate-pair protocols using Illumina HiSeq 2000 according to the manufacturer's instructions (Table 4.2). In addition, long-read sequences were obtained using PacBio RS II with C2 chemistry. Using 160 cells, a total of ca. 17 Gb were generated with the quality cutoff value of 0.75 (Table 4.2).

Table 4.2. DNA-seq libraries for genome sequencing of *Cephalotus follicularis*.

Sequence application	Read length	Insert size	# Forward read	# Reverse read	Identifier
Paired-end Illumina	93	170	103554132	103554132	SZABPI002897-7
	93	500	83584627	83584627	SZAIPI002896-8
	93	800	49645683	49645683	SZAMPI002895-1
	100	800	60152165	60152165	SZAMPI005087-17
	138	250	186215149	186215149	SZAXPI006993-22
	100	800	68285388	68285388	SZAXPI006994-45
	138	500	140177444	140177444	SZAXPI007015-23
	138	500	25913653	25913653	
	141	250	103122060	103122060	SZAXPI007016-22
Mate-pair Illumina	90	2k	103489594	103489594	CEPdaoDAFDWABPEI-19
	90	2k	36349304	36349304	
	90	2k	98094048	98094048	CEPdaoDAFDWAAPEI-13
	90	2k	29539185	29539185	
	90	5k	61474845	61474845	CEPdaoDAFDLAAPEI-57
	90	5k	47747843	47747843	SZABPI002897-7
	90	10k	80581456	80581456	CEPomgDAQDTAAPEI-20
	90	10k	106591757	106591757	CEPomgDAQDTBAPEI-110
	90	20k	19807160	19807160	CEPomgDAQDUAAPEI-35
	90	20k	21122424	21122424	CEPomgDAQDUCAPEI-37
PacBio	2141 (mean max sub-read length)	-	8114864	-	-

Transcriptome sequencing. Extracted RNA was subjected to two rounds of mRNA enrichment using Dynabeads mRNA Purification Kit (Life Technologies) according to the manufacturer's instructions. RNA-seq libraries were prepared using TruSeq RNA Sample Preparation kit v.2 (Illumina). Strand-specific mRNA libraries were constructed by the dUTP second-strand marking method (Levin et al. 2010). Those libraries were sequenced using Illumina HiSeq 2000 (Table 4.3).

Table 4.3. RNA-seq libraries for transcriptome sequencing of carnivorous plants.

Species	Cultivation condition	Sampled tissue	Batch	rRNA ratio	RIN	Sequence application	# HiSeq 2000 paired-end read *	Identifier
Cephalotus follicularis	Grown *in vitro*, 25°C, 24L0D	Root	1	1.7	9.90	Strand-specific paired end	128559707	120803_I205_FCD17GEACXX_L3_CHKPEI12070001
			2	1.3	9.90	Strand-specific paired end	134773041	120803_I205_FCD17GEACXX_L4_CHKPEI12070002
			3	1.3	10.0 0	Strand-specific paired end	130030190	120808_I617_FCC0YKBACXX_L1_CHKPEI12070003
	Grown *in vitro*, 15°C, 24L0D	Shoot apex with <1 mm leaf primordia	1	1.6	9.70	Strand-specific paired end	129466767	120808_I617_FCC0YKBACXX_L2_CHKPEI12070004
			2	1.0	6.20	Strand-specific paired end	118114950	120808_I617_FCC0YKBACXX_L3_CHKPEI12070005
			3	1.2	9.60	Strand-specific paired end	143989026	120808_I617_FCC0YKBACXX_L4_CHKPEI12070006
	Grown *in vitro*, 25°C, 24L0D	Shoot apex with <1 mm leaf primordia	1	1.8	9.70	Strand-specific paired end	134700055	120808_I617_FCC0YKBACXX_L6_CHKPEI12070007
			2	1.2	9.60	Strand-specific paired end	137425138	120808_I617_FCC0YKBACXX_L7_CHKPEI12070008
			3	2.1	9.70	Strand-specific paired end	125686029	120808_I617_FCC0YKBACXX_L8_CHKPEI12070009
	Grown *in vitro*, 25°C, 24L0D	Pitcher leaf	1	1.7	9.10	Strand-specific paired end	155433787	120808_I617_FCD14WWACXX_L1_CHKPEI12070010
			2	1.7	9.50	Strand-specific paired end	160963944	120808_I617_FCD14WWACXX_L2_CHKPEI12070011
			3	1.6	9.10	Strand-specific paired end	143304510	120808_I617_FCD14WWACXX_L3_CHKPEI12070012
	Grown *in vitro*, 25°C, 24L0D	Flat leaf	1	1.5	8.50	Strand-specific paired end	131421624	120808_I617_FCD14WWACXX_L4_CHKPEI12070013
			2	1.3	8.20	Strand-specific paired end	147956132	120808_I617_FCD14WWACXX_L7_CHKPEI12070014
			3	1.3	8.20	Strand-specific paired end	124888730	120808_I617_FCD14WWACXX_L8_CHKPEI12070015
Drosera adelae	Grown on Jiffy7, 25°C, 24L0D, harvested on Jul 22th, 2011	Mature pitcher	1	1.20	NA	Paired end	18966953	s_5_1_8
	Grown on Jiffy7, 25°C, 24L0D, harvested on Jul 22th, 2011	Young aerial part	1	1.35	NA	Paired end	15890071	s_5_1_1
Nepenthes alata	Greenhouse-grown, harvested on Jul 22th, 2011	Unopened pitcher	1	1.62	NA	Paired end	21234442	s_5_1_3
	Greenhouse-grown, harvested on Aug 13th, 2013	Basal flat part	1	1.0	7.10	Paired end	26715073	idx13_AGTCAA_L004_R1

		Pitcher part	2	0.8	6.60	Paired end	22951831	idx14_AGTTCC_L004_R1
			3	0.8	6.70	Paired end	26071946	idx15_ATGTCA_L004_R1
			1	1.2	7.60	Paired end	25369818	idx16_CCGTCC_L004_R1
			2	1.3	7.40	Paired end	18711518	idx18_GTCCGC_L004_R1
			3	0.7	7.30	Paired end	17489707	idx19_GTGAAA_L004_R1
Sarracenia purpurea	Field-grown, harvested on May 25th, 2011	ca. 100-mm unopened pitcher, pooled from 3 plants	1	1.66	NA	Paired end	16072289	s_5_1_9
	Field-grown, harvested on May 25th, 2011	Shoot apex with <10-mm leaf primordia, pooled from 6 plants	1	1.58	9.90	Paired end	28191254	s_8_1_2
		ca. 100-mm unopened pitcher, pooled from 3 plants	1	1.66	9.80	Paired end	28963454	s_8_1_4
		ca. 100-mm unopened pitcher stimulated with 20 *Drosophila melanogaster* in 5 ml of 1 mg/ml BSA for 20 h, pooled from 3 plants	1	1.6	9.70	Paired end	24536600	s_8_1_5
		ca. 200-mm opened pitcher, pooled from 3 plants	1	1.11	7.20	Paired end	24985287	s_8_1_6

* The read number represents the number of pairs in paired-end reads.

Genome size estimation. The size of the Cephalotus genome was estimated by k-mer frequency analysis using JELLYFISH (Marcais and Kingsford 2011).

Genome assembly. Illumina paired-end reads with all insert sizes and mate-pair reads with the insert sizes of 2 and 5 kb were first assembled into 43,308 scaffolds using Allpaths-LG v42381 (Gnerre et al. 2011). Gap filling and further scaffolding were performed by adding mate-pair reads with longer inserts. PacBio reads were subjected to two rounds of error correction using Sprai (http://zombie.cb.k.u-tokyo.ac.jp/sprai/) and used for four rounds of iterative gap-filling with PBJelly (English et al. 2012). Final assembly was comprised of 16,307 scaffolds with N50 of 287 kb.

Repeat identification. Repetitive elements of the Cephalotus genome were first identified and masked for gene prediction. *De novo* prediction of transposable elements was performed using RepeatMasker (http://repeatmasker.org). Known transposable elements were found with RepeatMasker and RepeatProteinMasker (http://repeatmasker.org). Tandem repeat sequences were screened using Tandem Repeats Finder (Benson 1999).

Gene prediction. Transcript-based and homology-based predictions were performed using Bowtie-Tophat-Cufflinks pipeline (Trapnell et al. 2010) and GeneWise (Birney and Durbin 2000), respectively. Those models were merged using GLEAN (http://glean-gene.sourceforge.net/) (Table 4.7).

Evaluation of genome assembly and gene prediction. Gene coverage of genome assembly as well as predicted gene sets were evaluated using CEGMA 2.4 (Parra et al. 2007) (Table 4.8).

Small RNA extraction and sequencing. Plant tissues were ground in liquid nitrogen with a mortar and pestle. Total RNA was extracted using PureLink Plant RNA Reagent (Life Technologies) and subsequently purified using miRNeasy (QIAGEN). DNase treatment was performed during the column purification. Small RNA-seq was performed using Illumina HiSeq 2000 (Table 4.9).

MicroRNA prediction. The miRNA loci were predicted in the Cephalotus genome by transcriptome-based and homology-based methods. Small RNA-seq reads (Table 4.9) were mapped onto genomic inverted repeats predicted by EMBOSS einverted (Rice et al. 2000). miRNA loci were identified from the mapping results using ShortStack v1.2.3(Axtell 2013). For homology-based prediction, 7,385 mature miRNA sequences of Viridiplantae species were retrieved from miRbase (release 20, Kozomara and Griffiths-Jones 2014). Those miRNA sequences were mapped onto the

Cephalotus genome by allowing one mismatch using patscan (Dsouza et al. 1997). Putative loci mapped by less than five independent miRNAs were excluded. Secondary structures were searched from franking regions of mapped loci (± 350 bp) using RNAfold of Vienna RNA Package 2.0 (Lorenz et al. 2011), and putative miRNA loci were predicted using miRcheck with the default parameters (Jones-Rhoades and Bartel 2004). When putative miRNAs were predicted on both strands of the same loci, the minor locus was collapsed.

Selection of differentially expressed genes between pitcher and flat leaves. Strand-specific RNA-seq reads of shoot apices were mapped to genome assembly v0.1 using Bowtie-Tophat-Cufflinks pipeline (Trapnell et al. 2012) with default settings except adjusted max intron length of 10 kb. This generated the gene model v0.1 (Table 4.7). Transcript abundance was normalized by differentially expressed gene elimination strategy of TbT pipeline (Kadota et al. 2012), which consists of sequential TMM-baySeq-TMM normalization (Hardcastle and Kelly 2010; Robinson and Oshlack 2010). Genes differentially expressed between 15°C and 25°C were identified by an exact test for negative binomial distribution (Robinson and Smyth 2008) and subsequent multiple correction by adjusting false discovery rate to 0.01 (Benjamini and Hochberg 1995). A gene set of plant transcription factors was retrieved from PlnTFDB (Perez-Rodriguez et al. 2010), and BLASTX search (E value < 1E-10, Altschul et al. 1990) was performed against Cephalotus gene model v0.1 to annotate transcription factor gene families. Gene model v0.1 was further characterized by InterProScan (Zdobnov and Apweiler 2001) and the annotated transcription factors were manually curated. Differentially expressed transcription factors were considered as candidate regulators of leaf dimorphisms and were subjected to knockdown screening by virus-induced gene silencing (Table 4.10).

4.3 Results

Experimental control of leaf dimorphism in *Cephalotus follicularis*. To establish an experimental system to control leaf dimorphism of *C. follicularis*, I tested different culture conditions for axenically grown plants. Since seasonal regulation of the leaf dimorphism occurs under natural conditions (Hamilton 1904; Lloyd 1942; McPherson 2009; Pavlovič 2011), I first examined effects of temperature (Fig. 4.2a-d). Strikingly, Cephalotus plants preferentially produced flat leaves when they were grown at 15°C, and produced pitcher leaves at 25°C (Fig. 4.2a-b). Periodic observation revealed that the dimorphic differences in newly formed leaves became obvious at eight to ten weeks after the start of experiments (Fig. 4.2c). Although exposure to 15°C suppressed ca. 21% of new leaf production after 20 weeks of cultivation, both conditions resulted in similar growth curves (Fig. 4.2d).

Next, I examined light conditions including photoperiod, light intensity, and light quality (Fig. 4.2e-g). Plants were grown under short day (8L16D), long day (16L8D), or continuous (24L0D) light conditions for 12 weeks, and newly formed leaves were observed. Plants produced at least 75% flat and pitcher leaves at 15 and 25°C, respectively, under any photoperiod except the short day conditions at 25°C; under those conditions, plants preferentially produced flat leaves even at 25°C. Light intensity and light quality appear to have small effects on the leaf dimorphism in comparison to temperature (Fig. 4.2f-g).

Since plant hormones often mediate organ development and environmental responses, I examined hormonal effects on the leaf dimorphism, and found that the ethylene precursor 1-aminocyclopropane-1-carboxylic acid (ACC) modulates the leaf dimorphisms. ACC treatment, to as high as 1 mM in concentration, caused preferential production of flat leaves at 25°C (Fig. 4.2h). Since ethylene is a gaseous hormone, it increases in concentration after submergence of the plant body (Voesenek et al. 2006); therefore, I submerged Cephalotus plants to examine whether submergence mimics the effect of ACC. As predicted, submerged plants mainly produced flat leaves, even at 25°C (Fig. 4.2i).

Taken together, these results demonstrate that we can control the leaf dimorphism of *C. follicularis* in experimental conditions, opening new avenues for understanding pitcher leaf evolution by comparative approaches using a single species.

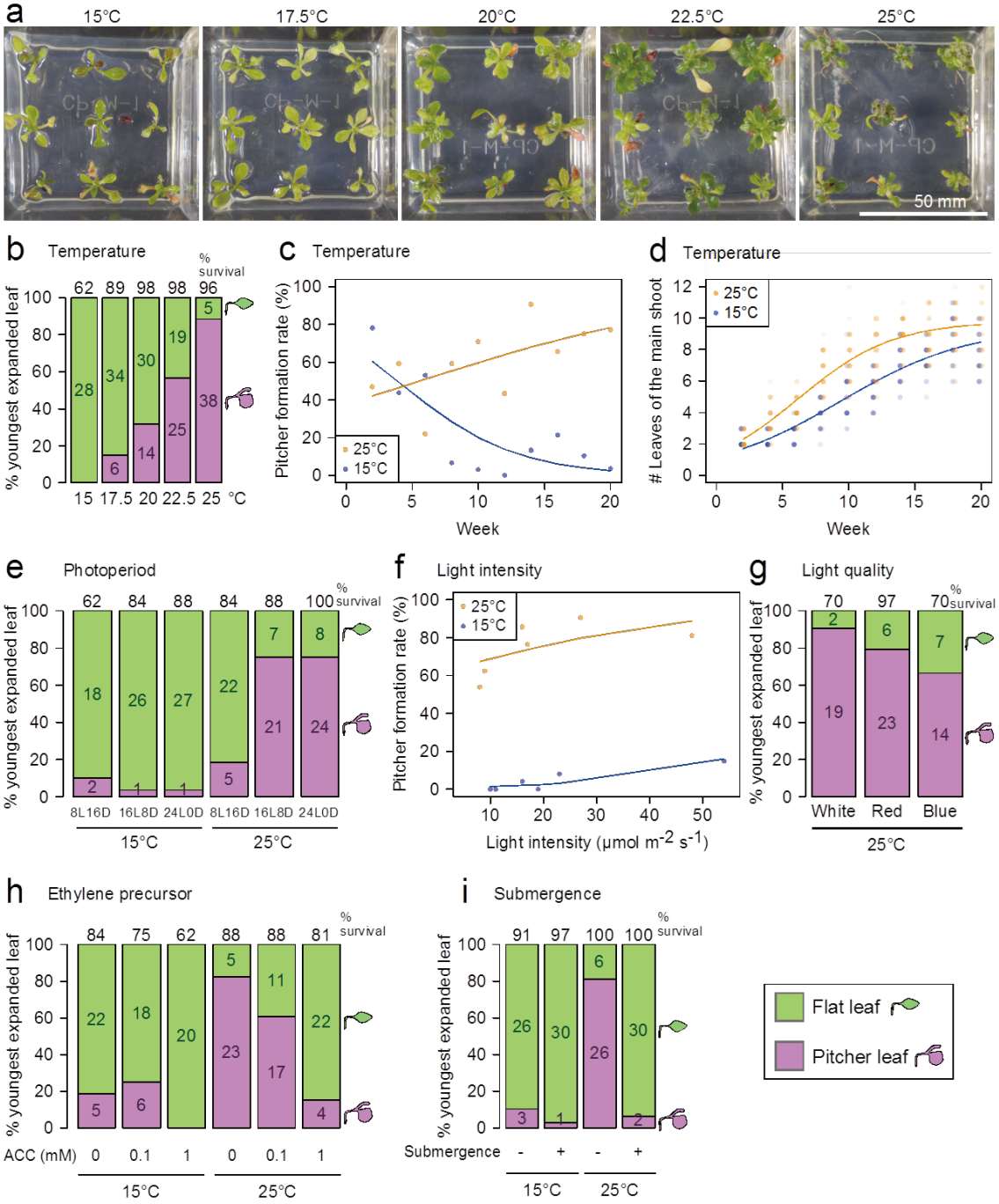

Figure 4.2. Effects of culture conditions on the leaf dimorphism of *Cephalotus follicularis*. (**a-d**) Thermoresponsive changes of leaf fate. Plants grown for 12 weeks at different temperatures (**a**). Stacked bar plots describe the proportion of pitcher and flat leaves in youngest expanded leaves after 12 weeks in culture (**b**). The number in each segment indicates total counts of each leaf type. Survival rates after 12 weeks in culture are indicated above the stacked bars. Scatter plots describe periodic observations of leaf fate (**c**) and growth rate (**d**) at 15°C and 25°C for 20 weeks. Best fitting logistic curves are given in the plots. (**e-g**) Photoresponsive changes. Photoperiod (**e**), light intensity (**f**), and light quality (**g**) are examined. (**h**) Effects of the ethylene precursor 1-aminocyclopropane-1-carboxylic acid (ACC). Different concentrations of ACC were added to the media. (**i**) Effects of submergence. Plants were grown on media for 4 weeks, and then the container was filled with water to submerge the plant bodies for additional 12 weeks of culture. Experiments were conducted using 30 (**g**), 32 (**c,d,f,h,i**), or 45 (**b,e**) plants. Effects of temperature (**b**), photoperiod (**e**), and ACC (**h**) were examined in two independent experiments, and others were conducted once (**c**,**d**,**f**,**g**,**i**).

Genome assembly and characterization. Since genomic data provide useful information allowing us to compare gene expression profiles between pitcher-inducing and flat leaf-inducing conditions, I and colleagues sequenced the nuclear genome of *C. follicularis*. The genome size of *C. follicularis* was estimated as 2.11 Gb by k-mer frequency analysis (Fig. 4.3), which raises questions about previous microdensitometry of Feulgen-stained chromosomes (625 Mb, Hanson et al. 2001). The chromosome number of the sequenced plants was $2n = 20$ (Fig. 4.4), concordant with previous reports (Johnson 1979; Keighery 1979; Kondo 1969). The genome sequences were reconstructed by shotgun assembly with Illumina short-read sequences and gap filling with PacBio long-read sequences. This approach yielded 16,307 scaffolds with an N50 of 287 kb (Table 4.4). Repetitive sequences were found to constitute 79% of the genomic sequences (Table 4.5). Long terminal repeats (LTRs) are the most abundant class of transposable elements, representing 75% of the Cephalotus genome (Table 4.6).

To construct gene models, mRNA of roots, shoot apices grown at 15°C and 25°C, pitcher leaves, and flat leaves were sequenced by strand-specific RNA-seq. On the basis of the RNA-seq reads, several versions of gene models were constructed on the assembled genome. A total of 36,503 protein-coding genes were predicted in the latest version, gene model v3 (Table 4.7). A dataset of 248 core eukaryotic genes was used to evaluate the completeness of the gene prediction (Parra et al. 2007), and 93.6% of the core genes were found in the gene model v3, at least in partial form (Table 4.8). Next, I examined gene length distribution of the Cephalotus and other sequenced genomes that cover different genome sizes: 135 Mb in *A. thaliana*, 975 Mb in *G. max*, 372 Mb in *O. sativa*, 423 Mb in *P. trichocarpa*, and 2.5 Gb in *Z. mays* (Fig. 4.5). Gene length of the Cephalotus genome is more similar to that of *Z. mays*, compared with the other genomes, which can be attributed to long intron length in the two species (Fig. 4.5c). This result indicates successful isolation of genes with long introns in the Cephalotus genome. In addition, 72 miRNAs, including 4 novel loci, were predicted by transcript-based and homology-based approaches (Table 4.9; Table 4.10; Fig. 4.6).

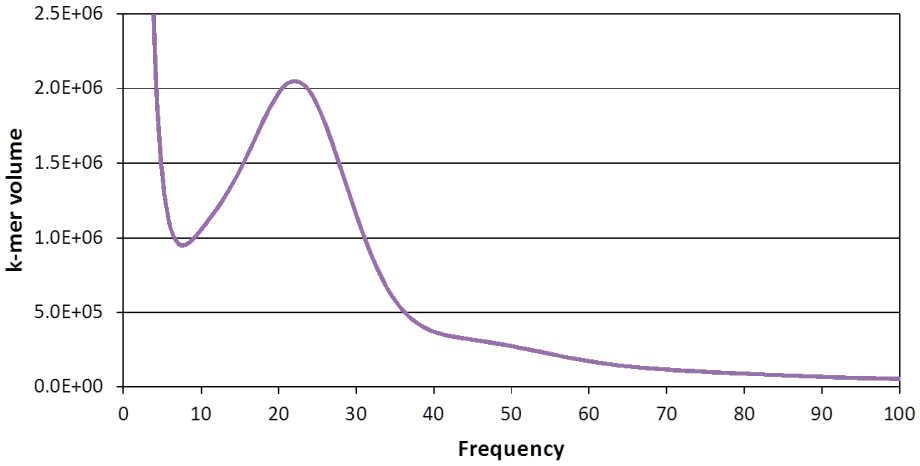

Figure 4.3. 17-mer frequency distribution of the genome sequencing reads. Occurrences of 17-mer DNA sequences were counted in a total of 56.07 Gb of Hiseq 2000 reads. Inflated k-mers in low-frequency ranges originate from sequence errors (ca. <10 counts in this analysis). The main peak is found at a frequency of 22. This would come from homozygous segments of the diploid genome. Sequence heterozygosity would appear as a peak at a half the frequency of the main peak (11), if present. A faint peak located around the frequency of 45 may represent segmental duplication of the Cephalotus genome. The genome size was estimated by dividing the total k-mer count (46,459,380,198) by the main peak depth (22), and therefore the size of Cephalotus genome would be 2.11 Gb.

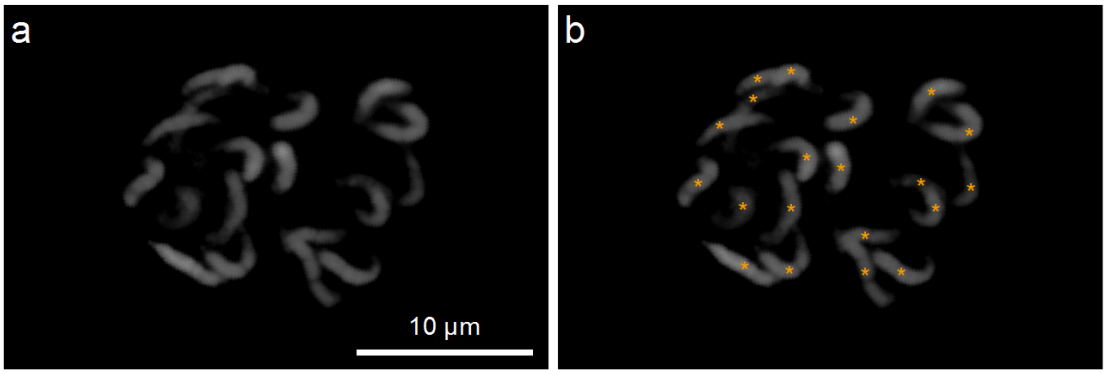

Figure 4.4. Chromosome spread of *Cephalotus follicularis*. A chromosome set is shown in **a** and positions of chromosomes are indicated with asterisks in **b**.

Table 4.4. Assembly statistics of the *Cephalotus follicularis* genome.

	Step	*De novo* assembly & Scaffolding		Scaffolding & Gap filling		Gap filling*	
	Tool	Allpaths-LG	In-house pipeline	Sprai(2)+ PBJelly(1)	Sprai(2)+ PBJelly(2)	Sprai(2)+ PBJelly(3)	Sprai(2)+ PBJelly(4)
	Version	0.1	-	-	-	-	1
Data	170 PE	+					
	250 PE	+					
	500 PE	+					
	800 PE	+					
	2k MP	+					
	5k MP	+					
	10k MP			+			
	20k MP			+			
	PacBio					+	
Contig	#Seqs	176,560	49,125	43,626	42,921	42,666	42,576
	Min	85	96	96	96	96	96
	1st Qu.	2,451	2,703	2,605	2,621	2,639	2,645
	Median	5,132	12,405	12,542	12,715	12,828	12,865
	Mean	8,808	31,992	36,124	36,741	36,969	37,051
	3rd Qu.	11,335	41,543	45,764	46,619	46,974	47,110
	Max	152,633	690,723	690,723	690,723	690,723	690,723
	Total	1,555,159,685	1,571,625,334	1,575,980,178	1,576,995,813	1,577,359,131	1,577,493,999
	n50	15,583	81,073	97,145	98,856	99,355	99,494
	n90	3,769	19,216	22,289	22,724	22,861	22,904
	n95	2,497	10,602	12,180	12,430	12,511	12,526
Scaffold	#Seqs	43,308	16,307	16,307	16,307	16,307	16,307
	Min	944	944	944	944	944	944
	1st Qu.	4,838	3,133	3,136	3,136	3,136	3,136
	Median	19,762	30,357	30,351	30,357	30,357	30,357
	Mean	38,562	98,941	98,981	98,998	99,005	99,007
	3rd Qu.	52,138	123,842	124,041	124,041	124,041	124,041
	Max	587,264	2,214,167	2,218,686	2,219,130	2,219,130	2,219,130
	Total	1,670,076,705	1,613,431,089	1,614,086,549	1,614,362,095	1,614,479,186	1,614,517,073
	n50	83,328	287,422	287,471	287,498	287,498	287,498
	n90	21,666	68,718	68,821	68,821	68,821	68,821
	n95	12,862	39,961	39,961	39,961	39,961	39,975
Gap	#Seqs	133,252	32,818	27,319	26,614	26,359	26,269
	Min	1	1	1	1	1	1
	1st Qu.	95	10	25	25	25	25
	Median	455	300	324	328	331	333
	Mean	862	1,273	1,394	1,404	1,408	1,409
	3rd Qu.	1,195	1,264	1,514	1,537	1,548	1,548
	Max	9,880	19,215	19,125	19,006	18,898	18,886
	Total	114,917,020	41,805,755	38,106,371	37,366,282	37,120,055	37,023,074
	n50	1,961	4,807	4,896	4,888	4,882	4,882
	n90	515	844	927	938	938	939
	n95	334	443	482	487	488	488

* The number of iterations is indicated in parentheses.

Table 4.5. Statistics of repeat elements in the *Cephalotus follicularis* genome.

Tool	Total size of identified repeats	% of genome
Tandem Repeats Finder	77,285,220	4.79
Repeatmasker	320,115,044	19.83
Proteinmask	453,527,842	28.09
Repeatmodeller	1,218,349,823	75.46
Total	1,275,339,348	78.99

Table 4.6. Composition of transposable elements in the *Cephalotus follicularis* genome.

Type	Length (bp)	% of genome
DNA	29,417,373	1.82
LINE	10,848,419	0.67
SINE	202,814	0.01
LTR	1,220,028,435	75.57
Other	548	0.00
Unknown	1,661,546	0.10
Total	1,249,887,436	77.42

Table 4.7. General statistics of predicted genes of *Cephalotus follicularis* in comparison with other plant genomes.

Genome	Gene number	Average gene length	Average CDS length	Average exon number	Average exon length	Average intron length
Cephalotus.v0.1	44,303	2,216	1,301	2.89	450	484
Cephalotus.v1	49,714	1,440	766	2.08	368	623
Cephalotus.v2	43,899	2,726	993	3.21	309	784
Cephalotus.v2.clean	32,973	3,194	1,022	3.83	267	768
Cephalotus.v3	36,503	2,943	961	3.57	269	770
Arabidopsis thaliana	27,416	2,187	1218	5.13	238	158
Linum usitatissimum	43,471	2,308	1201	5.03	239	275
Manihot esculenta	30,666	2,952	1168	4.88	239	400
Populus trichocarpa	41,335	3,072	1158	4.79	242	372
Ricinus communis	31,221	2,262	1004	4.14	242	378

Table 4.8. Statistics of the completeness of the *Cephalotus follicularis* genome sequence based on 248 core eukaryotic genes.

Sequence	# Gene	% Completeness	
		Complete	Partial
Genome assembly v0.1	-	85.9	95.6
Genome assembly v1	-	87.5	96.8
Gene model v0.1	44,303	84.7	95.0
Gene model v1	49,714	72.2	87.1
Gene model v2	43,899	79.4	92.7
Gene model v2.clean *	32,973	79.0	92.7
Gene model v3	36,503	79.4	93.6

* Gene model v2.clean was constructed by eliminating contamination of transposable elements from gene model v2.

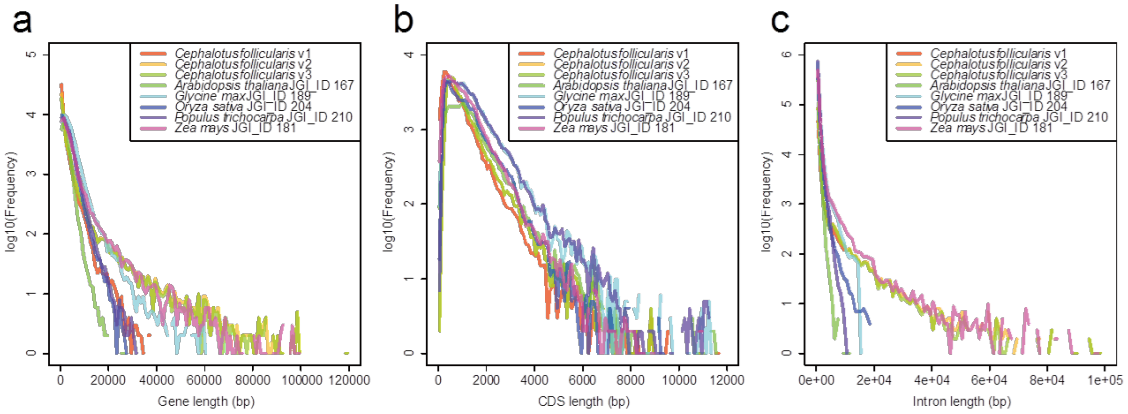

Figure 4.5. Length distribution of gene structures. Gene (**a**), CDS (**b**), and intron (**c**) lengths are shown. Keys for species are provided in the plot.

Table 4.9. Small RNA sequencing of *Cephalotus follicularis*.

Growth condition	Tissue	Insert size (bp)	Replicate	# Illumina read	Identifier
Grown *in vitro*, 25°C, 24L0D	Root	15-40	1	4,760,943	FCC1TF1ACXX_L7_PLAltgSACTAASE-9
Grown *in vitro*, 15°C, 24L0D	Shoot apex with <1 mm leaf primordia	15-40	1	5,102,847	FCC1TF1ACXX_L7_PLAltgSAATAASE-1
Grown *in vitro*, 25°C, 24L0D	Shoot apex with <1 mm leaf primordia	15-40	1	5,661,674	FCC1TF1ACXX_L7_PLAltgSABTAASE-5
Grown *in vitro*, 25°C, 24L0D	Pitcher leaf	15-40	1	4,440,248	FCC1TF1ACXX_L7_PLAltgSAETAASE-2
Grown *in vitro*, 25°C, 24L0D	Flat leaf	15-40	1	5,199,840	FCC1TF1ACXX_L7_PLAltgSADTAASE-13

Table 4.10. The list of identified miRNA loci in the *Cephalotus follicularis* genome.

miRNA family	Position					Prediction			Mature miRNA length	Mature miRNA sequence
	Scaffold	Hairpin		Mature miRNA		Strand	Transcript -based	Homology -based		
		Start	End	Start	End					
miR156	scaffold132	114205	114295	114210	114230	+	+	+	20	TGACAGAAGAGAGTGAGCAC
miR156	scaffold2798	227253	227343	227318	227338	-	+	+	20	GTGCTCACTCTCTTCTGTCA
miR156	scaffold4338	90930	91171	90977	90998	-	+	+	21	GTGCTCTCTATCTTCTGTCAA
miR156	scaffold5600	1409	1489	1409	1429	+		+	20	TTGACAGAAGATAGAGAGCA
miR156	scaffold665	807290	807373	807354	807373	-		+	19	GTGCTCTCTCTCTTCTGTC
miR159	scaffold1859	74929	75100	74929	74949	-		+	20	TAGAGCTCCCTTCAATCCAA
miR160	scaffold2369	175512	175593	175512	175532	+		+	20	TGCCTGGCTCCCTGTATGCC
miR160	scaffold5236	76132	76272	76225	76246	+	+	+	21	GCGTATGAGGAGCCATGCATA
miR160	scaffold631	411534	411616	411534	411554	+		+	20	TGCCTGGCTCCCTGGATGCC
miR160	scaffold823	95424	95505	95485	95505	-		+	20	TGGCATTCAGGGAGCCAGGC
miR162	scaffold2931	81620	81718	81698	81718	+		+	20	TCGATAAACCTCTGCATCCA
miR164	scaffold2271	136905	137090	136930	136951	+	+	+	21	TGGAGAAGCAGGGCACGTGCA
miR164	scaffold3114	17951	18049	17968	17989	+	+	+	21	TGGAGAAGCAGGGCACGTGCA
miR164	scaffold511	260290	260435	260387	260408	-	+	+	21	TGCACGTGCCCTGCTTCTCCA
miR166	scaffold107	77085	77320	77141	77162	-	+	+	21	GGGGAATGAAGCCTGGTCCGA
miR166	scaffold186	462206	462422	462265	462286	-	+	+	21	CGGGAATGAAGCCTGGTCCGA
miR166	scaffold2862	22567	22678	22652	22673	+	+	+	21	TCGGACCAGGCTTCATTCCCC
miR166	scaffold507	44682	44754	44734	44754	+		+	20	TCGGACCAGGCTTCATTCCC
miR166	scaffold5127	106635	106920	106702	106723	-	+	+	21	GGGGAATGAAGCCTGGTCCGA
miR166	scaffold734	746013	746097	746013	746033	-		+	20	GGGGAATGAAGCCTGGTCCG
miR167	scaffold1415	222708	222906	222829	222851	-	+	+	22	TCAGATCATGCTGGCAGCTTCA
miR167	scaffold342	536592	536922	536592	536612	+		+	20	TGAAGCTGCCAGCATGATCT
miR167	scaffold35	320415	320520	320481	320502	-	+	+	21	AAGATCATGCTGGCAGCTTCA
miR167	scaffold7018	31892	32013	31901	31922	+	+	+	21	TGAAGCTGCCAGCATGATCTA
miR168	scaffold2641	191718	191971	191775	191796	+	+	+	21	TCGCTTGGTGCAGGTCGGGAA
miR169	scaffold1035	255841	255931	255841	255861	+		+	20	CAGCCAAGGATGACTTGCCG
miR169	scaffold1126	62435	62586	62435	62455	+		+	20	CAGCCAAGGATGACTTGCCG

miR169	scaffold1591	149608	149823	149677	149697	-	+	+	20	AGTTAGCCAAGGAGACTGCC
miR169	scaffold269	505018	505123	505103	505123	-		+	20	CAGGCAAGTCATCCTTGGCT
miR169	scaffold313	479437	479523	479437	479457	+		+	20	CAGCCAAGGATGACTTGCCG
miR171	scaffold1829	193606	193750	193626	193647	-	+	+	21	GATATTGGCACGGCTCAATCA
miR171	scaffold3422	151162	151240	151220	151240	+		+	20	TGATTGAGCCGTGCCAATAT
miR171	scaffold3762	113273	113353	113333	113353	+		+	20	AGATTGAGCCGCGCCAATAT
miR171	scaffold5	30521	30702	30560	30581	-	+	+	21	GATATTGGCACGGCTCAATCA
miR171	scaffold511	474873	474957	474873	474893	-		+	20	CGTGATATTGGCACGGCTCA
miR171	scaffold951	90699	90778	90699	90719	-		+	20	GATATTGGCGCGGCTCAATC
miR172	scaffold1325	64782	64886	64866	64886	+		+	20	AGAATCTTGATGATGCTGCA
miR172	scaffold1772	246182	246283	246263	246283	+		+	20	GGAATCTTGATGATGCTGCA
miR172	scaffold259	388616	388749	388631	388652	-	+	+	21	ATGCAGCATCATCAAGATTCT
miR172	scaffold267	207744	207886	207850	207871	+	+	+	21	AGAATCTTGATGATGCTGCAT
miR319	scaffold1952	129705	129900	129880	129900	+		+	20	TTGGACTTAAGGGAGCTCCC
miR319	scaffold310	136330	136505	136330	136350	-		+	20	AGGGAGCTCCCTTCAGTCCA
miR319	scaffold586	154232	154407	154388	154407	+		+	19	CTTGGACTGAAGGGAGCTC
miR319	scaffold79	81777	81946	81777	81796	-		+	19	GGAGCTCCCTTCAGTCCAA
miR390	scaffold1544	78054	78173	78071	78092	+	+	+	21	AAGCTCAGGAGGGATAGCGCC
miR390	scaffold79	612161	612382	612301	612322	-	+	+	21	GGCGCTATCCCTCCTGAGCTT
miR393	scaffold1956	6256	6361	6341	6361	-		+	20	GATCAATGCGATCCCTTTGG
miR393	scaffold6	738874	738942	738922	738942	-		+	20	GATCAATGCGATCCCTTTGG
miR394	scaffold5	154701	154783	154701	154720	+		+	19	TTGGCATTCTGTCCACCTC
miR395	scaffold10243	2385	2450	2385	2405	-		+	20	GAGTTCCCCCAAACACTTCA
miR395	scaffold10243	3026	3087	3067	3087	+		+	20	CTGAAGTGTTTGGGGGAACT
miR396	scaffold1367	218415	218487	218415	218435	+		+	20	TTCCACAGCTTTCTTGAACT
miR396	scaffold156	132445	132544	132524	132544	-		+	20	CAGTTCAAGAAAGCTGTGGA
miR396	scaffold3762	120014	120128	120108	120128	-		+	20	CAGTTCAAGAAAGCTGTGGA
miR396	scaffold4645	54997	55100	54997	55017	+		+	20	TTCCACAGCTTTCTTGAACT
miR396	scaffold4645	61306	61386	61366	61386	-		+	20	AAGTTCAAGAAAGCTGTGGA
miR396	scaffold826	117873	118019	117999	118019	-		+	20	AAGTTCAAGAAAGCCGTGGA
miR397	scaffold548	269509	269673	269628	269649	-	+	+	21	CATCAACGCTGCACTCAATGA

miR398	scaffold239	800297	800393	800297	800317	-		+	20	CAGGGGCGACCTGAGAACAC
miR399	scaffold1974	244416	244512	244492	244512	+		+	20	CGCCAAAGGAGAGTTGCCCT
miR399	scaffold36	351130	351226	351130	351150	-		+	20	CCGGGCAAATCTCCTTTGGC
miR399	scaffold36	365007	365086	365066	365086	+		+	20	TGCCAAAGGAGAATTGCCCT
miR403	scaffold7014	24354	24432	24354	24374	-		+	20	CGAGTTTGTGCGTGAATCTA
miR403	scaffold931	836882	836980	836960	836980	+		+	20	TTAGATTCACGCACAAACTC
miR408	scaffold2644	78533	78615	78533	78553	-		+	20	GCCAGGGAAGAGGCAGTGCA
miR477	scaffold3171	283045	283144	283061	283082	-	+		21	CCACTCTCCCCAAAGGCCTCA
miR530	scaffold737	65868	65970	65951	65970	-		+	19	TAGGTGCAGGTGCAAATGC
miR535	scaffold1506	140597	140721	140615	140636	+	+	+	21	TGACAAGGAGAGAGAGCACGC
Novel1	scaffold126	62666	62828	62702	62723	-	+		21	TTCAATACTCTCATCAATGGA
Novel2	scaffold666	617101	617258	617196	617218	+	+		22	TTGACGGTCCCGCCGATTCCAA
Novel3	scaffold666	621083	621266	621142	621164	-	+		22	TTGGAATTTGCGGTGCCGGCAA
Novel4	scaffold929	462873	463022	462900	462921	+	+		21	TTTGTTGACAGCAGGTGACAG

* Positions were specified according to bed format.
* Minus strand sequences are reverse complement of actual miRNA sequences.

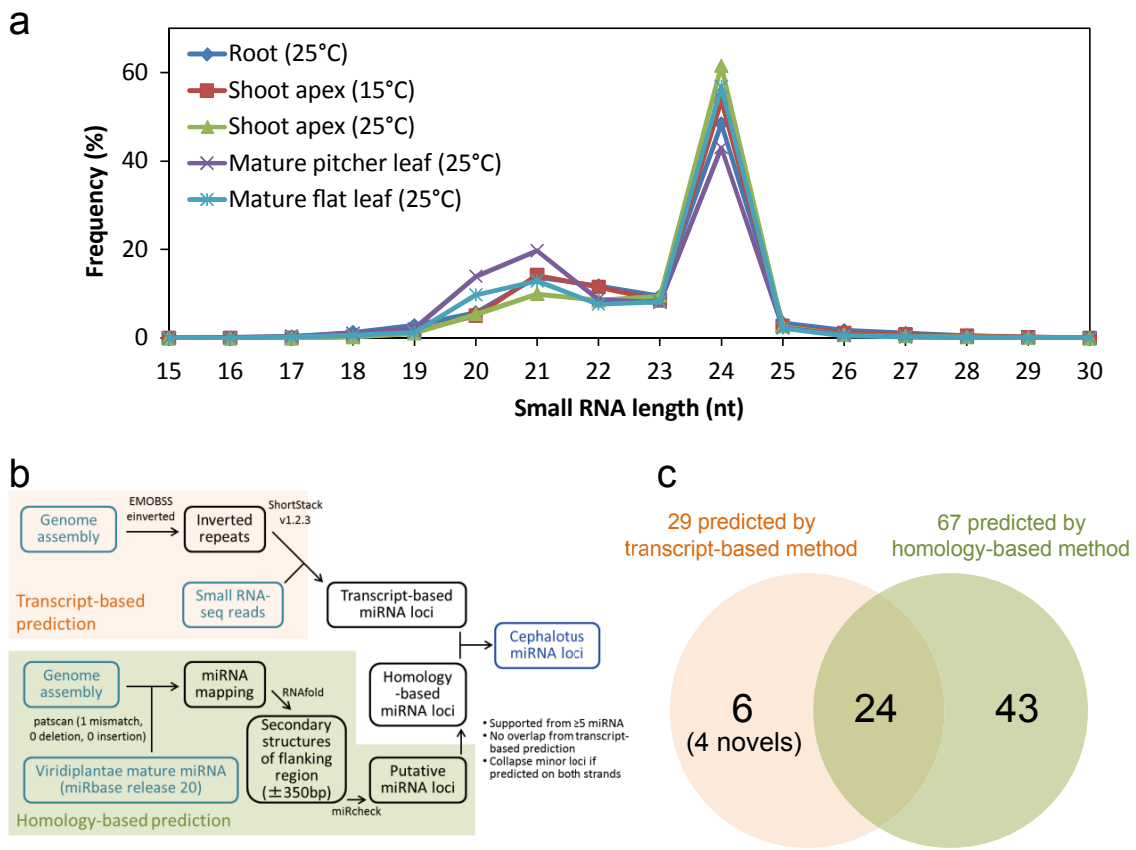

Figure 4.6. miRNA prediction in the *Cephalotus follicularis* genome. (**a**) Length distribution of small RNA-seq. Key for the five sequenced tissues is provided in the plot. (**b**) Pipelines for transcript-based and homology-based prediction of miRNA loci. (**c**) Venn diagram showing the numbers of miRNA loci detected by the two approaches.

Knockdown screening for the identification of a gene regulating pitcher morphogenesis. To identify genes regulating pitcher morphogenesis, I performed comparison of the transcriptomes of shoot apices grown at 15°C and 25°C, the culture conditions for induction of flat and pitcher leaves, respectively. Gene expression levels were obtained by RNA-seq reads mapped to the gene model v0.1. In total, 1,171 and 698 genes were up-regulated in shoot apices at 15°C and 25°C, respectively, to the other temperature with a cutoff value of false discovery rate of 0.01. Since transcription factors often participate in developmental processes, I performed knockdown screening of 111 differentially expressed transcription factors by VIGS (Table 4.11). Successful gene knockdown was evaluated by the photobleached phenotype in simultaneous knockdown of *PHYTOENE DESATURASE* (*PDS*) (Fig. 4.7a-c). As a result of the VIGS screening, I found that knockdown of LOB-domain genes (ID in gene model v3, Cfol_v3_25373 and Cfol_v3_32472) gives rise to defects in leaf development at 25°C (Fig. 4.7d-f). The knockdown lines of these genes produced ensiform-like leaves (Fig. 4.7d) and rod-like leaves (Fig. 4.7e,f), which are never observed in wild type. Although further sophistication of the knock-down technique, including a quantification of gene silencing efficiency, would be necessary, detailed functional characterization of these genes

and other candidates may give an insight into the evolution of pitcher morphology in carnivorous plants.

Table 4.11. Transcription factors that are differentially expressed between shoot apices grown at 15°C and 25°C (false discovery rate < 0.01).

Gene ID		Category of transcription factor	Preferential expression	Expression (FPKM)		BLAST best-hit Arabidopsis gene	Arabidopsis gene symbol
Gene model v0.1	Gene model v3			15° C	25°C		
CUFF.11161	Cfol_v3_34753	ABI3VP1	25°C	7.26	16.55	AT3G18990	VRN1, REM39
CUFF.17810	Cfol_v3_29939	ABI3VP1	25°C	0.03	1.05	AT1G19850	MP, ARF5, IAA24
CUFF.1853	Cfol_v3_21073	ABI3VP1	15°C	7.94	3.52	AT3G42170	NA
CUFF.8051	Cfol_v3_25935	ABI3VP1	25°C	1.52	3.41	AT3G15880	WSIP2, TPR4
CUFF.18172	Cfol_v3_07685	AP2-EREBP	25°C	102.62	218.47	AT3G16770	RAP2.3, ATEBP, ERF72, EBP
CUFF.21542	Cfol_v3_04988	AP2-EREBP	15°C	2.37	0.01	AT3G23220	NA
CUFF.31380	Cfol_v3_14868	AP2-EREBP	15°C	20.33	9.80	AT2G28550	RAP2.7
CUFF.31958	Cfol_v3_22947	AP2-EREBP	25°C	4.52	12.97	AT5G51190	NA
CUFF.35163	Cfol_v3_03736	AP2-EREBP	15°C	0.98	0.09	AT5G61890	NA
CUFF.36234	Cfol_v3_15578	AP2-EREBP	15°C	31.66	14.32	AT5G61890	NA
CUFF.44805	Cfol_v3_27246	AP2-EREBP	25°C	24.76	49.32	AT4G34100	NA
CUFF.9483	Cfol_v3_13942	AP2-EREBP	25°C	0.04	0.17	AT2G20880	NA
CUFF.13306	Cfol_v3_35179	ARF	25°C	16.88	42.95	AT4G23980	ARF9
CUFF.179	Cfol_v3_11188	ARID	25°C	1.54	4.41	AT1G04880	NA
CUFF.27297	Cfol_v3_19684	AUX/IAA	25°C	1.20	3.28	AT1G77690	LAX3
CUFF.29399	Cfol_v3_09125	bHLH	15°C	0.19	0.04	AT2G34820	NA
CUFF.35155	Cfol_v3_19413	bHLH	15°C	0.10	0.00	AT3G21330	NA
CUFF.36723	Cfol_v3_05371	bHLH	15°C	5.11	0.21	AT4G25410	NA
CUFF.38360	Cfol_v3_02953	bHLH	15°C	4.71	2.23	AT2G41130	NA
CUFF.42546	Cfol_v3_08635	bHLH	15°C	0.23	0.02	AT4G37850	NA
CUFF.6475	Cfol_v3_33109	bHLH	25°C	5.02	11.39	AT5G46690	bHLH071
CUFF.20117	Cfol_v3_02840	bZIP	15°C	6.28	2.72	AT1G77920	NA
CUFF.28497	Cfol_v3_21448	bZIP	25°C	1.64	4.30	AT2G36270	ABI5, GIA1
CUFF.12768	Cfol_v3_08856	C2C2	25°C	0.00	0.09	AT2G15740	NA
CUFF.13418	Cfol_v3_12598	C2C2	25°C	0.07	0.74	AT4G17810	NA
CUFF.18753	Cfol_v3_28711	C2C2	15°C	6.67	2.98	AT3G57670	NTT, WIP2
CUFF.24619	Cfol_v3_03127	C2C2	15°C	0.57	0.19	AT5G57520	ZFP2, ATZFP2
CUFF.39229	Cfol_v3_02315	C2C2	15°C	2.12	0.57	AT1G24625	ZFP7
CUFF.44362	Cfol_v3_13123	C2C2	15°C	44.22	23.98	AT2G36930	NA
CUFF.788	Cfol_v3_14165	C2C2	15°C	3.71	0.60	AT5G48890	NA
CUFF.25213	Cfol_v3_29925	C2C2-CO-like	25°C	16.50	37.47	AT1G25440	NA
CUFF.41689	Cfol_v3_20699	C2C2-CO-like	25°C	0.69	1.90	AT1G28050	NA
CUFF.6399	Cfol_v3_14844	C2C2-CO-like	25°C	6.01	17.15	AT1G28050	NA
CUFF.12869	Cfol_v3_28018	C2C2-GATA	25°C	0.73	2.06	AT3G60530	GATA4
CUFF.17562	Cfol_v3_25951	C2C2-YABBY	25°C	82.90	211.45	AT2G26580	YAB5

CUFF.29030	Cfol_v3_07401	C2C2-YABBY	25°C	0.23	2.38	AT1G08465	YAB2
CUFF.32963	Cfol_v3_24602	C3H	15°C	328.88	160.43	AT3G26420	ATRZ-1A
CUFF.35746	Cfol_v3_05310	C3H	25°C	3.80	17.00	AT5G42820	ATU2AF35B, U2AF35B
CUFF.1058	Cfol_v3_06753	CCAAT	15°C	724.57	394.65	AT1G08880	HTA5, H2AXA, G-H2AX, GAMMA-H2AX
CUFF.42840	Cfol_v3_33528	CCAAT	25°C	0.12	0.52	AT1G56170	HAP5B, ATHAP5B, NF-YC2
CUFF.6158	Cfol_v3_29281	CCAAT	15°C	57.58	23.14	AT4G02570	ATCUL1, CUL1, AXR6
CUFF.4303	Cfol_v3_11573	DBP	15°C	24.60	12.68	AT2G25620	AtDBP1, DBP1
CUFF.13422	Cfol_v3_31530	G2-like	15°C	2.34	0.57	AT1G14600	NA
CUFF.6655	Cfol_v3_04861	G2-like	25°C	2.38	6.58	AT1G14600	NA
CUFF.3677	Cfol_v3_19640	GRAS	25°C	0.71	1.96	AT1G50420	SCL3, SCL-3
CUFF.7061	Cfol_v3_02255	GRAS	25°C	1.07	3.26	AT3G49950	NA
CUFF.44756	Cfol_v3_32314	GRF	25°C	6.33	13.92	AT4G24150	AtGRF8, GRF8
CUFF.14252	Cfol_v3_15571	H2C2	25°C	0.00	0.05	NA	NA
CUFF.19817	Cfol_v3_10837	HB	25°C	1.81	4.69	AT2G01430	ATHB17, ATHB-17, HB17
CUFF.27008	Cfol_v3_06122	HB	15°C	17.48	8.02	AT4G08150	KNAT1, BP, BP1
CUFF.36896	Cfol_v3_11774	HB	25°C	1.29	6.01	AT4G36870	BLH2, SAW1
CUFF.44466	Cfol_v3_01962	HB	25°C	0.00	0.07	AT1G73360	HDG11, EDT1, ATHDG11
CUFF.44479	Cfol_v3_29639	HB	15°C	0.45	0.14	AT3G03660	WOX11
CUFF.4460	Cfol_v3_23111	HB	25°C	1.94	4.44	AT1G62990	KNAT7, IXR11
CUFF.9128	Cfol_v3_27227	HB	25°C	0.34	1.36	AT3G18010	WOX1
CUFF.21732	Cfol_v3_25584	HSF	25°C	8.29	25.36	AT3G24520	AT-HSFC1, HSFC1
CUFF.2284	Cfol_v3_31350	HSF	25°C	0.71	3.70	AT3G22830	AT-HSFA6B, HSFA6B
CUFF.28449	Cfol_v3_16791	Jumonji	25°C	2.77	6.38	AT1G11950	NA
CUFF.3504	Cfol_v3_13834	LOB	25°C	0.00	0.12	AT3G58190	LBD29, ASL16
CUFF.35874	Cfol_v3_32472	LOB	25°C	0.08	0.33	AT5G66870	ASL1, LBD36
CUFF.44243	Cfol_v3_25373	LOB	25°C	1.38	5.58	AT1G65620	AS2
CUFF.6474	Cfol_v3_34919	LOB	15°C	2.37	0.49	AT2G45410	LBD19
CUFF.18668	Cfol_v3_16164	LUG	15°C	27.87	4.12	AT1G52360	NA
CUFF.24672	Cfol_v3_18231	MADS	15°C	1.64	0.34	AT2G14210	ANR1, AGL44
CUFF.28288	Cfol_v3_15676	MADS	15°C	26.52	12.69	AT3G54340	AP3, ATAP3
CUFF.29046	Cfol_v3_07391	MADS	25°C	0.06	0.22	AT2G40210	AGL48
CUFF.29048	Cfol_v3_07392	MADS	25°C	0.04	0.26	AT5G48670	FEM111, AGL80
CUFF.33415	Cfol_v3_22117	MADS	15°C	0.24	0.04	AT5G60440	AGL62
CUFF.34813	Cfol_v3_31429	MADS	25°C	0.02	0.17	AT2G34440	AGL29
CUFF.38728	Cfol_v3_13348	MADS	25°C	0.01	0.14	AT1G69120	AP1, AGL7
CUFF.39623	Cfol_v3_22971	MBF1	25°C	2.66	11.70	AT3G24500	MBF1C, ATMBF1C
CUFF.22626	Cfol_v3_17920	MYB	25°C	1.91	6.03	AT4G21440	ATMYB102, ATM4, MYB102

CUFF.26365	Cfol_v3_14676	MYB	15°C	0.91	0.25	AT5G16770	AtMYB9, MYB9
CUFF.2910	Cfol_v3_12526	MYB	15°C	1.18	0.46	AT3G50060	MYB77
CUFF.3472	Cfol_v3_24589	MYB	25°C	0.09	0.30	AT3G53200	AtMYB27, MYB27
CUFF.38625	Cfol_v3_05696	MYB	25°C	0.14	0.65	AT5G57620	MYB36, AtMYB36
CUFF.41502	Cfol_v3_15158	MYB	15°C	1.20	0.34	AT3G06490	MYB108, AtMYB108, BOS1
CUFF.32151	Cfol_v3_32210	NAC	15°C	21.93	10.18	AT5G13180	ANAC083, VNI2, NAC083
CUFF.32258	Cfol_v3_15432	NAC	15°C	23.70	12.10	AT1G01720	ATAF1, ANAC002
CUFF.3681	Cfol_v3_34600	NAC	15°C	1.85	0.35	AT3G15510	ATNAC2, ANAC056, NARS1, NAC2
CUFF.43502	Cfol_v3_08267	NAC	15°C	14.72	7.60	AT3G10490	ANAC052, NAC052
CUFF.29129	Cfol_v3_07368	Orphans	25°C	0.21	1.33	AT5G26594	ARR24, RR24
CUFF.29131	Cfol_v3_07368	Orphans	25°C	0.01	0.08	AT5G26594	ARR24, RR24
CUFF.34849	Cfol_v3_04144	Orphans	25°C	11.35	26.01	AT1G29170	WAVE2, ATSCAR3, SCAR3
CUFF.6985	Cfol_v3_19374	Orphans	15°C	14.77	7.63	AT4G38960	NA
CUFF.10346	Cfol_v3_15495	PHD	25°C	7.56	16.95	AT1G33420	NA
CUFF.39914	Cfol_v3_04092	PHD	25°C	1.92	5.06	AT2G31650	ATX1, SDG27
CUFF.44489	Cfol_v3_15652	PHD	25°C	5.06	11.67	AT4G22140	EBS
CUFF.702	Cfol_v3_13295	PLATZ	15°C	1.05	0.18	AT5G46710	NA
CUFF.39695	Cfol_v3_14875	pseudo-ARR-B	25°C	7.61	18.00	AT5G02810	PRR7, APRR7
CUFF.608	Cfol_v3_06893	SBP	25°C	3.41	7.23	AT5G18830	SPL7
CUFF.10792	Cfol_v3_05277	SET	15°C	5.33	1.53	AT5G17240	SDG40
CUFF.27299	Cfol_v3_19692	SET	25°C	0.18	0.84	AT2G17900	SDG37
CUFF.16116	Cfol_v3_32785	SNF2	25°C	5.98	12.74	AT3G57300	INO80
CUFF.31308	Cfol_v3_03338	SNF2	25°C	0.15	0.61	AT1G24480	NA
CUFF.36691	Cfol_v3_06912	SNF2	25°C	2.76	6.76	AT2G28290	SYD, CHR3
CUFF.36362	Cfol_v3_17227	SWI-SNF-BAF 60b	15°C	125.62	73.54	AT2G14880	NA
CUFF.41642	Cfol_v3_10017	SWI-SNF-SWI3	25°C	0.68	3.30	AT1G67370	ASY1, ATASY1
CUFF.11491	Cfol_v3_25758	TCP	15°C	1.92	0.37	AT3G18550	BRC1, TCP18, ATTCP18
CUFF.28328	Cfol_v3_19463	TCP	15°C	2.56	1.01	AT3G15030	TCP4, MEE35
CUFF.41697	Cfol_v3_33820	TCP	25°C	0.02	0.14	AT1G67260	TCP1
CUFF.4500	Cfol_v3_07560	TCP	25°C	0.32	1.21	AT3G15030	TCP4, MEE35
CUFF.34261	Cfol_v3_32601	Tify	15°C	0.08	0.00	AT1G30135	JAZ8, TIFY5A
CUFF.36214	Cfol_v3_14971	Tify	15°C	3.12	1.32	AT5G13220	JAZ10, TIFY9, JAS1
CUFF.36858	Cfol_v3_04949	Tify	15°C	4.98	0.21	AT1G72450	JAZ6, TIFY11B
CUFF.21373	Cfol_v3_17440	Trihelix	25°C	7.46	20.01	AT2G35640	NA
CUFF.36011	Cfol_v3_07330	Trihelix	25°C	6.79	17.28	AT3G10040	NA
CUFF.39979	Cfol_v3_27116	WRKY	15°C	13.48	4.50	AT2G47260	WRKY23, ATWRKY23
CUFF.40682	Cfol_v3_14929	WRKY	15°C	1.76	0.48	AT1G80840	WRKY40, ATWRKY40
CUFF.20650	Cfol_v3_35810	zf-HD	15°C	0.13	0.02	AT1G14440	AtHB31, HB31, ZHD4

CUFF.23909	Cfol_v3_25181	zf-HD	25°C	0.00	0.06	AT3G28917	MIF2

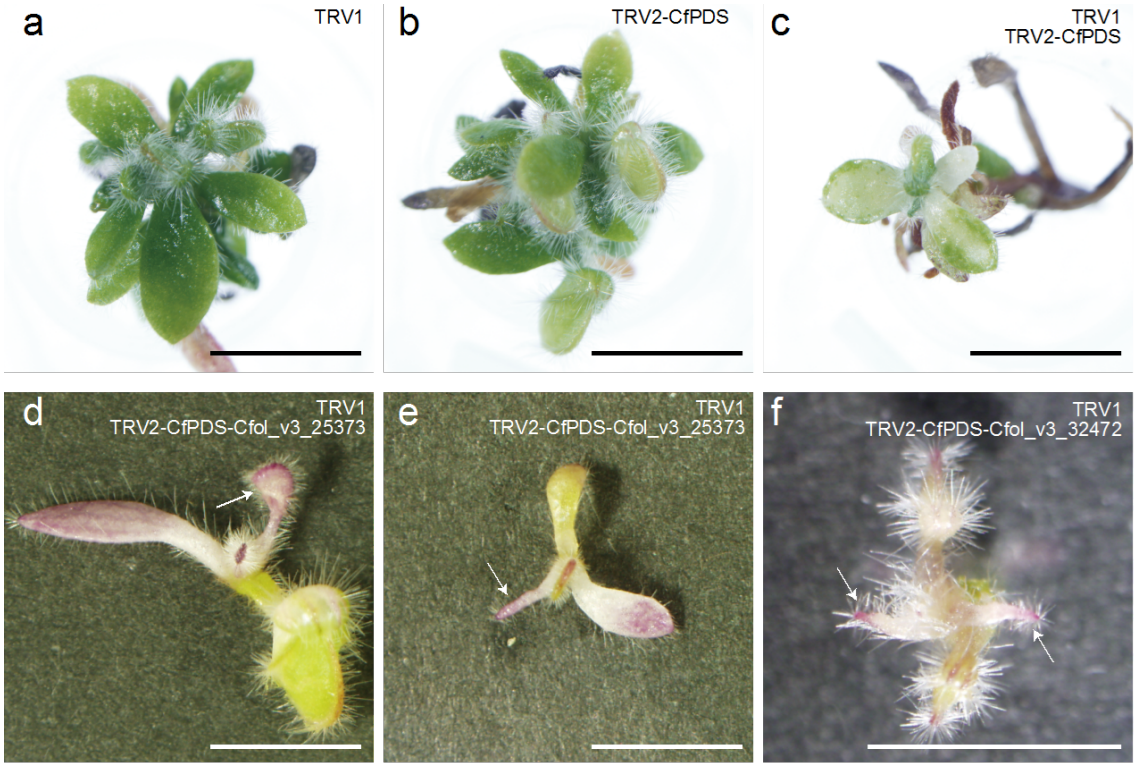

Figure 4.7. Examples of knockdown phenotypes observed in VIGS screening. Plasmid vectors of TRV1 (**a**), TRV2-CfPDS (**b**), TRV1 and TRV2-CfPDS (**c**), TRV1 and TRV2-CfPDS-Cfol_v3_25373 (**d,e**), and TRV1 and TRV2-CfPDS-Cfol_v3_32472 (**f**) were introduced into Cephalotus plants and cultured for one to two months at 25°C. Gene silencing of *CfPDS* is observed as photobleaching of leaves. Cfol_v3_25373 and Cfol_v3_32472 encode LOB-domain proteins. Arrows indicate malformed leaves with ensiform morphology (**d**) and cylindrical shape (**e,f**). Bars represent 5 mm.

4.4 Discussion

In this study, I established culture conditions for leaf fate control of Cephalotus (Fig. 4.2). Cultivation at different temperatures induced distinct types of leaves: flat leaves at 15°C and pitcher leaves at 25°C. Although the *in vitro* culture conditions are substantially different from natural environmental conditions, these results are concordant with previous observation in native habitats where these plants produce flat leaves in spring and pitcher leaves later in summer (Pavlovič 2011). Since photoperiod also affected the leaf dimorphism (Fig. 4.2), Cephalotus is likely to integrate multiple environmental cues to determine leaf fates.

I also established a knockdown technique of this plant using *TRV* (Fig. 4.1 and 4.7), which is a Geminivirus that can infect a broad range of eudicot plants (Becker and Lange 2010). VIGS using *TRV* allows transient knockdown, and therefore offers an opportunity to examine functions of Cephalotus genes. One advantage of this method is its simple handling. Unlike Agrobacterium-mediated transformation, VIGS does not require callus formation or plant regeneration. The short timeframe for VIGS experiments would be advantageous for large-scale knockdown experiments.

In addition, my collaborators and I sequenced the genome and transcripts of this species (Fig. 4.3, 4.4 and 4.6; Table 4.4 and 4.7). Distribution of gene lengths (Fig. 4.5) and coverage of essential genes (Table 4.8) suggest that the genome assembly and gene models successfully recover most of the genes in the genome. The number of genes in the Cephalotus genome is equivalent to those of other sequenced genomes in flowering plants (Table 4.7; Fig. 4.5), and it suggests that Cephalotus did not experience recent genome duplication. On the other hand, its large genome (2.11 Gb) is abundant in transposable elements (ca. 80% of the genome). Transposon-mediated recombination is a source of novel functional unit in a genome (Gray 2000). Therefore, the Cephalotus genome has a potential to generate a novel function by genomic rearrangements.

Knockdown screening of candidate genes identified genes that cause developmental defects of pitcher leaves under knockdown conditions (Fig. 4.7). Further functional analyses of candidate genes may give an insight into pitcher leaf evolution in Cephalotus.

5. MOLECULAR CONVERGENCE OF DIGESTIVE ENZYMES IN CARNIVOROUS PLANTS

5.1 Introduction

Convergence, in which a phenotypic similarity independently arises in different organisms, is a common evolutionary process across the entire tree of life (Futuyma 2009). Phenotypic convergence is often caused by similar or identical genetic changes under similar selective pressures, a process called adaptive molecular convergence (Stern 2013). For example, a combination of identical amino acid substitutions in the pancreatic RNases of independently evolved leaf monkeys conferred biochemical properties that allowed herbivory (Zhang 2006). Bats and toothed whales have echolocation abilities, and the genes involved in their auditory systems appear to have evolved convergently (Shen et al. 2012). The striking similarities of these molecular evolutionary patterns illustrate that a few accessible patterns of adaptive amino acid substitutions exist to achieve the same functional innovation of proteins.

Carnivorous plants, which degrade captured prey in trap leaves, evolved in five independent orders of flowering plants, and therefore, carnivory-related traits including digestive functions emerged in multiple lineages (Albert et al. 1992). For example, young traps of the carnivorous pitcher plant *Nepenthes* spp. maintain optimal fluid environments for digestion while avoiding microbial colonization, by accumulating antimicrobial molecules (Buch et al. 2013; Krolicka et al. 2008) and by acidifying the fluids to help digestion (An et al. 2001). A number of studies have successfully isolated genes encoding the digestive enzymes produced by various carnivorous plants (Table 5.1). For example, recent work employed mass spectrometry and transcriptome sequencing to identify 76 transcripts encoding secreted proteins from the digestive fluids of the Venus flytrap *Dionaea muscipula* (Schulze et al. 2012). However, previous studies focused on a specific species or a specific enzyme, and did not cover independently evolved lineages of carnivorous plants. Therefore, multiple comparisons of digestive enzymes from multiple carnivorous plant lineages are necessary to ascertain the genetic basis of convergent emergence of digestive enzymes. In this study, I identified digestive enzyme genes from *Cephalotus follicularis*, *Drosera adelae*, *Nepenthes alata*, and *Sarracenia purpurea*, which cover three independent carnivorous plant lineages, and compared their evolutionary trends. The origin and evolution of digestive enzymes are discussed.

Table 5.1. Previously identified secreted proteins in carnivorous plants.

Order	Species	Enzyme family	Enzyme	Evidence of secretion	GenBank accession	Reference
Oxalidales	*Cephalotus follicularis*	RNase T2	CF-I	Western blotting	AB811227 AB811228	Nishimura et al. 2013
Caryophyllales	*Dionaea muscipula*	GH19 chitinase	VF chitinase-I	Mass spectrometry	KF597524	Paszota et al. 2014
		RNase T2	DM-I	Western blotting	AB481098	Nishimura et al. 2013
		Cysteine protease	Dionain	Protein sequencing	-	Takahashi et al. 2011
	Drosera adelae	RNase T2	RNase DA-I	Protein sequencing	AB211503	Okabe et al. 2005
	Nepenthes gracilis	Aspartic protease	nepenthesin I	Protein sequencing	AB114914	Athauda et al. 2004
		Aspartic protease	nepenthesin II	Protein sequencing	AB114915	Athauda et al. 2004
	Nepenthes mirabilis	PR-1	NEMI1	Protein sequencing	GQ337079	Buch et al. 2014
	Nepenthes rafflesiana	Acidic chitinase	NrChit1	Protein sequencing	GQ338257	Rottloff et al. 2011
	Nepenthes alata	Aspartic protease	NaNEP1	Mass spectrometry	AB266803	Hatano and Hamada 2008
		Basic chitinase	NaCHIT1	Mass spectrometry	AB289807	Hatano and Hamada 2008
		Thaumatin-like protein	NaTLP1a	Mass spectrometry	AB267384	Hatano and Hamada 2008
			NaTLP1b	Mass spectrometry	AB267385	Hatano and Hamada 2008
			NaTLP1c	Mass spectrometry	AB267386	Hatano and Hamada 2008
		β-1,3-Glucanase	NaBGLUC1	Mass spectrometry	AB289559	Hatano and Hamada 2012
			NaBGLUC2	Mass spectrometry	AB518307	Hatano and Hamada 2012
		Acidic chitinase	NaCHIT3	Mass spectrometry	AB510164	Hatano and Hamada 2012
		Class III peroxidase	NaPrx1a	Mass spectrometry	AB476301	Hatano and Hamada 2012
			NaPrx1b	Mass spectrometry	AB476302	Hatano and Hamada 2012
			NaPrx1c	Mass spectrometry	AB476303	Hatano and Hamada 2012
Lamiales	ND					
Ericales	ND					
Poales	ND					

* ND means no data.

5.2 Materials and methods

Protein sequencing of digestive fluids. Digestive fluids of *C. follicularis*, *Dr. adelae*, *N. alata*, and *S. purpurea* were collected from soil-grown plants in a greenhouse. Fluids were freeze-dried and stored at room temperature. Dried samples were dissolved in protease inhibitor cocktail (cOmplete, Mini, EDTA-free, Roche), precipitated with 8% trichloroacetic acid (TCA), and then washed with 90% acetone. They were dissolved in SDS sample buffer (62.5 mM Tris-HCl, 2% SDS, 0.25% BPB, 10% glycerol, 5% 2-mercaptoethanol, pH 6.8), denatured at 95°C for 3 min, and then separated by 12% SDS-polyacrylamide gel electrophoresis. Negative staining was performed using the Gel-Negative Stain Kit (Nacalai tesque) according to manufacturer's instructions. After destaining, proteins were transferred to polyvinylidene difluoride (PVDF) membrane. N-terminal sequences of each protein band were determined by the Edman degradation method using ABI Procise 494-HT (Applied Biosystems). To obtain internal protein sequences, protein bands were dissected from the gel, destained, dehydrated with 100% acetonitrile for 5 min, dried using an evaporator, and then deoxidated by incubating in10 mM DTT and 25 mM ammonium bicarbonate at 56°C for 60 min. After washing with 25 mM ammonium bicarbonate, the proteins were alkylated in 55 mM iodoacetamide and 25 mM ammonium bicarbonate for 45 min at room temperature. After washing with 50% acetonitrile containing 25 mM ammonium bicarbonate, the samples were dried using an evaporator. The proteins were in-gel-digested with 10 ng/μg trypsin in 50 mM ammonium bicarbonate, 10 ng/μl lysyl endopeptidase in 25 mM Tris-HCl (pH 9.0) or 20 ng/μl V8 protease in 50 mM phosphate buffer (pH7.8) at 37°C overnight. The digested peptides were extracted twice by sonication in 50% acetonitrile containing 5% trifluoroacetic acid (TFA) for 10 min. The peptides were separated by high-performance liquid chromatography (HPLC) using Pharmacia SMART System and a reverse-phase column (μRPC C2/C18 PC 3.2/3, GE Healthcare Life Sciences or XBridge C8 5μm 2.1×100mm, Waters) under the following conditions: constant flow rate of 200 μl/min; solvent A, 0.5% TFA, solvent B, acetonitrile containing 0.5% TFA; linear gradient from 10 to 40% [B over A in % (v/v)] in 30 min (1%/min). Separated peptides were then used for protein sequencing by the Edman degradation method.

Transcriptome assembly and identification of transcripts encoding secreted proteins. RNA-seq reads of *Dr. adelae*, *N. alata*, and *S. purpurea* were assembled into transcripts by Trinity (version r2013-02-25, Grabherr et al. 2011) with 200 bp minimum contig length cutoff. Partial amino acid sequences of secreted proteins were subjected to TBLASTN searches (Altschul et al. 1990) against the transcriptome assemblies to identify the corresponding transcript.

Phylogenetic analyses. Phylogenetic relationships of digestive enzyme genes were examined with their homologs in the annotated genomes of *Arabidopsis thaliana* (TAIR10, Swarbreck et al. 2008), *Populus trichocarpa* (v3, Tuskan et al. 2006), *Mimulus guttatus* (v2.0, distributed by Department of Energy Joint Genome Institute [JGI] at http://www.jgi.doe.gov/), *Solanum lycopersicum* (ITAG2.3, Tomato Genome Consortium 2012), *Fragaria vesca* (v1.1, Shulaev et al. 2011), *Theobroma cacao* (v1.1, Argout et al. 2011), *Glycine max* (v1.1, Schmutz et al. 2010), and *Aquilegia coerulea* (v1.1, distributed by JGI). Coding sequence (CDS) datasets were obtained from The Arabidopsis Information Resource (TAIR, http://www.arabidopsis.org/), and Phytozome v9.1 (http://www.phytozome.net/). TBLASTX searches (Altschul et al. 1990) of digestive enzyme genes were performed against the above CDS datasets. After sequence retrieval, multiple alignments were prepared with MAFFT 6.956 (Katoh and Standley 2013), and ambiguous codons were removed using trimAl (Capella-Gutierrez et al. 2009) with the "gappyout" option implemented in Phylogears2-2.0.2013.03.15 (http://www.fifthdimension.jp/products/phylogears/). Phylogenetic trees were reconstructed by the maximum likelihood method using RAxML v8.0.26 (Stamatakis 2006) with the general time-reversible model of nucleotide substitution and four discrete gamma categories of rate heterogeneity (GTRGAMMA option). Support for nodes was estimated by rapid bootstrapping with 1000 replications.

Expression profiling of Arabidopsis genes. Affymetrix ATH1 (25K) microarray dataset of pathogen infection experiments were retrieved from AtGenExpress (http://www.weigelworld.org/resources/microarray/AtGenExpress/). The dataset covers gene expression after inoculation of *Pseudomonas syringae* pv. tomato (Pst) avrRpm1, Pst DC3000, Pst DC3000 hrcC-, *Pseudomonas syringae* pv. *phaseolicola*, and *Phytophthora infestans*. According to the gene classification in GreenPhyl v4 (Rouard et al. 2011), expression profiles of specific gene families were examined. GreenPhyl gene family ID of acidic chitinases, basic chitinases, β-1,3-glucanases, purple acid phosphatases, RNase T2, and thaumatin-like proteins are GP015464, GP015301, GP015069, GP000169, GP104239, and GP000141, respectively. The heatmap was drawn using the R package 'gplots'. Dendrograms are drawn by furthest neighbor method with Euclidian distances.

Evaluation of detection methods for molecular convergence. Since heavily converged genes attract each other in standard phylogenetic inferences and this results in underestimation of convergent substitutions (Christin et al. 2012), our analysis required another method that is robust to such topological disturbance. Given that molecular convergence is driven by selective pressure, less-selected information such as synonymous substitution distance, 3rd codon tree, and species tree are potentially useful.

To evaluate different tree reconstruction methods, simulated gene sequences were generated using the R package Phylosim (Sipos et al. 2011). I used publicly available simulated datasets for 16 fungi species (Rasmussen and Kellis 2011; Wu et al. 2013). This dataset contains 1000 simulated tree topologies of gene families, each of which is generated under different gene duplication and loss rates. Sequences of 300 codons were simulated on the tree topologies of the "fungi" dataset. Codon usage was sampled from actual frequency of *Saccharomyces cerevisiae* (Nakamura et al. 2000). κ (transition/transversion rate) was set to 1. ω (dN/dS rate) of each codon position was randomly sampled from a gamma distribution (shape = 0.5, rate = 1). To mimic molecular convergence, 2 to 4 genes were randomly selected to be converged. In terminal branches of selected genes, codon usage of *S. cerevisiae* was replaced with a biased matrix in which frequencies of codons coding for two randomly selected amino acids were increased. Increased frequency was calculated by multiplying the original value by 100, and then total frequencies of all codons were scaled to 1 in total.

Gene trees were inferred by the maximum-likelihood method using third codons (3rd-ML) or neighbor-joining method using a distance matrix of estimated synonymous substitution (dS-NJ). The 3rd-ML was generated using RAxML v8.0.26 (Stamatakis 2014). To obtain robust tree topology, the gene trees were reconciled with the species tree. 3rd-ML tree was reconciled with the species tree using Treefix 1.1.10, which incorporates duplication-loss parsimony and a test statistic for likelihood equivalence (Wu et al. 2013). Reconciliation was made with default settings in which 1,000 iterations were performed and rearrangements were accepted when likelihood was not significantly reduced by Shimodaira-Hasegawa test (threshold $P = 0.05$) (Shimodaira and Hasegawa 1999). To obtain the dS-NJ tree, a synonymous substitution distance matrix was generated with 1,000 bootstrapping by yn00 of PAML 4.7 (Yang 2007; Yang and Nielsen 2000), and topology was reconstructed using phylip 3.69 (Felsenstein 1989). The dS-NJ tree was reconciled with the species tree using NOTUNG 2.6, which incorporates duplication-loss parsimony (Chen et al. 2000). Reconciliation was made with "rearrange" mode in which the bootstrap threshold to be rearranged was set to <70. Branch lengths of reconciled trees were optimized using RAxML v8.0.26. Finally, the number of convergent and divergent substitutions were estimated with reconciled trees and original simulated alignments using CodeMLancestral (Castoe et al. 2009).

Detection of molecular convergence in digestive enzymes. Digestive enzyme genes identified in this study (Table 5.2-5.5) and previous work (Table 5.1) were analyzed. As an initial gene tree, a 3rd-ML tree was reconstructed. A dated large-scale phylogeny (Bell et al. 2010) was used as the species tree of flowering plants covering all lineages of carnivorous plants. The reconciled 3rd-ML and species tree was used as the tree topology in Bayesian ancestral state reconstruction and convergence quantification using CodeMLancestral (Castoe et al. 2009). Neutral background of convergent changes was expected by a linear model in which the numbers of convergent changes

was predicted by divergent changes (Castoe et al. 2009). Overaccumulation of convergent changes was examined by one-sided G-test.

Homology modeling of protein structures. Protein structures of digestive enzymes were constructed using SWISS-MODEL Workspace (Biasini et al. 2014). Template models were selected using "Template Identification" tool. SMTL IDs of selected templates were 2dkv.1.A, 3zk4.1.A, and 1iyb.1.A, for basic chitinases, purple acid phosphatases, and RNase T2, respectively. Predicted models were visualized using UCSF Chimera 1.10 (Pettersen et al. 2004). Relative exposure of amino acid surface was calculated by dividing solvent-excluded surface in protein structures by that of corresponding amino acids in Gly-X-Gly tripeptide contexts (Bendell et al. 2014).

5.3 Results

Identification of digestive enzyme genes. To understand the repeated origins of digestive functions in flowering plants, I analyzed digestive enzymes of four carnivorous plants (Fig. 5.1) that cover at least three lineages with different origins of carnivory. My colleagues and I first determined the partial amino acid sequences of secreted proteins in digestive fluids, and then identified the corresponding genes by transcriptome sequencing of trap leaves. As a result we identified 12, 9, 10, and 6 genes from *C. follicularis* (Table 5.2), *Dr. adelae* (Table 5.3), *N. alata* (Table 5.4), and *S. purpurea* (Table 5.5), respectively. Gene family classification of identified genes was performed by BLAST searches against the GreenPhyl database (Rouard et al. 2011). The results showed that among the 36 identified genes, 27 encode hydrolytic enzymes (Table 5.2-5.5).

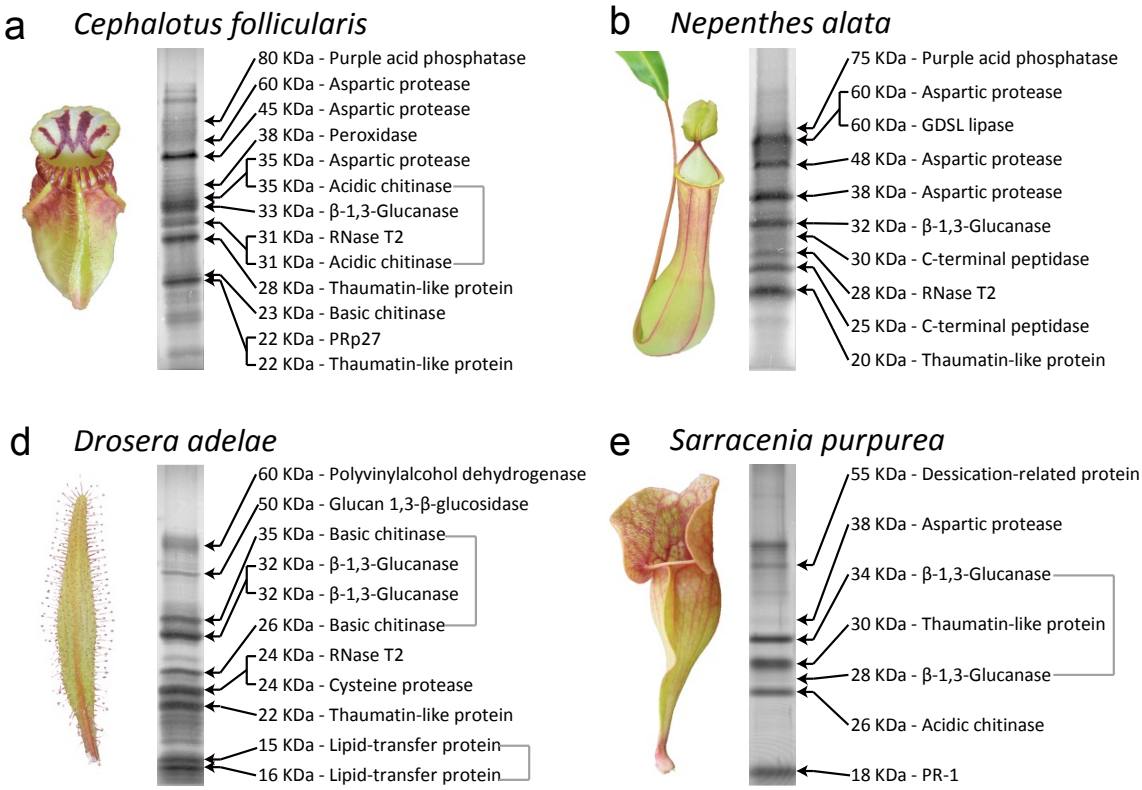

Figure 5.1. Protein compositions of digestive fluids. Secreted fluids of *Cephalotus follicularis* (a), *Nepenthes alata* (b), *Drosera adelae* (c), and *Sarracenia purpurea* (d) were analyzed. Negative-stained SDS-PAGE gels are shown. Band positions of identified proteins are indicated by arrows. Gray brackets denote protein bands originating from an identical gene.

Table 5.2. Identified digestive enzymes of *Cephalotus follicularis.*

Protein	MW (kDa)	Gene ID (gene model v3)	Peptide position / digestion method	Peptide identity [1] (1.Determined AA) (2.Match) (3.Translated gene)
Purple acid phosphatase	80	Cfol_v3_19644	N-terminal / -	INcPNLNPXRQMTIxSsnfPL ******** ***** *** ** INCPNLNPYRQMTINSSN-PL
Aspartic protease	60	Cfol_v3_21613	N-terminal / -	DKKMNGFSVELIHRDSPK ****************** DKKMNGFSVELIHRDSPK
Aspartic protease	45	Cfol_v3_23936	N-terminal / -	DIQAPMYFPGGGGEYLIEFGM ********************** DIQAPMYFPGGGGEYLIEFGM
			Internal / V8 protease	TALTNSISAQPVSDPSGSGLSPCYNSDGIQFPxAaVQFTN ******************************** ******* TALTNSISAQPVSDPSGSGLSPCYNSDGIQFPSAAVQFTN
Class III peroxidase	38	Cfol_v3_02176	Internal / lysylendopeptidase	XXXLLHSDQQLYNGGSTDs *************** EEGLLHSDQQLYNGGSTDS
			Internal / lysylendopeptidase	XXXcpSTAGsGDDNlAPLDV ***************** KKSCPSTAGSGDDNLAPLDV
Aspartic protease	35	Cfol_v3_33064	N-terminal / -	FEKGITqVPLKNFMDTVYYGEIGPgTP ********************** *** FEKGITQVPLKNFMDTVYYGEIGIGTP
			Internal / trypsin	IAYGSGYVLGYFSQDDL ***************** IAYGSGYVLGYFSQDDL
			Internal / lysylendopeptidase	RQDFTETLFESGFSGLPXDGILGLAFPxIxV **************** ********* * * RQDFTETLFESGFSGLPSDGILGLAFPSISV
			Internal / lysylendopeptidase	EGYWQFAFK ********* EGYWQFAFK
			Internal / lysylendopeptidase	TSCPAIADTGTSLFTGPTDAINK ********************** TSCPAIADTGTSLFTGPTDAINK
Acidic chitinase	35 & 31 [2]	Cfol_v3_20843	N-terminal / -	GGIAIYWGQNenEGTLa ***************** GGIAIYWGQNENEGTLA
β-1,3-Glucanase	33	Cfol_v3_33636	Internal / lysylendopeptidase	nNGGSLGIVVSETGwPTDGGAA ********************** NNGGSLGIVVSETGWPTDGGAA
			Internal / lysylendopeptidase	HWGLFYPDRGPK ********* ** HWGLFYPDRSPK
RNase T2	31	Cfol_v3_19641	N-terminal / -	FDFFYFVQQWPgSYxDTS ************* *** FDFFYFVQQWPGSYCDTS
Thaumatin-like protein	28	Cfol_v3_29167	N-terminal / -	ATVTITNNcPYTIWPATLTGGGgNQLSTT **************************** ATVTITNNCPYTIWPATLTGGGGNQLSTT
Basic chitinase	23	Cfol_v3_22778	Internal / lysylendopeptidase	NFYTRDAFLTAANYYSGFATGGSAD ***** ****************** NFYTRGAFLTAANYYSGFATGGSAD
PRp27	22	Cfol_v3_08624	N-terminal / -	VNYVVTNNARNTAGGVRFDNEIgADYSR **************************** VNYVVTNNARNTAGGVRFDNEIGADYSR
Thaumatin-like protein	22	Cfol_v3_18289	N-terminal / -	ANFNIVNNcPYTVWAAAVPGGGRQLNPGQTWSLDVNAGTag ** ANFNIVNNCPYTVWAAAVPGGGRQLNPGQTWSLDVNAGTAG

[1] Lower case in peptide sequences means low score in protein sequencing.
[2] Peptide fragments of the protein were detected from two different protein bands.

Table 5.3. Identified digestive enzymes of *Drosera adelae*.

Protein	MW (kDa)	Contig ID	Peptide position / digestion method	Peptide identity [1] (1.Determined AA) (2.Match) (3.Translated gene)
Polyvinylalcohol dehydrogenase	60	comp8359	Internal / trypsin	LGGYAGAAIWGSSPSIDVVR ********** LGGYAGAAIWGSSPSIDVVR
			Internal / trypsin	QLggYDVFY ********* QLGGYDVFY
			Internal / trypsin	DGFVWALERSsGDI ********** SGFVWALERSSGDI
Glucan 1,3-β-glucosidase	50	comp16664 & comp14244	Internal / V8 protease	DSPHVRGVNLGGWLVTEGFITPELFG ********** ******* DSPHVRGVNLGGWLVTEGWITPELFQ
			Internal / V8 protease	SQNGLNTVRVPVGwwIAYDPNPP ********** SQNGLNTVRVPVGWWIAYDPNPP
			Internal / trypsin	TEQNIQDTLHVIDFLANR ********** TEQNIQDTLHVIDFLANR
			Internal / lysyl endopeptidase	xxxxYVIWSARLGPADsREFL ********** YSNCYVIWSARLGPADSREFL
Basic chitinase	35 & 26 [2]	comp22438 & comp18618	N-terminal / -	GDVSSIITSQIFNQMLLHRNDNAxPaNxFYSYQafi ********** *** ******** GDVSSIITSQIFNQMLLHRNDNACPANGFYSYQAFI
			Internal / lysyl endopeptidase	NELAAFFGQTSHETTGGxStAPDxPYA ********** ***** *** NELAAFFGQTSHETTGGWSTAPDGPYA
			Internal / V8 protease	QGNPGDYcvPSSTYPcAPG ********** QGNPGDYCVPSSTYPCAPG
β-1,3-Glucanase	32	comp9359	N-terminal / -	IGTCYGMLGNdLPSPQRVVSDYnRYNi ********** IGTCYGMLGNDLPSPQRVVSDYNRYNI
		comp1331	Internal / lysyl endopeptidase	YIAVGNEIRPNNGASQYAPYVLPAMQNI ********** ********* YIAVGNEIRPNNGASQYAQYVLPAMQNI
RNase T2	24	comp10489	Internal / lysyl endopeptidase	SQANTLASLTNAGITPNNSFYNLSDVLAAIK ********** SQANTLASLTNAGITPNNSFYNLSDVLAAIK
Cysteine protease	24	comp5582	N-terminal / -	SVPASINWVTMGAVTPIRNQGTCGSxxAF ********** ** SVPASINWVTMGAVTPIRNQGTCGSCWAF
Thaumatin-like protein	22	comp168	N-terminal / -	ATFTITNNCPYTIWAAAVPGGG ********** ATFTITNNCPYTIWAAAVPGGG
Lipid-transfer protein	16 & 15 [2]	comp1614	N-terminal / -	AFIGYDwGTTFFYccKDYIQTGIDxALDYAccPVIaQFA ********** ********** AFIGYDWGTTFFYCCKDYIQTGIDCALDYACCPVIAQFA
			Internal / lysyl endopeptidase	DYIQTGIDCALDYACCPVIAQFAGAVNK ********** DYIQTGIDCALDYACCPVIAQFAGAVNK

[1] Lower case in peptide sequences means low score in protein sequencing.
[2] Peptide fragments of the protein were detected from two different protein bands.

Table 5.4. Identified digestive enzymes of *Nepenthes alata*.

Protein	MW (kDa)	Contig ID	Peptide position / digestion method	Peptide identity [1] (1.Determined AA) (2.Match) (3.Translated gene)
Purple acid phosphatase	75	comp20931	Internal / trypsin	TPLDPSIEHYIQPgAVsVIxa ****************** * TPLDPSIEHYIQPGAVSVIQA
			Internal / trypsin	TPPAgGSNELtFLAFADM ****************** TPPAGGSNELTFLAFADM
Aspartic protease	60	comp3584	N-terminal / -	NGPSGVETPVYAGDGEYLMxLSIxTPAQPF ****************** *** ****** NGPSGVETPVYAGDGEYLMNLSIGTPAQPF
GDSL lipase	60	comp9476	N-terminal / -	EPQVPcFFIFGDSLaDNgnN ******************** EPQVPCFFIFGDSLADNGNN
Aspartic protease	48	comp9350	Internal / lysyl endopeptidase	XPLSLPSQLPVS *********** GPLSLPSQLPVS
Aspartic protease	38	comp8857	N-terminal / -	SGVQTPVYSGGGEFLMNIAIGEPpNYyRAIMDTg ********************************** SGVQTPVYSGGGEFLMNIAIGEPPNYYRAIMDTG
			Internal / trypsin	ESTSYSTLLMGSLADQLPVAIK ********************** ESTSYSTLLMGSLADQLPVAIG
			Internal/ trypsin	MQVVYDLQNQLLGFTPT ***************** MQVVYDLQNQLLGFTPT
β-1,3-Glucanase	32	comp15862	N-terminal / -	RVGVCYGRNGNNLPxESQxV ************** * * * RVGVCYGRNGNNLPSEQQVV
			Internal / lysyl endopeptidase	NGGPLETYLFAMFDENQ ***************** KGGPLETYLFAMFDENQ
			Internal / lysyl endopeptidase	GSNIDLILDVPNDSLK **************** GSNIDLILDVPNDSLK
C-terminal peptidase	30	comp9476	N-terminal / -	SANTNHQYAVIAYFYGSASLQGAxATINIxnPT ********************** ***** *** SANTNHQYAVIAYFYGSASLQGANATINIWNPT
			Internal / trypsin	cYNYQFQQGSSELYLFYxgPG ****************** *** CYNYQFQQGSSELYLFYGGPG
RNase T2	28	comp3584	N-terminal / -	DYDFFYFVQQWPGSYxDTsE *************** **** DYDFFYFVQQWPGSYCDTSE
C-terminal peptidase	25	comp22917	Internal / trypsin	DLFYTEDTQNWVAVVA **************** DLFYTEDTQNWVAVVA
			Internal / V8 protease	ASYNNGHQYAVIHYFTQSQtIqGAqa ************************* ASYNNGHQYAVIHYFTQSQTIQGAQA
Thaumatin-like protein	20	comp3936	N-terminal / -	ATFVITNNcPYTVWAAASPGgGQQLNH ************************** ATFVITNNCPYTVWAAASPGGGQQLNH

[1] Lower case in peptide sequences means low score in protein sequencing.

Table 5.5. Identified digestive enzymes of *Sarracenia purpurea*.

Protein	MW (kDa)	Contig ID	Peptide position / digestion method	Peptide identity [1] (1.Determined AA) (2.Match) (3.Translated gene)
Desiccation-related protein	55	comp13116	N-terminal / -	TxLSCDPIYPPIKVPVSATDVELLQFAV * * ********** TNLTCDPIYPPIKVPVSATDVELLQFAV
			Internal / trypsin	ALLAGLLGVESGQDAVIR ********** ALLAGLLGVESGQDAVIR
Aspartic protease	38	Comp2140	N-terminal / -	VTLPAISGSSLGTGNYIVTiGLgSPxR ********** * VTLPAISGSSLGTGNYIVTIGLGSPKR
β-1,3-Glucanase	34 & 28 [2]	comp3326	N-terminal / -	PNPDALQALRxSNIEliLGVPNTxl ********** ********** * PNPDALQALRGSNIELILGVPNTDL
			Internal / lysyl endopeptidase	RMRLYDPNPDALQALRGSNIELILGVPNxDLQ ********** *** RMRLYDPNPDALQALRGSNIELILGVPNTDLQ
			Internal / V8 protease	SGWPSAGGGAATTVDNar ********** SGWPSAGGGAATTVDNAR
Thaumatin-like protein	30	comp1193	N-terminal / -	SIFTIKNNcPYTIYPATSTGQGSPASxTGFELV ********** ****** SIFTIKNNCPYTIYPATSTGQGSPASSTGFELV
Acidic chitinase	26	comp4791	N-terminal / -	GGIAIYWGQNGNEGTLAQTxATGRFSYVNIAFL ********** ********** GGIAIYWGQNGNEGTLAQTCATGRFSYVNIAFL
			Internal / lysyl endopeptidase	xVATYIWNNFLGGSSPSRPLxdAV ********** *** SVATYIWNNFLGGSSPSRPLGDAV
			Internal / lysyl endopeptidase	YGGVMLWLK ********* YGGVMLWLK
PR-1	18	comp817	Internal / trypsin	aqvgvgPISWDxNVAAYAQSYAN ********** ********** AQVGVGPISWDNNVAAYAQSYAN
			Internal / lysyl endopeptidase	gsgsftGTAAVNLWIGEK ********** GSGSFTGTAAVNLWIGEK
			Internal / trypsin	CNxGWWFISCNYDPPGNYVGQRPY ** ********** CNNGWWFISCNYDPPGNYVGQRPY

[1] Lower case in peptide sequences means low score in protein sequencing.
[2] Peptide fragments of the protein were detected from two different protein bands.

Functional origins of digestive enzymes. I found that the identified genes sometimes belonged to the same gene family even if they were isolated from independently evolved carnivorous plants. For example, *C. follicularis*, *N. alata*, and *S. purpurea* have aspartic proteases in their digestive fluids. Other than aspartic proteases, acidic chitinases, basic chitinases, β-1,3-glucanases, RNase T2, purple acid phosphatases, Class III peroxidases, and thaumatin-like proteins occur in at least two carnivorous plant lineages. To check the gene relationships, we reconstructed gene family-level phylogenetic trees of the digestive enzymes identified in this study (Table 5.2-5.5) and previous work (Table 5.1), and found orthologous relationships in six gene families amongst the eight families examined (Fig. 5.2a-c). I next examined the expression patterns of the Arabidopsis genes most closely related to the orthologous genes (Fig. 5.2d). Compared with other genes in the same families, such Arabidopsis genes showed a significant tendency to be up-regulated upon microbial infections (P = 2.2e-16, Wilcoxon rank sum test) (Fig. 5.3). This raises the possibility that the digestive enzyme genes were co-opted from ancestral genes that functioned in biological defense against pathogens, as previously suggested for some digestive enzymes (Hatano and Hamada 2008; Okabe et al. 2005; Rottloff et al. 2011) (reviewed in Mithofer 2011).

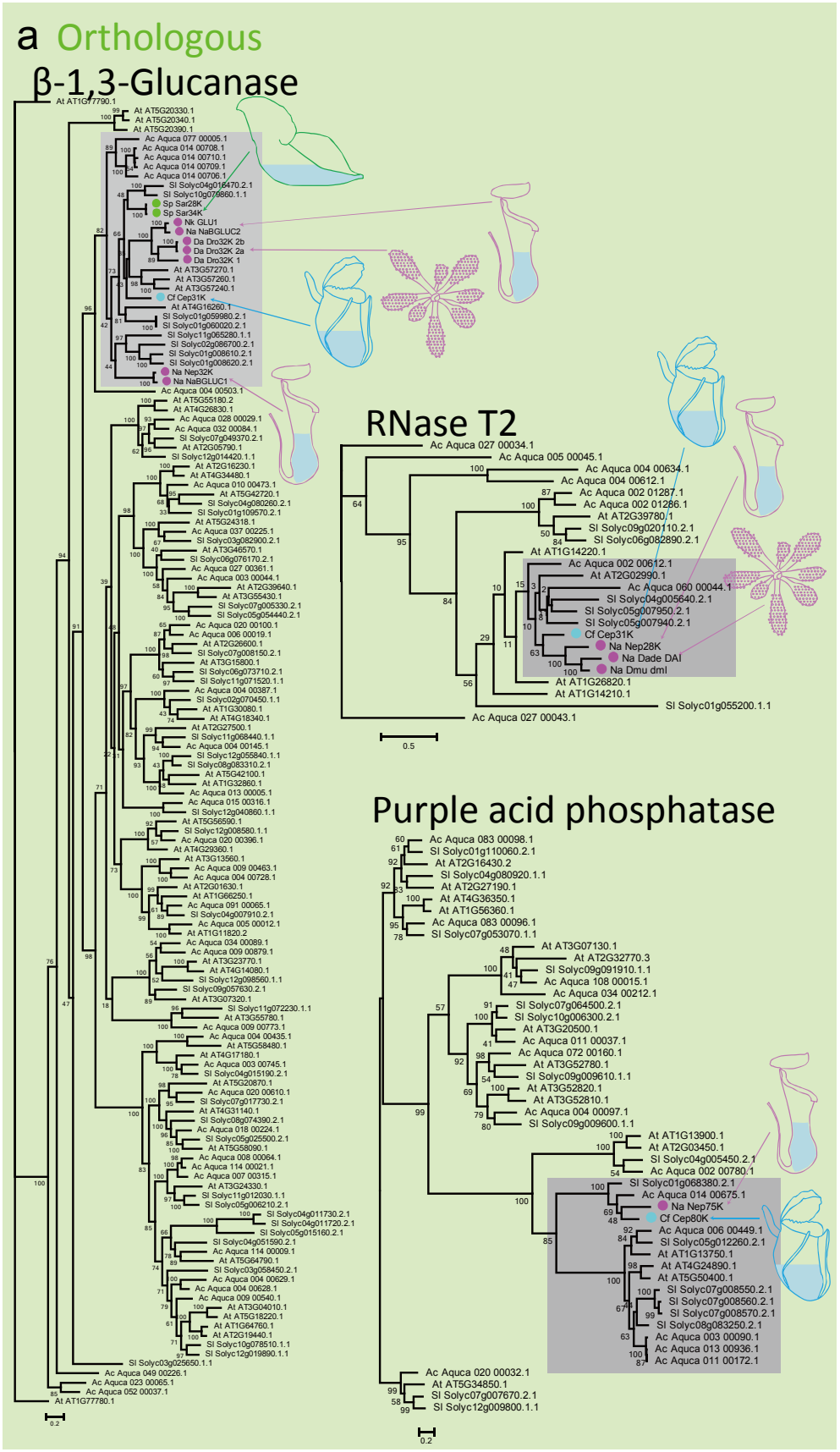
a Orthologous
β-1,3-Glucanase
RNase T2
Purple acid phosphatase

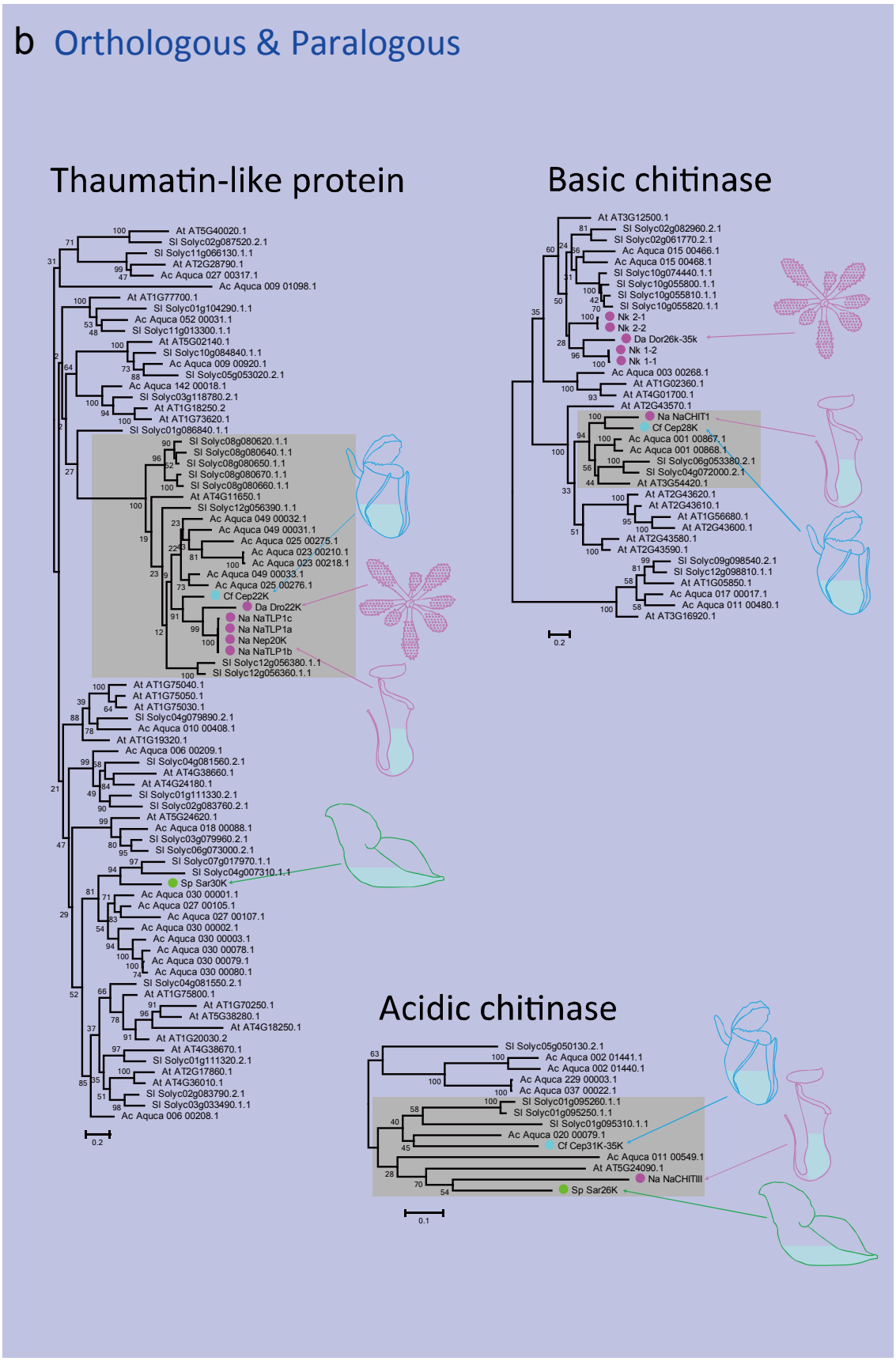
b Orthologous & Paralogous
Thaumatin-like protein
At AT5G40020.1
Sl Solyc02g087520.2.1
Sl Solyc11g066130.1.1
At AT2G28790.1
Ac Aquca 027 00317.1
Ac Aquca 009 01098.1
At AT1G77700.1
Sl Solyc01g104290.1.1
Ac Aquca 052 00031.1
Sl Solyc11g013300.1.1
At AT5G02140.1
Sl Solyc10g084840.1.1
Ac Aquca 009 00920.1
Sl Solyc05g053020.2.1
Ac Aquca 142 00018.1
Sl Solyc03g118780.2.1
At AT1G18250.2
At AT1G73620.1
Sl Solyc01g086840.1.1
Sl Solyc08g080620.1.1
Sl Solyc08g080640.1.1
Sl Solyc08g080650.1.1
Sl Solyc08g080670.1.1
Sl Solyc08g080660.1.1
At AT4G11650.1
Sl Solyc12g056390.1.1
Ac Aquca 049 00032.1
Ac Aquca 049 00031.1
Ac Aquca 025 00275.1
Ac Aquca 023 00210.1
Ac Aquca 023 00218.1
Ac Aquca 049 00033.1
Ac Aquca 025 00276.1
Cf Cep22K
Da Dro22K
Na NaTLP1c
Na NaTLP1a
Na Nep20K
Na NaTLP1b
Sl Solyc12g056380.1.1
Sl Solyc12g056360.1.1
At AT1G75040.1
At AT1G75050.1
At AT1G75030.1
Sl Solyc04g079890.2.1
Ac Aquca 010 00408.1
At AT1G19320.1
Ac Aquca 006 00209.1
Sl Solyc04g081560.2.1
At AT4G38660.1
At AT4G24180.1
Sl Solyc01g111330.2.1
Sl Solyc02g083760.2.1
At AT5G24620.1
Ac Aquca 018 00088.1
Sl Solyc03g079960.2.1
Sl Solyc06g073000.2.1
Sl Solyc07g017970.1.1
Sl Solyc04g007310.1.1
Sp Sar30K
Ac Aquca 030 00001.1
Ac Aquca 027 00105.1
Ac Aquca 027 00107.1
Ac Aquca 030 00002.1
Ac Aquca 030 00003.1
Ac Aquca 030 00078.1
Ac Aquca 030 00079.1
Ac Aquca 030 00080.1
Sl Solyc04g081550.2.1
At AT1G75800.1
At AT1G70250.1
At AT5G38280.1
At AT4G18250.1
At AT1G20030.2
At AT4G38670.1
Sl Solyc01g111320.2.1
At AT2G17860.1
At AT4G36010.1
Sl Solyc02g083790.2.1
Sl Solyc03g033490.1.1
Ac Aquca 006 00208.1
0.2
Basic chitinase
At AT3G12500.1
Sl Solyc02g082960.2.1
Sl Solyc02g061770.2.1
Ac Aquca 015 00466.1
Ac Aquca 015 00468.1
Sl Solyc10g074440.1.1
Sl Solyc10g055800.1.1
Sl Solyc10g055810.1.1
Sl Solyc10g055820.1.1
Nk 2-1
Nk 2-2
Da Dor26k-35k
Nk 1-2
Nk 1-1
Ac Aquca 003 00268.1
At AT1G02360.1
At AT4G01700.1
At AT2G43570.1
Na NaCHIT1
Cf Cep28K
Ac Aquca 001 00867.1
Ac Aquca 001 00868.1
Sl Solyc06g053380.2.1
Sl Solyc04g072000.2.1
At AT3G54420.1
At AT2G43620.1
At AT2G43610.1
At AT1G56680.1
At AT2G43600.1
At AT2G43580.1
At AT2G43590.1
Sl Solyc09g098540.2.1
Sl Solyc12g098810.1.1
At AT1G05850.1
Ac Aquca 017 00017.1
Ac Aquca 011 00480.1
At AT3G16920.1
0.2
Acidic chitinase
Sl Solyc05g050130.2.1
Ac Aquca 002 01441.1
Ac Aquca 002 01440.1
Ac Aquca 229 00003.1
Ac Aquca 037 00022.1
Sl Solyc01g095260.1.1
Sl Solyc01g095250.1.1
Sl Solyc01g095310.1.1
Ac Aquca 020 00079.1
Cf Cep31K-35K
Ac Aquca 011 00549.1
At AT5G24090.1
Na NaCHITIII
Sp Sar26K
0.1

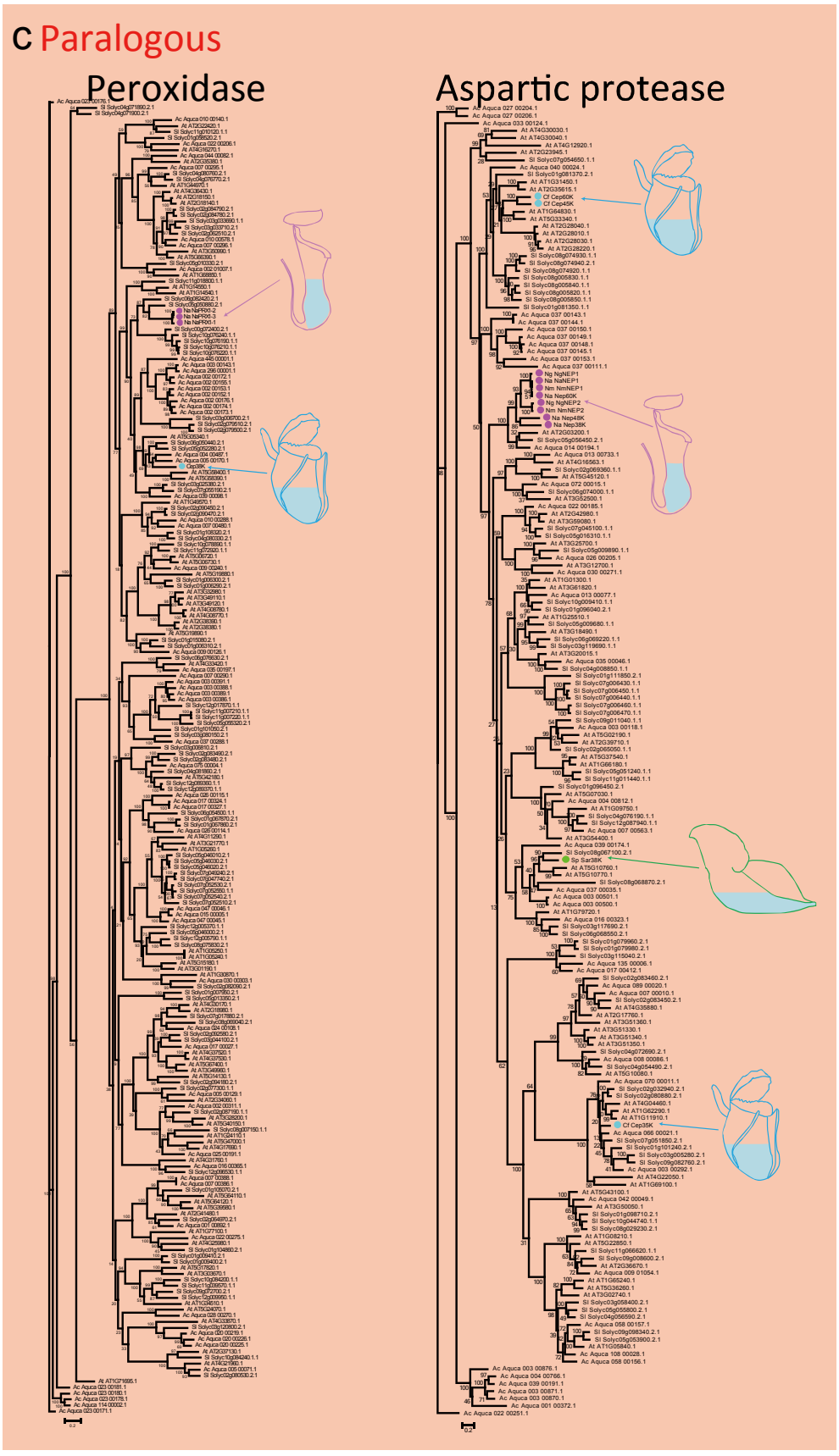
c Paralogous
Peroxidase
Aspartic protease

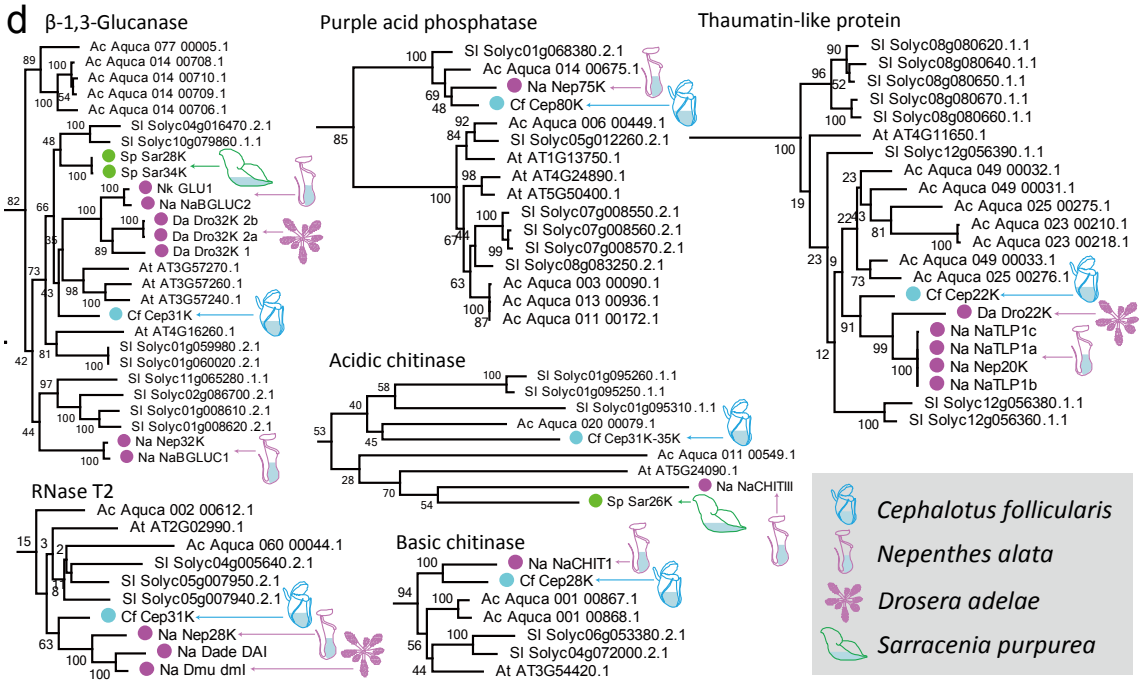

Figure 5.2. Phylogenetic analyses of digestive enzyme gene families. (**a-c**) Identified digestive enzyme genes were analyzed with their homologs in the genomes of a rosid species (*Arabidopsis thaliana*), an asterid species (*Solanum lycopersicum*), and a basal eudicot species (*Aquilegia coerulea*) by maximum-likelihood phylogenetic inferences. Orthologous relationships are defined if genes of interest make a cluster without any *A. coerulea* gene. (**d**) Magnified views of branches shaded with gray in **a-c** are provided. Positions of digestive enzyme genes are indicated by illustrations.

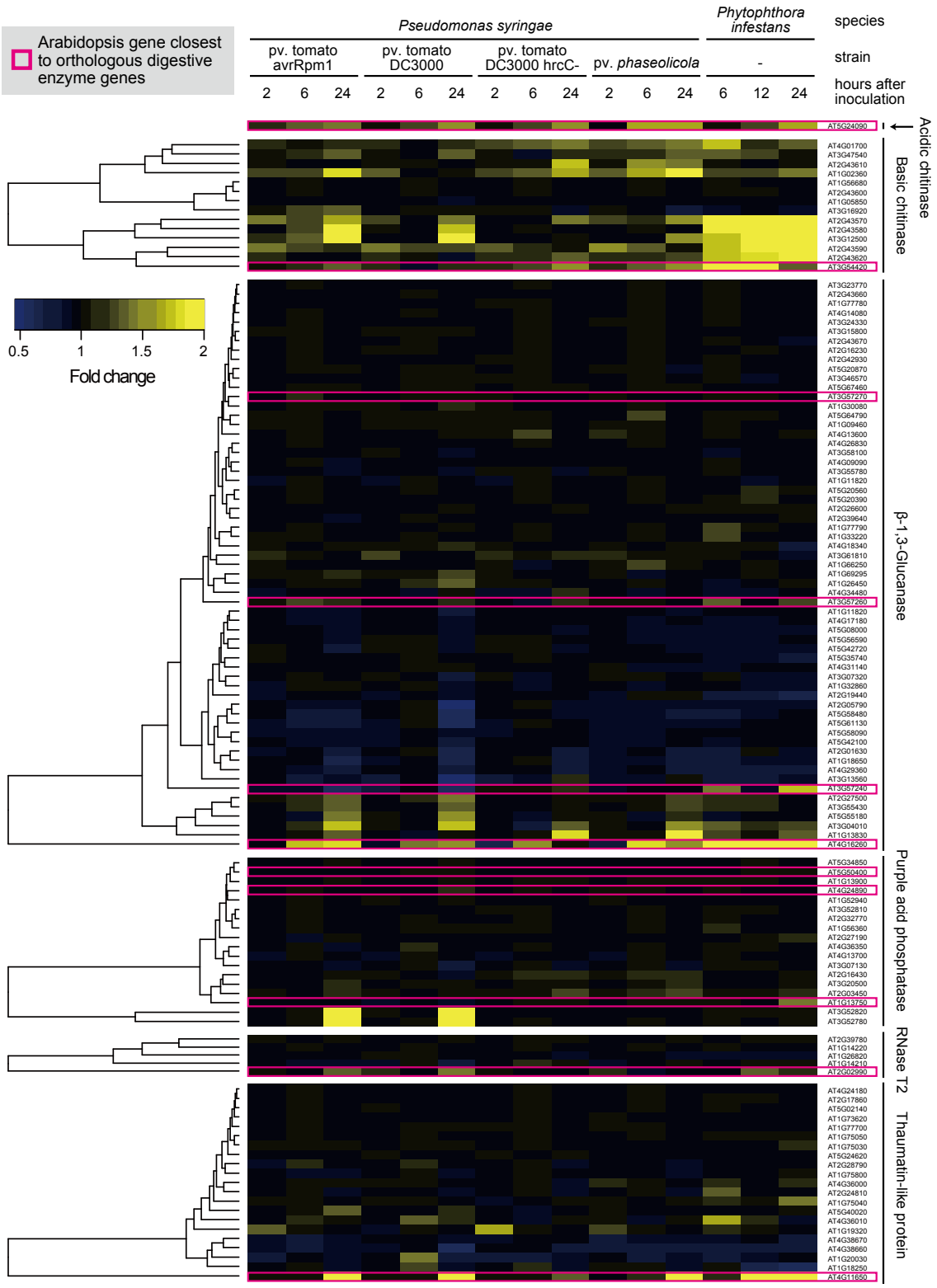

Figure 5.3. Transcriptional responses of Arabidopsis genes most closely related to the orthologous carnivorous plant genes encoding secreted proteins. AtGenExpress microarray data on pathogen infection are shown as a heat map. The dataset contains gene expression after inoculation with *Pseudomonas syringae* pv. tomato (Pst) avrRpm1, Pst DC3000, Pst DC3000 hrcC-, *Pseudomonas syringae* pv. *phaseolicola*, and *Phytophthora infestans*. Entire members of gene families are listed according to GreenPhyl v4, as long as Affymetrix ATH1 (25K) microarray contains corresponding probes. The closest relative Arabidopsis genes to the orthologous digestive enzyme genes are indicated in magenta. Dendrograms are drawn by the furthest neighbor method with Euclidean distances.

Expression patterns of digestive enzyme genes. Next I analyzed whether expression patterns of digestive enzyme genes are associated with carnivory. *Cephalotus follicularis* produces both carnivorous pitcher and non-carnivorous flat leaves. Leaves of *N. alata* are spatially subdivided into a non-carnivorous flat structure and a carnivorous pitcher part. Using these two species, I examined carnivory-associated expression by comparing pairs of carnivorous and non-carnivorous structures. Transcriptome comparisons by RNA-seq revealed that digestive enzyme genes were preferentially expressed in carnivorous organs both in *C. follicularis* (P = 9.8e-4, one sample t-test) and *N. alata* (P = 6.4e-3, one sample t-test) (Fig. 5.4). This indicates transcriptional specialization of digestive enzyme genes and implies the presence of trap-specific *cis*- or *trans*-regulatory mechanisms.

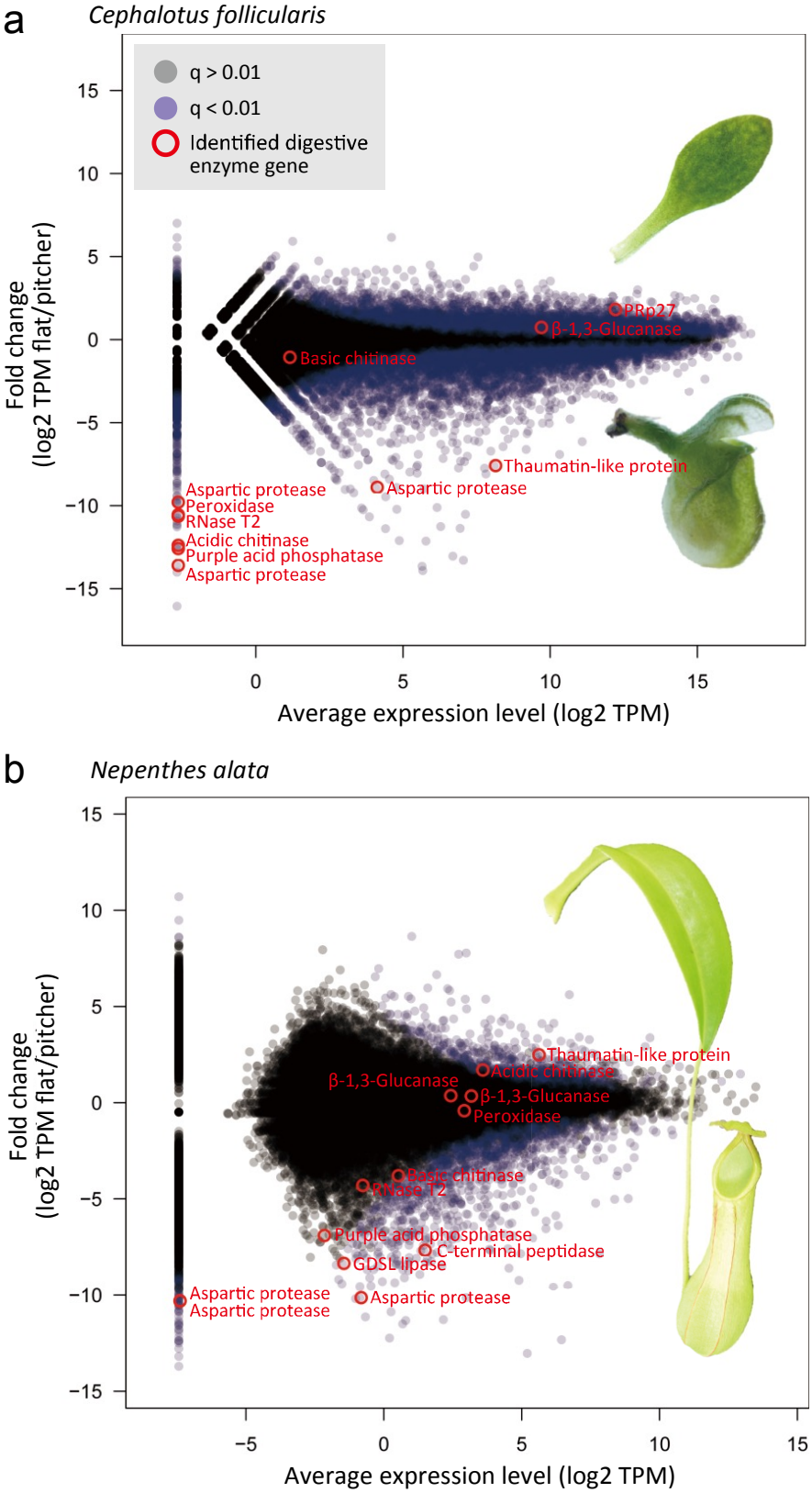

Figure 5.4. Transcriptome comparisons between carnivorous and non-carnivorous leaf parts. *Cephalotus follicularis* (**a**) and *N. alata* (**b**) were examined. Gene model v0.1 was used for the analysis of *C. follicularis*, and the transcriptome assembly was used for *N. alata*. Blue indicates genes differentially expressed between two samples with a cut-off false discovery rate of 0.01. Positions of digestive enzyme genes are shown in red.

Detection of molecular convergence in complex history of gene family evolution.
Neofunctionalization of genes can occur by regulatory changes, as well as changes in coding regions that alter protein properties. Since carnivory emerged repeatedly, as described above, digestive enzymes in the different species may have evolved by convergent amino acid substitutions in response to carnivorous plant-specific selective pressure.

A framework for detecting molecular convergence consists of the following three steps: (1) inferring phylogenetic relationships, (2) estimating substitution events, and (3) identifying convergent genes (Castoe et al. 2009). However, the first step has a technical problem. Convergently evolved genes accumulate the same amino acid substitutions independently. In standard phylogenetic inference, those independently occurring substitutions are often treated as a single substitution event, resulting in incorrect clustering of the convergently evolved genes, which leads to underestimation of the number of convergent substitutions (Christin et al. 2012). In other words, the results of molecular convergence can make it difficult to detect molecular convergence. Previous studies have circumvented this problem by using a species tree instead of a gene tree in convergence detection (e.g. Castoe et al. 2009; Parker et al. 2013; Shen et al. 2012). However, this method only allows the analysis of conserved genes without lineage-specific gene duplications and losses. Some digestive enzyme genes belong to relatively large gene families, such as β-1,3-glucanase and purple acid phosphatases, and tree topologies imply that gene duplications and losses are common (Fig. 5.2). Therefore, using only species trees is not a suitable approach, and duplicated/lost gene lineages must be considered for less-biased analysis of adaptive molecular convergence. Given that accelerated convergent substitutions result from selective pressure, tree reconstruction using only information either insensitive to selection or less sensitive to selection, such as synonymous substitutions, 3rd codons, and species trees, should work for detection of convergence. To combine the information, gene trees were first reconstructed using a synonymous substitution distance or 3rd codon information, and then the tree topology was improved by phylogenetic reconciliation with the species tree. Reconciliation between gene trees and species trees has been demonstrated to be a rigorous approach to reconstruct the complex evolutionary history of gene families (Doyon et al. 2011). Reconciled tree topologies enable us to infer patterns of duplication and loss while eliminating the artifacts of tree topology generated by molecular convergence. Evaluation of the performance of pipelines was conducted using a publicly available benchmark dataset (Rasmussen and Kellis 2011). Generally, reconciliation of the 3rd-ML tree and the species tree outperformed other methods over different tree lengths and different gene duplication and loss rates in convergent scenarios (Fig. 5.5). Therefore I used this method for further analyses of digestive enzymes.

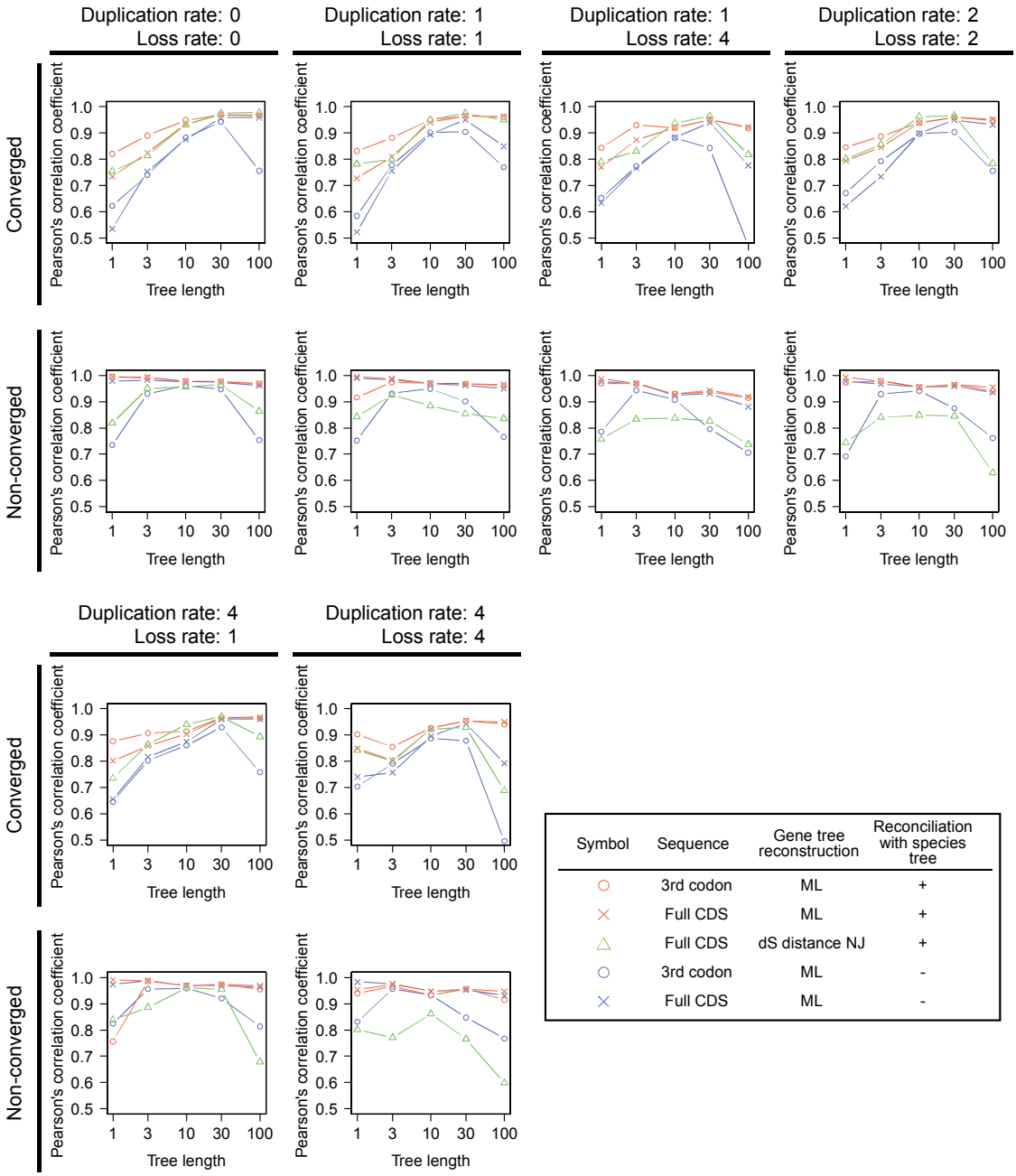

Figure 5.5. Performance evaluation of molecular convergence detection. Converged and non-converged molecular evolutionary patterns were generated on the basis of different tree topologies in publicly available "fungi" dataset, in which different gene duplication and loss rates are assumed. The simulated sequences were generated under different tree lengths. Pearson's correlation coefficients were calculated by comparing the number of convergent substitutions estimated from the true tree topology and the inferred topology. Different combinations of sequence information and tree reconstruction methods were examined, and keys are provided in the figure.

Molecular convergence of digestive enzymes. I next examined adaptive evolution in the protein-coding sequences of the digestive enzyme genes. Digestive enzyme genes and their homologs in eudicot genomes were subjected to tree reconstruction by phylogenetic reconciliation of 3rd-ML trees and species trees. This approach resolved branch attractions found in RNase T2, purple acid phosphatases, basic chitinases, and thaumatin-like proteins (Fig. 5.2 and 5.6). Unexceptional

branch lengths of digestive enzyme genes indicate that their evolutionary rates are comparable to those of their non-carnivorous homologs (Fig. 5.6). Ancestral protein sequences were inferred by Bayesian methods and posterior probabilities of convergent and divergent amino acid substitution pairs were obtained in all independent branch pairs (Castoe et al. 2009). Neutral backgrounds of convergent substitutions were expected by linear regression based on the number of divergent substitutions. By comparing convergent substitutions of digestive enzymes and the neutral expectations, I found that basic chitinases, purple acid phosphatases, and RNase T2 significantly accumulated convergent amino acid substitutions (Fig. 5.6). In the converged branch pairs, 12.8, 20.5, and 9.8 convergent substitutions were estimated for basic chitinases, purple acid phosphatases, and RNase T2, respectively. These numbers were approximately twice as many as neutral expectations (6.0, 10.0, and 3.8, respectively). In all three enzymes, two pitfall-type carnivorous plants, *C. follicularis* and *N. alata* were associated as convergent branch pairs. Furthermore, in RNase T2, significant molecular convergence was detected between the terminal branch of *C. follicularis* and the branch of the common ancestor of the three Caryphyllales species: *Dr. adelae*, *Di. muscipula*, and *N. alata* (Fig. 5.6e). *Nepenthes* spp., *Drosera* spp. and *Di. muscipula* produce pitfall, sticky, and snap traps, respectively. Parsimonious analyses of character evolution indicate that the trapping strategy has diversified after the establishment of carnivory in the Caryophyllales (Albert et al. 1992; Heubl et al. 2006; Meimberg et al. 2000). Since the convergence of RNase T2 was detected before the divergence of these three genera, the molecular convergence occurred during the evolution of carnivorous syndrome, rather than during the establishment of the specific capture strategy of pitfall traps.

Evolutionary constraints imposed on digestive enzymes. Since protein structure provides a major source of evolutionary constraint in amino acid substitution patterns (Sikosek and Chan 2014), I then examined the localizations of convergent amino acid residues in the protein molecule. Convergent amino acids do not localize to specific segments, neither in primary amino acid sequences (Fig. 5.7a-c) nor in three-dimensional protein structures (Fig. 5.7d-k). Furthermore, convergent positions do not overlap with the catalytically essential amino acids of basic chitinases (Passarinho and de Vries 2002), the metal-ligating residues of purple acid phosphatases (Schenk et al. 2000), or the catalytic histidines of RNase T2 (MacIntosh et al. 2010) (Fig. 5.7d-k). However, they significantly localize to exposed positions in basic chitinases and RNase T2, but not in purple acid phosphatases (Fig. 5.7l). Convergent substitutions in amino acids localized to the surface of basic chitinases and RNaseT2 may change their interactions with other molecules, rather than changing their protein conformation.

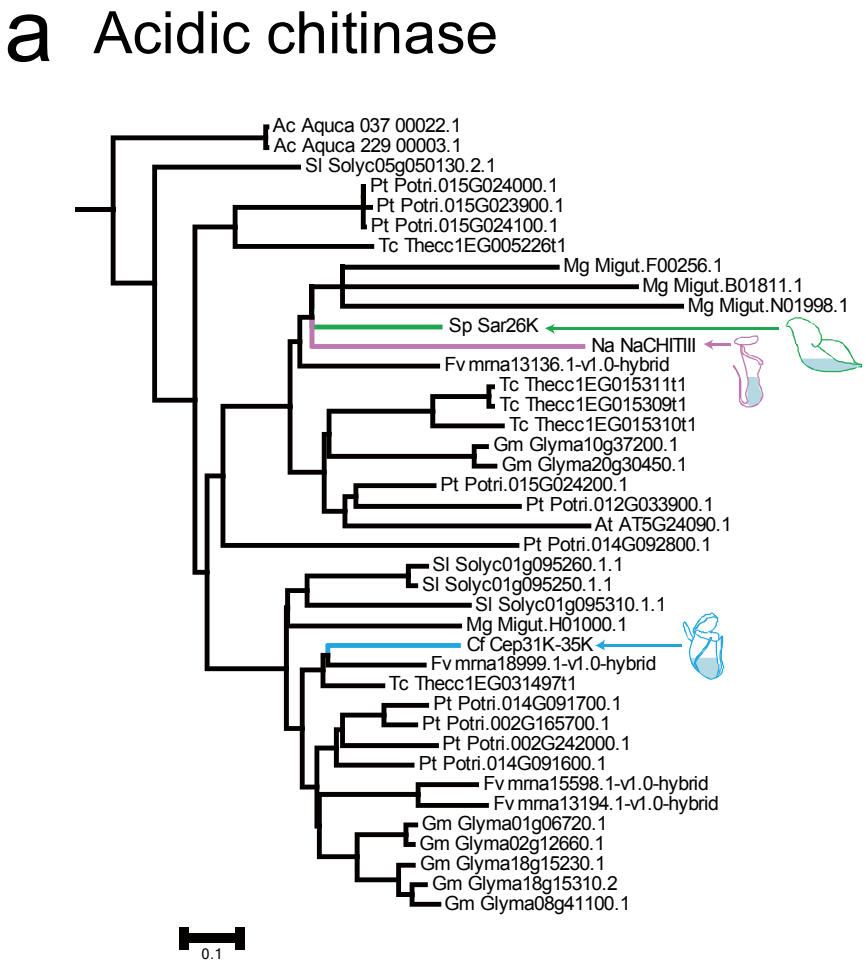
a Acidic chitinase
Ac Aquca 037 00022.1
Ac Aquca 229 00003.1
Sl Solyc05g050130.2.1
Pt Potri.015G024000.1
Pt Potri.015G023900.1
Pt Potri.015G024100.1
Tc Thecc1EG005226t1
Mg Migut.F00256.1
Mg Migut.B01811.1
Mg Migut.N01998.1
Sp Sar26K
Na NaCHITIII
Fv mrna13136.1-v1.0-hybrid
Tc Thecc1EG015311t1
Tc Thecc1EG015309t1
Tc Thecc1EG015310t1
Gm Glyma10g37200.1
Gm Glyma20g30450.1
Pt Potri.015G024200.1
Pt Potri.012G033900.1
At AT5G24090.1
Pt Potri.014G092800.1
Sl Solyc01g095260.1.1
Sl Solyc01g095250.1.1
Sl Solyc01g095310.1.1
Mg Migut.H01000.1
Cf Cep31K-35K
Fv mrna18999.1-v1.0-hybrid
Tc Thecc1EG031497t1
Pt Potri.014G091700.1
Pt Potri.002G165700.1
Pt Potri.002G242000.1
Pt Potri.014G091600.1
Fv mrna15598.1-v1.0-hybrid
Fv mrna13194.1-v1.0-hybrid
Gm Glyma01g06720.1
Gm Glyma02g12660.1
Gm Glyma18g15230.1
Gm Glyma18g15310.2
Gm Glyma08g41100.1
0.1

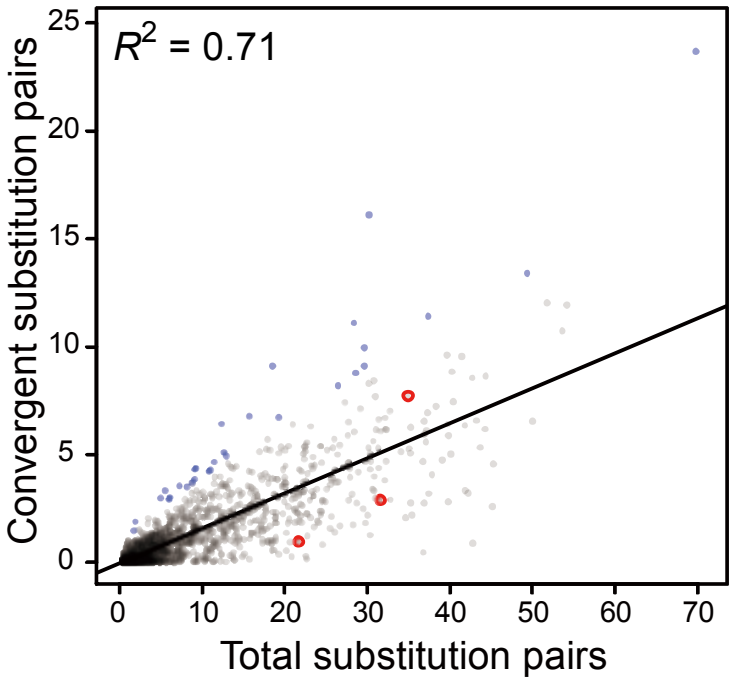
R^2 = 0.71
Convergent substitution pairs
Total substitution pairs
0
5
10
15
20
25
0
10
20
30
40
50
60
70

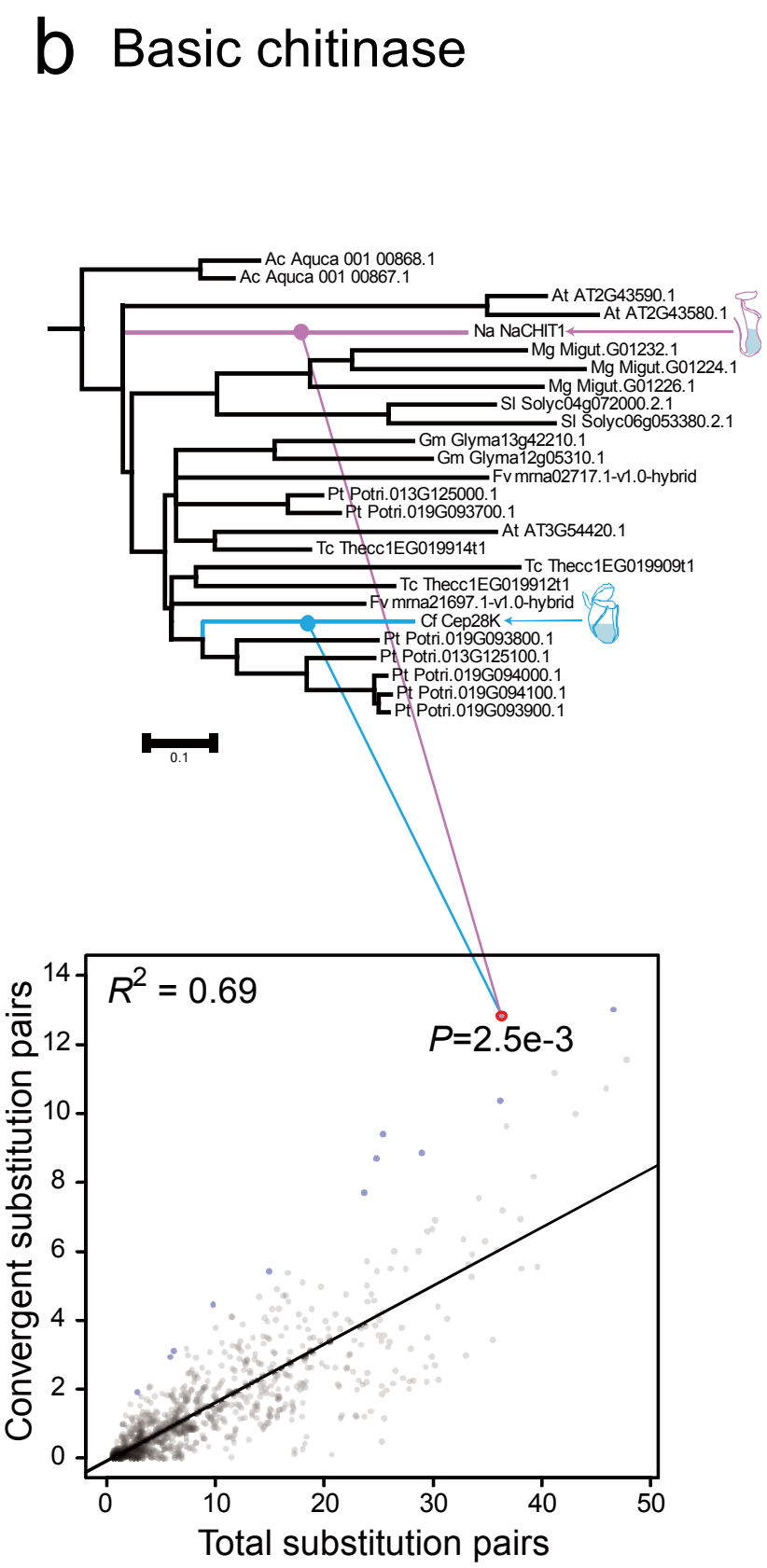
b Basic chitinase
Ac Aquca 001 00868.1
Ac Aquca 001 00867.1
At AT2G43590.1
At AT2G43580.1
Na NaCHIT1
Mg Migut.G01232.1
Mg Migut.G01224.1
Mg Migut.G01226.1
Sl Solyc04g072000.2.1
Sl Solyc06g053380.2.1
Gm Glyma13g42210.1
Gm Glyma12g05310.1
Fv mrna02717.1-v1.0-hybrid
Pt Potri.013G125000.1
Pt Potri.019G093700.1
At AT3G54420.1
Tc Thecc1EG019914t1
Tc Thecc1EG019909t1
Tc Thecc1EG019912t1
Fv mrna21697.1-v1.0-hybrid
Cf Cep28K
Pt Potri.019G093800.1
Pt Potri.013G125100.1
Pt Potri.019G094000.1
Pt Potri.019G094100.1
Pt Potri.019G093900.1
0.1
R^2 = 0.69
P=2.5e-3
Convergent substitution pairs
Total substitution pairs
0
2
4
6
8
10
12
14
0
10
20
30
40
50

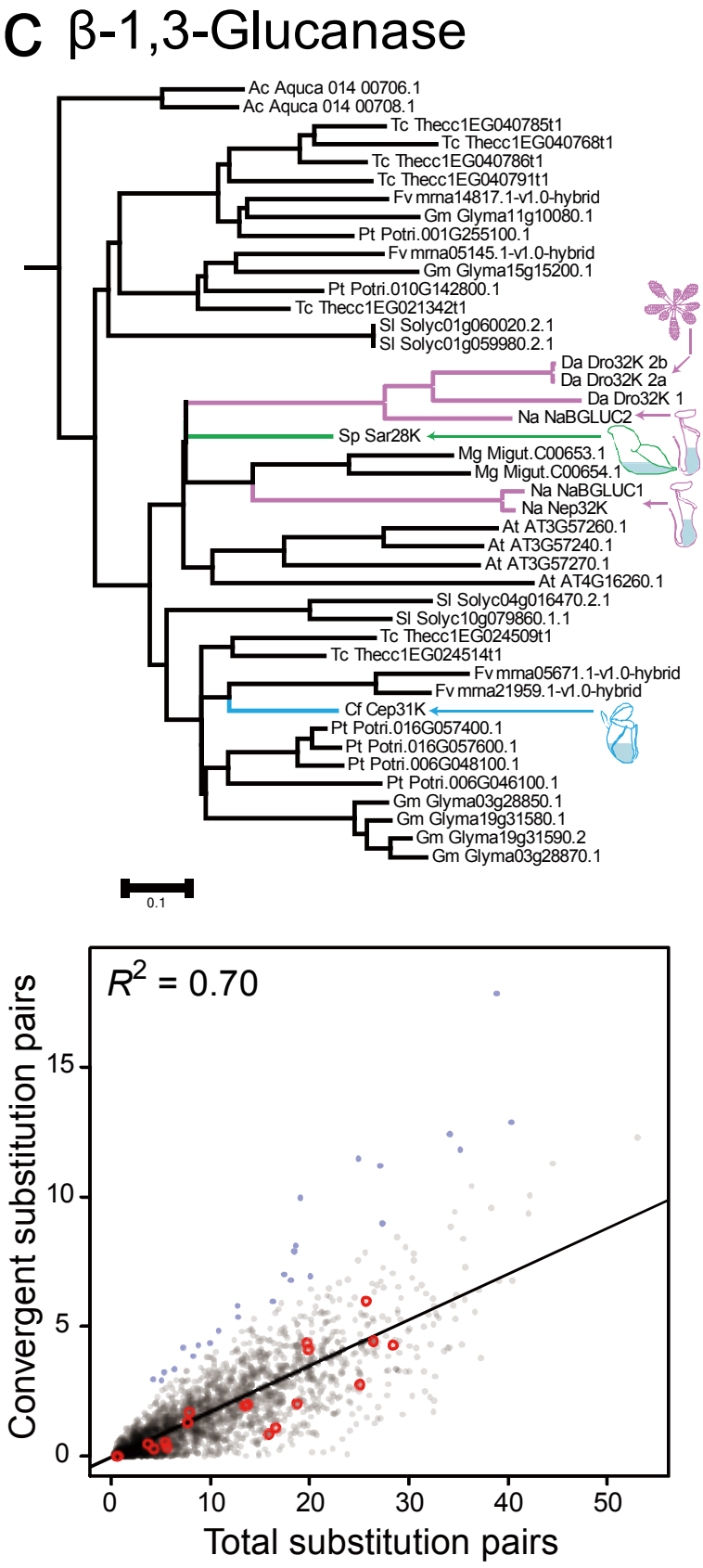
C β-1,3-Glucanase
Ac Aquca 014 00706.1
Ac Aquca 014 00708.1
Tc Thecc1EG040785t1
Tc Thecc1EG040768t1
Tc Thecc1EG040786t1
Tc Thecc1EG040791t1
Fv mrna14817.1-v1.0-hybrid
Gm Glyma11g10080.1
Pt Potri.001G255100.1
Fv mrna05145.1-v1.0-hybrid
Gm Glyma15g15200.1
Pt Potri.010G142800.1
Tc Thecc1EG021342t1
Sl Solyc01g060020.2.1
Sl Solyc01g059980.2.1
Da Dro32K 2b
Da Dro32K 2a
Da Dro32K 1
Na NaBGLUC2
Sp Sar28K
Mg Migut.C00653.1
Mg Migut.C00654.1
Na NaBGLUC1
Na Nep32K
At AT3G57260.1
At AT3G57240.1
At AT3G57270.1
At AT4G16260.1
Sl Solyc04g016470.2.1
Sl Solyc10g079860.1.1
Tc Thecc1EG024509t1
Tc Thecc1EG024514t1
Fv mrna05671.1-v1.0-hybrid
Fv mrna21959.1-v1.0-hybrid
Cf Cep31K
Pt Potri.016G057400.1
Pt Potri.016G057600.1
Pt Potri.006G048100.1
Pt Potri.006G046100.1
Gm Glyma03g28850.1
Gm Glyma19g31580.1
Gm Glyma19g31590.2
Gm Glyma03g28870.1
0.1
R^2 = 0.70
Convergent substitution pairs
0
5
10
15
0
10
20
30
40
50
Total substitution pairs

d Purple acid phosphatase

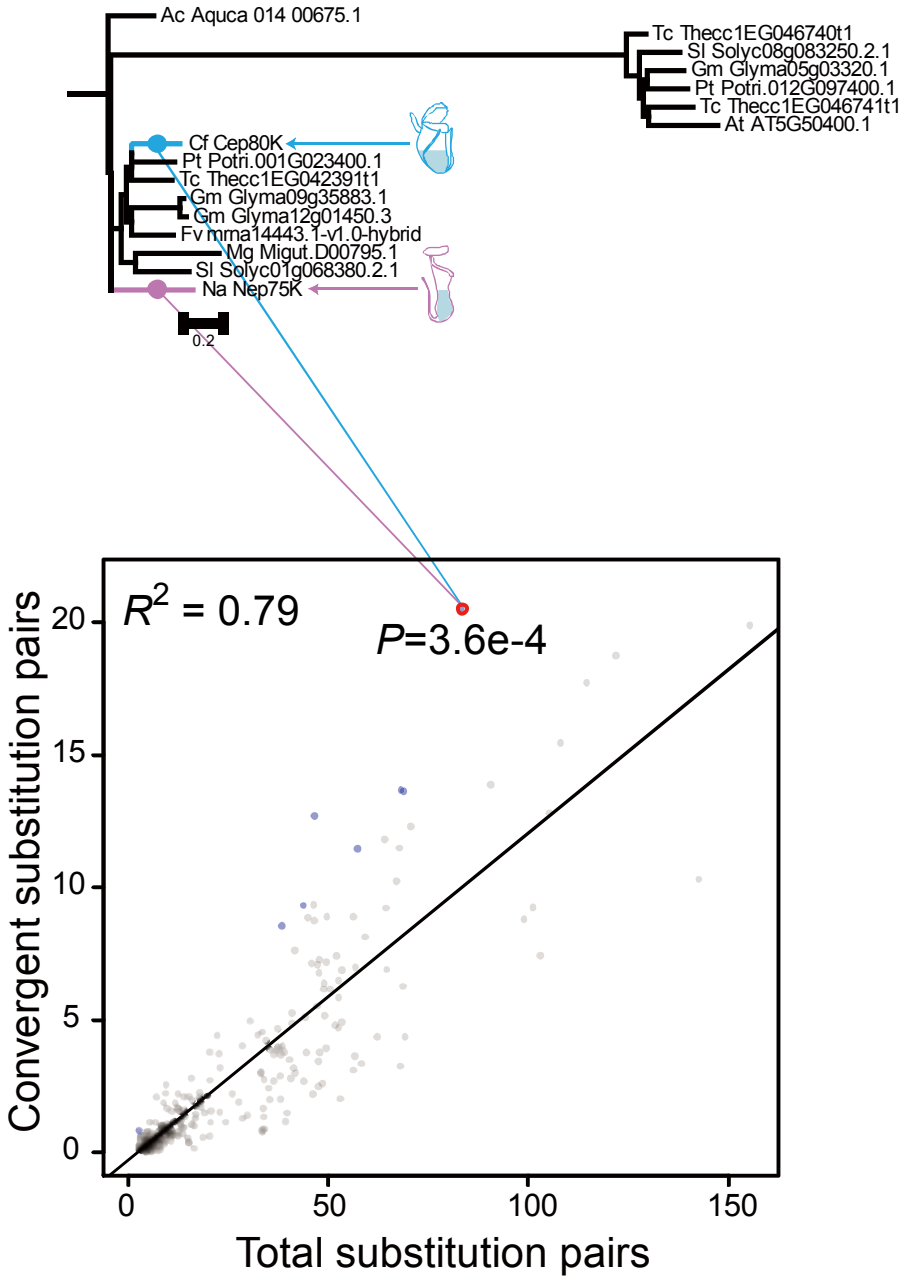

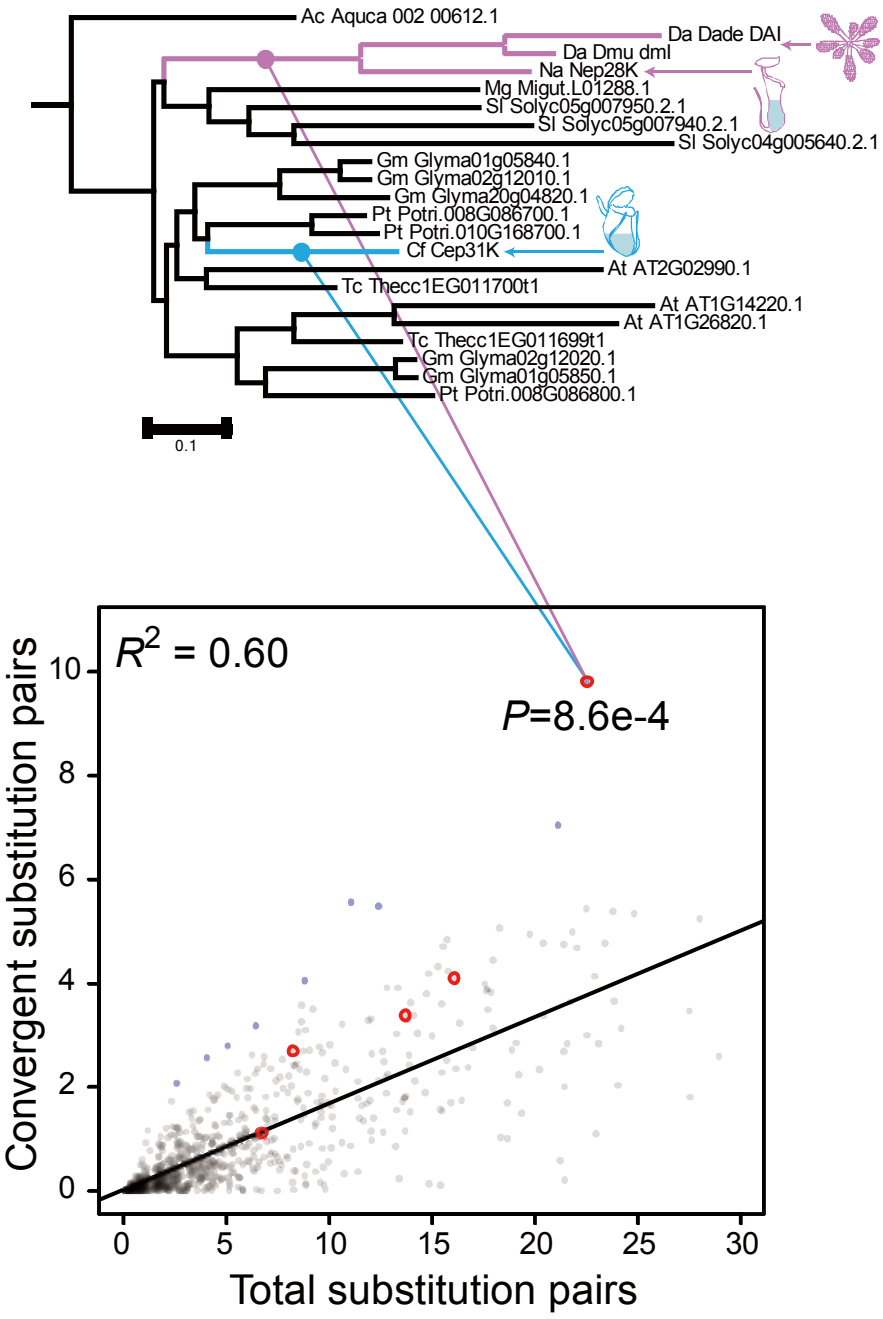
e RNase T2
Ac Aquca 002 00612.1
Da Dade DAI
Da Dmu dmI
Na Nep28K
Mg Migut.L01288.1
Sl Solyc05g007950.2.1
Sl Solyc05g007940.2.1
Sl Solyc04g005640.2.1
Gm Glyma01g05840.1
Gm Glyma02g12010.1
Gm Glyma20g04820.1
Pt Potri.008G086700.1
Pt Potri.010G168700.1
Cf Cep31K
At AT2G02990.1
Tc Thecc1EG011700t1
At AT1G14220.1
At AT1G26820.1
Tc Thecc1EG011699t1
Gm Glyma02g12020.1
Gm Glyma01g05850.1
Pt Potri.008G086800.1
0.1
R^2 = 0.60
P=8.6e-4
Convergent substitution pairs
Total substitution pairs
0
2
4
6
8
10
0
5
10
15
20
25
30

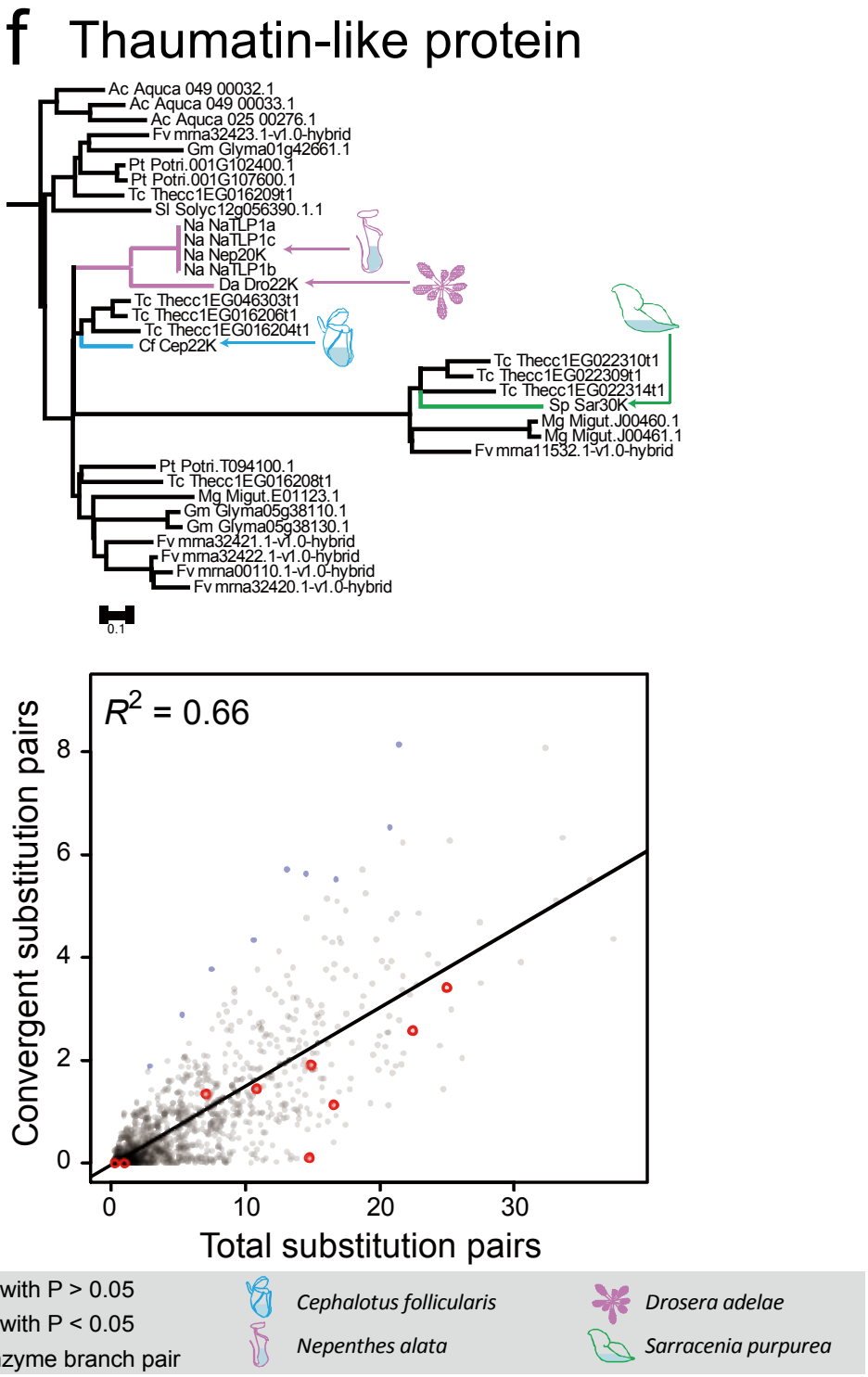

Figure 5.6. Quantification of convergent amino acid substitutions in digestive enzymes. Acidic chitinases (**a**), basic chitinases (**b**), β-1,3-glucanases (**c**), purple acid phosphatases (**d**), RNase T2 (**e**), and thaumatin-like proteins (**f**) were analyzed. Reference trees were reconstructed with identified digestive enzyme genes of carnivorous plants and homologous genes in *Fragaria vesca*, *Glycine max*, *Populus trichocarpa*, *Theobroma cacao*, *Arabidopsis thaliana*, *Solanum lycopersicum*, *Mimulus guttatus*, and *Aquilegia coerulea* by phylogeny reconciliation of maximum-likelihood trees of 3rd codons and species trees. Scatter plots show the inferred number of convergent substitutions. The positions of digestive enzyme branch pairs are indicated with red circles. *P* values of one-sided t-test are shown if digestive enzyme branch pairs significantly accumulate convergent substitutions. Adjusted R^2 of linear regression is provided in the plots.

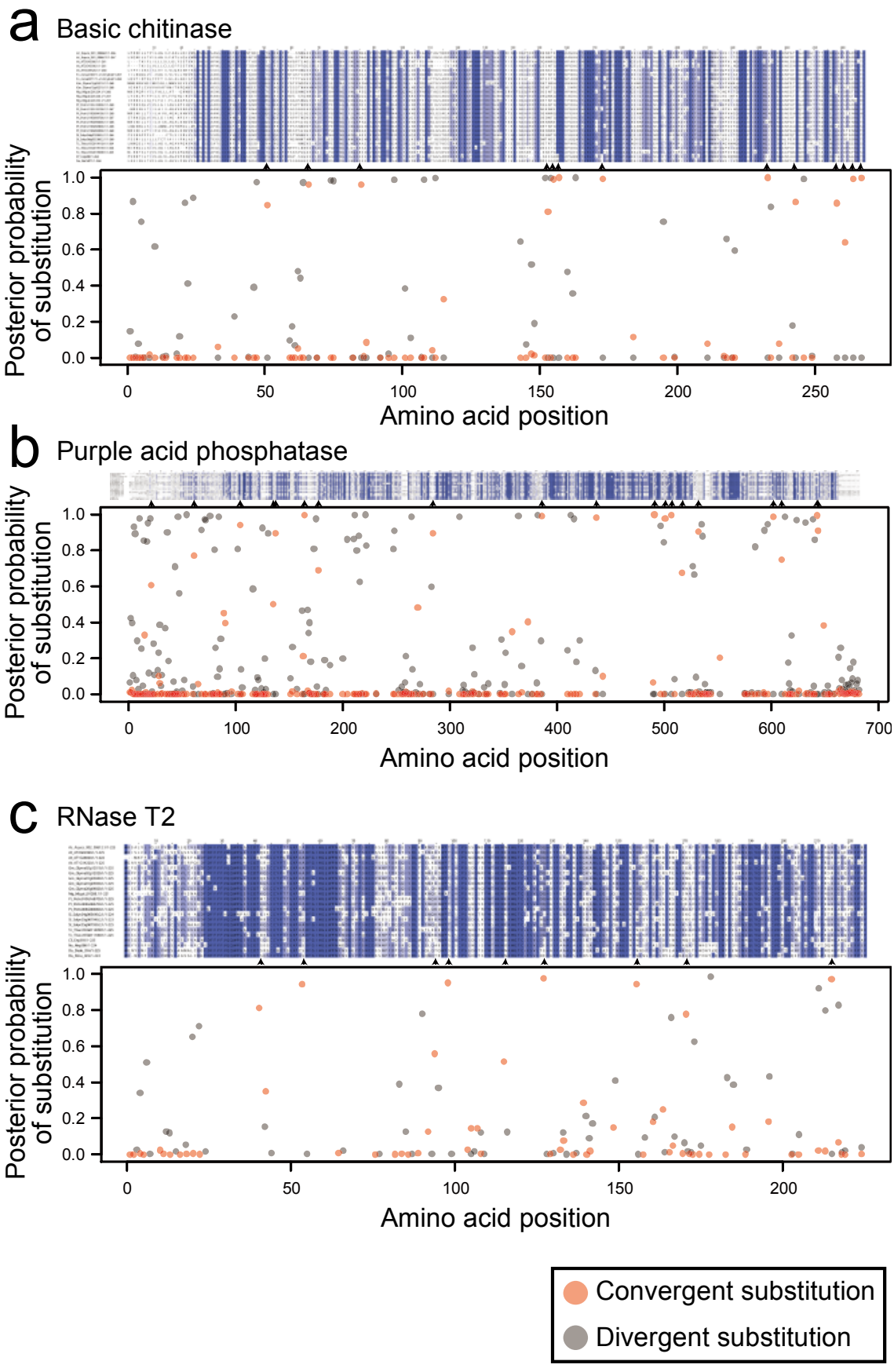
a
Basic chitinase
Posterior probability of substitution
1.0
0.8
0.6
0.4
0.2
0.0
0
50
100
150
200
250
Amino acid position
b
Purple acid phosphatase
Posterior probability of substitution
1.0
0.8
0.6
0.4
0.2
0.0
0
100
200
300
400
500
600
700
Amino acid position
c
RNase T2
Posterior probability of substitution
1.0
0.8
0.6
0.4
0.2
0.0
0
50
100
150
200
Amino acid position
Convergent substitution
Divergent substitution

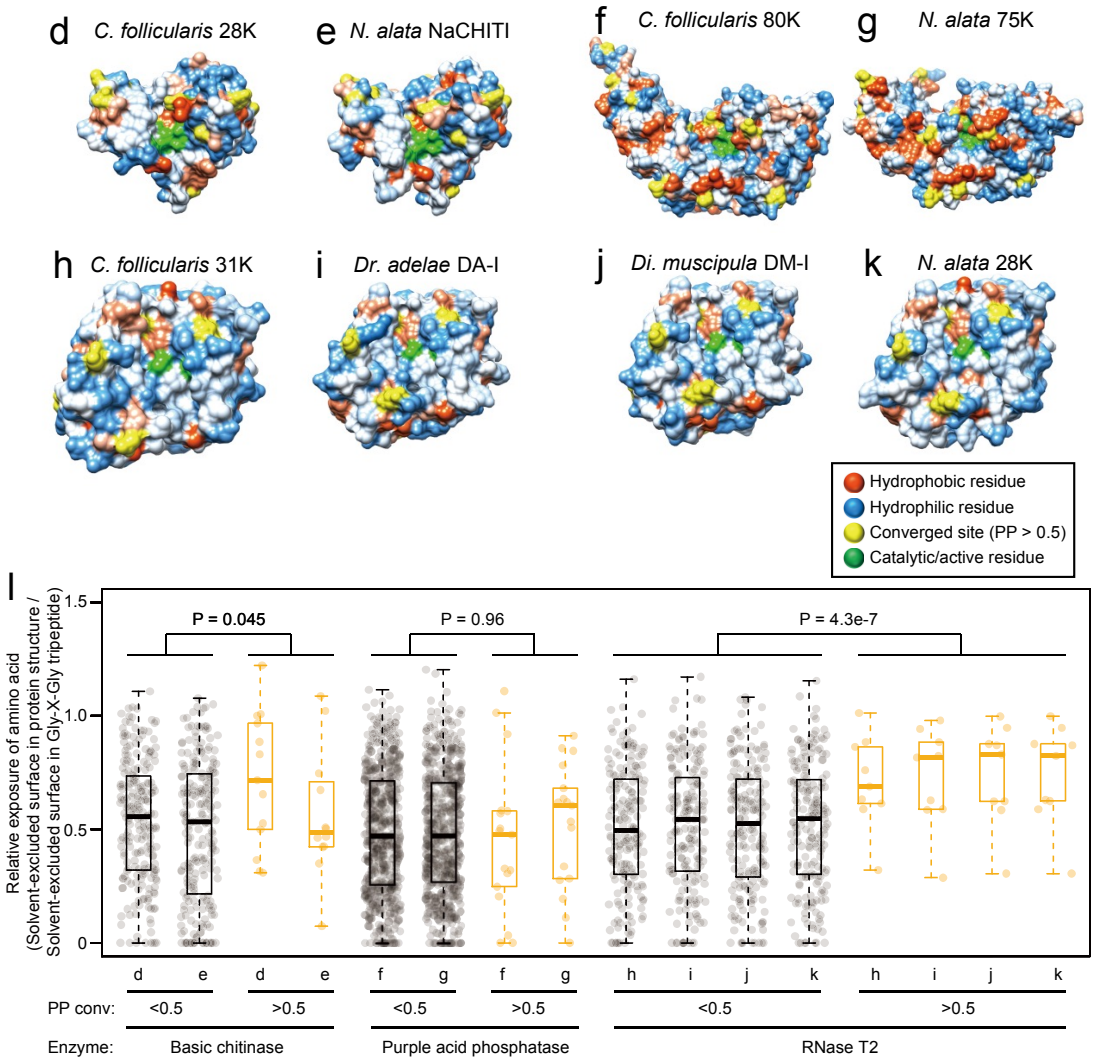

Figure 5.7. Structural localization of convergent residues. (**a-c**) Posterior probabilities of convergent (red) and divergent (gray) substitutions in protein primary sequences. Digestive enzyme branch pairs of basic chitinases (**a**), purple acid phosphatases (**b**), and RNase T2 (**c**) were analyzed. Sequence alignments trimmed using trimAl are shown above the plots. Conserved amino acids are shaded. (**d-k**) Protein structures of basic chitinases (**d,e**), purple acid phosphatases (**f,g**), and RNase T2 (**h-k**) were constructed by homology modeling. Red and blue sites indicate hydrophobic and hydrophilic residues, respectively. The amino acid positions having posterior probability of convergence of >0.5 are shown with yellow. Green indicates the catalytically essential amino acids of basic chitinases (Passarinho and de Vries 2002), metal-ligating residues of purple acid phosphatase (Schenk et al. 2000), and catalytic histidines of RNase T2 (MacIntosh et al. 2010). (**l**) Relative exposure of amino acids in the protein structure is examined. Convergent and undetected positions are classified by a threshold of posterior probability of 0.5. *P* values for the Student's *t*-test are shown in the plot.

5.4 Discussion

In this study, I identified digestive enzyme genes from four carnivorous plants covering three independent origins of carnivory (Fig. 5.1). The phylogenetic relationships of acidic chitinases, basic chitinases, β-1,3-glucanases, purple acid phosphatases, and RNase T2, thaumatin-like proteins suggest that those secreted proteins originated from conserved proteins in flowering plants (Fig. 5.2). Expression profiling of the most closely related genes in the Arabidopsis genome showed transcriptional responsiveness to microbial infections (Fig. 5.3). Pathogenesis-related functions of these Arabidopsis genes have been studied in previous work. The promoter of the acidic chitinase (ATHCHIA, At5g24090) responds to the fungal pathogens *Rhizoctonia solani*, *Alternaria solani*, and *Phytophthora infestans* (Samac and Shah 1991). Catalytic activity of the basic chitinase (AtEP3/AtchitIV, At3g54420) has been confirmed (Passarinho et al. 2001). Its transcripts rapidly accumulate in leaves after inoculation with *Xanthomonas campestris* (Gerhardt et al. 1997; Passarinho et al. 2001). Three β-1,3-glucanases (At3g57240, At3g57260, and At3g57270) are tandemly clustered in the Arabidopsis genome and its transcripts are induced by a virulent strain of *Pseudomonas syringae* but not by an avirulent strain (Dong et al. 1991). The expression of two of these β-1,3-glucanases (At3g57240 and At3g57260) and another β-1,3-glucanase (At4g16260) responds to diverse pathogens and is especially strongly induced by *A. brassicicola* and *P. infestans* (Doxey et al. 2007). Catalytic activity of At3g57240 was confirmed (Oide et al. 2013). A purple acid phosphatase (At1g13750) is up-regulated in response to *P. infestans* (Fig. 5.3), and is also induced by *A. brassicicola* (Lohrasebi et al. 2013), but no obvious pathogenesis-related transcriptional regulation has been found for the other two purple acid phosphatases (At4g24890 and At5g50400). RNase T2 (RNS1, At2g02990) is up-regulated by mechanical wounding (Hillwig et al. 2008). Thaumatin-like protein (AtOSM34, At4g11650) is induced by *Agrobacterium tumefaciens* (Ditt et al. 2006) and *A. brassicicola* (Mukherjee et al. 2010). Thus, the Arabidopsis genes are involved in diverse pathogen-related responses, and represent functions of the homologs of digestive enzyme in non-carnivorous plants. Therefore, antimicrobial proteins might be exapted for carnivory as digestive enzymes. Whether they are currently bifunctional, having non-carnivorous and carnivorous roles, has not been examined, but digestive enzyme genes likely function mainly in carnivory, since they are preferentially expressed in the carnivorous trap rather than in non-carnivorous flat structures (Fig. 5.4).

In addition to regulatory changes, functional innovations can also be achieved by changes in coding sequences that alter protein properties. I detected significant accumulation of convergent amino acid substitutions in basic chitinases, purple acid phosphatases, and RNase T2 among six enzyme families that show orthologous relationships (Fig. 5.6). By contrast, significant molecular convergence was not found in acidic chitinases, β-1,3-glucanases, or thaumatin-like proteins, which

may reflect differences in modes and levels of selective pressures imposed on the secreted proteins in carnivorous plants.

Protein sequences show heterogeneous evolutionary conservation of amino acid compositions due to constraints imposed by protein conformation (Sikosek and Chan 2014). For example, amino acid positions that are buried in protein structures tend to be conserved, and fewer amino acids are accessible because substitutions in such positions are most likely to disturb the protein's structural integrity and hence impair its biochemical function (Bustamante et al. 2000; Choi et al. 2006; Goldman et al. 1998). By contrast, positions that are exposed on protein surfaces can easily tolerate replacement of amino acids because they have fewer interactions with other residues. If few amino acids are accessible, there is a good chance that convergent substitutions may be generated; if many amino acids are allowed at a position, the chance of convergent substitutions is low. Therefore, two alternative pathways can shape adaptive molecular convergence from the viewpoint of protein structures: (1) accelerating evolutionary rates at structurally constrained protein positions where amino acid compositions are originally limited, and (2) limiting amino acid compositions in structurally less-constrained positions where evolutionary rates are originally high. Our analyses of basic chitinases and RNase T2 showed that convergent changes tend to locate in exposed sites (Fig. 5.7), which have high degrees of freedom in amino acid compositions and therefore are less-constrained (Choi et al. 2006). On the other hand, in the evolution of mitochondrial proteins of snakes and agamid lizards, convergent amino acid substitution occurred in more-constrained positions, as judged from amino acid compositions (Castoe et al. 2009). Differences in protein properties may lead to those contrasting results. During the evolution of digestive enzymes, selective pressures may come from the specific environments in digestive fluids, which include: the presence of insect-derived substrates, high proteolytic activity, low pH, and microbial invasion. Since exposed residues constitute the protein-environment interface, the convergent amino acid substitutions may affect molecular adaptation to those digestive fluid-specific micro-environments.

6. GENERAL DISCUSSION

6.1 Evolution of complex traits in carnivorous plants

Carnivorous syndrome consists of attraction, trapping, digestion, and absorption of prey insects (Juniper et al. 1989). Therefore, the evolution of carnivorous plants required the emergence of multiple traits. In carnivorous plants, morphological evolution often involves a trapping strategy. Especially in pitcher plants, drastic morphological changes are necessary to construct functional pitfall traps. In Chapter 2, I described evidence showing that changes in adaxial-abaxial patterning generate variable leaf shapes. However, pitcher leaves of *Sarracenia purpurea* unexpectedly develop through a characteristic cell division pattern after standard establishment of adaxial-abaxial patterning, as described in Chapter 3. This suggests the existence of unexplored mechanisms in the evolution of leaf morphology. To explore the mechanisms of pitcher development, as described in Chapter 4, I have developed genomic resources and transgenic techniques in *Cephalotus follicularis*. Based on its leaf dimorphism, and our ability to induce the two different types of leaves in the lab, *C. follicularis* will be a good material for characterization of the genetic changes that regulate leaf morphology.

In the evolution of both leaf morphology and digestive enzymes, preexisting mechanisms appear to have been co-opted and modified for novel functions. For example, in Chapter 5, I found that digestive enzymes likely originated from pathogenesis-related hydrolytic enzymes that are conserved in flowering plants. No novel genes were found, indicating that co-option from preexisting genes has driven the evolution of digestive functions. Such evolutionary modifications likely occurred with fewer genetic changes compared with constructing traits from ground zero, and have the potential to drive the evolution of complex traits.

In this study, I analyzed pitcher development and digestive enzymes, mainly involved in trapping and digestion processes, respectively. Other studies have examined the evolutionary mechanisms of other carnivorous processes such as attraction and absorption. *Nepenthes rafflesiana*, *Sarracenia* spp. and *Dionaea muscipula* employ floral scents to attract prey (Di Giusto et al. 2010; Jürgens et al. 2009; Kreuzwieser et al. 2014). Related to absorptive functions, ammonium transporters have been identified from gland cells of *Di. muscipula* and *N. alata* (Scherzer et al. 2013; Schulze et al. 1999). In addition to transporter-mediated absorption, endocytotic uptake has been reported from multiple lineages of carnivorous plants (Adlassnig et al. 2012). Together with our results, the evolutionary analyses of those molecules would advance our understanding of complex trait evolution in carnivorous plants.

6.2 *Cephalotus follicularis* as a model system for carnivorous plants

Because of their unusual characteristics, carnivorous plants have received substantial attention from evolutionary biologists; for example, Charles Darwin compiled his intensive observations in the book "Insectivorous Plants" (Darwin 1875). Although physiological, morphological, and ecological knowledge have accumulated (reviewed in Ellison and Gotelli 2009), the molecular mechanisms of carnivorous syndrome remain unclear. This could be because of the lack of a model system in carnivorous plants. In this study, I established *Cephalotus follicularis* as a model system for studying carnivorous traits, since this plant has phenotypic plasticity of carnivorous characters. Genome sequences and a gene knockdown technique have been developed in this species, enabling us to analyze gene functions *in vivo*. Establishment of Agrobacterium-mediated transformation will be necessary for further genetic manipulation, including gene knock-in and genome editing.

One drawback of this plant is its long, perennial life cycle. It takes four to six years from germination to maturity (McPherson 2009), and therefore it is difficult to conduct forward genetic analyses in *C. follicularis*. Recently, various efforts have been made to shorten the generation time in flowering plants. One innovative technique is virus-induced precocious flowering in which viral infection is used to deliver the flowering integrator FLOWERING LOCUS T (FT) to the plant (Yamagishi et al. 2011; Yamagishi and Yoshikawa 2011). In the case of apple, maturity takes more than five years after seed germination; however, time-to-maturity can be as short as seven months by FT delivery through *Apple latent spherical virus* (*ALSV*) (Yamagishi et al. 2011). Since *ALSV* can infect a broad range of host plants covering both rosids and asterids (Igarashi et al. 2009), it has a potential to open avenues for forward genetic analyses in *C. follicularis*.

6.3 Constraints of evolutionary pathways in molecular convergence

Recent studies have unraveled the molecular underpinnings of phenotypic convergence and have illustrated the importance of convergent genetic changes (Stern 2013). However, understanding the evolutionary constraints that drive adaptive molecular convergence has been a challenging problem. In this study, I revealed the presence of molecular convergence of digestive enzymes in independently-evolved carnivorous plant lineages, and those convergent loci tended to localize in protein surfaces (Chapter 5), where amino acid composition is generally less-constrained (Sikosek and Chan 2014). On the other hand, convergent tendency in more-constrained sites has been reported in mitochondrial proteins of reptiles (Castoe et al. 2009). Understanding how evolutionary constraints act differently in protein evolution will be a challenge for future work.

ACKNOWLEDGMENTS

I am deeply indebted to Professor Mitsuyasu Hasebe for his generous supports, advices, and helpful discussion. Genomics and Evo-Devo works of carnivorous plants would have not been possible without his understandings and supports.

I sincerely wish to thank many colleagues for collaborations works. Hironori Fujita developed and performed the computational simulation of *Sarracenia* leaf development. Naomi Sumikawa cloned *PHABULOSA* and *FILAMENTOUS FLOWER* from *S. purpurea* in Chapter 3. She also contributed to the project of Chapter 4 in which she determined amino acid sequences of digestive enzymes. Takahiro Yamaguchi designed the molecular cloning of the developmental genes in *S. purpurea* and supervised the works in Chapter 3. Hirokazu Tsukaya and Masayoshi Kawaguchi also supervised the works in Chapter 3. Shoko Ooi, Tomoko Shibata, and Shuji Shigenobu supported genome and transcriptome sequencing of carnivorous plants. Huimin Cai, Likai Mao, Hongyan Zhang, and Xiaodong Fang supported sequencing and characterization of the Cephalotus genome. Tomoaki Nishiyama helped a lot in genome assembly of the Cephalotus. He also supported me to get started learning about bioinformatics. Takamasa Imai, and Masahiro Kasahara conducted error correction of PacBio reads and gap filling of the Cephalotus genome. Yumiko Makino performed protein sequencing by Edman degradation method. Yoko Matsuzaki supported me in plasmid construction, virus-induced gene silencing, and plant cultivation.

I also thank the Functional Genomics Facility, Model Plant Research Facility, and Data Integration and Analysis Facility of the National Institute for Basic Biology. I thank Ikumi Kajikawa for plant cultivation. I am also grateful to Takeshi Shimada and Tomomi Sugaya for giving us *Heliamphora nutans* and Arabidopsis plants, respectively. Elena Kramer kindly provided *Tobacco Rattle Virus* vectors and trained me for experimental techniques of virus-induced gene silencing. Masanao Sato kindly taught me a basic lesson about statistics from scratch. I thank all the past and present members of Prof. Hasebe's laboratory for giving me many helps.

This thesis was partly supported by Japan Society for the Promotion of Science.

Finally, I thank my family and friends for many supports.

LIST OF REFERENCES

Abera MK, Verboven P, Defraeye T, Fanta SW, Hertog ML, Carmeliet J, Nicolai BM (2014) A plant cell division algorithm based on cell biomechanics and ellipse-fitting. Ann Bot 114: 605-617

Adenot X, Elmayan T, Lauressergues D, Boutet S, Bouche N, Gasciolli V, Vaucheret H (2006) DRB4-dependent *TAS3 trans*-acting siRNAs control leaf morphology through AGO7. Curr Biol 16: 927-932

Adlassnig W, Koller-Peroutka M, Bauer S, Koshkin E, Lendl T, Lichtscheidl IK (2012) Endocytotic uptake of nutrients in carnivorous plants. Plant J 71: 303-313

Albert VA, Williams SE, Chase MW (1992) Carnivorous plants: phylogeny and structural evolution. Science 257: 1491-1495

Allen E, Xie Z, Gustafson AM, Carrington JC (2005) microRNA-directed phasing during trans-acting siRNA biogenesis in plants. Cell 121: 207-221

Altschul SF, Gish W, Miller W, Myers EW, Lipman DJ (1990) Basic local alignment search tool. J Mol Biol 215: 403-410

Altschul SF, Madden TL, Schaffer AA, Zhang J, Zhang Z, Miller W, Lipman DJ (1997) Gapped BLAST and PSI-BLAST: a new generation of protein database search programs. Nucleic Acids Res 25: 3389-3402

An CI, Fukusaki E, Kobayashi A (2001) Plasma-membrane H+-ATPases are expressed in pitchers of the carnivorous plant *Nepenthes alata* Blanco. Planta 212: 547-555

Anastasiou E, Kenz S, Gerstung M, MacLean D, Timmer J, Fleck C, Lenhard M (2007) Control of plant organ size by *KLUH/CYP78A5*-dependent intercellular signaling. Dev Cell 13: 843-856

Arber A (1918) The phyllode theory of the monocotyledonous leaf, with special reference to anatomical evidence. Ann Bot os-32: 465-501

Arber A (1921) The leaf structure of the Iridaceae, considered in relation to the phyllode theory. Ann Bot os-35: 301-336

Arber A (1923) Leaves of the Gramineae. Bot Gaz 76: 374-388

Argout X, Salse J, Aury JM, Guiltinan MJ, Droc G, Gouzy J, Allegre M, Chaparro C, Legavre T, Maximova SN, Abrouk M, Murat F, Fouet O, Poulain J, Ruiz M, Roguet Y, Rodier-Goud M, Barbosa-Neto JF, Sabot F, Kudrna D, Ammiraju JS, Schuster SC, Carlson JE, Sallet E, Schiex T, Dievart A, Kramer M, Gelley L, Shi Z, Berard A, Viot C, Boccara M, Risterucci AM, Guignon V, Sabau X, Axtell MJ, Ma Z, Zhang Y, Brown S, Bourge M, Golser W, Song X, Clement D, Rivallan R, Tahi M, Akaza JM, Pitollat B, Gramacho K, D'Hont A, Brunel D, Infante D, Kebe I, Costet P, Wing R, McCombie WR, Guiderdoni E, Quetier F, Panaud O, Wincker P, Bocs S, Lanaud C (2011) The genome of *Theobroma cacao*. Nat Genet 43: 101-108

Athauda SB, Matsumoto K, Rajapakshe S, Kuribayashi M, Kojima M, Kubomura-Yoshida N, Iwamatsu A, Shibata C, Inoue H, Takahashi K (2004) Enzymic and structural characterization of nepenthesin, a unique member of a novel subfamily of aspartic proteinases. Biochem J 381: 295-306

Axtell MJ (2013) ShortStack: comprehensive annotation and quantification of small RNA genes. RNA 19: 740-751

Böcher TW (1981) Evolutionary trends in Ericalean leaf structure. Biol Skr Kgl Danske Vidensk Selsk 23: 1-64

Barton NH, Briggs DEG, Eisen JA, Goldstein DB, Patel NH (2007) Evolution. Cold Spring Harbor Laboratory Press, New York

Becker A, Lange M (2010) VIGS—genomics goes functional. Trends Plant Sci 15: 1-4

Bell AD, Bryan A (2008) Plant Form: An Illustrated Guide to Flowering Plant Morphology. Timber Press, London

Bell CD, Soltis DE, Soltis PS (2010) The age and diversification of the angiosperms re-revisited. Am J Bot 97: 1296-1303

Bendell CJ, Liu S, Aumentado-Armstrong T, Istrate B, Cernek PT, Khan S, Picioreanu S,

Zhao M, Murgita RA (2014) Transient protein-protein interface prediction: datasets, features, algorithms, and the RAD-T predictor. BMC Bioinformatics 15: 1471-2105
Benjamini Y, Hochberg Y (1995) Controlling the false discovery rate: a practical and powerful approach to multiple testing. J R Stat Soc Ser B Stat Methodol: 289-300
Benson G (1999) Tandem repeats finder: a program to analyze DNA sequences. Nucleic Acids Res 27: 573-580
Biasini M, Bienert S, Waterhouse A, Arnold K, Studer G, Schmidt T, Kiefer F, Cassarino TG, Bertoni M, Bordoli L, Schwede T (2014) SWISS-MODEL: modelling protein tertiary and quaternary structure using evolutionary information. Nucleic Acids Res 42: 29
Birney E, Durbin R (2000) Using GeneWise in the *Drosophila* annotation experiment. Genome Res 10: 547-548
Bohmert K, Camus I, Bellini C, Bouchez D, Caboche M, Benning C (1998) *AGO1* defines a novel locus of *Arabidopsis* controlling leaf development. EMBO J 17: 170-180
Boke NH (1940) Histogenesis and morphology of the phyllode in certain species of Acacia. Am J Bot 27: 73-90
Bonaccorso O, Lee JE, Puah L, Scutt CP, Golz JF (2012) *FILAMENTOUS FLOWER* controls lateral organ development by acting as both an activator and a repressor. BMC Plant Biol 12: 1471-2229
Bowman J (1994) *ARABIDOPSIS*: An Atlas of Morphology and Development. Springer New York
Bozorg B, Krupinski P, Jonsson H (2014) Stress and strain provide positional and directional cues in development. PLoS Comput Biol 10: 9
Braybrook SA, Kuhlemeier C (2010) How a plant builds leaves. Plant Cell 22: 1006-1018
Buch F, Pauchet Y, Rott M, Mithofer A (2014) Characterization and heterologous expression of a PR-1 protein from traps of the carnivorous plant *Nepenthes mirabilis*. Phytochemistry 100: 43-50
Buch F, Rott M, Rottloff S, Paetz C, Hilke I, Raessler M, Mithofer A (2013) Secreted pitfall-trap fluid of carnivorous *Nepenthes* plants is unsuitable for microbial growth. Ann Bot 111: 375-383
Buchmann A, Alber M, Zartman JJ (2014) Sizing it up: The mechanical feedback hypothesis of organ growth regulation. Semin Cell Dev Biol 35: 73-81
Bustamante CD, Townsend JP, Hartl DL (2000) Solvent accessibility and purifying selection within proteins of *Escherichia coli* and *Salmonella enterica*. Mol Biol Evol 17: 301-308
Byrne ME, Barley R, Curtis M, Arroyo JM, Dunham M, Hudson A, Martienssen RA (2000) *Asymmetric leaves1* mediates leaf patterning and stem cell function in *Arabidopsis*. Nature 408: 967-971
Candela H, Johnston R, Gerhold A, Foster T, Hake S (2008) The *milkweed pod1* gene encodes a KANADI protein that is required for abaxial/adaxial patterning in maize leaves. Plant Cell 20: 2073-2087
Capella-Gutierrez S, Silla-Martinez JM, Gabaldon T (2009) trimAl: a tool for automated alignment trimming in large-scale phylogenetic analyses. Bioinformatics 25: 1972-1973
Carlsbecker A, Lee JY, Roberts CJ, Dettmer J, Lehesranta S, Zhou J, Lindgren O, Moreno-Risueno MA, Vatén A, Thitamadee S, Campilho A, Sebastian J, Bowman JL, Helariutta Y, Benfey PN (2010) Cell signalling by microRNA165/6 directs gene dose-dependent root cell fate. Nature 465: 316-321
Castoe TA, de Koning AP, Kim HM, Gu W, Noonan BP, Naylor G, Jiang ZJ, Parkinson CL, Pollock DD (2009) Evidence for an ancient adaptive episode of convergent molecular evolution. Proc Natl Acad Sci USA 106: 8986-8991
Charlton WA (1993) The rotated-lamina syndrome. I. Ulmaceae. Can J Bot 71: 211-221
Chen K, Durand D, Farach-Colton M (2000) NOTUNG: a program for dating gene duplications and optimizing gene family trees. J Comput Biol 7: 429-447
Chitwood DH, Nogueira FT, Howell MD, Montgomery TA, Carrington JC, Timmermans MC (2009) Pattern formation via small RNA mobility. Genes Dev 23: 549-554
Cho S-H, Yoo S-C, Zhang H, Pandeya D, Koh H-J, Hwang J-Y, Kim G-T, Paek N-C (2013)

The rice *narrow leaf2* and *narrow leaf3* loci encode WUSCHEL-related homeobox 3A (OsWOX3A) and function in leaf, spikelet, tiller and lateral root development. New Phytol 198: 1071-1084

Choi SS, Vallender EJ, Lahn BT (2006) Systematically assessing the influence of 3-dimensional structural context on the molecular evolution of mammalian proteomes. Mol Biol Evol 23: 2131-2133

Christin PA, Besnard G, Edwards EJ, Salamin N (2012) Effect of genetic convergence on phylogenetic inference. Mol Phylogenet Evol 62: 921-927

Cunninghame ME, Lyndon RF (1986) The relationship between the distribution of periclinal cell divisions in the shoot apex and leaf initiation. Ann Bot 57: 737-746

Dai M, Hu Y, Zhao Y, Liu H, Zhou DX (2007) A *WUSCHEL-LIKE HOMEOBOX* gene represses a *YABBY* gene expression required for rice leaf development. Plant Physiol 144: 380-390

Darwin C (1875) Insectivorous plants. D. Appleton and Company, New York

De Vries H (1905) Species and Varieties: Their Origin by Mutation. The Open Court Publishing Co., Chicago

Dengler N, Kang J (2001) Vascular patterning and leaf shape. Curr Opin Plant Biol 4: 50-56

Di Giusto B, Bessière J-M, Guéroult M, Lim LBL, Marshall DJ, Hossaert-McKey M, Gaume L (2010) Flower-scent mimicry masks a deadly trap in the carnivorous plant *Nepenthes rafflesiana*. J Ecol 98: 845-856

Ditt RF, Kerr KF, de Figueiredo P, Delrow J, Comai L, Nester EW (2006) The *Arabidopsis thaliana* transcriptome in response to *Agrobacterium tumefaciens*. Mol Plant Microbe Interact 19: 665-681

Dong X, Mindrinos M, Davis KR, Ausubel FM (1991) Induction of *Arabidopsis* defense genes by virulent and avirulent *Pseudomonas syringae* strains and by a cloned avirulence gene. Plant Cell 3: 61-72

Douglas RN, Wiley D, Sarkar A, Springer N, Timmermans MC, Scanlon MJ (2010) *ragged seedling2* encodes an ARGONAUTE7-like protein required for mediolateral expansion, but not dorsiventrality, of maize leaves. Plant Cell 22: 1441-1451

Doxey AC, Yaish MW, Moffatt BA, Griffith M, McConkey BJ (2007) Functional divergence in the *Arabidopsis* beta-1,3-glucanase gene family inferred by phylogenetic reconstruction of expression states. Mol Biol Evol 24: 1045-1055

Doyon JP, Ranwez V, Daubin V, Berry V (2011) Models, algorithms and programs for phylogeny reconciliation. Brief Bioinform 12: 392-400

Dsouza M, Larsen N, Overbeek R (1997) Searching for patterns in genomic data. Trends Genet 13: 497-498

Dunoyer P, Schott G, Himber C, Meyer D, Takeda A, Carrington JC, Voinnet O (2010) Small RNA duplexes function as mobile silencing signals between plant cells. Science 328: 912-916

Dupuy L, Mackenzie J, Rudge T, Haseloff J (2008) A system for modelling cell–cell interactions during plant morphogenesis. Ann Bot 101: 1255-1265

Ellison AM, Gotelli NJ (2002) Nitrogen availability alters the expression of carnivory in the northern pitcher plant, *Sarracenia purpurea*. Proc Natl Acad Sci USA 99: 4409-4412

Ellison AM, Gotelli NJ (2009) Energetics and the evolution of carnivorous plants—Darwin's 'most wonderful plants in the world'. J Exp Bot 60: 19-42

Emery JF, Floyd SK, Alvarez J, Eshed Y, Hawker NP, Izhaki A, Baum SF, Bowman JL (2003) Radial patterning of *Arabidopsis* shoots by class III HD-ZIP and KANADI genes. Curr Biol 13: 1768-1774

English AC, Richards S, Han Y, Wang M, Vee V, Qu J, Qin X, Muzny DM, Reid JG, Worley KC, Gibbs RA (2012) Mind the gap: upgrading genomes with Pacific Biosciences RS long-read sequencing technology. PLoS One 7: 21

Esau K (1977) Anatomy of Seed Plants. Wiley, New York

Eshed Y, Baum SF, Bowman JL (1999) Distinct mechanisms promote polarity establishment in carpels of *Arabidopsis*. Cell 99: 199-209

Eshed Y, Baum SF, Perea JV, Bowman JL (2001) Establishment of polarity in lateral organs of plants. Curr Biol 11: 1251-1260

Eshed Y, Izhaki A, Baum SF, Floyd SK, Bowman JL (2004) Asymmetric leaf development and blade expansion in *Arabidopsis* are mediated by KANADI and YABBY activities. Development 131: 2997-3006

Farhadifar R, Roper JC, Aigouy B, Eaton S, Julicher F (2007) The influence of cell mechanics, cell-cell interactions, and proliferation on epithelial packing. Curr Biol 17: 2095-2104

Felsenstein J (1989) PHYLIP-phylogeny inference package (version 3.2). Cladistics 5: 164-166

Finet C, Berne-Dedieu A, Scutt CP, Marletaz F (2013) Evolution of the ARF gene family in land plants: old domains, new tricks. Mol Biol Evol 30: 45-56

Finet C, Fourquin C, Vinauger M, Berne-Dedieu A, Chambrier P, Paindavoine S, Scutt CP (2010) Parallel structural evolution of auxin response factors in the angiosperms. Plant J 63: 952-959

Fletcher AG, Osterfield M, Baker RE, Shvartsman SY (2014) Vertex models of epithelial morphogenesis. Biophys J 106: 2291-2304

Fozard JA, Lucas M, King JR, Jensen OE (2013) Vertex-element models for anisotropic growth of elongated plant organs. Front Plant Sci 4

Franck DH (1975) Early histogenesis of the adult leaves of *Darlingtonia californica* (Sarraceniaceae) and its bearing on the nature of epiascidiate foliar appendages. Am J Bot 62: 116-132

Franck DH (1976) The morphological interpretation of epiascidiate leaves —An historical perspective—. Bot Rev 42: 345-388

Fu Y, Xu L, Xu B, Yang L, Ling Q, Wang H, Huang H (2007) Genetic interactions between leaf polarity-controlling genes and *ASYMMETRIC LEAVES1* and *2* in *Arabidopsis* leaf patterning. Plant Cell Physiol 48: 724-735

Fukushima K, Hasebe M (2014) Adaxial–abaxial polarity: the developmental basis of leaf shape diversity. genesis 52: 1-18

Futuyma D (2009) Evolution (2nd ed). Sinauer Associates, Inc, Sunderland, MA, USA

Garcia D, Collier SA, Byrne ME, Martienssen RA (2006) Specification of leaf polarity in *Arabidopsis* via the *trans*-acting siRNA pathway. Curr Biol 16: 933-938

Gerhardt L, Sachetto-Martins G, Contarini M, Sandroni M, de PFR, de Lima V, Cordeiro M, de Oliveira D, Margis-Pinheiro M (1997) *Arabidopsis thaliana* class IV chitinase is early induced during the interaction with *Xanthomonas campestris*. FEBS Lett 419: 69-75

Gibson G, Dworkin I (2004) Uncovering cryptic genetic variation. Nat Rev Genet 5: 681-690

Gibson WT, Veldhuis JH, Rubinstein B, Cartwright HN, Perrimon N, Brodland GW, Nagpal R, Gibson MC (2011) Control of the mitotic cleavage plane by local epithelial topology. Cell 144: 427-438

Givnish TJ, Vermeij GJ (1976) Sizes and shapes of liane leaves. Am Nat 110: 743-778

Gleissberg S, Groot EP, Schmalz M, Eichert M, Kolsch A, Hutter S (2005) Developmental events leading to peltate leaf structure in *Tropaeolum majus* (Tropaeolaceae) are associated with expression domain changes of a YABBY gene. Dev Genes Evol 215: 313-319

Gnerre S, Maccallum I, Przybylski D, Ribeiro FJ, Burton JN, Walker BJ, Sharpe T, Hall G, Shea TP, Sykes S, Berlin AM, Aird D, Costello M, Daza R, Williams L, Nicol R, Gnirke A, Nusbaum C, Lander ES, Jaffe DB (2011) High-quality draft assemblies of mammalian genomes from massively parallel sequence data. Proc Natl Acad Sci USA 108: 1513-1518

Goldman N, Thorne JL, Jones DT (1998) Assessing the impact of secondary structure and solvent accessibility on protein evolution. Genetics 149: 445-458

Golz JF, Roccaro M, Kuzoff R, Hudson A (2004) *GRAMINIFOLIA* promotes growth and polarity of *Antirrhinum* leaves. Development 131: 3661-3670

Gonzalez N, Vanhaeren H, Inze D (2012) Leaf size control: complex coordination of cell

division and expansion. Trends Plant Sci 17: 332-340
Grabherr MG, Haas BJ, Yassour M, Levin JZ, Thompson DA, Amit I, Adiconis X, Fan L, Raychowdhury R, Zeng Q, Chen Z, Mauceli E, Hacohen N, Gnirke A, Rhind N, di Palma F, Birren BW, Nusbaum C, Lindblad-Toh K, Friedman N, Regev A (2011) Full-length transcriptome assembly from RNA-Seq data without a reference genome. Nat Biotechnol 29: 644-652
Gray YHM (2000) It takes two transposons to tango:transposable-element-mediated chromosomal rearrangements. Trends Genet 16: 461-468
Groff PA, Kaplan DR (1988) The relation of root systems to shoot systems in vascular plants. Bot Rev 54: 387-422
Hagemann W, Gleissberg S (1996) Organogenetic capacity of leaves: the significance of marginal blastozones in angiosperms. Plant Syst Evol 199: 121-152
Hagerup O (1946) Studies on the Empetraceae. Kgl Danske Vidensk Selsk Biol Medd 20: 1-49
Hamilton A (1904) Notes on the West Australian pitcher plant (*Cephalotus follicularis* Labill.). Proc Linn Soc NSW 29: 36-56
Hanson L, McMahon KA, Johnson MAT, Bennett MD (2001) First Nuclear DNA C-values for 25 Angiosperm Families. Ann Bot 87: 251-258
Hardcastle TJ, Kelly KA (2010) baySeq: empirical Bayesian methods for identifying differential expression in sequence count data. BMC Bioinformatics 11: 1471-2105
Hatano N, Hamada T (2008) Proteome analysis of pitcher fluid of the carnivorous plant *Nepenthes alata*. J Proteome Res 7: 809-816
Hatano N, Hamada T (2012) Proteomic analysis of secreted protein induced by a component of prey in pitcher fluid of the carnivorous plant *Nepenthes alata*. J Proteomics 75: 4844-4852
Hawkins RD, Hon GC, Ren B (2010) Next-generation genomics: an integrative approach. Nat Rev Genet 11: 476-486
Heubl G, Bringmann G, Meimberg H (2006) Molecular phylogeny and character evolution of carnivorous plant families in Caryophyllales — revisited. Plant Biol 8: 821-830
Hileman LC, Drea S, Martino G, Litt A, Irish VF (2005) Virus-induced gene silencing is an effective tool for assaying gene function in the basal eudicot species *Papaver somniferum* (opium poppy). Plant J 44: 334-341
Hillson CJ (1979) Leaf development in *Senecio rowleyanus* (Compositae). Am J Bot 66: 59-63
Hillwig MS, Lebrasseur ND, Green PJ, Macintosh GC (2008) Impact of transcriptional, ABA-dependent, and ABA-independent pathways on wounding regulation of RNS1 expression. Mol Genet Genomics 280: 249-261
Hofer J, Turner L, Moreau C, Ambrose M, Isaac P, Butcher S, Weller J, Dupin A, Dalmais M, Le Signor C, Bendahmane A, Ellis N (2009) *Tendril-less* regulates tendril formation in pea leaves. Plant Cell 21: 420-428
Honda H, Tanemura M, Nagai T (2004) A three-dimensional vertex dynamics cell model of space-filling polyhedra simulating cell behavior in a cell aggregate. J Theor Biol 226: 439-453
Huang W, Pi L, Liang W, Xu B, Wang H, Cai R, Huang H (2006) The proteolytic function of the *Arabidopsis* 26S proteasome is required for specifying leaf adaxial identity. Plant Cell 18: 2479-2492
Igarashi A, Yamagata K, Sugai T, Takahashi Y, Sugawara E, Tamura A, Yaegashi H, Yamagishi N, Takahashi T, Isogai M, Takahashi H, Yoshikawa N (2009) *Apple latent spherical virus* vectors for reliable and effective virus-induced gene silencing among a broad range of plants including tobacco, tomato, *Arabidopsis thaliana*, cucurbits, and legumes. Virology 386: 407-416
Ishiwata A, Ozawa M, Nagasaki H, Kato M, Noda Y, Yamaguchi T, Nosaka M, Shimizu-Sato S, Nagasaki A, Maekawa M, Hirano H-Y, Sato Y (2013) Two *WUSCHEL-related homeobox* genes, *narrow leaf2* and *narrow leaf3*, control leaf width in rice. Plant Cell

Physiol 54: 779-792
Iwasaki M, Takahashi H, Iwakawa H, Nakagawa A, Ishikawa T, Tanaka H, Matsumura Y, Pekker I, Eshed Y, Vial-Pradel S, Ito T, Watanabe Y, Ueno Y, Fukazawa H, Kojima S, Machida Y, Machida C (2013) Dual regulation of *ETTIN* (*ARF3*) gene expression by AS1-AS2, which maintains the DNA methylation level, is involved in stabilization of leaf adaxial-abaxial partitioning in *Arabidopsis*. Development 140: 1958-1969
Jürgens A, El-Sayed AM, Suckling DM (2009) Do carnivorous plants use volatiles for attracting prey insects? Funct Ecol 23: 875-887
James SA, Bell DT (2000) Leaf orientation, light interception and stomatal conductance of *Eucalyptus globulus* ssp. *globulus* leaves. Tree Physiol 20: 815-823
Johnson MAT (1979) Chromosome Numbers in *Akania* and *Cephalotus*. Kew Bull 34: 37-38
Johnston R, Candela H, Hake S, Foster T (2010) The maize *milkweed pod1* mutant reveals a mechanism to modify organ morphology. genesis 48: 416-423
Jones-Rhoades MW, Bartel DP (2004) Computational identification of plant microRNAs and their targets, including a stress-induced miRNA. Mol Cell 14: 787-799
Juarez MT, Kui JS, Thomas J, Heller BA, Timmermans MC (2004a) microRNA-mediated repression of *rolled leaf1* specifies maize leaf polarity. Nature 428: 84-88
Juarez MT, Twigg RW, Timmermans MCP (2004b) Specification of adaxial cell fate during maize leaf development. Development 131: 4533-4544
Juniper BE, Robins RJ, Joel DM (1989) The Carnivorous Plants. Academic Press, London
Kadota K, Nishiyama T, Shimizu K (2012) A normalization strategy for comparing tag count data. Algorithms Mol Biol 7: 1748-7188
Kaplan D (1975) Comparative developmental evaluation of the morphology of unifacial leaves in the monocotyledons. Bot Jahrb Syst 95: 1-105
Kaplan DR (1970) Comparative foliar histogenesis in *Acorus calamus* and its bearing on the phyllode theory of monocotyledonous leaves. Am J Bot 57: 331-361
Kaplan DR (1973) The problem of leaf morphology and evolution in the monocotyledons. Q Rev Biol 48: 437-457
Kaplan DR (2001) Fundamental concepts of leaf morphology and morphogenesis: a contribution to the interpretation of molecular genetic mutants. Int J Plant Sci 162: 465-474
Katoh K, Standley DM (2013) MAFFT multiple sequence alignment software version 7: improvements in performance and usability. Mol Biol Evol 30: 772-780
Kaul RB (1977) The role of the multiple epidermis in foliar succulence of Peperomia (Piperaceae). Bot Gaz 138: 213-218
Kawade K, Horiguchi G, Usami T, Hirai MY, Tsukaya H (2013) ANGUSTIFOLIA3 signaling coordinates proliferation between clonally distinct cells in leaves. Curr Biol 23: 788-792
Keighery GJ (1979) Chromosome counts in *Cephalotus* (*Cephalotaceae*). Plant Syst Evol 133: 103-104
Kelley DR, Arreola A, Gallagher TL, Gasser CS (2012) ETTIN (ARF3) physically interacts with KANADI proteins to form a functional complex essential for integument development and polarity determination in *Arabidopsis*. Development 139: 1105-1109
Kerstetter RA, Bollman K, Taylor RA, Bomblies K, Poethig RS (2001) *KANADI* regulates organ polarity in *Arabidopsis*. Nature 411: 706-709
Kidner CA, Martienssen RA (2004) Spatially restricted microRNA directs leaf polarity through ARGONAUTE1. Nature 428: 81-84
Kidner CA, Wrigley S (2010) Patches, pegs and piggies. New Phytol 187: 13-17
Kim M, McCormick S, Timmermans M, Sinha N (2003a) The expression domain of *PHANTASTICA* determines leaflet placement in compound leaves. Nature 424: 438-443
Kim M, Pham T, Hamidi A, McCormick S, Kuzoff RK, Sinha N (2003b) Reduced leaf complexity in tomato wiry mutants suggests a role for *PHAN* and *KNOX* genes in generating compound leaves. Development 130: 4405-4415
Kojima S, Iwasaki M, Takahashi H, Imai T, Matsumura Y, Fleury D, Van Lijsebettens M,

Machida Y, Machida C (2011) ASYMMETRIC LEAVES2 and Elongator, a histone acetyltransferase complex, mediate the establishment of polarity in leaves of *Arabidopsis thaliana*. Plant Cell Physiol 52: 1259-1273

Kondo K (1969) Chromosome numbers of carnivorous plants. Bull Torrey Bot Club 96: 322-328

Korn RW (2010) Naturally occurring ectopic growths in certain *Xanthosoma* and *Begonia* cultivars and the problem of leaf dorsiventral polarity. New Phytol 187: 9-13

Kozomara A, Griffiths-Jones S (2014) miRBase: annotating high confidence microRNAs using deep sequencing data. Nucleic Acids Res 42: D68-73

Kreuzwieser J, Scheerer U, Kruse J, Burzlaff T, Honsel A, Alfarraj S, Georgiev P, Schnitzler JP, Ghirardo A, Kreuzer I, Hedrich R, Rennenberg H (2014) The Venus flytrap attracts insects by the release of volatile organic compounds. J Exp Bot 65: 755-766

Krolicka A, Szpitter A, Gilgenast E, Romanik G, Kaminski M, Lojkowska E (2008) Stimulation of antibacterial naphthoquinones and flavonoids accumulation in carnivorous plants grown *in vitro* by addition of elicitors. Enzyme Microb Tech 42: 216-221

Kron K, Judd W, Stevens P, Crayn D, Anderberg A, Gadek P, Quinn C, Luteyn J (2002) Phylogenetic classification of Ericaceae: molecular and morphological evidence. Bot Rev 68: 335-423

La Rota C, Chopard J, Das P, Paindavoine S, Rozier F, Farcot E, Godin C, Traas J, Moneger F (2011) A data-driven integrative model of sepal primordium polarity in *Arabidopsis*. Plant Cell 23: 4318-4333

Lee SW, Feugier FG, Morishita Y (2014) Canalization-based vein formation in a growing leaf. J Theor Biol 353: 104-120

Levin JZ, Yassour M, Adiconis X, Nusbaum C, Thompson DA, Friedman N, Gnirke A, Regev A (2010) Comprehensive comparative analysis of strand-specific RNA sequencing methods. Nat Methods 7: 709-715

Levine E, McHale P, Levine H (2007) Small regulatory RNAs may sharpen spatial expression patterns. PLoS Comput Biol 3: e233

Lewis FT (1928) The correlation between cell division and the shapes and sizes of prismatic cells in the epidermis of Cucumis. Anat Rec 38: 341-376

Li H, Xu L, Wang H, Yuan Z, Cao X, Yang Z, Zhang D, Xu Y, Huang H (2005) The Putative RNA-dependent RNA polymerase *RDR6* acts synergistically with *ASYMMETRIC LEAVES1* and *2* to repress *BREVIPEDICELLUS* and MicroRNA165/166 in Arabidopsis leaf development. Plant Cell 17: 2157-2171

Liu Q, Yao X, Pi L, Wang H, Cui X, Huang H (2009) The *ARGONAUTE10* gene modulates shoot apical meristem maintenance and establishment of leaf polarity by repressing miR165/166 in Arabidopsis. Plant J 58: 27-40

Lloyd FE (1942) The carnivorous plants. Chronica Botanica Campany, Waltham, MA, USA

Lohrasebi T, Zamani K, Sabet MS, Malboobi MA (2013) Fungal infection alters phosphate level and phosphatase profiles in *Arabidopsis*. Progr Biol Sci 2: 42-57

Lorenz R, Bernhart SH, Honer Zu Siederdissen C, Tafer H, Flamm C, Stadler PF, Hofacker IL (2011) ViennaRNA Package 2.0. Algorithms Mol Biol 6: 1748-7188

MacIntosh GC, Hillwig MS, Meyer A, Flagel L (2010) RNase T2 genes from rice and the evolution of secretory ribonucleases in plants. Mol Genet Genomics 283: 381-396

Magnani E, Barton MK (2011) A per-ARNT-sim-like sensor domain uniquely regulates the activity of the homeodomain leucine zipper transcription factor REVOLUTA in *Arabidopsis*. Plant Cell 23: 567-582

Mallory AC, Reinhart BJ, Jones-Rhoades MW, Tang G, Zamore PD, Barton MK, Bartel DP (2004) MicroRNA control of *PHABULOSA* in leaf development: importance of pairing to the microRNA 5' region. EMBO J 23: 3356-3364

Marcais G, Kingsford C (2011) A fast, lock-free approach for efficient parallel counting of occurrences of k-mers. Bioinformatics 27: 764-770

McConnell JR, Barton MK (1998) Leaf polarity and meristem formation in *Arabidopsis*.

Development 125: 2935-2942
McConnell JR, Emery J, Eshed Y, Bao N, Bowman J, Barton MK (2001) Role of *PHABULOSA* and *PHAVOLUTA* in determining radial patterning in shoots. Nature 411: 709-713
McHale NA (1993) *LAM-1* and *FAT* genes control development of the leaf blade in *Nicotiana sylvestris*. Plant Cell 5: 1029-1038
McHale NA, Koning RE (2004a) MicroRNA-directed cleavage of *Nicotiana sylvestris PHAVOLUTA* mRNA regulates the vascular cambium and structure of apical meristems. Plant Cell 16: 1730-1740
McHale NA, Koning RE (2004b) *PHANTASTICA* regulates development of the adaxial mesophyll in Nicotiana leaves. Plant Cell 16: 1251-1262
McPherson S (2009) Pitcher plants of the old world. Redfern Natural History Productions, Poole, Dorset, England
Mecchia MA, Debernardi JM, Rodriguez RE, Schommer C, Palatnik JF (2013) MicroRNA miR396 and *RDR6* synergistically regulate leaf development. Mech Dev 130: 2-13
Meimberg H, Dittrich P, Bringmann G, Schlauer J, Heubl G (2000) Molecular phylogeny of Caryophyllidae s.l. based on *matK* sequences with special emphasis on carnivorous taxa. Plant Biol 2: 218-228
Merks RM, Guravage M, Inze D, Beemster GT (2011) VirtualLeaf: an open-source framework for cell-based modeling of plant tissue growth and development. Plant Physiol 155: 656-666
Mineyuki Y, Marc J, Palevitz BA (1988) Formation of the oblique spindle in dividing guard mother cells of *Allium*. Protoplasma 147: 200-203
Mithofer A (2011) Carnivorous pitcher plants: insights in an old topic. Phytochemistry 72: 1678-1682
Miyashima S, Honda M, Hashimoto K, Tatematsu K, Hashimoto T, Sato-Nara K, Okada K, Nakajima K (2013) A comprehensive expression analysis of the Arabidopsis *MICRORNA165/6* gene family during embryogenesis reveals a conserved role in meristem specification and a non-cell-autonomous function. Plant Cell Physiol 54: 375-384
Miyashima S, Koi S, Hashimoto T, Nakajima K (2011) Non-cell-autonomous microRNA165 acts in a dose-dependent manner to regulate multiple differentiation status in the *Arabidopsis* root. Development 138: 2303-2313
Molnar A, Melnyk CW, Bassett A, Hardcastle TJ, Dunn R, Baulcombe DC (2010) Small silencing RNAs in plants are mobile and direct epigenetic modification in recipient cells. Science 328: 872-875
Mukherjee AK, Carp M-J, Zuchman R, Ziv T, Horwitz BA, Gepstein S (2010) Proteomics of the response of *Arabidopsis thaliana* to infection with *Alternaria brassicicola*. J Proteomics 73: 709-720
Murashige T, Skoog F (1962) A revised medium for rapid growth and bio assays with tobacco tissue cultures. Physiol Plantarum 15: 473-497
Nagai T, Honda H (2001) A dynamic cell model for the formation of epithelial tissues. Philos Mag B 81: 699-719
Nagasaki H, Itoh J, Hayashi K, Hibara K, Satoh-Nagasawa N, Nosaka M, Mukouhata M, Ashikari M, Kitano H, Matsuoka M, Nagato Y, Sato Y (2007) The small interfering RNA production pathway is required for shoot meristem initiation in rice. Proc Natl Acad Sci USA 104: 14867-14871
Nakamura Y, Gojobori T, Ikemura T (2000) Codon usage tabulated from international DNA sequence databases: status for the year 2000. Nucleic Acids Res 28: 292
Nakata M, Matsumoto N, Tsugeki R, Rikirsch E, Laux T, Okada K (2012) Roles of the middle domain-specific *WUSCHEL-RELATED HOMEOBOX* genes in early development of leaves in *Arabidopsis*. Plant Cell 24: 519-535
Nakayama H, Yamaguchi T, Tsukaya H (2012) Acquisition and diversification of cladodes: leaf-like organs in the genus *Asparagus*. Plant Cell 24: 929-940

Nardmann J, Ji J, Werr W, Scanlon MJ (2004) The maize duplicate genes *narrow sheath1* and *narrow sheath2* encode a conserved homeobox gene function in a lateral domain of shoot apical meristems. Development 131: 2827-2839

Nardmann J, Zimmermann R, Durantini D, Kranz E, Werr W (2007) *WOX* gene phylogeny in *Poaceae*: a comparative approach addressing leaf and embryo development. Mol Biol Evol 24: 2474-2484

Nishimura E, Kawahara M, Kodaira R, Kume M, Arai N, Nishikawa J, Ohyama T (2013) S-like ribonuclease gene expression in carnivorous plants. Planta 238: 955-967

Nishimura T, Wada T, Okada K (2004) A key factor of translation reinitiation, ribosomal protein L24, is involved in gynoecium development in *Arabidopsis*. Biochem Soc Trans 32: 611-613

Nishimura T, Wada T, Yamamoto KT, Okada K (2005) The *Arabidopsis* STV1 protein, responsible for translation reinitiation, is required for auxin-mediated gynoecium patterning. Plant Cell 17: 2940-2953

Nogueira FT, Madi S, Chitwood DH, Juarez MT, Timmermans MC (2007) Two small regulatory RNAs establish opposing fates of a developmental axis. Genes Dev 21: 750-755

Nystedt B, Street NR, Wetterbom A, Zuccolo A, Lin YC, Scofield DG, Vezzi F, Delhomme N, Giacomello S, Alexeyenko A, Vicedomini R, Sahlin K, Sherwood E, Elfstrand M, Gramzow L, Holmberg K, Hallman J, Keech O, Klasson L, Koriabine M, Kucukoglu M, Kaller M, Luthman J, Lysholm F, Niittyla T, Olson A, Rilakovic N, Ritland C, Rossello JA, Sena J, Svensson T, Talavera-Lopez C, Theissen G, Tuominen H, Vanneste K, Wu ZQ, Zhang B, Zerbe P, Arvestad L, Bhalerao R, Bohlmann J, Bousquet J, Garcia Gil R, Hvidsten TR, de Jong P, MacKay J, Morgante M, Ritland K, Sundberg B, Thompson SL, Van de Peer Y, Andersson B, Nilsson O, Ingvarsson PK, Lundeberg J, Jansson S (2013) The Norway spruce genome sequence and conifer genome evolution. Nature 497: 579-584

Oide S, Bejai S, Staal J, Guan N, Kaliff M, Dixelius C (2013) A novel role of PR2 in abscisic acid (ABA) mediated, pathogen-induced callose deposition in *Arabidopsis thaliana*. New Phytol 200: 1187-1199

Okabe T, Yoshimoto I, Hitoshi M, Ogawa T, Ohyama T (2005) An S-like ribonuclease gene is used to generate a trap-leaf enzyme in the carnivorous plant *Drosera adelae*. FEBS Lett 579: 5729-5733

Okuda S, Inoue Y, Eiraku M, Sasai Y, Adachi T (2013) Reversible network reconnection model for simulating large deformation in dynamic tissue morphogenesis. Biomech Model Mechanobiol 12: 627-644

Oud JL, Nanninga N (1992) Cell shape, chromosome orientation and the position of the plane of division in *Vicia faba* root cortex cells. J Cell Sci 103: 847-855

Ouyang S, Zhu W, Hamilton J, Lin H, Campbell M, Childs K, Thibaud-Nissen F, Malek RL, Lee Y, Zheng L, Orvis J, Haas B, Wortman J, Buell CR (2007) The TIGR Rice Genome Annotation Resource: improvements and new features. Nucleic Acids Res 35: D883-887

Ozerova LV, Timonin AC (2009) On the evidence of subunifacial and unifacial leaves: developmental studies in leaf-succulent *Senecio* L. species (Asteraceae). Wulfenia 16: 61-77

Palevitz B, Hepler P (1974) The control of the plane of division during stomatal differentiation in *Allium*. Chromosoma 46: 297-326

Parker J, Tsagkogeorga G, Cotton JA, Liu Y, Provero P, Stupka E, Rossiter SJ (2013) Genome-wide signatures of convergent evolution in echolocating mammals. Nature 502: 228-231

Parra G, Bradnam K, Korf I (2007) CEGMA: a pipeline to accurately annotate core genes in eukaryotic genomes. Bioinformatics 23: 1061-1067

Passarinho PA, de Vries SC (2002) Arabidopsis chitinases: a genomic survey. Arabidopsis Book 1: e0023

Passarinho PA, Van Hengel AJ, Fransz PF, de Vries SC (2001) Expression pattern of the

Arabidopsis thaliana AtEP3/AtchitIV endochitinase gene. Planta 212: 556-567
Paszota P, Escalante-Perez M, Thomsen LR, Risor MW, Dembski A, Sanglas L, Nielsen TA, Karring H, Thogersen IB, Hedrich R, Enghild JJ, Kreuzer I, Sanggaard KW (2014) Secreted major Venus flytrap chitinase enables digestion of Arthropod prey. Biochim Biophys Acta 2: 374-383
Pavlovič A (2011) Photosynthetic characterization of Australian pitcher plant *Cephalotus follicularis*. Photosynthetica 49: 253-258
Pekker I, Alvarez JP, Eshed Y (2005) Auxin response factors mediate *Arabidopsis* organ asymmetry via modulation of KANADI activity. Plant Cell 17: 2899-2910
Perez-Rodriguez P, Riano-Pachon DM, Correa LG, Rensing SA, Kersten B, Mueller-Roeber B (2010) PlnTFDB: updated content and new features of the plant transcription factor database. Nucleic Acids Res 38: D822-827
Pettersen EF, Goddard TD, Huang CC, Couch GS, Greenblatt DM, Meng EC, Ferrin TE (2004) UCSF Chimera — a visualization system for exploratory research and analysis. J Comput Chem 25: 1605-1612
Pigliucci M, Murren CJ, Schlichting CD (2006) Phenotypic plasticity and evolution by genetic assimilation. J Exp Biol 209: 2362-2367
Pinon V, Prasad K, Grigg SP, Sanchez-Perez GF, Scheres B (2013) Local auxin biosynthesis regulation by PLETHORA transcription factors controls phyllotaxis in *Arabidopsis*. Proc Natl Acad Sci USA 110: 1107-1112
Prigge MJ, Otsuga D, Alonso JM, Ecker JR, Drews GN, Clark SE (2005) Class III homeodomain-leucine zipper gene family members have overlapping, antagonistic, and distinct roles in Arabidopsis development. Plant Cell 17: 61-76
Prusinkiewicz P, Lindenmayer A (1990) The Algorithmic Beauty of Plants. Springer, New York
Rasmussen MD, Kellis M (2011) A Bayesian approach for fast and accurate gene tree reconstruction. Mol Biol Evol 28: 273-290
Ratcliff F, Martin-Hernandez AM, Baulcombe DC (2001) Technical Advance: Tobacco rattle virus as a vector for analysis of gene function by silencing. Plant J 25: 237-245
Reinhardt D, Frenz M, Mandel T, Kuhlemeier C (2005) Microsurgical and laser ablation analysis of leaf positioning and dorsoventral patterning in tomato. Development 132: 15-26
Rhoades MW, Reinhart BJ, Lim LP, Burge CB, Bartel B, Bartel DP (2002) Prediction of plant microRNA targets. Cell 110: 513-520
Rice P, Longden I, Bleasby A (2000) EMBOSS: the European Molecular Biology Open Software Suite. Trends Genet 16: 276-277
Robinson MD, Oshlack A (2010) A scaling normalization method for differential expression analysis of RNA-seq data. Genome Biol 11: 2010-2011
Robinson MD, Smyth GK (2008) Small-sample estimation of negative binomial dispersion, with applications to SAGE data. Biostatistics 9: 321-332
Rosado A, Li R, van de Ven W, Hsu E, Raikhel NV (2012) *Arabidopsis* ribosomal proteins control developmental programs through translational regulation of auxin response factors. Proc Natl Acad Sci USA 109: 19537-19544
Roth I (1952) Beiträge zur Entwicklungsgeschichte der Schildblätter. Planta 40: 350-376
Rottloff S, Stieber R, Maischak H, Turini FG, Heubl G, Mithofer A (2011) Functional characterization of a class III acid endochitinase from the traps of the carnivorous pitcher plant genus, *Nepenthes*. J Exp Bot 62: 4639-4647
Rouard M, Guignon V, Aluome C, Laporte MA, Droc G, Walde C, Zmasek CM, Perin C, Conte MG (2011) GreenPhylDB v2.0: comparative and functional genomics in plants. Nucleic Acids Res 39: D1095-1102
Rudall PJ, Buzgo M (2002) Evolutionary history of the monocot leaf. In: Cronk QCB, Bateman RM, Hawkins JA (eds) Developmental genetics and plant evolution. Taylor and Francis, London, pp 431-458
Rudge T, Haseloff J (2005) A computational model of cellular morphogenesis in plants. In:

Capcarrère M, Freitas A, Bentley P, Johnson C, Timmis J (eds) Advances in Artificial Life. Springer Berlin Heidelberg, Heidelberg, pp 78-87

Samac DA, Shah DM (1991) Developmental and pathogen-induced activation of the Arabidopsis acidic chitinase promoter. Plant Cell 3: 1063-1072

Sarojam R, Sappl PG, Goldshmidt A, Efroni I, Floyd SK, Eshed Y, Bowman JL (2010) Differentiating Arabidopsis shoots from leaves by combined YABBY activities. Plant Cell 22: 2113-2130

Sawa S, Watanabe K, Goto K, Liu YG, Shibata D, Kanaya E, Morita EH, Okada K (1999) *FILAMENTOUS FLOWER*, a meristem and organ identity gene of *Arabidopsis*, encodes a protein with a zinc finger and HMG-related domains. Genes Dev 13: 1079-1088

Scanlon MJ, Chen KD, McKnight CI (2000) The *narrow sheath* duplicate genes: sectors of dual aneuploidy reveal ancestrally conserved gene functions during maize leaf development. Genetics 155: 1379-1389

Scanlon MJ, Freeling M (1997) Clonal sectors reveal that a specific meristematic domain is not utilized in the maize mutant *narrow sheath*. Dev Biol 182: 52-66

Scanlon MJ, Schneeberger RG, Freeling M (1996) The maize mutant *narrow sheath* fails to establish leaf margin identity in a meristematic domain. Development 122: 1683-1691

Schenk G, Guddat LW, Ge Y, Carrington LE, Hume DA, Hamilton S, de Jersey J (2000) Identification of mammalian-like purple acid phosphatases in a wide range of plants. Gene 250: 117-125

Scherzer S, Krol E, Kreuzer I, Kruse J, Karl F, von Ruden M, Escalante-Perez M, Muller T, Rennenberg H, Al-Rasheid KA, Neher E, Hedrich R (2013) The *Dionaea muscipula* ammonium channel DmAMT1 provides NH(4)(+) uptake associated with Venus flytrap's prey digestion. Curr Biol 23: 1649-1657

Schmutz J, Cannon SB, Schlueter J, Ma J, Mitros T, Nelson W, Hyten DL, Song Q, Thelen JJ, Cheng J, Xu D, Hellsten U, May GD, Yu Y, Sakurai T, Umezawa T, Bhattacharyya MK, Sandhu D, Valliyodan B, Lindquist E, Peto M, Grant D, Shu S, Goodstein D, Barry K, Futrell-Griggs M, Abernathy B, Du J, Tian Z, Zhu L, Gill N, Joshi T, Libault M, Sethuraman A, Zhang XC, Shinozaki K, Nguyen HT, Wing RA, Cregan P, Specht J, Grimwood J, Rokhsar D, Stacey G, Shoemaker RC, Jackson SA (2010) Genome sequence of the palaeopolyploid soybean. Nature 463: 178-183

Schneeberger R, Tsiantis M, Freeling M, Langdale JA (1998) The *rough sheath2* gene negatively regulates homeobox gene expression during maize leaf development. Development 125: 2857-2865

Schulze W, Frommer WB, Ward JM (1999) Transporters for ammonium, amino acids and peptides are expressed in pitchers of the carnivorous plant *Nepenthes*. Plant J 17: 637-646

Schulze WX, Sanggaard KW, Kreuzer I, Knudsen AD, Bemm F, Thogersen IB, Brautigam A, Thomsen LR, Schliesky S, Dyrlund TF, Escalante-Perez M, Becker D, Schultz J, Karring H, Weber A, Hojrup P, Hedrich R, Enghild JJ (2012) The protein composition of the digestive fluid from the venus flytrap sheds light on prey digestion mechanisms. Mol Cell Proteomics 11: 1306-1319

Schwab R, Maizel A, Ruiz-Ferrer V, Garcia D, Bayer M, Crespi M, Voinnet O, Martienssen RA (2009) Endogenous tasiRNAs mediate non-cell autonomous effects on gene regulation in *Arabidopsis thaliana*. PLoS One 4: e5980

Semiarti E, Ueno Y, Tsukaya H, Iwakawa H, Machida C, Machida Y (2001) The *ASYMMETRIC LEAVES2* gene of *Arabidopsis thaliana* regulates formation of a symmetric lamina, establishment of venation and repression of meristem-related homeobox genes in leaves. Development 128: 1771-1783

Sessions A, Nemhauser JL, McColl A, Roe JL, Feldmann KA, Zambryski PC (1997) *ETTIN* patterns the *Arabidopsis* floral meristem and reproductive organs. Development 124: 4481-4491

Sessions RA, Zambryski PC (1995) *Arabidopsis* gynoecium structure in the wild and in *ettin*

mutants. Development 121: 1519-1532
Shen YY, Liang L, Li GS, Murphy RW, Zhang YP (2012) Parallel evolution of auditory genes for echolocation in bats and toothed whales. PLoS Genet 8: 28
Shimodaira H, Hasegawa M (1999) Multiple comparisons of log-likelihoods with applications to phylogenetic inference. Mol Biol Evol 16: 1114-1116
Shubin N, Tabin C, Carroll S (2009) Deep homology and the origins of evolutionary novelty. Nature 457: 818-823
Shulaev V, Sargent DJ, Crowhurst RN, Mockler TC, Folkerts O, Delcher AL, Jaiswal P, Mockaitis K, Liston A, Mane SP, Burns P, Davis TM, Slovin JP, Bassil N, Hellens RP, Evans C, Harkins T, Kodira C, Desany B, Crasta OR, Jensen RV, Allan AC, Michael TP, Setubal JC, Celton JM, Rees DJ, Williams KP, Holt SH, Ruiz Rojas JJ, Chatterjee M, Liu B, Silva H, Meisel L, Adato A, Filichkin SA, Troggio M, Viola R, Ashman TL, Wang H, Dharmawardhana P, Elser J, Raja R, Priest HD, Bryant DW, Jr., Fox SE, Givan SA, Wilhelm LJ, Naithani S, Christoffels A, Salama DY, Carter J, Lopez Girona E, Zdepski A, Wang W, Kerstetter RA, Schwab W, Korban SS, Davik J, Monfort A, Denoyes-Rothan B, Arus P, Mittler R, Flinn B, Aharoni A, Bennetzen JL, Salzberg SL, Dickerman AW, Velasco R, Borodovsky M, Veilleux RE, Folta KM (2011) The genome of woodland strawberry (*Fragaria vesca*). Nat Genet 43: 109-116
Siegfried KR, Eshed Y, Baum SF, Otsuga D, Drews GN, Bowman JL (1999) Members of the *YABBY* gene family specify abaxial cell fate in *Arabidopsis*. Development 126: 4117-4128
Sikosek T, Chan HS (2014) Biophysics of protein evolution and evolutionary protein biophysics. J R Soc Interface 11
Sipos B, Massingham T, Jordan GE, Goldman N (2011) PhyloSim - Monte Carlo simulation of sequence evolution in the R statistical computing environment. BMC Bioinformatics 12: 1471-2105
Snow M, Snow R (1959) The dorsiventrality of leaf primordia. New Phytol 58: 188-207
Snow R, Snow M (1954) Experiments on the cause of dorsiventrality in leaves. Nature 174: 352-353
Soma S (1965) Developmental studies on the orientation and the dorsiventrality of the leaf of *Zelkova serrata* Makino. J Fac Sci Univ Tokyo Sec III Bot 9: 1-17
Stahle MI, Kuehlich J, Staron L, von Arnim AG, Golz JF (2009) YABBYs and the transcriptional corepressors LEUNIG and LEUNIG_HOMOLOG maintain leaf polarity and meristem activity in Arabidopsis. Plant Cell 21: 3105-3118
Stamatakis A (2006) RAxML-VI-HPC: maximum likelihood-based phylogenetic analyses with thousands of taxa and mixed models. Bioinformatics 22: 2688-2690
Stamatakis A (2014) RAxML version 8: a tool for phylogenetic analysis and post-analysis of large phylogenies. Bioinformatics 30: 1312-1313
Staple DB, Farhadifar R, Roper JC, Aigouy B, Eaton S, Julicher F (2010) Mechanics and remodelling of cell packings in epithelia. Eur Phys J E Soft Matter 33: 117-127
Steeves TA, Sussex IM (1989) Patterns in Plant Development. Cambridge University Press, New York
Stern DL (2013) The genetic causes of convergent evolution. Nat Rev Genet 14: 751-764
Sun Y, Zhou Q, Zhang W, Fu Y, Huang H (2002) *ASYMMETRIC LEAVES1*, an *Arabidopsis* gene that is involved in the control of cell differentiation in leaves. Planta 214: 694-702
Sussex IM (1951) Experiments on the cause of dorsiventrality in leaves. Nature 167: 651-652
Sussex IM (1954) Experiments on the cause of dorsiventrality in leaves. Nature 174: 351-352
Sussex IM (1955) Morphogenesis in *Solanum tuberosum* L.: experimental investigation of leaf dorsiventrality and orientation in the juvenile shoot. Phytomorphology 5: 286-300
Swarbreck D, Wilks C, Lamesch P, Berardini TZ, Garcia-Hernandez M, Foerster H, Li D, Meyer T, Muller R, Ploetz L, Radenbaugh A, Singh S, Swing V, Tissier C, Zhang P, Huala E (2008) The Arabidopsis Information Resource (TAIR): gene structure and

function annotation. Nucleic Acids Res 36: D1009-1014
Tadege M, Lin H, Bedair M, Berbel A, Wen J, Rojas CM, Niu L, Tang Y, Sumner L, Ratet P, McHale NA, Madueno F, Mysore KS (2011) *STENOFOLIA* regulates blade outgrowth and leaf vascular patterning in *Medicago truncatula* and *Nicotiana sylvestris*. Plant Cell 23: 2125-2142
Takahashi K, Suzuki T, Nishii W, Kubota K, Shibata C, Isobe T, Dohmae N (2011) A cysteine endopeptidase ("Dionain") is involved in the digestive fluid of *Dionaea muscipula* (Venus's fly-trap). Biosci Biotechnol Biochem 75: 346-348
Talbert PB, Adler HT, Parks DW, Comai L (1995) The *REVOLUTA* gene is necessary for apical meristem development and for limiting cell divisions in the leaves and stems of *Arabidopsis thaliana*. Development 121: 2723-2735
Tameshige T, Fujita H, Watanabe K, Toyokura K, Kondo M, Tatematsu K, Matsumoto N, Tsugeki R, Kawaguchi M, Nishimura M, Okada K (2013) Pattern dynamics in adaxial-abaxial specific gene expression are modulated by a plastid retrograde signal during *Arabidopsis thaliana* leaf development. PLoS Genet 9: e1003655
Tang G, Reinhart BJ, Bartel DP, Zamore PD (2003) A biochemical framework for RNA silencing in plants. Genes Dev 17: 49-63
Tattersall AD, Turner L, Knox MR, Ambrose MJ, Ellis TH, Hofer JM (2005) The mutant *crispa* reveals multiple roles for *PHANTASTICA* in pea compound leaf development. Plant Cell 17: 1046-1060
Tepfer SS (1960) The shoot apex and early leaf development in Clematis. Am J Bot 47: 655-664
Timmermans MC, Hudson A, Becraft PW, Nelson T (1999) ROUGH SHEATH2: a Myb protein that represses *knox* homeobox genes in maize lateral organ primordia. Science 284: 151-153
Tomato Genome Consortium (2012) The tomato genome sequence provides insights into fleshy fruit evolution. Nature 485: 635-641
Toriba T, Ohmori Y, Hirano H-Y (2011) Common and distinct mechanisms underlying the establishment of adaxial and abaxial polarity in stamen and leaf development. Plant Signal Behav 6: 430-433
Toriba T, Suzaki T, Yamaguchi T, Ohmori Y, Tsukaya H, Hirano HY (2010) Distinct regulation of adaxial-abaxial polarity in anther patterning in rice. Plant Cell 22: 1452-1462
Toyokura K, Watanabe K, Oiwaka A, Kusano M, Tameshige T, Tatematsu K, Matsumoto N, Tsugeki R, Saito K, Okada K (2011) Succinic semialdehyde dehydrogenase is involved in the robust patterning of Arabidopsis leaves along the adaxial-abaxial axis. Plant Cell Physiol 52: 1340-1353
Trapnell C, Roberts A, Goff L, Pertea G, Kim D, Kelley DR, Pimentel H, Salzberg SL, Rinn JL, Pachter L (2012) Differential gene and transcript expression analysis of RNA-seq experiments with TopHat and Cufflinks. Nat Protoc 7: 562-578
Trapnell C, Williams BA, Pertea G, Mortazavi A, Kwan G, van Baren MJ, Salzberg SL, Wold BJ, Pachter L (2010) Transcript assembly and quantification by RNA-Seq reveals unannotated transcripts and isoform switching during cell differentiation. Nat Biotechnol 28: 511-515
Troll W (1932) Morphologie der schildförmigen Blätter. Planta 17: 231-314
Tsiantis M, Schneeberger R, Golz JF, Freeling M, Langdale JA (1999) The maize *rough sheath2* gene and leaf development programs in monocot and dicot plants. Science 284: 154-156
Tsukaya H (2013) Leaf development. The Arabidopsis Book. The American Society of Plant Biologists, p e0163
Turchi L, Carabelli M, Ruzza V, Possenti M, Sassi M, Penalosa A, Sessa G, Salvi S, Forte V, Morelli G, Ruberti I (2013) *Arabidopsis* HD-Zip II transcription factors control apical embryo development and meristem function. Development 140: 2118-2129
Tuskan GA, Difazio S, Jansson S, Bohlmann J, Grigoriev I, Hellsten U, Putnam N, Ralph S,

Rombauts S, Salamov A, Schein J, Sterck L, Aerts A, Bhalerao RR, Bhalerao RP, Blaudez D, Boerjan W, Brun A, Brunner A, Busov V, Campbell M, Carlson J, Chalot M, Chapman J, Chen GL, Cooper D, Coutinho PM, Couturier J, Covert S, Cronk Q, Cunningham R, Davis J, Degroeve S, Dejardin A, Depamphilis C, Detter J, Dirks B, Dubchak I, Duplessis S, Ehlting J, Ellis B, Gendler K, Goodstein D, Gribskov M, Grimwood J, Groover A, Gunter L, Hamberger B, Heinze B, Helariutta Y, Henrissat B, Holligan D, Holt R, Huang W, Islam-Faridi N, Jones S, Jones-Rhoades M, Jorgensen R, Joshi C, Kangasjarvi J, Karlsson J, Kelleher C, Kirkpatrick R, Kirst M, Kohler A, Kalluri U, Larimer F, Leebens-Mack J, Leple JC, Locascio P, Lou Y, Lucas S, Martin F, Montanini B, Napoli C, Nelson DR, Nelson C, Nieminen K, Nilsson O, Pereda V, Peter G, Philippe R, Pilate G, Poliakov A, Razumovskaya J, Richardson P, Rinaldi C, Ritland K, Rouze P, Ryaboy D, Schmutz J, Schrader J, Segerman B, Shin H, Siddiqui A, Sterky F, Terry A, Tsai CJ, Uberbacher E, Unneberg P, Vahala J, Wall K, Wessler S, Yang G, Yin T, Douglas C, Marra M, Sandberg G, Van de Peer Y, Rokhsar D (2006) The genome of black cottonwood, *Populus trichocarpa* (Torr. & Gray). Science 313: 1596-1604

Vandenbussche M, Horstman A, Zethof J, Koes R, Rijpkema AS, Gerats T (2009) Differential recruitment of *WOX* transcription factors for lateral development and organ fusion in Petunia and *Arabidopsis*. Plant Cell 21: 2269-2283

Vatén A, Dettmer J, Wu S, Stierhof YD, Miyashima S, Yadav SR, Roberts CJ, Campilho A, Bulone V, Lichtenberger R, Lehesranta S, Mähönen AP, Kim JY, Jokitalo E, Sauer N, Scheres B, Nakajima K, Carlsbecker A, Gallagher KL, Helariutta Y (2011) Callose biosynthesis regulates symplastic trafficking during root development. Dev Cell 21: 1144-1155

Voesenek LA, Colmer TD, Pierik R, Millenaar FF, Peeters AJ (2006) How plants cope with complete submergence. New Phytol 170: 213-226

Waddington CH (1953) Genetic assimilation of an acquired character. Evolution 7: 118-126

Waites R, Hudson A (1995) *phantastica*: a gene required for dorsoventrality of leaves in *Antirrhinum majus*. Development 121: 2143-2154

Waites R, Selvadurai HR, Oliver IR, Hudson A (1998) The *PHANTASTICA* gene encodes a MYB transcription factor involved in growth and dorsoventrality of lateral organs in *Antirrhinum*. Cell 93: 779-789

Wang W, Xu B, Wang H, Li J, Huang H, Xu L (2011) *YUCCA* genes are expressed in response to leaf adaxial-abaxial juxtaposition and are required for leaf margin development. Plant Physiol 157: 1805-1819

Wenkel S, Emery J, Hou BH, Evans MM, Barton MK (2007) A feedback regulatory module formed by LITTLE ZIPPER and HD-ZIPIII genes. Plant Cell 19: 3379-3390

Whibley AC, Langlade NB, Andalo C, Hanna AI, Bangham A, Thebaud C, Coen E (2006) Evolutionary paths underlying flower color variation in *Antirrhinum*. Science 313: 963-966

Williams L, Carles CC, Osmont KS, Fletcher JC (2005) A database analysis method identifies an endogenous trans-acting short-interfering RNA that targets the *Arabidopsis ARF2*, *ARF3*, and *ARF4* genes. Proc Natl Acad Sci USA 102: 9703-9708

Wolpert L, Tickle C, Lawrence P, Meyerowitz EM, Robertson E, Smith J, Jessell T (2011) Principles of development. Oxford Univ. Press, Oxford

Wu G, Lin WC, Huang T, Poethig RS, Springer PS, Kerstetter RA (2008) KANADI1 regulates adaxial-abaxial polarity in *Arabidopsis* by directly repressing the transcription of *ASYMMETRIC LEAVES2*. Proc Natl Acad Sci USA 105: 16392-16397

Wu YC, Rasmussen MD, Bansal MS, Kellis M (2013) TreeFix: statistically informed gene tree error correction using species trees. Syst Biol 62: 110-120

Xu D, Huang W, Li Y, Wang H, Huang H, Cui X (2012) Elongator complex is critical for cell cycle progression and leaf patterning in *Arabidopsis*. Plant J 69: 792-808

Xu L, Xu Y, Dong A, Sun Y, Pi L, Huang H (2003) Novel *as1* and *as2* defects in leaf adaxial-abaxial polarity reveal the requirement for *ASYMMETRIC LEAVES1* and *2* and *ERECTA* functions in specifying leaf adaxial identity. Development 130: 4097-4107

Xu L, Yang L, Pi L, Liu Q, Ling Q, Wang H, Poethig RS, Huang H (2006) Genetic interaction between the *AS1-AS2* and *RDR6-SGS3-AGO7* pathways for leaf morphogenesis. Plant Cell Physiol 47: 853-863

Xu Y, Sun Y, Liang WQ, Huang H (2002) The *Arabidopsis AS2* gene encoding a predicted leucine-zipper protein is required for the leaf polarity formation. Acta Bot Sin 44: 1194-1202

Yamada T, Yokota S, Hirayama Y, Imaichi R, Kato M, Gasser CS (2011) Ancestral expression patterns and evolutionary diversification of YABBY genes in angiosperms. Plant J 67: 26-36

Yamagishi N, Sasaki S, Yamagata K, Komori S, Nagase M, Wada M, Yamamoto T, Yoshikawa N (2011) Promotion of flowering and reduction of a generation time in apple seedlings by ectopical expression of the *Arabidopsis thaliana FT* gene using the *Apple latent spherical virus* vector. Plant Mol Biol 75: 193-204

Yamagishi N, Yoshikawa N (2011) Expression of *FLOWERING LOCUS T* from *Arabidopsis thaliana* induces precocious flowering in soybean irrespective of maturity group and stem growth habit. Planta 233: 561-568

Yamaguchi T, Nagasawa N, Kawasaki S, Matsuoka M, Nagato Y, Hirano HY (2004) The *YABBY* gene *DROOPING LEAF* regulates carpel specification and midrib development in *Oryza sativa*. Plant Cell 16: 500-509

Yamaguchi T, Tsukaya H (2010) Evolutionary and developmental studies of unifacial leaves in monocots: *Juncus* as a model system. J Plant Res 123: 35-41

Yamaguchi T, Yano S, Tsukaya H (2010) Genetic framework for flattened leaf blade formation in unifacial leaves of *Juncus prismatocarpus*. Plant Cell 22: 2141-2155

Yan S, Yan CJ, Zeng XH, Yang YC, Fang YW, Tian CY, Sun YW, Cheng ZK, Gu MH (2008) *ROLLED LEAF 9*, encoding a GARP protein, regulates the leaf abaxial cell fate in rice. Plant Mol Biol 68: 239-250

Yang L, Huang W, Wang H, Cai R, Xu Y, Huang H (2006) Characterizations of a hypomorphic *argonaute1* mutant reveal novel *AGO1* functions in *Arabidopsis* lateral organ development. Plant Mol Biol 61: 63-78

Yang Z (2007) PAML 4: phylogenetic analysis by maximum likelihood. Mol Biol Evol 24: 1586-1591

Yang Z, Nielsen R (2000) Estimating synonymous and nonsynonymous substitution rates under realistic evolutionary models. Mol Biol Evol 17: 32-43

Yao X, Wang H, Li H, Yuan Z, Li F, Yang L, Huang H (2009) Two types of *cis*-acting elements control the abaxial epidermis-specific transcription of the *MIR165a* and *MIR166a* genes. FEBS Lett 583: 3711-3717

Yifhar T, Pekker I, Peled D, Friedlander G, Pistunov A, Sabban M, Wachsman G, Alvarez JP, Amsellem Z, Eshed Y (2012) Failure of the tomato *trans*-acting short interfering RNA program to regulate AUXIN RESPONSE FACTOR3 and ARF4 underlies the wiry leaf syndrome. Plant Cell 24: 3575-3589

Yoshida S, Barbier de Reuille P, Lane B, Bassel GW, Prusinkiewicz P, Smith RS, Weijers D (2014) Genetic control of plant development by overriding a geometric division rule. Dev Cell 29: 75-87

Yuan Z, Luo D, Li G, Yao X, Wang H, Zeng M, Huang H, Cui X (2010) Characterization of the *AE7* gene in Arabidopsis suggests that normal cell proliferation is essential for leaf polarity establishment. Plant J 64: 331-342

Zdobnov EM, Apweiler R (2001) InterProScan—an integration platform for the signature-recognition methods in InterPro. Bioinformatics 17: 847-848

Zhang GH, Xu Q, Zhu XD, Qian Q, Xue HW (2009) SHALLOT-LIKE1 is a KANADI transcription factor that modulates rice leaf rolling by regulating leaf abaxial cell development. Plant Cell 21: 719-735

Zhang J (2006) Parallel adaptive origins of digestive RNases in Asian and African leaf monkeys. Nat Genet 38: 819-823

Zhang X, Zong J, Liu J, Yin J, Zhang D (2010) Genome-wide analysis of *WOX* gene family in

rice, sorghum, maize, *Arabidopsis* and poplar. J Integr Plant Biol 52: 1016-1026

Zhong R, Ye ZH (2004) *amphivasal vascular bundle 1*, a gain-of-function mutation of the *IFL1/REV* gene, is associated with alterations in the polarity of leaves, stems and carpels. Plant Cell Physiol 45: 369-385

Zhu H, Hu F, Wang R, Zhou X, Sze SH, Liou LW, Barefoot A, Dickman M, Zhang X (2011) *Arabidopsis* Argonaute10 specifically sequesters miR166/165 to regulate shoot apical meristem development. Cell 145: 242-256

Zhuang LL, Ambrose M, Rameau C, Weng L, Yang J, Hu XH, Luo D, Li X (2012) LATHYROIDES, encoding a WUSCHEL-related Homeobox1 transcription factor, controls organ lateral growth, and regulates tendril and dorsal petal identities in garden pea (*Pisum sativum* L.). Mol Plant 5: 1333-1345

Zoulias N, Koenig D, Hamidi A, McCormick S, Kim M (2012) A role for *PHANTASTICA* in medio-lateral regulation of adaxial domain development in tomato and tobacco leaves. Ann Bot 109: 407-418